PD-AAW-320
52161

AGENCY FOR INTERNATIONAL DEVELOPMENT
WASHINGTON, D.C. 20523

DATE: 8/7/87

MEMORANDUM

TO: AID/PPC/CDIE/DI, room 209 SA-18

FROM: AID/SCI, Victoria Ose VO

SUBJECT: Transmittal of AID/SCI Progress Report(s)

Attached for permanent retention/proper disposition is the following:

AID/SCI Progress Report No. 4 298
Trial

Attachment

2 cys

ROUTING AND TRANSMITTAL SLIP

Date: July 31, 1987

TO: (Name, office symbol, room number, building, Agency/Post)	Initials	Date
1. Dr. Irvin M. Asher Director, Science Program		
2. AID/SCI, Room 720, SA-18 AID/W		
3.		
4.		
5.		

	Action		File		Note and Return
	Approval		For Clearance		Per Conversation
X	As Requested		For Correction		Prepare Reply
	Circulate		For Your Information		See Me
	Comment		Investigate		Signature
	Coordination		Justify		

REMARKS

SUBJECT: PSTC Grant No. 936-5542-G-SS-4003-00 (4.298), P.I. Xavier

Subject Grant was completed June 30, 1987 and the final report submitted to USAID (10 copies). 8 copies of such report are transmitted herewith for AID/W distribution. 1 copy has been passed to Mission Science Officer, John Struble (ECON).
Enclosures: a/s

Note: Report copies pouched to AID/SCI in 4 separate packages of 2 copies each.

DO NOT use this form as a RECORD of approvals, concurrences, disposals, clearances, and similar actions

FROM: (Name, org. symbol, Agency/Post)	Room No.—Bldg.
USAID/Lisbon - Luz Rezende PS	Phone No. 726-66-00 (Lisbon)

5041-102

OPTIONAL FORM 41 (Rev. 7-76)
Prescribed by GSA
FPMR (41 CFR) 101-11.206

☆ GPO : 1981 O - 341-529 (25)

Rec'd in SCI. AUG 7 1987

4298

CENTRO DE QUÍMICA ESTRUTURAL
COMPLEXO INTERDISCIPLINAR
INSTITUTO SUPERIOR TÉCNICO
1096 LISBOA-CODEX PORTUGAL

Telefs. 57 26 16 - 55 38 09 - 56 20 96

To: AID Project Support Officer

Subject: Final Report

Grant: No. 936-5542-G-SS-4003-00

Title: Optimization of Bioconversion of Liquid and Solid Residues.

Principal Investigator: António V.Xavier, Ph.D.

Applicant Organization: Centro de Química Estrutural

Period Covered: July 3, 1984 to June 30, 1987.

2

1 - BIOCHEMICAL ENGINEERING SIDE OF THE PROJECT

1.1 - INTRODUCTION

These studies were described in the proposal on pages 11 to 18 (4.4.5 to 4.3.2), 22 to 23 (5), 24 to 28 (6.1), 29 to 32 (6.4.1.) and 35 to 36 (8) and were mainly intended to:

- use three different residues: molasses slops from ethanol prodcution, corn stover and eucalyptus;
- use phase separated systems, i.e. acidogenic reactors followed by methanogenic reactors with emphasis on the acidogenic phase;
- use different reactor types, not only the traditional continuously stirred tank reactor but mainly fixed bed, expanded bed, fluidised bed reactor types; these reactor types rely on biological film formation to increase biomass retention and thus allow smaller hydraulic retention times to be used without washout of the microorganisms.

1.2 - EVOLUTION OF WORLDWIDE RESEARCH ON THESE TOPICS AND ADJUSTEMENTS MADE THROUGHOUT THE PROJECT

1.2.1 - Residues

Further problems on sulphide toxicity and an increase in the fundamental knowledge on sulphate reducing bacteria, meant that the large sulphate contents in the molasses slops rendered it an even more interesting waste than originally forecasted. Much work on mixed cultures of sulphate reducers and methanogenic bacteria appeared in the literature; on the acidogenic phase though, little activity took place, increasing the interest in our work.

This work is going to be orally presented under the title "Sulphate reduction in acidogenic phase anaerobic digestion" at the IAWPRC Specialized Conference on the Microbiology of Waters and Wastewaters in Newport Beach, California, February 8-11, 1988.

The sharp drop in oil prices meant that many of the biomass projects were reduced/reassessed: furthermore, the difficulties faced by "microbial/enzymatic" hydrolysis of cellulose, specially if lignin is present, meant that the "general trend" is to assume that only chemical, namely acid hydrolysis, could be contemplated in the near future. Thus as indicated in earlier reports, we started the study of propionic/acetic acid production using substrates reproducing eucalyptus hydrolysates. As for corn stover, with a much smaller lignin content (approx. 8%), kinetic assessment of hydrolysis/acidification is important for two reasons: i) it is common to have particulates, mainly cellulosics, in many industrial/agricultaral/domestic effluents and thus these kinetics are important for effluent treatment; ii) some substrates for fermentations contain particulates similar to these and/or they can be used as support for fermentations conducted under acid pH's.

1.2.2 - Phase Separation

Some phase separated systems, namely Gist Brocades fluidized bed systems, have become operational from late 1984 onwards. These and continous research carried out over the last years,

seem to indicate that this strategy is mainly appropriate whenever: i) substrates/products that can hinder methanogenesis can be accomodated/separated/degraded in the acidogenic phase and thus not proceed to the methanogenic phase; ii) whenever there is a clear need tp carry out much slower hydrolysis, for which an acidogenic phase will be benefitial.

For other situations, the increased complexity of two separate reactors does not seem to be a worthy choice, even though a better control is possible.

We were only using the acidogenic approach for the corn stover (hydrolis is required) and molasses slops (eventually leading to sulphide removal prior to methanogenesis) i.e., we have not had to change the original approach. The main strategy is now either to "produce acids" (corn stover) or to remove sulphur and not so much to "optimize" the acidogenic reactor from the point of view of "reactor productivity".

1.2.3 - Reactor Types

Of the reactors indicated, expanded/fluidised bed systems have not, as yet, made major inroads in actual treatment systems as fixed bed systems are more reliable even though less productive

We have conducted tests with CSTR, fixed bed and expanded bed systems only.

1.3 - ACHIEVEMENTS

1.3.1 Operational

As stated in earlier reports, some major hurdles took place, namely due to a delay in the delivery of the new laboratory (more than one year) and, after that, a long start up problem with one central part of the equipment, namely the gas chromatograph.

a) From an analytical point of view, we finally implemented all the fourteen major parameters indicated (6.4.1, pg 29-32). The main difficulties/modifications that took place were (nomenclature as in the original proposal):

pH - under continous monitoring/control, the presence of sulphide "destroyed" the electrodes in about one month or less; we have recently started to use an Ingold Xerolyt electrode, specifically designed to "stand" high sulphide concentrations.

Sulfur species - proved much more awesome to determine than originally expected due not only to the dark colour of the effluent but also to the need to conduct all sulfide sampling and determinations in the liquid phase anaerobically, to avoid oxidation; furthermore, soluble and precipitated parts have to be examined/determined separately, increasing the analytical load. Modifications:

- sulfide in the liquid effluent samples was anaerobically removed into zinc acetate to avoid oxidation; to remove all other components this sample is now digested with sulphuric acid, with nitrogen reflux, and the sulfide in the gas is precipitated with zinc acetate and analysed by the titrimetric (iodine) method;

b

- hydrogen sulfide in the gas samples is precipitated in a trap containing zinc acetate and titrated.

ii) The reactor lay outs include CSTR with pH control as an acidogenic test reactor, fixed bed on porous supports (kindly given by Glasswerk Schott, Mainz, FR Germany) with pH control and large recirculation for the acidogenic phase and fixed bed for the methanogenic phase: the last reactor is used as a "test" for the effluents obtained from the two acidogenic reactors. An expanded bed reactor is used for the milled corn stover acidogenic reactor; no pH control is used.

For the pure cultures of Propionibacterium working on dual substrate (xylose plus glucose) columnar fixed bed reactors, CSTR and, now being assembled, CSTR with cell recycle on ultrafiltration membranes have been used.

iii) Industrial support now includes the two largest ethanol producing companies (Soc.Lusitânia de Destilação and Vieira e Irmãos) for the biogas side - they have put together a pilot plant with two reactors of, 200 and 400 liters for each phase, respectively, using ceramic rasching rings as support.

The work on Propionibacterium and ylose/glucose substrates is parthly sponsored by the largest portuguese pulp and paper manufacturer, Portucel, a state holding company, IFE and the National Board for Science and Technology, JNICT.

iv) Corn stover is being assessed as a support for the

1

production of lactic acid starter cultures of Lactobacillus plantarum to be used for sillage.

1.3.f Scientific

Many of the scientific results have now either been presented, and/or published or accepted for publication; copies of these are being forwarded and, as the reprints get available, we will be sending them to U.S.A.I.D.

1.3.f.1 - Mixed culture work

Results published/presented in communications A-1, 3, 6 and 7 (cf. Publication List 1.4).

i) Molasses slops

On the "liquid" molasses slops effluent we are working at approximately 1 day hydraulic retention time in the acidogenic fermenters(both CSTR and fixed bed); pH's, now under control in both reactors, have been dropped from 7 to 6.6, 6.2 and work is now starting at 5.8. Main points: sulfate reduction has always been above 80%, with concentrations of sulfide in the liquid effluent of approximately 500 mg/l (easily precipitable with iron oxides) and gas concentrations reaching 18%, on a weight basis; surprisingly enough, even under these conditions methane can be formed in the gas, approximately 10 to 12% for the CSTR and more than 20% for the support fixed bed reactors, which is consistent with the original hypothesis for the advantages of fixed/supported biomass; hydrogen could also be detected in the gas from the CSTR (less than 1%) but not from the fixed bed systems. Gas production averaged 1 l/l effluent day. The

volatile fatty acid production is consistent with current knowledge: an increase in concentration of higher acids follows a decrease of the hydraulic retention time.

Once sulphides are precipitated, the sulphate still present on the methane reactor (less than 1 g/l from the original 5 g/l in the sloss) does not seem to be inhibitory. High gas production rates (higher than 4 l/l reactor day) and methane contents (up to 88%) have been observed.

ii) Corn stover

Concentrations of 1,25 % and 2,5 % (W/V) have been used for the kinetics. Only the last concentration was used for the expanded bed acidogenic reactor.

It has become apparent that, since only broad measurements were used, many of the results published in the literature on kinetic rates are almost irrelevant (e.g., volatile suspended solids do not distinguish between bacterial or corn stover solids); the Kjeldahl method is rather insensitive for low bacterial concentrations and accounts both for protein and for ammonium nitrogen (in the corn stover). We are now trying to "balance" out the reaction using, among others, the Bradford protein method.

Otherwise, acid production rates are reasonably easy to follow and, as hypothesised, the natural lowering of pH, down to 5.5, increases the rate of acid production, both in batch and expanded bed tests. Comparatively, using identical retention

times (4 months) and solids concentrations (2.5 %), 3 g/l and 5.5 g/l of acetic acid were produced in batch and expanded bed systems respectively. An identical concentration of butyric 0.5 g/l and traces of other acids, were obtained in both tests.

1.3.2.2 - Pure culture work

Results published/presented in communication A-1, 2, 4 and 5 (cf. Publication List, 1.4).

Given the characterization obtained for the Eucalyptus globulus (25 % lignin and extractables, 49% celulose 26%, hemicelulose, of which approximately 80% are pentosans) we have targeted the "appropriate" substrate to 2/3 glucose and 1/3 xylose.

Batch tests were conducted and glucose/xylose consumption, as well as product inhibition equations, are presented; no substrate inhibition is apparent with the sugar concentrations tested (up to 120 g/l total sugars); maximum acid concentrations of 15 g/l are obtained. (12 g/l propionic and 3 g/l acetic, i.e., a molar ratio of 3:1, above and thus better than the theoretical stoicheometric ratio of 2:1); acid yields of 78 to 80% are close to the theoretical maximum (82 %).

Under pH control at 6.0, batch tests yielded higher acids concentrations: 25 g/l propionic and 7 g/l acetic.

We have proved that xylose consumption rate is a function of both glucose concentration and microorganism specific growth rate. Maximum xylose consumption rates of 0.2 g/l.h have been achieved but at the opposite xylose/glucose ratio (2:1) to the

one obtained from eucalyptus (1:3).

Various continuous reactor systems have been assessed for propionic acid production: namely continuous stirred tank reactor (CSTR), immmobilized cell columnar reactors (ICR), and CSTR with cell recycle on ultrafiltration membranes (UFR). The ICR presented the best yields, as well as the larger propionic/acetic ratio (6.5); as the propionic price is approximately three timer higher than acetic, ratio increase is favorable. As no pH control was used the last third of the column was no longer used as pH attained an inhibitory value of 5.2. The UFR also yielded good acid ratios, by far the best productivities, and the largest final acid concentrations; the yield for total acids was no better than under the CSTR tests only.

Since the observed cell mass yield coefficients for this facultative anaerobe are high, at 0.263 g cell/g substrate, we have also followed vitamin B_{12} production capabilities. For batch-tests - under straight anaerobic conditions and with no percursor added (cobalt or 5,6-dimethylbenzimidazole), the vitamin B12 in the broth reaches 0.35 mg/l. This value compares well with those reported for the "industrial" microorganism Propionibacterium freundenrichii subsp. shermanii. Under UFR, we have achieved 5,28 mg/l at 66 g cell/l, i.e., 80μg/g cell dry weight.

11

1.4 - PUBLICATION LIST

A-1. M.J.T.CARRONDO, M.A.M.REIS, J.P.S.G.CRESPO - Mixed and pure culture immobilized reactors for acidogenic fermentations VII Conference on Global Impact of Applied Microbiology, Helsinki, August 1985.

A-2. J.P.CRESPO, M.MOURA and M.J.T.CARRONDO - Propionibacterium fermentation using c5 sugars for production of propionic acid and Vitamin B12 - Conference Biotechnology and Agriculture in the Mediterranean, June 1986.

A-3. M.J.T.CARRONDO et al - Optimization of bioconversion of solid and liquid residues in M.M.El - Halwagi (Ed.) Biogas Technology, Transfer and Diffusion, Elsevier - Applied Sci.Publ., London 1986, 331-391.

A-4. MJ.T.CARRONDO, J.P.S.G.CRESPO and M.J.MOURA - Propionic acid and vitamin B12 production using a xylose utilising Propionibacterium and different bioreactors in Proc. 4th Eur.Cong.Biotechnology, Amsterdam, July 1987, 97-100.

A-5. M.J.T.CARRONDO, J.P.S.G.CRESPO and M.J.MOURA - Production of propionic acid using a xylose utilizing Propionibacterium - Appl.Biochem.Biotechnol. in press.

A-6. * M.J.T.CARRONDO and M.A.M.REIS - Fixed Film Anaerobic Digestion in D.L.Wise (Ed.) Global Bioconversions vol.i, CRC Press Florida, in press.

A-7. M.A.M.REIS, L.M.D.GONÇALVES, M.J.T.CARRONDO - Sulfate reduction in acidogenic phase anaerobic digestion to be presented at IAWPRC Specialised Conference on the Microbiology of Waters and Wastewaters, Newport Beach, Cal., USA, Feb. 8-11, 1988.

* Copy not included. To be sent when reprints become available.

12

2 - SCREENING OF ENZYMES AND COFACTORS

During the three year period of the AID grant, screening and characterization of electron transfer proteins (ETP), as well as enzyme cofactors, from different bacterial groups relevant for anaerobic digestion of organic matter (sulfate reducers and methane forming bacteria). was extensively carried out. natural extention was also made to denitrifier organisms, complementing our approach to the understanding of inorganic elemental cycles (sulfur, carbon, and nitrogen). During the last period thermophilic organisms were also studied, using the same strategy.

Our work originated several publications. A complete list of these publications is added, together with copies of the articles which are either published, in press or submited for publication.

We now ist the organisms used as well as the main achievements resulting from our research in this area during the three year period (The numbers in brackets refer to the Publications List, cf. 2.3).

2.1 - ORGANISMS USED

Sulfate reducers:

Desulfovibrio gigas (NCIB 9334)

Desulfovibrio vulgaris (Hildenborough)

Desulfovibrio salexigens (British Guiana)

Desulfovibrio baculatus (DSM 1743)

Desulfovibrio desulfuricans (27774)

	Desulfovibrio thermophilus	(DSM 1276)
Methanogenic	Methanosarcina barkeri	(DSM 800)
	Methanosarcina barkeri	(DSM 804)
	Methanosarcina barkeri	(MST)
Denitrifiers	Wolinella succinogenes	(VPI 10659)
	Archromobacter cycloclastes	(IAM 105)

2.2 - RESULTS

2.2.1 - Bacterial hydrogenase - our work resulted in a proposal for a new classification for bacterial hydrogenases based on chemical, spectroscopic, activity and genetic data. The [Fe], [Ni-Fe] and [NiFeSe] hydrogenases where caracterized. A mechanistic pathway for hydrogen utilization was postulated, and the intermediate reactive species involved were studied. Bacterial hydrogenases from thermophilic organisms were also characterized. The role of bacterial hydrogenase in the methanogenic pathways was established (B-1, 8, 9, 11, 13, 14, 18, 19, 29, 30).

2.2.2 - Sulfite reductases

A new type of sulfite reductases from sulfate reducers and methane forming bacteria (low spin type), was isolated.

Desulfoviridine, desulforubidine and desulfofucsidine (high spin sulfite reductases) were characterized and their substrate bound species as well as their reactivities towards external ligands were studied (B-2, 9, 14, 19, 24, 31).

2.2.3 - APS reductases

The enzyme responsable for the first steps of sulfate activation was, for the first time, fully characterized in terms of its active site. The relevant intermediate catalytic species formed upon reaction with AMP, AMP + $SO_3^=$, and ascorbate, were studied. Mechanistic implications were established (B-7).

2.2.4 - Multiheme cytochrome c_3

The tetraheme cytochrome c_3 purified from different Desulfovibrio spp. was studied from the point of view of its potential use for the coupled transfer of two-electrons and two-protons to hydrogenase. The microscopic midpoint redox potentials of its four hemes, as well as their pH dependences, were interpreted as an evidence for such a role. Furthermore, a regulatory role by the redox state of two hemes was postulated (B-4, 5, 16).

2.2.5 - Heme proteins involved in denitrification

The cytochrome system (monoheme and diheme proteins) of Wolinella succinogenes, a nitrate respiring organism, was studied. The membrane bound nitrite reductase (hexaheme) present in the same organism as well as the analogous enzyme present in the sulfate reducer D.desulfuricans (27774), induced when the bacteria are grown in nitrate, were isolated and characterized (B-3, 4, 5, 15, 28).

2.2.6 - B_{12} proteins

B_{12}-containing proteins, as well as the B_{12}-cofactor, were

isolated and the cofactor was identified as factor III in three methanogenic species (DSM 800, 804 and MST). Different redox and coordinated states were obtained, including a methylated form naturaly occuring in the MST strain, which is involved in the methyl transfer pathway to methane formation (B-12, 26).

2.2.7 - Other proteins

Flavodoxin and rubredoxin from D.desulfuricans (Berre-eau) were purified and characterized (B-22).

The [Mo-Fe-S] protein was further characterized. In particular, its possible catalytic function was screened and it was shown to have aldehyde oxidase activity (B-6, 25).

2.2.8 - Model systems

Novel metal clusters were produced, using the polypeptide chain of D.gigas ferredoxin, in order to mimic active site of enzymes as well as to test new catalytic possibilities (B-10, 19, 20, 21, 23, 27).

2.3 - PUBLICATION LIST

B-1. EPR STUDIES ON THE MECHANISM OF ACTIVATION AND CATALYTIC CYCLE OF THE NICKEL CONTAINING HYDROGENASE FROM DESULFOVIBRIO GIGAS
M.Teixeira, I.Moura, A.V.Xavier, B.H. Huynh, D.V. DerVartanian, H.D.Peck, Jr., J.LeGall and J.J.G.Moura
J.Biol.Chem., 260, 8942-8950 (1985).

B-2. CHARACTERIZATION OF TWO LOW-SPIN BACTERIAL SIROHEME PROTEINS
A.R.Lino, J.J.G.Moura, A.V.Xavier, G.Fauque, J.LeGall and I.Moura
Rev.Portuguesa de Química, 27, 215 (1985).

B-3. NMR STUDIES OF MONOHEME CYTOCHROME FROM WOLINELLE SUCCINOGENES A NITRATE RESPIRING ORGANISM.
I.Moura, M.C.Liu, G.Pai, W.J.Payne. H.D.Peck,Jr., J.LeGall.

16

A.V.Xavier and J.J.G.Moura
Rev.Portuguesa de Química, 27, 210-211 (1985).

B-4. STRUCTURAL HOMOLOGY OF TETRAHEME CYTOCHROME C_3
I.Moura, A.V.Xavier, J.J.G.Moura, G.Fauque, J.LeGall, G.R.Moore, B.H.Huynh
Rev.Portuguesa de Química, 27, 212-215 (1985).

B-5. MECHANISM AND REGULATION FOR A COUPLED TWO-ELECTRON TRANSFER IN A TETRAHEME CYTOCHROME
A.V.Xavier, H.Santos, J.J.G.Moura, I.Moura, and J.LeGall
Rev.Portuguesa de Química, 27, 149-150 (1985).

B-6. EPR AND MOSSBAUER STUDIES ON DESULFOVIBRIO GIGAS Mo(Fe-S) PROTEIN
B.Barata, I.Moura, A.V.Xavier, J.J.G.Moura, J.Liang, B.H.Huynh, and J.LeGall
Rev.Portuguesa de Química, 27, 174 (1985).

B-7. EPR STUDIES ON ADENYL SULFATE (APS) REDUCTASE - A FLAVIN, IRON-SULFUR CONTAINING PROTEIN
J.Lampreia, I.Moura, A.V.Xavier, J.J.G.Moura, H.D.Peck,Jr. and J.LeGall
Rev.Portuguesa de Química, 27, 189-190 (1985).

B-8. NICKEL-IRON-SULFUR-SELENIUM CONTAINING HYDROGENASES ISOLATED FROM DESULFOVIBRIO BACULATUS STAIN 9974
M.Teixeira, I.Moura, A.V.Xavier, J.J.G.Moura, G.Fauque, B.Pickril and J.LeGall
Rev.Portuguesa de Química, 27, 194-195 (1985).

B-9. A LINK BETWEEN HYDROGEN AND SULFUR METABOLISM METHANOSARCINA BARKERI (DSM 800)
G.Fauque, M.Teixeira, I.Moura, A.R.Lino, P.Lespinat, A.V.Xavier, D.V.DerVartanian, H.D.Peck,Jr., J.Le Gall and J.J.G.Moura
In: A.A.Antonopoulos, ed., "Biotechnological Advances in Processing Municipal Wastes for Fields and Chemicals", Proc. First National Symp. National Lab. (1985) pp. 76-111.

B-10. EVIDENCE FOR THE FORMATION OF A CoFe3S4 CLUSTER IN DESULFOVIBRIO GIGAS FERREDOXIN II
I.Moura, J.J.G.Moura, E.Münck, V.Papaefthymiou and J.Le Gall
J.Am.Chem.Soc., 108, 349-351 (1986).

B-11. DESULFOVIBRIO GIGAS HYDROGENASE; CATALYTIC CYCLE AND ACTIVATION PROCESS
J.J.G.Moura, M.Teixeira, I.Moura, A.V.Xavier and J.LeGall
In: A.V.Xavier, ed.: "Frontiers in Bioinorganic Chemistry", VCH Publishers, RFG (1986) 3-10 (also, Rev.Portuguesa de Química, 27, 63-66 (1985)).

B-12. COBALT CONTAINING B COFACTORS FROM METHANOGENIC BACTERIA

- SPECTROSCOPIC CHARACTERIZATION
A.R.Lino, A.V.Xavier, I.Moura, J.LeGall and L.G.Ljundgahl
Rev.Portuguesa de Química, 27, 175-177 (1985).

B-13. REDOX PROPERTIES AND ACTIVITY STUDIES ON A NICKEL CONTAINING HYDROGENASE ISOLATED FROM A HALOPHILIC SULFATE REDUCER - DESULFOVIBRIO SALEXIGENS
M.Teixeira, I.Moura, G.Fauque, M.Chzechowski, Y.Berlier, P.A.Lespinat, J.LeGall, A.V.Xavier and J.J.G.Moura, Biochimie, 68, 65-84 (1986).

B-14. PURIFICATION AND CHARACTERIZATION OF THREE PROTEINS FROM A HALOPHILIC SULFATE REDUCING BACTERIUM: DESULFOVIBRIO SALEXIGENS
M.Czechowski, G.Fauque, N.Galliano, B.Dimon, I.Moura, J.J.G.Moura, A.V.Xavier, B.A.S.Barata, A.R.Lino and J.LeGall
J. of Indust. Microbi., 1, 1-8 (1986).

B-15. CHARACTERIZATION OF THE CYTOCHROME SYSTEM OF A NITROGEN FIXING STRAIN OF A SULFATE REDUCING BACTERIUM: DESULFOVIBRIO DESULFURICANS BERRE EAU
I.Moura, G.Fauque, J.LeGall, A.V.Xavier and J.J.G.Moura (1986), Eur.J.Biochem, 162, 547-554.

B-16. ENERGY TRANSDUCTION COUPLING MECHANISMS IN MULTIREDOX CLUSTER PROTEINS
A.V.Xavier
J.Inorg.Biochem. 28, 239-243 (1986)

B-17. LOW-SPIN SULFITE REDUCTASES: A NEW HOMOLOGOUS GROUP OF NON-HEME IRON-SIROHEME PROTEINS IN ANAEROBIC BACTERIA
I.Moura, A.R.Lino, J.J.G.Moura, A.V.Xavier, G.Fauque, H.D.Peck Jr. and J.LeGall
Biochem.Biophys.Res.Comm., (1986) 141, 1032-1041.

B-18. * [Ni-Fe] HYDROGENASES FROM SULFATE REDUCING BACTERIA: NICKEL CATALYTIC AND REGULATORY ROLES
J.J.G.Moura, M.Teixeira, I.Moura and J.LeGall
in:"Nickel in Biochemistry", J.R.Lancaster.ed., in press (1987).

B-19. ON THE ACTIVE SITES OF THE [Ni-Fe] HYDROGENASES FROM D.GIGAS: MOSSBAUER AND REDOX TITRATION STUDIES
B.H.Huynh, D.S.Patil, I.Moura, M.Teixeira, J.J.G.Moura, D.V.DerVartanian, M.H.Czechowski, B.C.Pickril, H.D.Peck,Jr., and J.LeGall (1987) J.Biol.Chem., 262, 795-800.

B-20. IRON-SULFUR CLUSTER INTERCONVERSION
J.J.G.Moura
Proceedings of the Symposium "Frontiers of Iron-Sulfur Protein Research", (ed. Matsubara,H., Katsube,Y. and Wada,K.) Osaka (1987), Japan Scientific Soc.Press and Springer Verlag.

B-21. EVIDENCE FOR THE FORMATION OF A $ZnFe_3S_4$ CLUSTER IN

DESULFOVIBRIO GIGAS FERREDOXIN II
K.Surerus, E.Münck, I.Moura, J.J.G.Moura and J.LeGall
(1987) JACS 109, 3805-3807.

B-22. ISOLATION AND CHARACTERIZATION OF A RUBREDOXIN AND A FLAVODOXIN FROM DESULFOVIBRIO DESULFURICANS BERRE-EAU
G.D.Fauque, I.Moura, J.J.G.Moura, A.V.Xavier, N.Galliano, and J.LeGall
FEBS Lett., 215, 65-67 (1987).

B-23. SYNTESIS OF MIXED METAL CLUSTERS FROM A [Fe3S4] CORE
J.J.G.Moura, I.Moura, K.Surerus, V.Papaefthymiou, E.Münck and J.LeGall
Recueill des travaux chimiques des Pays-Bas 106, 225 (1987)

B-24. A COMPARATIVE STUDY OF TWO DISSIMILATORY SULFITE REDUCTASES FROM SULFATE-REDUCING BACTERIA
I.Moura, A.R.Lino, J.J.G.Moura, A.V.Xavier, G.Fauque, D.V.DerVartanian, H.D.Peck, Jr. J.LeGall and B.H.Huynh
Recueill des travaux chimiques des Pays-Bas 106, 284 (1987)

B-25. THE ALDEHYDE OXIDASE ACTIVITY OF DESULFOVIBRIO GIGAS Mo(Fe,S) PROTEIN
B.A.S.Barata, N.Turner, R.C.Bray, A.V.Xavier, J.LeGall and J.J.G.Moura
Recueill des travaux chimiques des Pays-Bas 106, 306 (1987)

B-26. EVIDENCE FOR THE PRESENCE OF A NATIVE METHYLATED B12 PROTEIN IN A THERMOPHILIC METHANOGENIC BACTERIUM
A.R.Lino, J.J.G.Moura, J.LeGall, A.V.Xavier and I.Moura
Recueill des travaux chimiques des Pays-Bas 106, 350-351 (1987)

B-27. SPECTROSCOPIC STUDIES OF COBALT AND NICKEL SUBSTITUTED RUBREDOXIN
I.Moura, M.Teixeira, A.V.Xavier, J.J.G.Moura, P.A.Lespinat, J.LeGall, Y.Berlier, P.Saint-Martin and G.Fauque (1987)
Recueill des travaux chimiques des Pays-Bas 106, 418 (1987)

B-28. CHARACTERIZATION OF ELECTRON TRANSFER PROTEINS FROM THE NITROGEM-FIXING SULFATE-REDUCING BACTERIUM DESULFOVIBRIO DESULFURICANS BERRE-EAU
G.Fauque, I.Moura, A.V.Xavier, N.Galliano, J.J.G.Moura and J.LeGall
Biochem.Soc.Trans. (1987) in press.

B-29. NICKEL-[IRON-SULFUR]-SELENIUM CONTAINING HYDROGENASES FROM DESULFOVIBRIO BACULATUS DSM 1743
M.Teixeira, G.D.Fauque, I.Moura, P.A.Lespinat, Y.Berlier, B.C.Pickril, H.D.Peck,Jr., A.V.Xavier, J.LeGall and J.J.G.Moura, Eur.J.Biochem., (1987) in press.

B-30. * NICKEL CONTAINING HYDROGENASES
J.J.G.Moura, I.Moura, M.Teixeira, A.V.Xavier, G.D.Fauque and J.LeGall
in: "Metal Ions in Biological Systems", Vol. 23, ed. H.Sigel, Marcel Decker, NY and Basel (1987) in Press.

B-31. CHARACTERIZATION OF TWO DISSIMILATORY SULFITE REDUCTASES (DESULFORUBIDIN AND DESULFOVIRIDIN) FROM THE SULFATE-REDUCING BACTERIA. MÖSSBAUER AND EPR STUDIES
I.Moura, J.LeGall, A.P.Lins, H.D.Peck, Jr., G.Fauque, A.V.Xavier, D.V.DerVartanian, J.J.G.Moura and B.H.Huynh
J.Am.Chem.Soc. (1987) submitted to publication.

* Copies of references B-18 and B-30 (revision articles) will be sent when the reprints become available.

3 - LINKS ESTABLISHED WITH U.S. INSTITUTIONS

3.1 - BIOCHEMICAL ENGINEERING

A close collaboration has been established with the University of Arkansas, Fayetteville, with the group of Prof.James Gaddy, Head of Chemical Engineering. Mr. João Paulo Crespo paid a four month visit in 1985 following the program established for Prof.Manuel Carrondo, in his visit in 1984. This led to work on the pure culture side of the project and the results have been discussed, namely in May 1987 with Prof.Clausen. Since this group now only maintains a small activity in the field (biomass and xylose research funds have dropped as indicated under 1.2), we keep exchanging results and experience on a less formal basis and intend to keep on doing so.

3.2 - BIOCHEMISTRY

As was originally forseen, the project gave us the opportunity to strenghten our previous links with the University

of Georgia at Athens (Profs. J.LeGall, H.D.Peck, Jr. and W.J.Payne). This collaboration was essential in order to obtain the biomass necessary to purify the proteins which we have been studying. More importantly, the regular visits to Portugal of Prof. J.LeGall as well as of portuguese researchers to Athens, Georgia, gave us the possibility to fully discuss the results as they were being acquired.

The Mössbauer Spectroscopy Studies [Mo-Fe-S] protein and sulfite reductase of hydrogenase was carried in Dr.B.H.Huynh's laboratory at Emory University and that of novel metal clusters in D.gigas ferredoxin was carried out in Prof.E.Münck's laboratory at the University of Minnesota.

4 - SUGGESTIONS FOR FUTURE WORK

The work undertaken under this project opened a number of lines which we intend to pursure:

i) Molasses slops

The sulphate reducing/acid production activities are to be studied in order to assess sinergism/antagonism of sulphide and pH inhibition of the sulphate reducing bacteria; at the same time, the reactors will be operated under lower pH and HRT to push the concept to its limits and then to allow optimization.

ii) Corn stover

Given the delays indicated above (see 1.3.2.1 ii) this part of the work did not fulfil our expectations. We do intend to keep working allong the lines of the proposal, namely by reducing the

21

retention times in the expanded bed reactor.

Furthermore, a material balance for carbon within the reactor is the goal for the next twelve months of work: concomitantly the Bradford protein test will, hopefully, help in distinguishing the study of kinetics of biomass hydrolysis on a sounder basis.

(ii) Pure culture work

Using fed batch techniques, we expect to develop the mathematical model for the consumption of xylose as dependent from glucose concentration and specific growth rate. This will, hopefully, allow an increase in yield for both the production of propionic acid and vitamin B12.

In the cell recycle reactor using ultrafiltration membrane, attemps will be made on "no growth" or "low-growth" strategies, by using biomass purge. The objective is to shift a larger proportion of the substrate to propionic acid production, as well as to increase the propionic acid/acetic acid molar ratio.

In the columnar reactor, attempts will be made to partly control pH, so as to be able to use the whole column volume at larger substrate concentrations and throughputs.

Seventh International Conference on GLOBAL IMPACTS OF APPLIED MICROBIOLOGY

PARTNERSHIP FOR PROGRESS

BOOK OF ABSTRACTS

12—16 August 1985
Helsinki Finland

GROUP D
Poster 86 OPTIMIZATION OF BIOCONVERSION OF AGROINDUSTRIAL RESIDUES

CARRONDO, M.J.T.; CRESPO, J.P.S.G; REIS, M.A.M.

BIOCHEMISTRY SECTION, UNIVERSIDADE NOVA DE LISBOA, 2825 MONTE DA CAPARICA, PORTUGAL

Strategies are presented for operation of a bioconversion process based on mi biology, biochemical and engineering studies in an interdisciplinary program, cently funded by the Programme in Science and Tecnhology Cooperation, U.S.A.i.: The main objective of this project is to optimize the biogasification process solid and liquid residues (agroindustrial, crop and foresty) by using two st anaerobic fixed film reactors. In the first stage (acid reactor) attention is cused on the optimization of acid phase for maximum production of volatile fa acids either for chemicals production or to yield the optimum substrate for methanogenic reactor. On the methanogenic reactor the emphasis is placed on a eving maximum methane contend in the gas (e.g. by seeding and fixing or addin immobilized hydrogen producing bacteria) so as to reduce or elliminate the purification step.
For one of the effluents (molasses destillation slops) stategies to eliminate majority of the sulphide produced in the acidogenic phase will be used in orde to reduce its toxic efect on the methanogens. Simultaneously with the laborato experiments a similar pilot scale installation shall be operated with molasse destillation slops as part of a cooperation programme between the industry university.
Concomitantly, immobilised pure cultures of Propionibacterium-propionici cel. will be used to convert pentoses and hexoses from wood hydrolysates to aceti and propionic acid - this will be used as a model fermentation for physical mathematical modelling.

MIXED AND PURE CULTURE IMMOBILIZED CELL REACTORS FOR ACIDOGENIC/METHANOGENIC FERMENTATION OF RESIDUES

M.A.M.REIS, J.P.G. CRESPO, M.J.T.CARRONDO

SECÇÃO AUTÓNOMA DE BIOQUÍMICA
FACULDADE DE CIÊNCIAS E TECNOLOGIA
UNIVERSIDADE NOVA DE LISBOA
2825 MONTE DA CAPARICA - PORTUGAL

1. RESEARCH OBJECTIVES

1.1. MIXED CULTURE SYSTEMS PRODUCING ACIDS/METHANE

A) BALANCE TWO STAGE PHASE SEPARATED (ACIDOGENIC-METHANOGENIC) SYSTEMS BY:

- PRODUCING THE BEST MIXTURE OF ACIDS TO BE FED AS SUBSTRATE TO THE METHANOGENIC REACTOR;
- REACH MAXIMUM STABLE PRODUCTIVITY BY TESTING START UP AND SEEDING PROCESSES, LOADING CAPACITY AND IMMOBILIZED CELL CONCENTRATION;
- OPTIMIZE METHANOGENIC PRODUCTION AND CONCENTRATION IN THE GAS.

B) MAXIMIZE HIGHER ORGANIC ACIDS PRODUCTION FOR POTENTIAL USE AS CHEMICALS.

1.2. PURE CULTURE SYSTEMS

- INCREASE THE SELECTIVITY OF THE ACIDS PRODUCING PROCESS;
- OPTIMIZATION AND MATHEMATICAL MODELLING OF THE PROPIONIC ACID PRODUCING FERMENTATION UNDER IMMOBILIZED CELL CONDITIONS;
- UTILIZATION OF C_5 AND C_6 SUGARS FROM HEMI- AND CELLULOSE HYDROLYSIS.

2. PROCESSES UTILIZED

2.1. MIXED CULTURE

- SOLUBLE RESIDUES - EXPANDED BED REACTOR FOR ACIDOGENESIS FOLLOWED, WHEN METHANE PRODUCTION IS ENVISAGED, BY UPFLOW ANAEROBIC FILTER WITH RASCHIG RINGS;
- HIGH SOLID RESIDUES - UPFLOW SLUDGE BLANKET REACTOR FOR ACIDOGENESIS, SOLIDS IN THE FEED USED AS NUCLEI FOR CELL ATTACHMENT; REST AS ABOVE.

2.2. PURE CULTURE

- TUBULAR PLUG FLOW COLUMN FILLED WITH RASCHIG RINGS COATED WITH AGAR AND GLUTARALDEHYDE.

3. RESIDUES

SOLUBLE - CANE MOLESSES SLOPS (WASTEWATER FROM ETHANOLIC FERMENTATION).

HIGH SOLID CONTENT - WITHOUT PRETREATMENT - CORN STOVER FOR METHANE PRODUCTION.
- WITH MILD ACID HYDROLYSIS - CORN STOVER AND EUCALYPTUS RESIDUES FOR BOTH ACIDS AND METHANE PRODUCTION.

4. ADVANTAGES OF IMMOBILIZED CELL REACTORS

- VERY LOW SUSCEPTIBILITY TO WASHOUT;
- INCREASED REACTOR PRODUCTIVITY;
- HIGHER TOLERANCE TO SHOCK LOADINGS (DUE TO REDUCED SUBSTRATE INHIBITION);
- HIGHER FINAL PRODUCT CONCENTRATION PERMITTED (DUE TO REDUCED PRODUCT INHIBITION);
- LITTLE EXPENDITURE OF SUBSTRATE FOR CELL GROWTH.

5. ADVANTAGES OF PHASE - SEPARATION FOR METHANE PRODUCTION

- PHYSIOLOGICAL: pH OPTIMA IN EACH REACTOR (5 TO 6 IN ACIDOGENIC, 7 TO 8 IN THE METHANOGENIC);
- NUTRITIONAL: METHANOGENES CAN PROFIT FROM HIGHER QUANTITY OF SUBSTRATE BEING PRESENT AS ACETATE;
- INHIBITION: IF TOXICS CAN BE CONFINED TO ACIDOGENIC REACTORS A MORE ROBUST PROCESS IS POSSIBLE AS METHANOGENES ARE MORE SUSCEPTIBLE;
- ENGINEERING: EASIER TO OPTIMIZE, MONITOR AND CONTROL. THUS INCREASED STABILITY; IF RUN IN CSTR MODE, EASE OF DISPOSAL OF FAST GROWING ACID FORMING SLUDGE WITHOUT LOSS OF METHANE PRODUCING BACTERIA; FOR LESS SOLUBLE SUBSTRATES, HYDROLYSIS PRECEDING ACIDOGENESIS IS IMPROVED BY LOWER pH AVAILABLE IN THE ACIDOGENIC REACTOR.

6. PROCESS CONTROL PARAMETERS TESTED

TO OBTAIN THE KINETICAL EQUATIONS AND DEVELOP THE MODELS, THE FOLLOWING PARAMETERS ARE MONITORED:

INFLUENT COMPOSITION: COD, PH, P_ε, ALKALINITY, SUSPENDED SOLIDS, N, P, S, CELLULOSE, HEMICELLULOSE, AND LIGNIN; FOR PURE CULTURE, ALSO SUGAR CONTENT, FURFURAL AND HYDROXIMETHYL-FURFURAL.

REACTOR PARAMETERS: HYDRAULIC RETENTION TIME, RECYCLE RATIOS, SUBSTRATE LOADING, CELL DENSITY.

EFFLUENT COMPOSITION: ORGANIC ACIDS (COMPOSITION AND CONCENTRATION). ALSO THOSE MENTIONED UNDER "INFLUENT COMPOSITION"

CALCULATED: CONVERSIONS, YIELDS, PRODUCTIVITIES.

TEMPERATURE IS KEPT AT 35°C.

7. EXPECTED RESULTS

GENERAL

- BETTER UNDERSTANDING OF ALTERNATIVES FOR RESIDUE BIOCONVERSION;
- UTILIZATION OF C_5 SUGARS FROM HEMICELLULOSES AS SUBSTRATES;
- MODEL BUILDING AND BIOCHEMICAL REACTOR DESIGN EXPERTISE DEVELOPPED.

SPECIFIC

- REDUCTION OF TOXICITY OF H_2S IN MOLASSES SLOPS TREATMENT (LARGELY CONFINED TO ACIDOGENIC REACTOR);
- HIGH PRODUCTIVITY/STABILITY OF THE METHANOGENIC REACTOR;
- SELECTIVE PRODUCTION OF ACIDS OF INDUSTRIAL IMPORTANCE;

IN THE MIXED CULTURE ACIDOGENIC REACTORS, ABSENCE OF LOW LEVELS OF METHANOGENES PERMIT HIGH CONVERSIONS TO MORE VALUABLE ACIDS.

- KEY REFERENCES

- M.J.T.CARRONDO AND M.A.M.REIS, "FIXED FILM ANAEROBIC DIGESTION" IN: ENVIRONMENTAL BIOCHEMISTRY, CRCPRESS, FL. USA (IN PRESS).
- E.C.CLAUSEN AND J.L.GADDY, "ORGANIC ACIDS FROM BIOMASS BY CONTINUOUS FERMENTATION", CHEM.ENG.PROG., DECEMBER 1984.

ACKNOWLEDGEMENTS

THE AUTHORS ACKNOWLEDGE THE CALOUSTE GULBENKIAN FOUNDATION, JNICT AND U.S.A.I.D. FOR FINANCIAL SPONSORSHIP.

liquid residues

MIXED CULTURE LAY OUTS

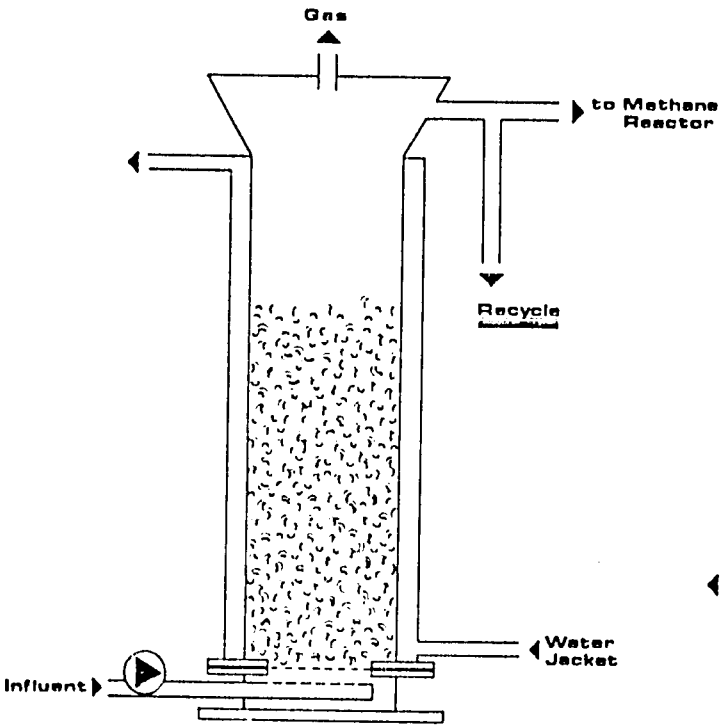

EXPANDED BED REACTOR
(ACIDOGENIC REACTOR)

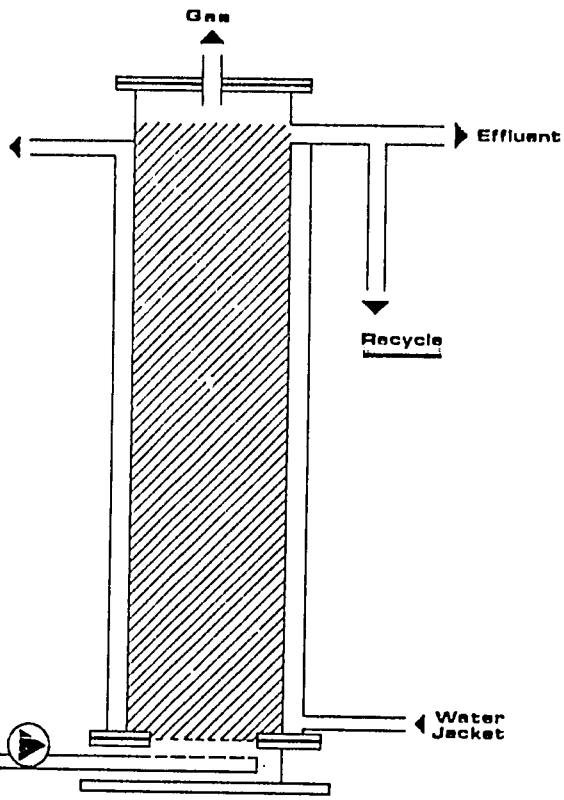

ANAEROBIC FILTER
(METHANOGENIC REACTOR)

solid residues

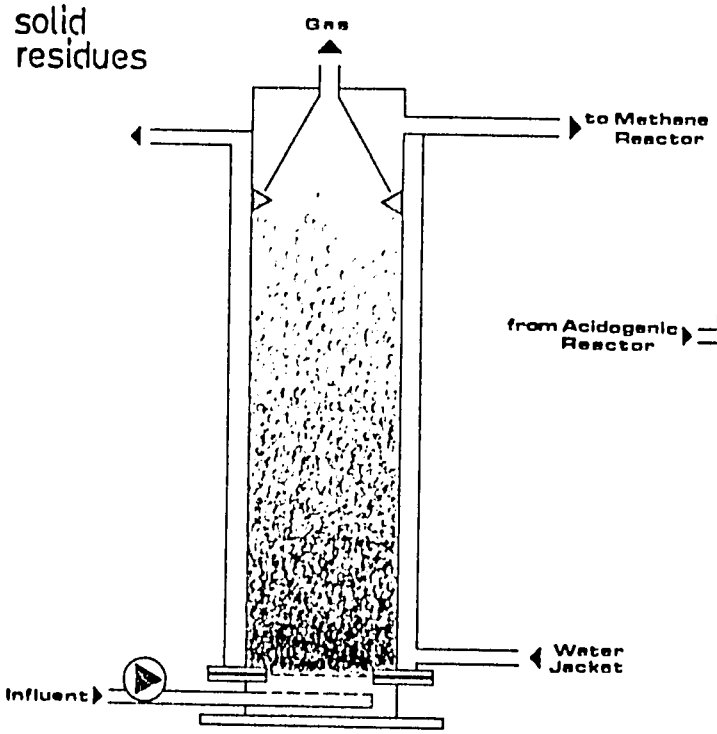

UPFLOW BLUDGE BLANKET REACTOR
(ACIDOGENIC REACTOR)

PROPIONIBACTERIUM FERMENTATION USING C5 SUGARS FOR PRODUCTION OF PROPIONIC ACID AND VITAMIN B 12

J.P.S.G.CRESPO, M.J.MOURA, M.J.T.CARRONDO*

Laboratório de Engenharia Bioquímica, Faculdade de Ciéncias e Tecnologia, Universidade Nova de Lisboa, 2825 MONTE DA CAPARICA, PORTUGAL

SUMMARY

Propionibacterium acidipropionici, a xylose utiliser, has been tested for its kinetic behaviour. Different sugar concentrations and different xylose proportions were used and its inhibitory behaviour, from substrate and product, was assessed. Specific rates of growth and production, yield coefficients for cell mass and propionic acid, ratios of propionic to acetic acid produced and volumetric productivities are reported; the culture broth has also been assessed for vitamin B12 production.

Strong propionic acid inhibition at above 10 g/l, low xylose utilisation at high sugar initial concentrations and absence of diauxic growth for glucose/xylose mixtures are reported. Molar ratios of propionic/acetic acid higher than the theoretical and vitamin B12 concentrations similar to those obtained for other propionibacterium species under cobalt addition are also presented.

INTRODUCTION

Vitamin B12 or cyanocobalamin is an important biological compound active as an hematopoietic factor in mammals and as a growth factor for many microbial and animal species. Although a full chemical synthesis was achieved, with 70 steps required, it is of little value for industrial purposes and all the vitamin B12 group of compounds is obtained by fermentation processes. Over the last years the market volume has been stable at approximately 10000 Kg/year, fetching a price fluctuating between 3 and 6 US dollars per gram. Mainly considering its use as an animal feed supplement, market size could expand, namely if its price could be reduced [1-4].

Propionic acid bacteria, namely Propionibacterium freundenrichii, and specially subsp.Shermanii have been used in the most successful industrial processes for B12. Some of the advantages of these microorganisms include acid formation, decreasing contamination as propionate is in itself a bacteriostatic and fungistatic agent, and little energy requirements as the majority of the fermentation is run under anaerobic conditions for biomass growth; cell growth is product (propionic acid) inhibited but, as with other weak acids this is

predominantly due to the undissociated form[6] and thus pH control is currently used in industrial processes[1-4]. In the majority of processes a second phase under aerobic conditions usually with the addition of a precursor (5,6 dimethylbenzimidazole) is run either in the same or in a separate reactor; in this last case, fedbatch operation is common[1-4].

On top of its current uses as a grain preserver/antifungal agent for foods, plasticizer, herbicide, perfumes,[7,8] propionic acid production via fermentation has been advocated because weight yields are greater than those for ethanol fermentation and because the conversion by hydrogenation and dehydration to propylene gives a one third greater weight yield than conversion of ethanol to ethylene[9]. Although fermentation patents have been taken as early as 1923[1] all the propionic acid is nowadays produced either by liquid phase oxidation of propane or from ethylene via propionaldehyde by the catalytic oxo process[8,11].

Looking ahead to the days when oil will become scarcer much research is now taking place on utilization of mixtures of c5 and c6 sugars as would be obtained from hydrolisis (enzymatic or chemical) of cellulose containing residues or raw materials (e.g. straw, wood, corn stover, potato pulp liquors)[12,13]. Propionibacterium acidipropionici (also know as P.pentasoceum or P.arabinosum[14] is a xylose utilising microorganism already assessed by Gaddy's group,[7,15,16] as a potential producer of propionic acid under immobilized conditions, xylose being utilised with glucose; Goma's group has used lactose for the same purpose. At least one of the early patents for the production of vitamin B12 reviewed by Noyes[3] uses P.acidipropionici.

Whenever propionic acid production is the objective, processes that minimize product inhibition, namely plug flow immobilized reactors are more suitable or cell recycled reactors with external acid removal; for either situation, conducting the bioreactor at lower pH would help acid extraction[18-19] even if, as is normal with weak acids, inhibition is mainly due to the undissociated acid form[20]. With vitamin B12 production as the objective, biomass production strategies are required, namely fed-batch processes, optimally at exponential rate of feed,[21] cell recycle[22], through extraction/membrane systems for detoxification[23].

We present preliminary results on the kinetics of P.acidipropionici growth, propionic acid production and vitamin B12 in the fermentation broth.

MATERIALS AND METHODS

Batch Tests

Propionibacterium acidi-propionici was obtained from the American Type culture collection (ATCC 25562) in a freeze dried form. The organism was grown in a standard nutrient containing peptone and yeast extract with phosphate buffer. Seed cultures grown for 24 to 48 hours were used for innoculation. Initial pH in all reactors was 7 ± 0.2; tests were carried out at $37^{o}C$ in

agitated 100 ml glass flasks (useful volume of 70 ml) kept under mild agitation, each test performed under duplication.

Samples, taken periodically during fermentation, were analysed for pH, optical density and, after centrifugation at 10000 r.p.m. for 10 minutes, for sugars and organic acids.

Analytical methods

Cell concentration was determined using optical density measured at 540 nm (Bausch & Lomb Spectronic 21) and comparison with a calibration curve obtained with cell densities determined after filtration through Millipore (GVW 1 04700) filter and dry weighing at 105°C.

The dinitrosalicyclic acid (DNS) method for reducing sugar analysis [24] was used troughout for measurement of total sugars. Glucose was determined enzymatically using either Yellow Springs YSI model 27 or Sigma test N°. 510 both based on the utilisation of glucose oxidase; xylose was obtained as the difference.

Organic acids propionic and acetic were determined by gas chromatography using an United Technologies Packard 439 instrument with flame ionization detector. A glass column 1.8m long and 0.2 cm internal diameter, packed with 10% SP 1200 1% H3P04 on chromosorb WAW 80/100 mesh; helium was used as carrier gas (at 40 ml/min), oven temperature of 130°C injector of 170°C and detector of 175°C were used throughout.

For these preliminary tests, vitamin B12 production was measured from 48 hour cultures only, averaging 5 to 6 g dry cell/l. The broth was centrifuged at 15 000 rpm for 10 min., resuspension with phosphate buffer - centrifugation being repeated twice. The concentrated cells were then disrupted in an Eaton press, resuspended in phosphate buffer and 1,1% sodium cyanide solution and autoclaved at 120°C for 15 min; the absorbance of the supernatant at 580 nm is then measured in a Spectronic 21 using a blank containing hydrochloric acid instead of sodium cyanide [25-28].

RESULTS AND DISCUSSION

A set of batch reactor studies were performed in order to obtain a kinetic description of the fermentation. These included tests conducted under different sugar compositions, under different initial glucose concentration to ckeck substrate inhibition and to confirm inhibitiory product mechanisms, with acids added to the broth.

The data obtained from the tests conducted under external acid addition to the broth at a concentration range of 0 to 20 g/l acetic or propionic acid can be described by hyperbolic models of the type:

$$\frac{\mu_m^i}{\mu_m^o} = \frac{k_p}{k_p + P_a^m} \qquad \text{(eq. 1)}$$

where μ_m^o and μ_m^i are the maximum specific growth rates without and with product addition to the fermentation media, Kp is a parameter related to the resistance to the added product and n, the exponent of the added product concentration Pa, represents the degree of tolerance of the strain to each added product. Data fitting yielded the following results:

- acetic acid

$$\frac{\mu_m^i}{\mu_m^o} = \frac{2943.8}{2943.8 + Pa^{2,179}} \qquad r=0.92 \quad (eq.2)$$

- propionic acid

$$\frac{\mu_m^i}{\mu_m^o} = \frac{76.1}{76.1 + Pa^{1.209}} \qquad r=0.984 \quad (eq.3)$$

As can be seen from a much lower Kp, the inhibitory effect is much stronger with propionic acid, being irrelevant foracetic acid at potential process concentrations (see Fig.5).

To determine the effect of initial glucose concentration, a set of batch tests at 2% 3%, 5%, 8.5% and 12% initial glucose concentrations were conducted. Similar substrate consumption curves and substrate utilisations were obtained irrespective of initial glucose concentration for the range tested.

The inhibitory effect due to propionic acid product during fermentation is apparent in Figure 1 where the specific growth rate μ and the specific production rate ν are plotted against the propionic acid produced P. As can be seen, specific growth rate tappers off at rather lower concentration than specific production rate i.e., production takes place at higher concentrations than those sufficient to stop growth. The relationship between μ and P can be described linearly up to 4g/l of propionic acid and exponentially thereafter.

$$P < 4 \text{ g/l} \qquad \mu = 0.211 - 0.0355\ P \quad (eq.\ 4)$$

$$P > 4 \text{ g/l} \qquad \mu = 1.2804 \exp(-0.726\ P) \quad (eq.\ 5)$$

On the other hand, ν and P can be described exponentially throughout the whole range

$$\nu = 0.366 \exp(-0.328\ P) \quad (eq.6)$$

Comparing the inhibitory effect of added versus produced propionic acid one can conclud for a stronger inhibition in the case of produced acid, also apparent in the case of ethanol [27].

The yield coefficients of propionic acids $Y_{P/S}$ and cell mass $Y_{X/S}$ for all fermentations performed were obtained from Fig. 2 and 3. The propionic yield coefficient is constant throughout the whole range with a value of 0.452 g product/g substrate whereas, as expected, cell yield coefficient changed dramatically when reaching the stationary phase; cell mass yield

was 0.263.

The propionic acid yield coefficient corresponds to 82.4% of the theoretical maximum obtained from the stoicheometry

$$1.5\ C_6H_{12}O_6 \text{ ------ } 2CH_3CH_2COOH + CH_3COOH + CO_2 + H_2O$$

whereas the total acids produced correspond to 80.1% of the theoretical maximum but at a propionic/acetic molar ratio varying between 2.5 and 3.2 as compared to the stoicheometic, theoretical value of 2. Although this ratio is said to be very variable (7, 28) in our tests even those conducted at controlled pH (not reported here) it always stood within 2.5 and 3.2.

To assess xylose utilisation at high sugar concentrations we performed a set of batch studies using glucose/xylose ratios of 3:1, 1:1 and 1:3 for a total sugar concentration of 50 g/l; the organic acids produced are plotted versus fermentation time in Fig.4. Fermentation curves for experiments carried out at 25% and 50% of xylose are similar and do not differ from product curves obtained from fermentations using glucose as the only substrate. However, if glucose becomes limitant as happens at 75% xylose concentrations, organic acid production is dramatically affected under those batch tests. Under continuous (CSTR and immobilized cell reactors) studies xylose utilisations reaching 12 g/l at 100 h retention time were reported [7], as compared to our values increasing from 1.4 to 2.5 g/l under batch tests of increasing xylose concentration.

The corresponding volumetric productivity curves are represented in Fig.5. Cell mass productivity is almost unchanged within the range 0.13-0.14 g cell/l/h but propionic acid volumetric productivity is affected by xylose concentration, presenting a maximum value of 0.19 g/l/h at 25% xylose and a minimum of 0.13 g/l.h at 75% xylose. A time shift is also apparent with cell mass productivity peaking at 41 h fermentation time and acid productivity peaking at 50 h, in correspondance to the different effect of propionic acid concentrations regarding μ and ν described above (see Fig. 1).

Preliminary results for vitamin B12 content were performed, using the same media and conditions as for organic acids production. The results obtained range from 0.32 to 0.39 mg/l and thus compare well with early 1960's results [3] yielding 0.3 to 0.4 mg/l when P.arabinosus and P.pentosaceun were used with cobalt addition not used here; for P.shermanii with cobalt addition but no agration nor DBI addition reported values range from 0.45 to 0.88 [2,25].

CONCLUSIONS

From the kinetic studies reported here a few conclusions are worth mentioning:

1 - For the concentrations to be expected in a continuous process, no inhibition is apparent for glucose as substrate or

acetic acid produced; propionic acid is a strong inhibitor and thus maximum concentrations obtained in the batch tests peak at 12 g/l;

2 - At high total sugar initial concentrations of 50 g/l (one normal batch tests uses slightly less than 25 g/l) xylose utilisation in batch conditions is low (maximum of 2.5 g/l at 75% xylose) and no diauxic growth seems to take place; glucose limitation at 75% xylose dramatically reduced acid production. It is worth remembering that hydrolis of agricultural and foresty residues will yield concentrations of C_5 sugars ranging from 15 to 35% of the total sugars;

3 - Acids were produced at a ratio close to 3:1 propionic/acetic (molar basis) as compared to 2:1 theoretical ratio; since propionic has a higher cost, this shift should be increased; acid yields are close to the theoretical maximum (80 to 82%);

4 - Cell mass yield coefficients are high at 0.263 g cell/ g substr. for this facultative anaerobe; this might be an adavantage for vitamin B12 production but lowered the product yield to 0.452 g product/g substrate. Thus acid production strategies should aim at low cell growth, namely by using cell immobilisation or high cell concentration reactors, concomitant with product removal for inhibition control.

5 - Even though no cobalt was added, vitamin B12 contents in the broth at 0.35 mg/l compare well with those reported in the literature under anaerobic conditions with cobalt addition (0.3 to 0.9 mg/l) for Propionibacterium species.

ACKNOWLEDGEMENTS

J.P.Crespo carried out some of the glucose tests at Prof.James Gaddy's laboratory at the University of Arkansas, Fayetteville; we hereby express our recognition for this on-going collaboration.

We acknowledge the finantial support of Junta Nacional de Investigação Cientifica e Tecnológica, Lisboa under contract n$^{o.}$ 720.85.74, U.S. Programme in Science and Technology Cooperation, Washington, D.C., U.S.A., Grant n$^{o.}$ 936-5542-G-SS-4003-00, as well as the sponsorship of IPE - Investimentos e Participações do Estado, SARL and Portucel, E.P.

BIBLIOGRAPHY

1. FLORENT, L.J. and L.NINET - Vitamin B12 in H.Peppler and D.Perlman (Eds) Microbial Technology, vol 1, 497-519, N.Y., 1979.

2. FRIEDMAN, H.C. and C.M.CAGEN - Microbial Biosynthesis of B12 like compounds in Ann.Rev.Microbial., 24, 159-208, 1970.

3. NOYES, R. - Vitamin B12 manufacture, Chem.Proc.Review, n°. 40, Noyes Devel.Corp., Park Ridge, N.Y., 1969.

4. SPEEDIE, J.D. and HULL, G.W., U.S.Patent 2,951,017/1960.

5. NANBA, A. et al, J.Ferment.Technol., 61,(1983) 551-556.

6. SALMOMD, C.V. et al., J.Gen.Microbiol., 130, (1984) 2845-2850.

7. CLAUSEN, E.C., et al., Chem.Engrg.Progr., 80, (1984) n°.12, 59-63,

8. PLAYNE, M.J. - Comprehensive Biotechnology, M.M.Young (Ed.) vol.3 Sect.3, Pergamon Press, London, 1985.

9. HUMPHREY, A.E. - Chem.Engrg Progr., 73, (1977) n°.5, 85-91.

10. SHERMAN, J.M. and R.H.SHAW - U.S.Patent 1,459,959/1923.

11. STANDER, A. (Ed.) Kirk-Othmer Encyclopaedia of Chemical Technology, vol.3, 2nd Ed., Wiley, N.Y., 868-883, 1964.

12. SERI, Fermentation Chemicals and Biomass, II SERI/TR -754, 1981.

13. REXEN, F. and MUNCK, Cereal Crops for industrial use in Europe, Comm.Europ.Comm.Rep. N.EUR 9617 EN, Brussels, 1984.

14. HOLDEMAN, L. and W.E.C.MOORE - Anaerobe Laboratory Manual, 3rd Ed. VPI Anaerobe Laboratory, Blacksburg, USA, 1975.

15. SHAH, R.B. et al. -Chem.Engrg.Progr., 80, (1984) n°. 1, 76-80.

16. CLAUSEN, E.C. et al. -Biotechnol.Bioenerg.Symp., 12, (1982) 67-72,

17. GOMA, G. - personal communication, 1985.

18. HELSEL, R.W. - Chem.Engrg.Progr., 73,(1977) n°.5, 55-59.

19. BUSCHE, R.M. -Biotechnol.Bioenerg.Symp., 13,(1983) 597-615.

20. SALMOND, C.V. et al. - J.Gen.Microbiol., 130, (1984) 2845--2850,

21. YAMANE, T. and S.SHIMIZU -Adv.Biochem.Eng.Biotechnol., 30,

(1984) 148-194.

22. GOTO, S. et al. -J.Ferment.Technol., 57, (1979) 47-52.

23. GABLER, F.R. -Comprehensive Biotechnology, M.M.Young (Ed.), Pergamon Press, London, 1985, vol.2, 351-366.

24. NOELTING, F. and A.BERNFELD - Helv.Chim.Acta, 31, (1948) 286-291,

25. IRION, E. and L.LJUNGDAHL, Biochem., 4, (1965), 2780-2790.

26. BERNAHAUER, K. et al. Arch.Biochem.Biphys., 83, (1959) 248--256,

27. MOTA, M. - Thesis, docteur engenieur, INSA, Toulose, France, 1985.

28. ALLEN, S.M.G. et al, J.Bacteriol, 87 (1964), 171-176.

29. MERVYN, L. and E.L.SMITH, The Biochemistry of Vitamin B12 Fermentation in Progr.Ind.Microbiol., D.J.D.Hockenhull (Ed.), vol.5, Heywood, London, 1964, 151-201.

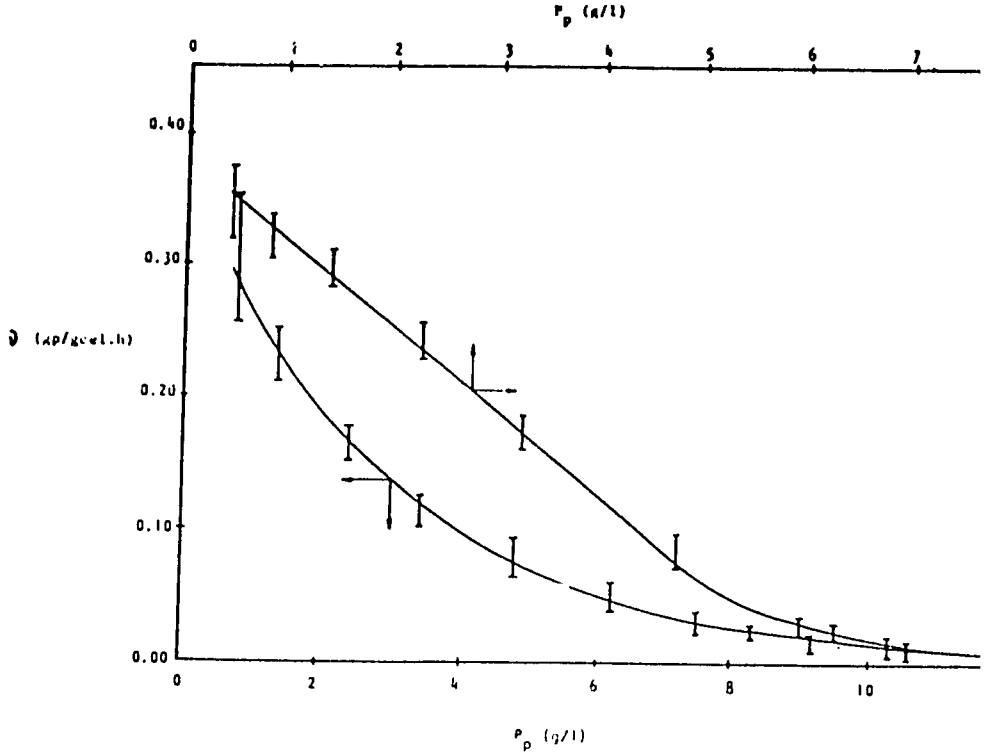

Fig. 1 - Specific rates of growth and propionic acid production.

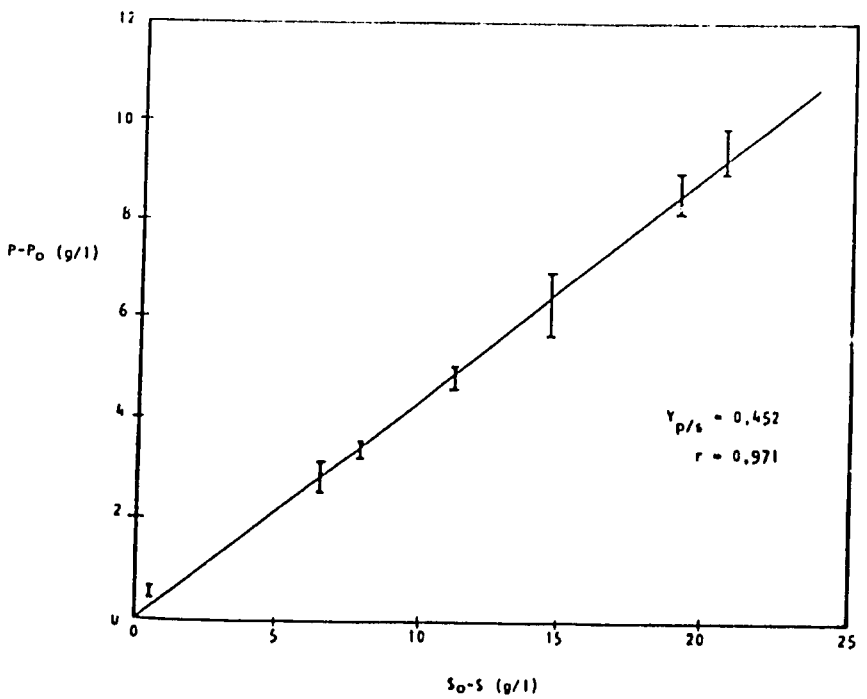

Fig. 2 - Yield coefficient for propionic acid.

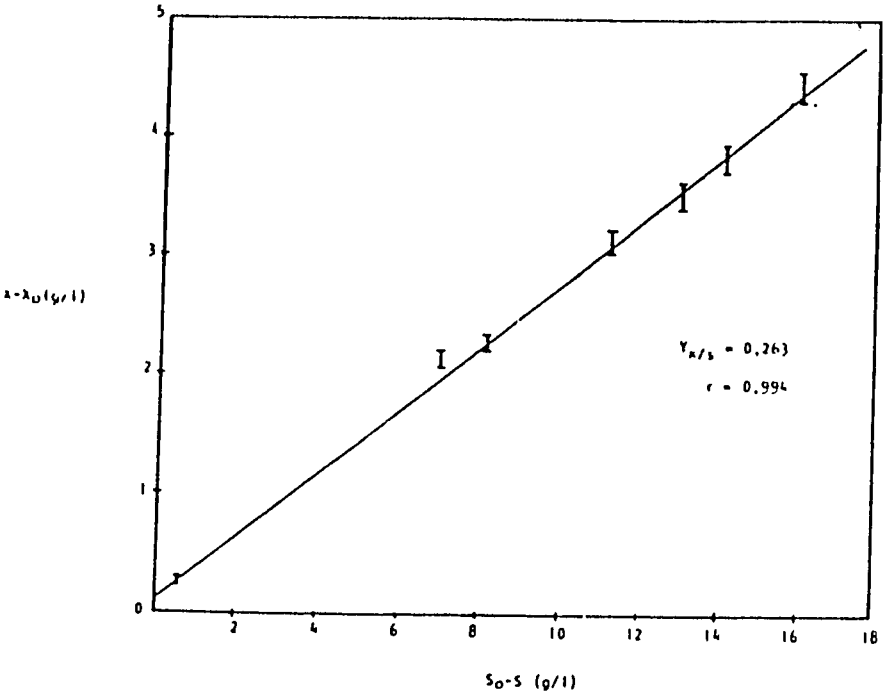

Fig.3 - Yield coefficient for cell mass

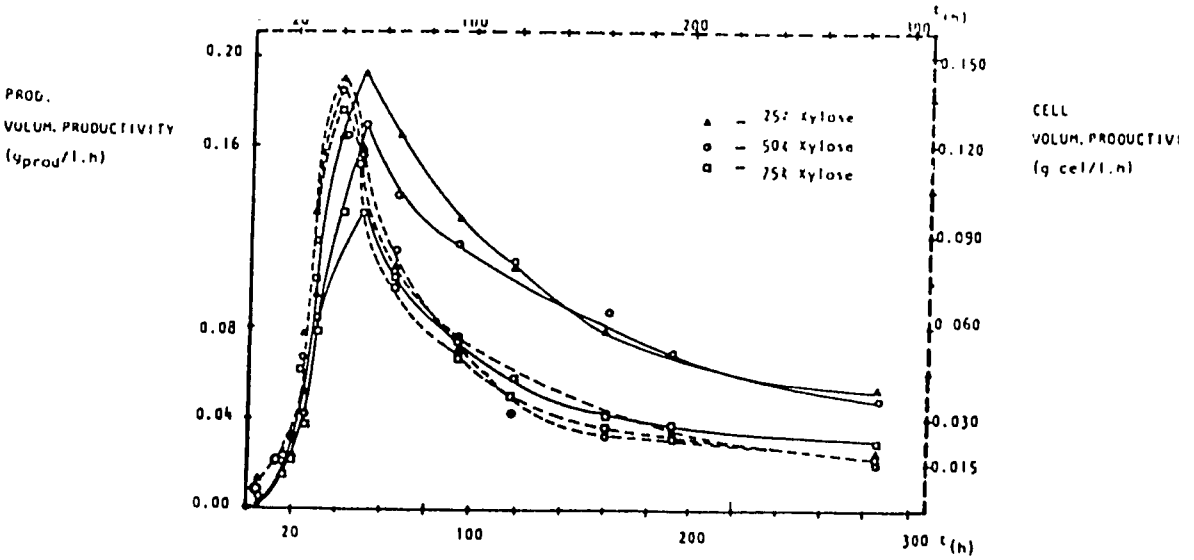

Fig. 5 - Volumetric productivities for cell mass and propionic acid

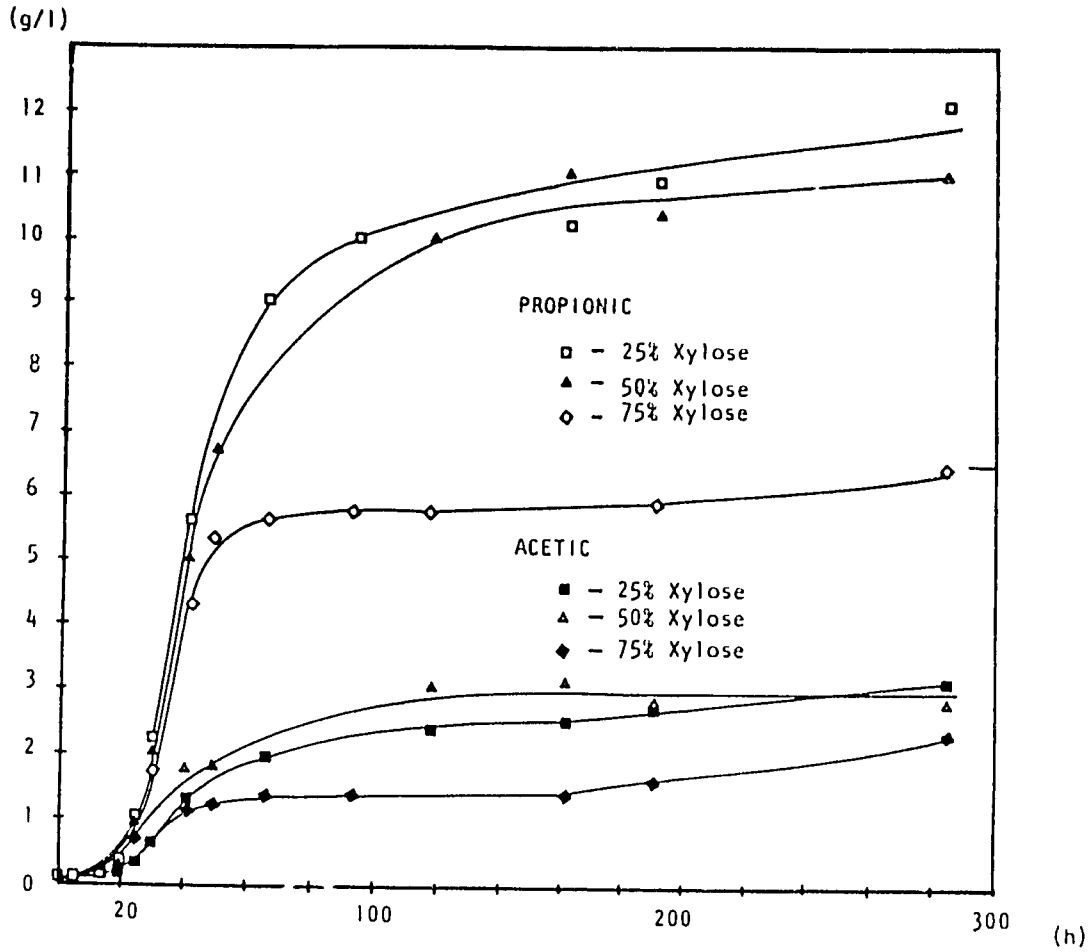

Fig. 4 - ropionic and acetic acids production by fermentation

41

Biogas Technology, Transfer and Diffusion

Edited by
M.M.EL-HALWAGI

ELSEVIER APPLIED SCIENCE PUBLISHERS

Table 4 Barriers to Widespread Application of Farm Digesters

Barrier	Probable Solution
Materials handling problems feeding, effluent withdrawal	Need efficient feed system design
Inert plug digesters	Develop effective separation techniques
Net biogas production does not match variation of farm energy use	Need low-cost waste-storage fermentation system, and gas storage
Biogas-to-electric power conversion is inefficient, uneconomical, maintenance-intensive, marginally attractive.	Need more efficient and low cost gas-to-power system
Use of biogas as truck or tractor fuel not feasible	Develop centralized system so that such uses are feasible
Other uses of biogas not developed	Investigate methanol or ammonia production or other uses
Effluent processing and disposal are problematic	Develop low-cost dewatering processes. Develop alternate uses of residue for aquaculture and algal growth. Need governmental subsidy/tax subsidy as credits for intangible benefits.
Process needs maintenance and expert service, quality control	Develop low-maintenance fool-proof system designs. Organize service groups.
Economy of scale unfavorable for family digesters	Organize community plants.
Gas production low at high loading rates	Need improved high-efficiency high-solids digestion systems. Need cost-effective chemical pretreatment techniques.
Low social and cultural acceptance	Reduce failures, increase reliability, provide assurance of service and safety.

OPTIMIZATION OF BIOCONVERSION OF SOLID AND LIQUID RESIDUES

M.J.T. Carrondo, I. Coutinho, J. Lampreia, J. LeGall, A.R. Lino, I. Moura, J.J.G. Moura, M.A.M. Reis, M. Teixeira and A.V. Xavier

Centro de Quimica Estrutural INIC, Universidade Nova de Lisboa, FCT, 2825 Monte da Caparica, Portugal

and

Dept. of Biochemistry, University of Georgia, Athens, Georgia 30602, USA

ABSTRACT

This paper presents strategies to scale up, start up, and operate a bioconversion process based on microbiological, biochemical, and engineering studies in an interdisciplinary program recently funded by the Program in Science and Technology Cooperation, United States Agency for International Development.

Two main objectives in this project are:

i) Optimization of the biogasification process of solid and liquid residues (agroindustrial, crop, and forestry) by using phased two-stage anaerobic fixed film reactors.

Two presumably different strategies will be adopted for the acid phase reactor:

- Operation of the acid phase reactor to yield maximum production of volatile fatty acids for chemicals production;
- Operation of the acid phase reactor to yield the best mixture of substrates for the methanogenic reactor.

In the case of molasses distillation slops, it is further expected that the acidogenic reactor will eliminate most of the sulphide produced before it can become "toxic" to the methanogens.

In the case of the methanogenic reactor, emphasis will be placed on achieving maximum methane content of the gas (e.g., by seeding and fixing or adding immobilized hydrogen-producing bacteria) to reduce or eliminate the gas purification stage.

ii) The microbiological biochemical effort will entail screening and

characterization of electron transfer proteins and enzymes relevant for the metabolic pathways involved (e.g., hydrogen and methane production). Also, quantification of cofactors relevant to the operation of the digesters will be examined.

INTRODUCTION

Although anaerobic digestion presents many advantages for residue biogasification, the "black box" approach used until recently gave rise to many operational difficulties, namely during the start up and occasionally when complete failure occurred.

Recent basic knowledge of the kinetics, microbiology, and biochemistry, the use of fixed film reactors and phase-separated operations should allow an increased expectation in overcoming large scale operational difficulties, with a higher stability of biogas production as well as elimination of later gas purification stages.

The screening and characterization of the electron transport proteins, as well as the enzymes involved in the metabolic production of methane and hydrogen, and the quantification of cofactors, could conceivably allow for the development of novel start up and operational techniques.

This paper is a brief presentation of the background knowledge which allowed our group to develop a multidisciplinary research strategy, recently funded by USAID.

TECHNOLOGICAL ASPECTS

In traditional digestion systems, one single reactor, generally with suspended growth by stirring, carries out the whole anaerobic treatment. Sometimes, e.g., in domestic wastewater treatment, a secondary digester exists, whose role is mainly that of a solid-liquid separator.

More recently, three process layouts or their combinations have been considered (Figure 1).

1. Parallel operation - after an initial soluble-suspended phase separation, both lines of treatment carry out the acid and methanogenic steps;

2. Series (stages) operation - two or more anaerobic reactors exist in series, each one with acid and methanogenic steps;

3. Phased operation - acid and methanogenic phases are separated in different reactors.

An important factor in deciding which lay-out to choose can be described by the solubility index[1] of the effluent stream. Residues with average solubility indexes (0.2-0.8) might benefit from the parallel operation, separating the soluble from the suspended fraction, whereas low (0-0.2, almost entirely suspended matter) or high (0.8-1, almost entirely soluble matter) solubility indexes should be processed in only one process line, with either one reactor or series or phased operation.

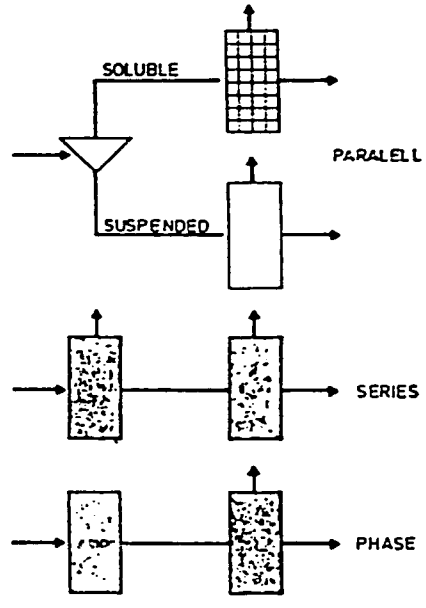

Figure 1 Anaerobic Processes

Advantages of Phased Separation

Phased separation for anaerobic digestion has both theoretical and practical advantages.

From the kinetic viewpoint, since the growth rate of the acidogenic microorganisms is much higher than the methanogens, different wash out velocities will take place and more economical

dimensioning of the reactors is possible. Nutritionally, the methanogens can only operate if metabolites from the acidogenic microorganisms are already available. Physiologically, their behavior is also rather diverse. In particular, the importance of controlling pH within 6.6–7.4 in a single reactor is in effect an optimization between the low pH optima (5–6) of the acidogenic organisms[2] and the high pH optima (7–8) of the methanogens[1]. Those reasons substantiate the conceptual proposal of Pohland and Ghosh[3] of operating the first reactor until acids (acetate) are produced and the second reactor for methane production.

Further theoretical advantages of two phase operation are: i) larger toxic resistance, if the toxins can be confined in the first reactor [sulphate, pulp, and paper xenobiotics [1,4]]; ii) the lower pH available in the acidogenic reactor also improves the hydrolysis step which precedes acidogenesis[5,6].

The engineering advantages of two-phase separation include: optimization of the overall process, increasing stability with easier process monitoring and control, and ease of disposal of fast growing acid forming sludge without loss of methane producing bacteria[3,7,8]. Operationally, phase separation is normally maintained by kinetic control (short residence time) chemical control (low pH values or addition of methanogenic inhibitors) or a combination of both[5,7-10]. Optimization of such a process may concentrate on acid formation or hydrolysis in the acid reactor, depending on the substrate or on the slow-growing methanogenic system and the contact time of the effluents from the first phase[5,7].

Economically, the extraction of chemicals from the acidogenic reactor may be feasible if more expensive residues are used which require chemical or enzymatic pretreatment. The products which can be obtained range from organic acids, to their salts or esters[9,11-13]. These processes will be strongly dependent upon the separation operations needed, e.g., liquid-liquid extraction, adsorption-esterification, or membranes[9,12,14].

Fixed Film and Suspended Growth Reactors

Conceptually one might consider five types of fixed film reactors and three types of suspended growth reactors [of which some might become fixed film if the floc shows a tendency to granulate throughout its operation[1,15]].

The types of anaerobic fixed film reactors are (Figure 2):

I - Fixed bed - uses various filling materials and can be operated up- or down-flow[15]; usually operated without recirculation as a large plug flow system even though gas bubbling mixes it to some extent; recirculation might be needed if there is a need to control biofilm thickness, toxicity or if the pH at the inlet is too low;

II - Expanded bed - introduced by Jewell and Switzenbaum[16] These utilize slightly larger solid supports than fluidized beds, expanded by the upflow rate obtained with recirculation. The particles keep their position within the bed and the thickness of biofilm is controlled by physical contact.

III - Fluidized bed [17] - operated at higher upflow rates with faster recirculation rates; the particles are kept within a reasonably small "parking" space. Biofilm thickness is controlled by the bed regeneration strategy and size and density of the inert materials in relation to the upflow rate.

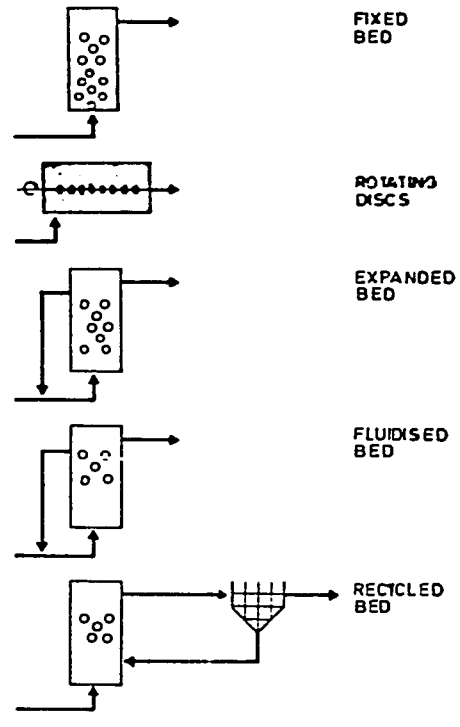

Figure 2 Fixed Film Anaerobic Reactors

IV Anaerobic rotating discs [18] - biofilm is formed on discs slowly rotating in liquid; the angular velocity controls biofilm thickness.

V Recycled bed - inert materials are kept in suspension by mechanical agitation or gas bubbling[19], a large part of the biomass exists as flocs; a phase separator allows recycling of the bed to the reactor.

Anaerobic suspended growth reactors can be classified as follows (Figure 3):

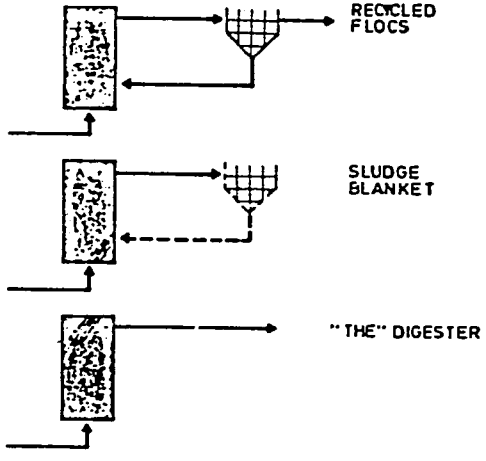

Figure 3 Suspended Growth Anaerobic Reactors

A - Contact or recycled floc[20] - conceptually similar to the recycled bed mentioned above, without explicit addition of inert solids apart from those existing in the residue or due to floc "granulation".

B - Fluidized floc or sludge blanket[21] - conceptually similar to the contact reactor except upflow and gas bubbling are responsible for fluidization; a solid profile exists along the reactor.

C - "The Digestor" - the classical reactor used for wastewater sludges high in suspended solids, operating under similar hydraulic and solids retention time thus requiring long hydraulic retention times and consequently large reactor volumes.

When compared with suspended growth reactors, the fixed film types are less susceptible to washout, can be operated at much shorter hydraulic detention time, are more likely to cope with shock loadings and sustain active microbial cultures even after long periods of starvation; given their long mean cell residence time, they have higher conversion efficiencies and reduced nutrient requirements[1,15]. Furthermore, their plug flow operation (unless high recirculation rates are used) produces some phase separation, perhaps increasing the stability and possibly also increasing the methane production rate and final methane concentration in the gas [1,22].

Choice of Process and Reactor Type

Where no phase separation is envisaged, the solubility index criteria allows us to decide for or against parallel operation[1]. Fixed film reactors should be considered the optimum choice for effluents with a high solubility index; the choice between fixed film and other systems will depend on size, energy efficiency required, and acceptable level of complexity.

If phase separation is chosen, (as in our project) the different limiting steps and engineering behavior of the reactors determine that[1-11, 15-25]:

a. For soluble, easily fermentable substrates from the agro-industries, the acid stage can probably be operated at very high loading rates as hydrolysis should not be rate- limiting; much of the engineering optimization strategies can thus focus on the quality of intermediary metabolites, either as methanogenic substrates or as chemicals. Thus, for the acidogenic phase, either expanded or fluidized beds seem appropriate, given their high loading rate capabilities and smaller requirement of sludge settling properties; we propose to utilize an expanded bed reactor as it is easier to operate, uses less energy and lower effluent recycle rates, thus being closer to plug flow than the fluidized bed.

b. For particulate feeds, such as those arising from crop or forestry residues less information is available. It looks as if long solids retention times, as well as high solids concentrations, and as low pH as reactionally feasible will be helpful for enzymatic action and further increase hydrolysis. Almost certainly much of the engineering strategies will focus on increasing the rate of hydrolysis for which culture seeding and breeding or cell immobilization of interesting bacteria might have to be contemplated. The most probably correct choice of reactor lies with the recycled bed type of the upflow solids blanket to which the former ultimately reduces, given the internal settling stage and the fact that part of the solids will operate as inert-floc support. We intend to use the sludge blanket reactor as it reduces the amount of equipment required and does not add a settling stage which also has to be kept anaerobic. The acid production rate and concentration distribution will, to a certain extent, have to yield to the first strategical priority of guaranteeing extended hydrolysis.

c. The methanogenic reactor will have similar constraints for both the soluble and particulate original feeds high biological solids

retention times, average hydraulic retention times (larger than is usual for the acidogenic reactor for soluble substrates), feed almost completely made up of solubilized substrate. The most appropriate reactor type for the job is generally recognized to be the upflow fixed bed or anaerobic filter, although the expanded bed might still be a good choice, but will probably yield lower methane concentrations in the gas; we therefore selected the former.

MICROORGANISMS

At the moment, we are characterizing the following microorganisms: Desulfovibrio gigas (NCIB 9932); Desulfovibrio vulgaris (Hildenborough) - this last one being a very interesting bacterium, because its hydrogenase is extremely active (specific activity of about 3000 micro liter H_2 evolved per minute per miligram protein, as compared to about 400 micro liter H_2/min mg in D. gigas); Desulfovibrio desulfuricans (Berre Eau), a sulfate reducing bacterium which is able to fix N_2; and Methanosarcina barkerii (DSM 800 and 804), the most versatile mesophylic methanogenic bacterium, as it can grow in methane acetate, CO_2+H_2 and methylamine.

BIOCHEMICAL STUDY OF THE PROCESS

Screening of the Electron Transfer Proteins and Enzymes

Purification Processes The purification processes used will depend on the organism and the cell quantity. In some cases, depending on the enzyme purified, the purification scheme may be altered. For instance, in the purification process of the D. gigas hydrogenase, an extremely active fraction can be obtained if the periplasmic space fraction (corresponding to the cell washing) is previously treated, thus making unnecessary some of the cromatographic steps, with an overall decrease of purification time.

All the purification steps are carried out at 4°C , in cooled chambers and columns, and the cromatographic elution processes are done with appropriate buffers of controlled molarity and pH.

The cells are either washed or broken in a French-Gaulin pressure cell, to obtain the periplasmic fraction or the crude extract respectively. In the last case, DNase is added to the medium to decrease its viscosity. The fractionating of the cellular extract is achieved through a series of cromatographic steps (in batch or column), using mainly sephadex, ultragel, DEAE-sephadex, alumina, silica gel, hydroxylapatik, DEAE, and CMC as cromatographic materials.

Bacterial Control of the Digestor through Cofactor Analysis

Previous studies of enzyme and cofactor contents present in some bacterial species lead to the following conclusions:

- The methanogenic bacteria have unique cofactors, which can be used as their activity indicators (e.g. F 420, F 430 (containing nikel) and corrinoid B-12).

- One of the largest components of the enzymatic apparatus of sulfate-reducing organisms is the dissimilatory sulfite reductase, which is used as a taxonomic label [26] of the bacteria D. gigas, D. Salexigens and D. Vulgaris (desulfoviridin), D. desulfuricans (Norway 4) and D. 9974(desulforubidin), and D. desulfotomaculun (P582). The chemical treatment of these enzymes with acetone/HCl produces an extract containing sirohydrochlorine (a demetalized siroheme), which presents a characteristic fluorescence.

The analysis of these cofactors may be relevant in the control and identification of the bacterial populations present in the system, when other experimental parameters (such as the pH and the [$SO_4^=$] present in the medium) are changed.

ACKNOWLEDGEMENTS

The authors acknowledge the INIC, JNICT, and Calouste Gulbenkian Foundation, Portugal, and the Agency for International Development, United States, for financial assistance.

REFERENCES

1 HENZE, M. and P. HARREMOES. June 1982. Anaerobic treatment of wastewater in fixed film reactors. Literature review in Proc. IAWPR Seminar, pp. 1-90. Copenhagen.

2 ZOETEMEYER, R.J. et al., pH influence on acidogenic dissimilation of glucose in an anaerobic digestor. Water Res. 16:303-311.

3 POHLAND, F.G. and S. GHOSH. 1971. Anaerobic stabilization of organic wastes: two phase concept. Env. Letters. 1:255-266.

4 CARRONDO, M.J.T., et al. 1983. Anaerobic filter treatment for molasses fermentation wastewater. Water Sci. Technol. 15:117-124.

5 GHOSH, S., J.R. CONRAD, and D.L. KLASS. 1975. Anaerobic acidogenesis of wastewater sludge. J. Water Pollut. Control Fed. 47:30-45.

6 EASTMAN, J.A. and J.F. FERGUSON. 1981. Solubilization of particulate organic carbon during the acid phase of anaerobic digestion. J. Water Pollut. Control Fed. 53:352-366.

7 VERSTRAETE, W., L. De BAERE and A. ROZZI. 1981. Phase separation in anaerobic digestion: motives and methods. Trib. Cebedeau, No. 453-454, 367-375.

8 COHEN, A., et al. 1979. Anaerobic digestion of glucose with separated acid production and methane formation. Water Res. 13:571-580.

9 LEVY, P.F., J.E. SANDERSON, and D.L. WISE. 1981. Development of a process for production of liquid fuels from biomass. Biotechnol. Bioeng. Symp. 11:239-248.

10 MASSEY, M.C., and F.G. POHLAND. "Phase separation of anaerobic stabilization by kinetic control. J. Water Pollut. Control. Fed. 9(=978): 2004-2222.

11 GHOSH, S. 1981. Kinetics of acid-phase fermentation anaerobic digestion. Biotechnol. Bioeng. Symp. 11:301-313.

12 DATA, R. 1981. Production of organic acid esters from biomass-novel processes and concepts. Biotechnol. Bioeng. Symp. 11:521-532.

13 CLAUSEN, E.C., R.B. SHAH, G. NAJAFFOUR, and J.L. GADDY. 1982. Production of organic acids from biomass by acid hydrolysis and fermentation. Biotechnol. Bioeng. Symp. 12:238-248.

14 OMSTEAD, D.R. et al. 1980. Membrane controlled digestion: anaerobic production of methane and organic acids. Biotechnol. Bioeng. Symp. 10:247-258.

15 YOUNG, J.C., and P.L. McCARTY. 1969. The anaerobic filter for water treatment. J. Water Pollut. Control. Fed. 41: R 160 - R 173.

16 SWITZENBAUM, M.S. and W.J. JEWELL. 1980. Anaerobic attached film expanded bed reactor treatment. J. Water Pollut. Control Fed. 52: 1953-1965.

17 SHIEH, W.K. 1980. Suggested kinetics model for fluidized biofilm reactor. Biotechnol. Bioeng. 22:667-676.

18 TAIT, S.J. and A.A. FRIEDMAN. 1980. Anaerobic rotating biological contactor for carbonaceous wastewaters. J. Water Pollut. Control Fed. 52:2257-2269.

19 MARTENSSON, L. and B. FROSTELL. June 1982. Anaerobic wastewater treatment in a carrier assisted sludge bed reactor. In: Proc. NAWPR Seminar on Anaerobic Treatment, pp. 179-192. Copenhagen.

20 SCHROEPFER, G.F. and N.R. ZIEMKE. 1959. Development of the anaerobic contact process. Sew. Ind. Waste 31:164-190.

21 LETTINGA, G. et al. 1980. Use of the upflow sludge flanked reactor concept for biological wastewater treatment, especially for anaerobic treatment. Biotechnol. Bioeng. 22:699-734.

22 CHYNOWETH, D.P. 1981. Microbial conversion of biomass to methane. 8th Ann. Energy Conf. and Exposition, p.25. Washington, March 1981.

23 DATTA, R. 1981. Acidogenic fermentation of corn stover. Biotechnol. Bioeng. 23:61-77.

24 JEWELL, W.J. et al. 1978. Anaerobic fermentation of agricultural residues: potential improvement and implementation. Final U. S. Department of Energy Report. EY-76-5-02-2981-7.

25 JERGER, D.E., J.R. CONRAD, K.F. FANNIN, and D.P. CHYNOWETH. 1982. Biogasification of woody biomass. In: Energy from Biomass and Wastes VI, p.27. Florida.

26 LeGALL, J. and J.R. POSTGATE. 1973. The sulfate reducing bacteria. In: Advances in Microbial Physiology (A.H. Rose and D.W. Tempest (eds.), pp. 81-133. Academic Press. London.

A - 4

Proceedings 4th European Congress on Biotechnology 1987

Amsterdam, June 14-19, 1987

Volume 1: Abstracts/Extended Abstracts

Edited by

O.M. Neijssel
Department of Microbiology, Biotechnology Centre, University of Amsterdam, Nieuwe Achtergracht 127, Amsterdam, The Netherlands

R.R. van der Meer
HOM Business and Venture Development, Scheveningseweg 9, The Hague, The Netherlands

K.Ch.A.M. Luyben
Department of Biochemical Engineering, Delft University of Technology, Julianalaan 67, Delft, The Netherlands

ELSEVIER
Amsterdam — Oxford — New York — Tokyo 1987

49

Proc. 4th European Congress on Biotechnology 1987, Volume 1.
edited by O.M. Neijssel, R.R. van der Meer and K.Ch.A.M. Luyben
Elsevier Science Publishers B.V., Amsterdam, 1987 — Printed in The Netherlands

PROPIONIC ACID AND VITAMIN B_{12} PRODUCTION USING A XYLOSE UTILIZING PROPIONIBACTERIUM AND DIFFERENT BIOREACTORS

M.J.T.Carrondo, J.P.S.G.Crespo and M.J.Moura
Biochemical Engineering Laboratory, Department of Chemistry, Faculdade de Ciências e Tecnologia, Universidade Nova de Lisboa, 2825 Monte de Caparica, Portugal.

Propionic acid production by fermentation might be required for utilization in foods, animal feed and grain preservation; also weight yields to propylene are substantially larger than those from the ethylene from fermentation ethanol route (1-3). Industrial vitamin B_{12} production utilizes Propionibacterium freundenrichii, namely subsp. shermanii, the bacteriostatic effect of the acid produced being responsible for decreased contamination (4,5).

The kinetics of P. acidipropionici (ATCC 25562), a xylose utilizing rumen microorganism, have been studied to assess its use to propionic acid and vitamin B_{12} production from cellulose - hemicellulose hydrolysates.

From experiments conducted under batch conditions, uncontrolled pH (initial pH 7) and different xylose: glucose ratios (1:3, 1:1, 3:1) at 50 g/l total sugars the following conclusions can be drawn (6):

1- For the concentrations to be expected in a continuous process, no inhibition is apparent for glucose as substrate or acetic acid produced; propionic acid is a strong inhibitor and thus maximum concentrations obtained in the batch tests peak at 12 g/l (at 3 g/l acetic acid);

2- Xylose utilisation is low (maximum of 2.5 g/l at 75% xylose) and no diauxic growth seems to take place; glucose limitation at 75% xylose dramatically reduced acid production to 6.5 g/l propionic acid. It is worth remembering that hydrolis of agricultural and forestry residues will yield concentrations of C_5 sugars ranging from 15 to 35% of the total sugars;

3- Acids were produced at a ratio close to 3:1 propionic/acetic (molar basis) as compared to 2:1 theoretical ratio; since propionic has a higher cost, this shift should be increased; acid yields are close to the theoretical maximum (80 to 82%, at 60% acids to sugar yields;

4- Cell mass yield coefficients are high at 0.263 g cell/g substr. for this facultative anaerobe; this might be an adavantage for vitamin B_{12} production but lowered the product yield to 0.452 g propionic/g substrate. Maximum specific growth rates of 0.11 h^{-1} and maximum biomass concentrations of 4.3 g/l were obtained.

5- Cell mass productivities of 0.14 g cell/l.h are average and maximum volumetric productivity of 0.19 g propionic/l.h was obtained at 25% xylose; a time shift is apparent, cell mass productivities peaking at 41 h fermentation time whereas acid productivity peaks at 50 h. Thus, acid production takes place at higher concentrations than those sufficient to stop growth;

6- Even though no cobalt was added, vitamin B_{12} contents in the broth at 0.35 mg/l compare well with those reported in the literature under anaerobic conditions with cobalt addition (0.3 to 0.9 mg/l) for Propionibacterium species (4,5).

Controlling pH at 6.0, batch tests conducted with total sugars at 75 g/l yielded the results presented in Table 1. Thus, pH control permits higher acid and biomass final concentrations at a decreased product yield and higher maximum volumetric

Table 1 - Batch tests under pH controlled at 6.0

Sugar conc.,g/l		75glu	54gl+18xy	38gl+37xy	19gl+55xy
μ_{max},h^{-1}		0.143	0.140	0.130	0.127
X_{max},g/l		7.2	7.35	6.25	5.9
Final ac. conc.,g/l	Prop.	24.6	22.9	16.6	9.6
	Acet.	6.9	7.6	5.9	4.0
Consumption, g/l	Glu.	61.3	54	38	19
	Xyl.	-	4.9	8.5	12.3
Prod.(P+A)yield,Wt%		51	52	48	44
Max.vol. Prod.,g/l.h	Prop.	0.24	0.24	0.22	0.18
	P+A	0.29	0.30	0.29	0.25
P/A molar ratio		2.9	2.4	2.3	2.0

productivities but for the 1:3 glucose:xylose ratio. The increased initial concentration of xylose is accompanied by a decrease in the molar ratio propionic/acetic acids.

The sugar consumption pattern is crucial for the potential development of the process from biomass hydrolysates. As can be seen from Table 1, glucose consumption is complete and thus higher final acid concentrations are possible (approximately 30 g/l as propionic); xylose consumption has increased regarding the tests conducted without pH control but never went above 25% of the xylose present. A more clear picture for the glucose and xylose consumption for these four experiments is depicted in Figure 1 where glucose concentrations in the broth and xylose consumption are plotted versus fermentation time; it is aparent that no xylose consumption takes place once glucose is exhausted.

From Figure 1, xylose and glucose consumption rates are calculated for the time periods when these are maximum and approximately constant - the corresponding results are presented in Table 2. Care must be taken in interpreting the data for 3:1

Table 2 - Sugar consumption rates in batch tests,pH 6.0 (23 to 52hrs)

	3:1glu/xyl	1:1glu/xyl	1:3glu/xyl
Xylose cons.rate,g/l.h	0.04	0.18	0.21
Glucose cons.rate,g/l.h	0.87	0.87	0.56
Range of glucose conc.,g/l	47-22	35-9	17-1

glucose:xylose ratio as, when glucose concentration gets small, the microorganism is no longer growing exponentially and no increase is apparent in xylose consumption rate. As glucose: xylose ratios are decreased to 1:1 and 1:3, xylose consumption rate shoots up as glucose concentration is lowered within the exponential growth phase.

Three continuous reactor types were assessed at 3:1 glucose/ /xylose ratios, namely CSTR, immobilized cells columnar reactor (ICR) and CSTR with ultrafiltration cell recycle (UFR).

CSTR tests conducted at pH 6.0 washed out at 5 to 7 hours, in agreement with the variable specific growth rates quoted here. For the high sugar concentrations of 75 g/l, maximum xylose consumption was low at 1.3 g/l. Maximum volumetric productivities were reached at 17.6 h (D=0,057 h^{-1}) as 0.42 g/l.h and 0.57 g/l.h for propionic and total acids, respectively, at low acid concentrations of 7.3 g prop./l and 2.7 g acet./l. Maximum total yield of 61% was obtained at 42 h at 13.4 g prop./l and 5.2 g acet./l and total volumetric productivity of 0.45 g/l.h.Propionic to acetic molar ratios were almost constant at 2.2.

ICR tests, using agar+glutaraldehyde on 4 mm glass beads and a 32 mm internal diameter acrilic column 50 cm in height with 5 sampling ports, were carried out over a period of 6 months. Degassing became a major problem and as no pH control was available, full use of the column proved difficult to achieve, pH reaching an inhibitory 5.2 (6) still within the column. Starting from 25 g/l total sugars and at a residence time of 16.5 hr, final concentrations of 9.5 g prop./l and 1.2 g acet./l, i.e. a 6.4 molar ratio, were achieved at productivities of 0.95 g/l.h for propionic acid and 1.03 g/l,h for total acids. Xylose consumption was low at 1 g/l with very high product yields of 80%.

UFR tests on carbon-zirconium oxide membranes, pH control at 6.0 and 50 g/l total sugars were conducted for two dilution rates. At 0.09 h^{-1} (11.1 h residence time), 18.5 g prop./l and 4.3 g acet./l were achieved, at propionic and total acids volumetric productivities of 1.6 and 2.0 g/l.h but low xylose consumptions of 0.7 g/l. Increasing dillution rate to 0.12 h^{-1} (8.33 h residence time) increased propionic and total acids volumetric productivities to 2.2 and 2.7 g/l.h, with final acids concentrations almost unchanged at 18 and 4 g/l propionic and acetic acids, respectively, and increasing xylose consumption to 2.7 g/l. The molar ratio for the acids was 3.5 and the yield for total acids was 58%. Final cell concentrations reached 95 g/l in the system still within a newtonian rheology at 13.3 centipoises.

CONCLUSIONS

In order to achieve higher xylose consumption, a better understanding of the xylose consumption rate as a function of growth rate and glucose concentration must be sought. Given the sugar concentrations to be expected in real situations (3:1 glucose/xylose) a glucose consumption rate three times higher than xylose would be ideal; such a result was obtained in the batch tests for the opposite sugar ratio of 1:3 (see Table 2).

As the price of propionic acid is higher than acetic acid, a larger P/A molar ratio is desirable. UFR and ICR systems,possibly due to larger populations of non-growing cells, seem most appropriate for the purpose, ICR allowing larger product yields. These high cell concentration reactors might perform even better if operated under extractive/product removal conditions and/or pH control to decrease inhibition.

The UFR system might prove to be the most appropriate for vitamin B_{12} production, under still to be established conditions.

ACKNOWLEDGEMENTS

J.P.Crespo carried out some of the glucose batch tests without pH control at Prof. James Gaddy's laboratory at the University of Arkansas, Fayetteville and the UFR at Prof. Gerard Goma's laboratory at INSA, Toulouse, France. We hereby express our recognition for these ongoing collaborations.

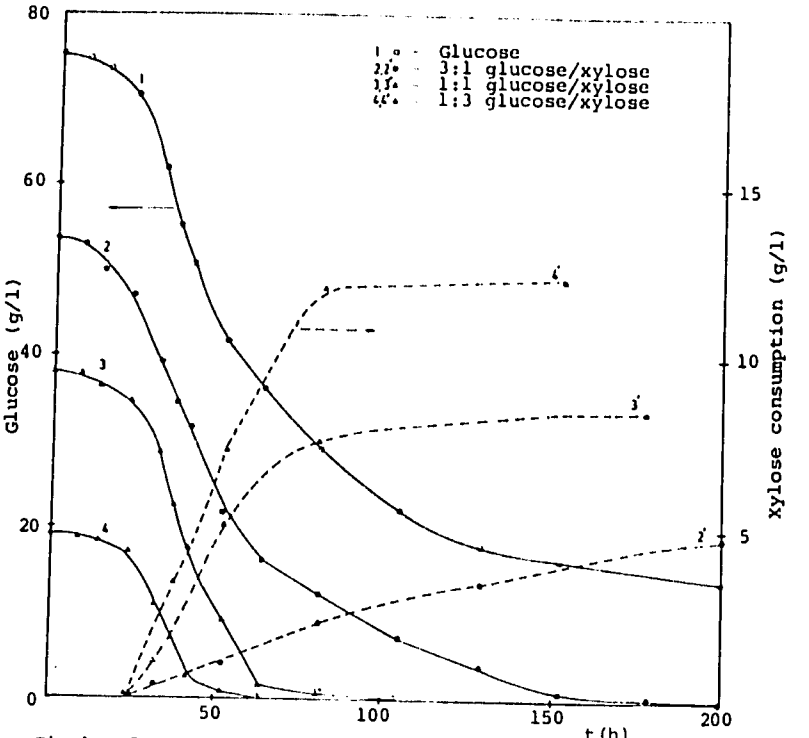

Fig.1 - Sugar consumption during batch tests at pH 6.0.

M.J.Moura acknowledges a research studentship awarded by Junta Nacional de Investigação Científica e Tecnológica, Lisboa (JNICT) We acknowledge: financial support of JNICT under contract nº720.85.74; U.S. Programme in Science and Technology Cooperation, Washington, D.C., U.S.A., Grant nº936-5542-G-SS-4003-00, as well as the sponsorship of IPE - Investimentos e Participações do Estado, SARL and Portucel, E.P.

REFERENCES

1. E.C.Clausen et al., Chem.Engrg Prog., 80 (1984) n.12, 59-63.
2. M.J.Playne, Propionic Acid, in: M.Moo Young (Ed.)Comprehensive Biotechnology, Vol.3, Sec.3, Pergamon Press, London, 1985.
3. A.E.Humphrey, Chem.Engrg Prog., 73 (1977) n.5, 85-91.
4. L.J.Florent and F.M.Ninet, Vitamin B_{12}, in: H.Peppler and D. Perlman (Eds.) Microbiol Technology, Vol.1 Academic Press, New York, 1979, 497-519.
5. H.C.Friedman and C.M.Cagen, Microbiol Biosynthesis of B_{12} like compounds, Ann.Rev.Microbiol., 24 (1970) 159,208.
6. J.P.S.G.Crespo et al, in Biotechnology and Agriculture in the Mediterranean, Athens, Greece, June 1986, CEE Conf.Proc. in Press.

REVISED VERSION A.5

PRODUCTION OF PROPIONIC ACID USING A XYLOSE UTILIZING PROPIONIBACTERIUM

M.J.T.Carrondo, J.P.S.G.Crespo and M.J.Moura*
Biochemical Engineering Laboratory, Department of Chemistry, Faculdade de Ciências e Tecnologia, Universidade Nova de Lisboa, 2825 Monte da Caparica, Portugal.

SUMMARY

The kinetics of P. acidipropionici (ATCC25562), a xylose-utilizing rumen microorganism, was studied to assess its use for propionic acid production from wood hydrolyzates.

Propionic acid has been shown to have a stronger inhibitory effect than acetic acid, with the undissociated acid form being responsible for the majority of the inhibitory effect. Thus, in batch tests with pH controlled at 6.0, the propionic acid concentration reaches 25 g/L and the acetic acid 7 g/L. Xylose uptake rate is dependent on the specific growth rate and glucose concentration.

An immobilized cell columnar reactor at very high product yields (80%) proved adequate for propionic production. At cell concentrations of 95 g/L with high product concentration, volumetric productivities of 2.7 g/L·h were obtained in ultrafiltration cell recycle systems.

INTRODUCTION

Propionic acid production via fermentation has been advocated for use as a grain preserver and antifungal agent for feeds, a plasticizer, and as a herbicide *(1)*. Weight yields are greater than those for ethanol fermentation, and the conversion by hydrogenation and dehydration to propylene gives a one third greater weight yield than conversion of ethanol to ethylene *(2)*.

Propionic acid bacteria, namely P. freudeurichii, and especially subsp. shermanii have been used in some industrial processes for vitamin B_{12} production. Advantages of this organism include *(1)* decreased contamination (since propionate is in itself a bacteriostatic and fungistatic agent) and *(2)* low energy requirements since the majority of the fermentation is run under anaerobic conditions for cell growth. P. acidi-propionici (also known as P. pentosaceum) has already been assessed by Prof. Gaddy's group *(3)* as

a potential propionic acid producer under immobilized conditions. Playne *(4)*, has also studied propionic fermentation, comparing results of Propionibacterium with Veillonella parvula, an organism which cannot use carbohydrates but uses lactate, pyruvate, and succinate.

MATERIAL AND METHODS

STRAIN

The organism utilized in all the studies, Propionibacterium acidi-propionici, was obtained from the American Type Culture Collection (ATCC 25562) in a freeze-dried form.

MEDIA

Conservation media consists of a standard nutrient containing peptone (1%), yeast extract (1%), and phosphate buffer (0.15 M, pH 7). The carbon source was a mixture of glucose: xylose (3:1) at 25 g/L.

Magnesium and manganese salts were added (0.01% and 0.001%, resp.) and also agar powder (3%), to provide for solid medium tubes which were inoculated in depth, incubated for 36h at 37°C and kept at 4 C. Transfer was made every two months.

During assays, the organism was kept in a liquid medium (same conditions as for conservation but without agar powder) and transfered every 48 h. The flasks were kept constantly shaking at 37°C.

The carbon source (glucose + xylose, 3:1, 2.5%) was separately sterilized and added to the flasks by injection with sterilized needles.

INOCULUM PREPARATION

Seed cultures, grown for 24 to 48 h, were used for the inoculation. The organism was kept and prepared for inoculation with 2.5% glucose + xylose; transfer was made by sterile injection.

ANALYTICAL METHODS

Biomass determination

Cell concentration was determined using the optical density measured at 540 nm and comparing with a calibration curve (optical density versus cell

dry weight). On all readings, uninoculated medium was used for zero correction.

Acetic and propionic acid determination

The organic acids propionic and acetic were determined by gas chromatography using a United Technologies Packard G C - 439 chromatograph. A glass column 1.8 m long and 2 mm internal diameter, packed with 10% SP 1 200 1% H_3PO_4 on chromosorb waw 80/100 mesh was used. Nitrogen was used as a carrier gas (at 40 mL/min). An oven temperature of 115°C, injector temperature of 130°C and detector of 135°C were maintained throughout.

Prior to injection, all samples were centrifuged at 6 000 rpm for 10 minutes, and the cells discarded. To ensure total conversion of all acids to a nondissociated form, an oxalic acid solution (0.5 M) was used for dilutions. A sample volume of 0.6 µL was used. After every three injections 0.6 µL of oxalic acid solution was injected in order to avoid ghosting or tailing of the peaks.

An integrator (Shimadzu C R 3 - A) on-line with the chromatograph was used to determine the composition of each sample. A two point calibration, external standard method was used. Standards were equally diluted with oxalic acid solution.

Glucose and xylose determination

Glucose was determined enzymatically using a Yellow Springs (YSI 27) instrument. Xylose determination was carried out on a HPLC chromatograph (Waters Model - 410). A Sugarpack column was used with demineralized water as the solvent phase at a flow rate of 0.5 mL/min. A two-point, external standard method was used, achieving very good linearity. Prior to injection, samples were centrifuged at 6 000 rpm and the cells discarded. Samples were then filtered through Sartorius membranes (0.45 µm) and diluted with demineralized water.

Viscosity assay

Broth viscosity was estimated with a couette viscometer (Rheomat 15 TFC) at 37°C.

BATCH REACTORS

All reactors were sterilized at 121°C for 20 min. Sugar solutions separately sterilized, were added after cooling to room temperature. Inocula were 3% (v/v), 24 to 48 h old.

Batch reactors without pH control

Borosilicate glass flasks (100 mL) were used with a 70 mL working volume. Flasks were sealed with rubber stoppers and aluminum capsules with a central sampling point allowed aseptic conditions during fermentation.

Substrate addition and inoculation were made by injection under aseptic conditions. During fermentation, flasks were kept in a thermostatic bath with longitudinal shaking, at 37°C and 140 strokes/min.

Batch reactors with pH control

A poli-batch battery was used, with 2 L fermenters (Setric 2 M), which allowed temperature, pH, and mixing speed control. Substrate and inocula were added by sterile connection with glass connectors. Temperature was kept at 37°C, revolution speed at 150 rpm, and pH at 6.00, by addition of diluted ammonia (13.4 M).

CHEMOSTAT REACTORS

Setric Fermenters (2 L and 7 L) were used, operated as a CSTR. Temperature revolution speed, and pH were controlled in the same way as for the batch reactors.

IMMOBILIZED CELL REACTOR

A columnar reactor was used built from a plexiglass tube, 3.16 cm in internal diameter, 47 cm in height, and 0.3 cm wall thickness. The reactor was closed at both ends by plexiglass plates; the bottom was fixed and the top removable, to allow for filling and washing of the column. A NPT Swagelok (1/4 in. connection) was fixed at the center of each plate for feeding (bottom) and effluent discharge (top).

Five sampling ports, at 8 cm intervals along the column, were made using 1/8 in. NPT Swagelok, screwed to the column and sealed with rubber septa.

The bed was made up of 4 mm glass beads covered with a solution of agar (1%) and gelatin (25%), which was subjected to attack with glutaraldehyde solution (3%) prior to sterilization with ethylene oxide. The system (including medium reservoir, reactor, pumps, etc.) was kept in a temperature-controlled chamber at 37°C.

CELL RECYCLE ULTRAFILTRATION SYSTEM

This system consisted of a Setric fermenter (2 L), working on-line with two parallel ultrafiltration modules (CARBOSEP M 6, manufactured by SFEC) with zirconium oxide membranes on a carbon support. The ultrafiltration modules were tubular, with seven separate type M 6 membranes, containing a maximum of 1.5 L of medium. The filtration surface was 0.0226 m^2 with a cutoff of 500,000 d. The second module was used in case of flow interruption by cell accumulation on the working module and allowance was made for rinsing and change under sterile conditions (Fig. 1).

RESULTS AND DISCUSSION

FERMENTATION KINETIC STUDIES

Batch reactor studies were undertaken to describe product inhibition conditions during fermentation and to assess glucose-xylose consumption kinetics. The inhibitory effects were clearly demonstrated by data obtained from tests conducted using *(1)* external acid addition to the broth in a concentration range of 0 to 20 g/L and *(2)* pH control. In both cases, acetic or propionic acid inhibitory effects can be described by hyperbolic model of the type *(5)*:

$$\frac{\mu_m^i}{\mu_m^o} = \frac{K_p}{Kp + P_a^m} \qquad (1)$$

Where μ_m^o and μ_m^i are the maximum specific growth rates, without and with product addition to the fermentation media, resp.; K_p is a parameter related to the resistance to the added product; and m, the exponent of the added product concentration P_a, represents the degree of strain tolerance to each product. Data fitting yielded the following results:

1. Acetic acid:

$$\frac{\mu_m^i}{\mu_m^o} = \frac{2943.8}{2943.8 + P_a^{2.179}} \qquad r = 0.92 \qquad (2)$$

2. Propionic acid:

$$\frac{\mu_m^i}{\mu_m^o} = \frac{76.1}{76.1 + P_a^{1.209}} \qquad r = 0.98 \qquad (3)$$

The inhibitory effect is much stronger with propionic acid, being very small for acetic acid (large K_p) at potential process concentrations. A set of batch tests at 2%, 3%, 5%, 8.5% and 12% initial glucose concentrations was also conducted. Since glucose consumption curves and final glucose utilization were the same in all the experiments, fermentation was not controlled by the initial glucose concentration within the range tested.

The inhibitory effect due to propionic acid produced during fermentation is shown in Fig. 2, where the specific growth rate, μ, and the specific production rate, ν, are plotted against propionic acid concentration. As can be seen, specific growth rate tapers off at somewhat lower concentrations than the specific production rate; i.e., production still takes place at higher concentrations than those sufficient to stop growth. The relationship between μ and P can be linearly described up to 4 g/L of propionic acid and exponentially thereafter:

$$P < 4 \text{ g/L} \qquad \mu = 0.211 - 0.0355\ P \qquad (4)$$

$$P > 4 \text{ g/L} \qquad \mu = 1.2804 \exp(-0.726\ P) \qquad (5)$$

On the other hand, ν and P can be described exponentially throughout the whole range:

$$\nu = 0.366 \exp(-3.328\ P) \qquad (6)$$

Comparing the inhibitory effect of added versus produced propionic acid, one can conclude that a stronger inhibition occurs in the case of the produced acid which is also apparent in other fermentation systems *(6)*.

To assess xylose utilization, a set of batch studies was performed using glucose/xylose ratios of 3:1, 1:1, and 1:3 at total sugar concentrations of 50 g/L. Xylose utilization was low (maximum of 2.5 g/L at 75% xylose) and no diauxic growth seems to take place. Fermentation curves for experiments carried out at 25% and 50% of xylose are similar and do not differ from curves obained from fermentationsusing glucose as the only substrate. However, if glucose becomes limiting, as happens at 75% xylose concentration, organic acid production is dramatically affected, reaching a maximum of only 6.5 g/L of propionic acid and 1.9 g/L of acetic acid.

Acids were produced at a ratio close to 3:1 propionic/acetic (mol basis) as compared to 2:1 theoretical ratio, obtained from the stoichiometry *(7)*.

$$1.5\ C_6H_{12}O_6 \longrightarrow 2\ CH_3CH_2COOH + CH_3COOH + CO_2 + H_2O \quad (7)$$

Since propionic acid has a higher cost, this shift is favorable and should be increased as much as possible. Table 1 shows the average performance obtained in batch assays with no substrate limitation. These results fit well with those obtained by B. Hendricks et al. *(8)*. The cell mass yield coefficient is somewhat high for a facultative anaerobe, probably lowering the product yields. At the low final pH values obtained in these experiments (in spite of the presence of phosphate buffer), propionic and acetic acid are essentially in their undissociated forms. Thus, transport through the cell membrane is easier. Consequently, its inhibitory effect becomes rather important *(9)*.

To overcome this inhibitory effect, batch tests were conducted with pH controlled at 6.0. The results obtained are summarized in Table 2. Total sugar concentrations of 75 g/L and different sugar ratios were utilized: glucose only, 3:1 glucose/xylose, 1:1 glucose/xylose, and 1:3 glucose/xylose. Higher acid concentrations and volumetric productivities were apparent as compared to the uncontrolled batch tests (Fig. 3 and 4). A clearer picture for glucose and xylose consumption is depicted in Fig. 5 where glucose concentration in the broth and xylose consumption are plotted versus fermentation time. It is clear that both sugars can be fermented simultaneously but with a higher uptake rate for glucose. However, there is no uptake of xylose during the first 23 h and the fermentation kinetics are initially close to that observed with glucose

alone. After glucose exhaustion, no xylose consumption takes place, which agrees with the fact that fermentation does not proceed with xylose only. From Fig. 5, xylose and glucose consumption rates were calculated for the time periods when these were maximum and approximately constant. These results are presented in Table 3.

It seems evident that there is an inhibition of xylose uptake by an excess of glucose. So the xylose consumption rate varies inversely with glucose concentration. However, care must be taken in interpreting this data. For instance, for the 3:1 glucose/xylose ratio essay and when glucose concentration gets small, the microorganism is no longer growing exponentially and no increase in xylose consumption rate is apparent. As glucose:xylose ratios are decreased to 1:1 and 1:3, xylose consumption rate shoots up, as the glucose concentration range is lowered (within the exponential growth phase). These results suggest that the xylose uptake rate, in the presence of glucose, might be described by a model of the type:

$$-\frac{1}{X}\frac{dC_{xyl}}{dt} = f(\mu, C_{glu}) \qquad (8)$$

CONTINUOUS REACTOR STUDIES

There continuous reactor types were assessed at 3:1 glucose/xylose ratios: *(1)* continuous stirred tank reactor (CSTR), *(2)* immobilized-cell columnar reactor (ICR), and *(3)* a CSTR with ultrafiltration cell recycle (UFR).

CSTR tests conducted without pH control and with pH control at 6.0 (feed sugar concentrations of 30 g/L and 75 g/L, resp.), were performed essentially to compare its performance with the batch reactors. Figures 6, 7 and 8 show the results obtained. The CSTR at pH 6.0 washed out at 6 to 7 h, in agreement with the maximum specific growth rate of 0.140 h^{-1} obtained in batch tests under similar conditions. Maximum xylose consumption was low at 1.3 g/L, while glucose concentration in the broth remained high. Maximum volumetric productivities were reached at 17.6 h ($D = 0.057\ h^{-1}$) at 0.42 g/L·h and 0.57 g/L·h for propionic and total acids, respectively. Nevertheless acid concentrations were low at 7.3 g/L propionic acid and 2.7 g/L acetic acid. Maximum total yield of 61% was

obtained at 42 h with 13.4 g/L propionic acid and 5.2 g/L acetic acid at a total volumetric productivity of 0.45 g/L·h. It is worth mentioning that the propionic to acetic mol ratio remains almost constant at 2.2, a value closer to the theoretical ratio than obtained under batch conditions.

As expected, the CSTR without pH control yields very low acid concentrations - in spite of good volumetric productivities (see Fig. 7 and 8). This effect becomes more noticeable when the pH drops below 6, at approximately 12 h retention time. At such a retention time, volumetric and specific productivities are almost identical with and without pH control at 6 (see Fig. 8). Furthermore, productivities drop much faster without pH control.

ICR tests were carried out over a period of six months. During its operation, degassing of CO_2 (produced during fermentation) became a major problem. It reduced the useful reactor volume and the immobilized cells-nutrient broth contact. Since the column was operated without pH control, a strong inhibitory pH value of 5.2 was reached within the column. With these conditions full use of the column proved difficult to achieve. Starting from 25 g/L total sugars and at a residence time of 16.5 h, final concentrations of 9.5 g/L propionic acid and 1.2 g/L acetic acid, i.e. a 6.4 mol ratio, were obtained at productivities of 0.95 g/L·h for propionic acid and 1.03 g/L·h for total acids. Product yields were high at 80% since less substrate was utilized for cell growth purposes. Xylose consumption was low at 1 g/L, a result to be expected since glucose concentration was low only at very low pH.

UFR tests were performed with pH control at 6.0 and a total sugar concentration of 50 g/L. Figure 9 presents the fermentation curves. The system was initially operated in a batch way and after that period, it was run continuously for two dilution rates. At 0.09 h^{-1} (11.1 h residence time), 18.5 g/L propionic acid and 4.3 g/L acetic acid were achieved at propionic and total acids volumetric productivities of 1.6 and 2.0 g/L·h. Increasing the dilution rate to 0.12 h^{-1} (8.33 h residence time) increased propionic and total acids volumetric productivities to 2.2 and 2.7 g/L·h, with final acids concentrations almost unchanged at 18 g/L propionic acid and 4 g/L acetic acid. Blanc *(10)*, using lactose substrates, increased propionic productivity to 2.15 g/L·h at a dilution rate of 0.3 h^{-1} but with a low propionic concentration in the effluent (9 g/L). The results we

obtained are encouraging, since a good compromise between productivities and acids concentration was achieved. This compromise is important and will be reflected on downstream process costs for product recovery. The mol ratio for the acids was 3.5 and the yield for total acids was 59%. The productivity reported here is 14 times greater than productivity obtained in the batch reactor without pH control and 9 times that in the batch with pH control at 6.0.

Since the final cell concentration reached 95 g/L in the system i.e., 14 times higher than in the batch with pH control, but the productivity was only 9 times that in the batch, it can be concluded that a loss of cell activity occurred. This might be explained by a decay of cell viability due to shear stress developed along the system, the rheological conditions associated with such high cell concentrations, and accumulation of inhibitory co-metabolites. The system still presents a Newtonian rheology behavior, with a final apparent viscosity of 13.3 $mP_a \cdot s$.

Figure 10 shows the apparent viscosity versus cell concentration. This relationship can be described by a model of the type:

$$\eta_{app} = 1 + AX^n \qquad (9)$$

Data fitting yielded the following results:

$$\eta_{app} = 1 + 6.156 \times 10^{-4} X^{2.186} \qquad r = 0.987 \qquad (10)$$

Performance results obtained from continuous fermentation systems are summarized on Table 4.

CONCLUSIONS

1. In order to achieve higher xylose consumption, a better understanding of the xylose uptake rate as a function of specific growth rate and glucose concentration must be sought. Given the sugar concentrations to be expected in real situations (3:1 glucose/xylose), a glucose consumption rate three times higher than xylose would be ideal. Such a result was obtained in the batch tests for the opposite sugar ratio of 1:3 (see Table 3).

To develop a model, the utilization of a chemostat fed with nutrient broth containing xylose and with a separate glucose solution feed, seems to be appropriate (fed batch situation). The use of different dilution rates would allow the study of the influence of specific growth rate on the kinetics of xylose utilization, while on-line glucose control would allow keeping its concentration within a desirable range.

2. The ICR reactor presented higher yields than any of the other reactor types tested; pH control and degassing are important requirements to be improved for better operability of this reactor type.

3. Since the price of propionic acid is higher than that of acetic acid, a larger P/A mol ratio is desirable. UFR and ICR systems, possibly due to larger populations of non-growing cells, seem most appropriate for the purpose. These high-cell-concentration reactors might perform even better if operated under extractive/product removal conditions and/or pH control to decrease inhibition.

ACKNOWLEDGEMENTS

J.P.Crespo carried out some of the glucose batch tests without pH control at Prof. James Gaddy's laboratory at the Univerisity of Arkansas, Fayetteville and the UFR at Prof. Gerard Goma's laboratory at INSA, Toulouse, France. We hereby express our recognition for these ongoing collaborations.

M.J.Moura acknowledges a research studentship awarded by Junta Nacional de Investigação Científica e Tecnológica, Lisboa (JNICT). We acknowledge: financial support of JNICT under contract No. 720.85.74; U.S. Programme in Science and Technology Cooperation, Washington, D.C., U.S.A., Grant No. 936-5542-G-SS-4003-00, as well as the sponsorship of IPE - Investimentos e Participações do Estado, SARL and Portucel, E.P.

NOMENCLATURE

t Time (h)
G Glucose concentration (g/L)
G_o Initial glucose concentration (g/L)
X Biomass concentration (g/L)
A Acetic acid concentration (g/L)

P Propionic acid concentration (g/L)

P_a Product concentration added to broth (g/L)

μ Specific growth rate (h^{-1})

μ_m Maximum specific growth rate (h^{-1})

ν Specific production rate (g product/g cell·h)

$Y_{X/S}$ Biomass yield (g cell/g substrate)

$Y_{P/S}$ Product yield (g product/g substrate)

D Dilution rate (h^{-1})

η_{app} Apparent viscosity (m P_a·s)

REFERENCES

1. Anon., Chemical Economics Handbook, SRI International, Stanford, Cal, U.S.A., May (1981).
2. Humphrey, A.E., Chem.Eng.Prog., 73 (5), 85-91 (1977).
3. Clausen, E.C. and Gaddy, J.L., Chem.Eng.Prog., 80 (12), 59-63 (1984).
4. Playne, M.J., *Propionic and Butyric Acids* in M. Moo-Young (Ed.) Comprehensive Biotechnology, Pergamon Press, London (1985).
5. Mota, M.J., Docteur Ingenieur Thesis, INSA, Toulouse (1985).
6. Nagodawithana, T.W., Steinkraus, K.H., J. Appl.Environ.Microbiol., 31, 158 (1976).
7. Allen, S.H.G., Kellermeyer, R.W., Stjernholm, R., Wood, H.G., J. Bacteriol., 87, 171-187 (1964).
8. Hendricks,B., Korus, R.A., Heimsch, R.C., Biotechnol.Bioenerg.Symp., 17, 241-245 (1985).
9. Samson, F.E., Katz, A.M., Harris, D.L., Arch.Biochem.Biophys., 54, 406-423 (1955).
10. Blanc, P., Docteur Ingenieur Thesis, INSA, Toulouse (1986).

KEY WORDS

Propionic acid, production from Propionibacterium acidi-propionici; Xylose utilization, kinetics of; Immobilized cell system (ICR), production of propionic acid by; Tangential ultrafiltration cell recycle reactor (UFR), production of propionic acid by; High cell concentration system for propionic acid production.

Table 1 - Batch tests without pH control

Maximum specific growth rate, μ_{max}		(h^{-1})	0.11
Maximum cell concentration, X_{max}		(g/L)	4.3
Final acid concentration	Propionic acid	(g/L)	11.0
	Acetic acid		3.0
Glucose consumption		(g/L)	22.0
Total product yield		(wt%)	63.6
Cell yield, $Y_{X/S}$		(g cell/g substrate)	0.263
Maximum volumetric productivity		(g prod./L·h)	0.19
Maximum cell mass productivity		(g cell/L·h)	0.13
P/A mol ratio			3.0
Final pH			4.7

Table 2 - Batch tests under pH controlled at 6.0

Sugar concentration, g/L		75glu[a]	54glu + 18xyl[a]	38glu + 37xyl	19glu + 55xyl
Maximum specific growth rate, μ_{max}, h^{-1}		0.143	0.140	0.130	0.127
Maximum cell concentration, X_{max}, g/L		7.2	7.35	6.25	5.9
Final acid concentration, g/L	Propionic	24.6	22.9	16.6	9.6
	Acetic	6.9	7.6	5.9	4.0
Consumption, g/L	Glucose	61.3	54	38	19
	Xylose	-	4.9	8.5	12.3
Total product yield, wt%		51	52	48	44
Maximum volumetric Productivities, g/L·h	Propionic	0.24	0.24	0.22	0.18
	Propionic + Acetic	0.29	0.30	0.29	0.25
P/A mol ratio		2.9	2.4	2.3	2.0

[a] glu - glucose
xyl - xylose

Table 3 - Sugar consumption rates in batch tests, pH 6.0 (23 to 52 h)

	3:1glu/xyl [a]	1:1glu/xyl	1:3glu/xyl
Xylose consumption rate, g/L·h	0.04	0.18	0.21
Glucose consumption rate, g/L·h	0.87	0.87	0.56
Range of glucose conc., g/L	47-22	35-9	17-1

[a] glu/xyl = glucose/xylose

Table 4 - Performance comparison in continuous fermentation systems.

		CSTR pH 6.0	CSTR	ICR	UFR
Maximum volumetric productivity(g prod./L·h)	Propionic	0.42	0.34	0.95	2.20
	Total	0.57	0.49	1.03	2.70
Corresponding acid concentration(g/L)	Propionic	7.3	3.9	9.5	18.0
	Acetic	2.7	1.7	1.2	4.0
Yield for total acids(W/W%)		61	66	80	59
Percentage of theoretical maximum yield [a]		79	86	104	77
P/A mol ratio		2.2	1.9	6.5	3.5

[a] Assuming Stoichiometry given by Eq.7.

LIST OF FIGURES - DESCRIPTIVE LEGENDS

Fig. 1 - Schematic representation of the ultrafiltration cell recycle system.

Fig. 2 - Specific rates of growth and propionic acid production.

Fig. 3 - Acetic and propionic acids production in batch reactor at pH=6.00.

Fig. 4 - Specific and volumetric productivities in batch reactor at pH=6.00.

Fig. 5 - Glucose concentration and xylose consumption in batch reactor at pH=6.00.

Fig. 6 - Glucose consumption, cell growth, propionic and acetic acids production in CSTR at pH=6.00.

Fig. 7 - pH, glucose consumption, cell growth, propionic and acetic acids production in CSTR without pH control.

Fig. 8 - Specific and volumetric productivities (propionic acid) in CSTR without pH control (▲,●) and with pH=6.00 (Δ,o).

Fig. 9 - Glucose consumption, cell growth, propionic and acetic acids production in UF system.

Fig. 10 - Apparent viscosity versus cell growth in UF system.

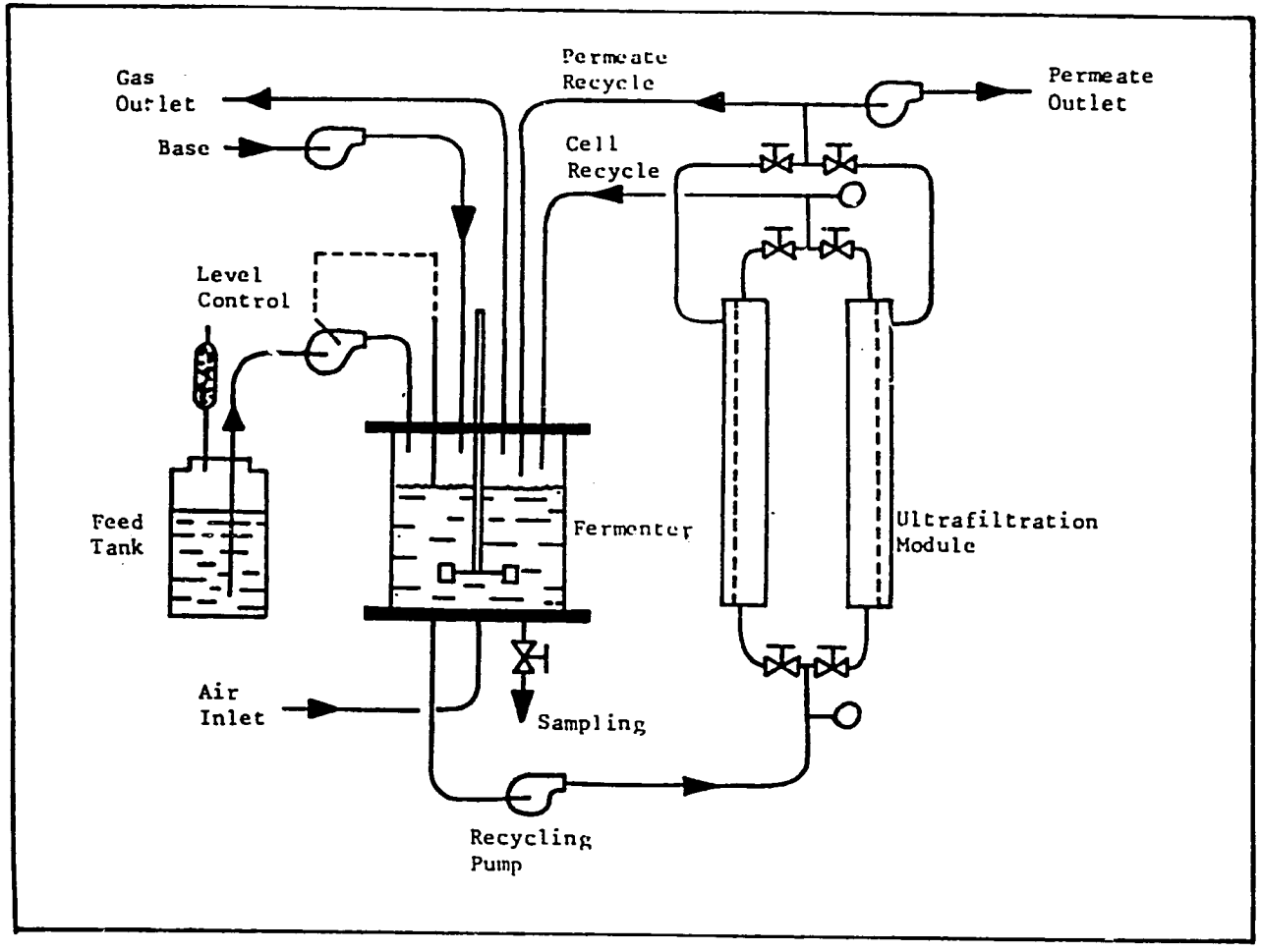
Gas
Outlet
Permeate
Recycle
Permeate
Outlet
Base
Cell
Recycle
Level
Control
Feed
Tank
Fermenter
Ultrafiltration
Module
Air
Inlet
Sampling
Recycling
Pump

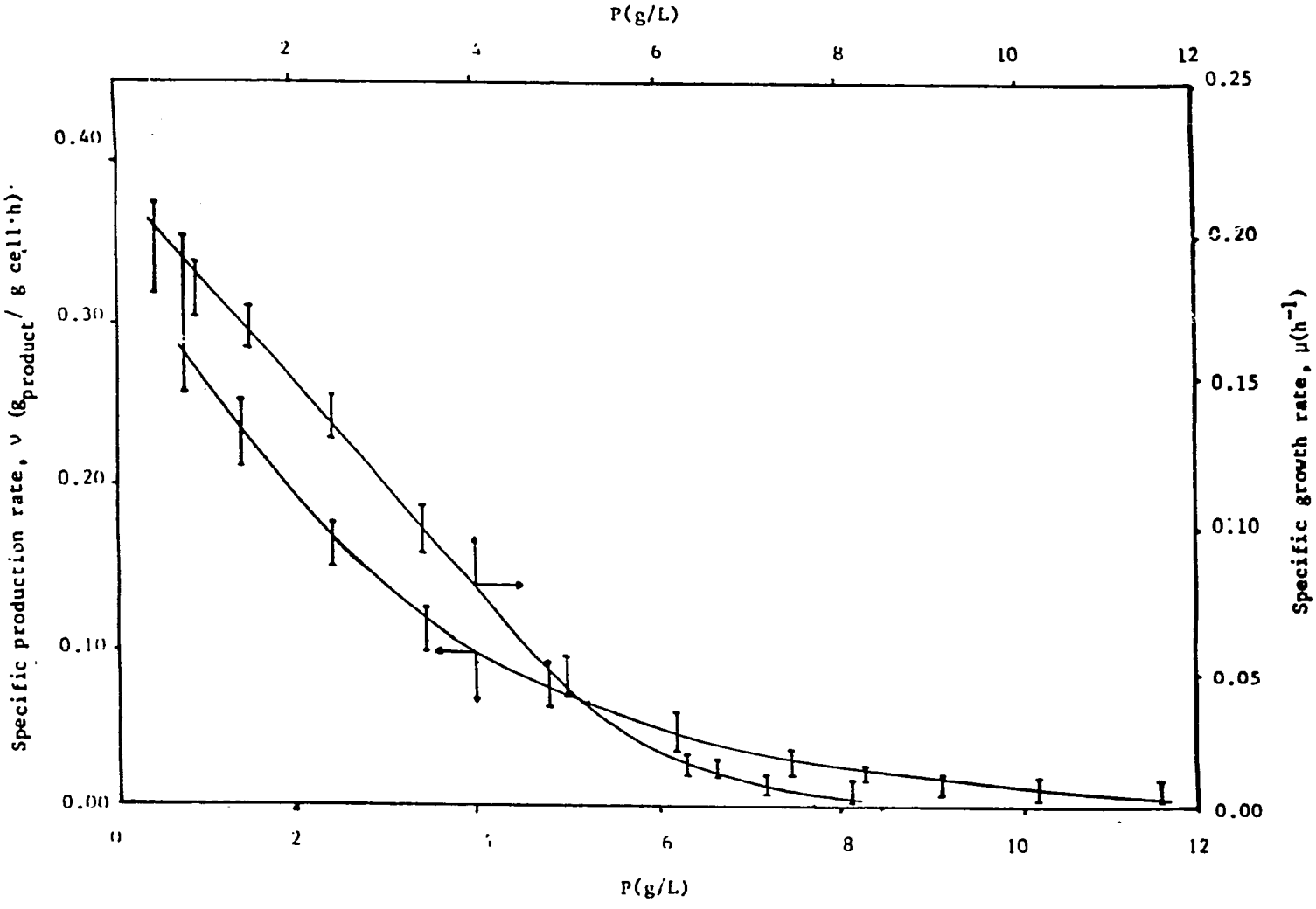
P(g/L)
2
4
6
8
10
12
0.40
0.30
0.20
0.10
0.00
Specific production rate, ν (g product / g cell·h)
0.25
0.20
0.15
0.10
0.05
0.00
Specific growth rate, μ(h⁻¹)
0
2
4
6
8
10
12
P(g/L)

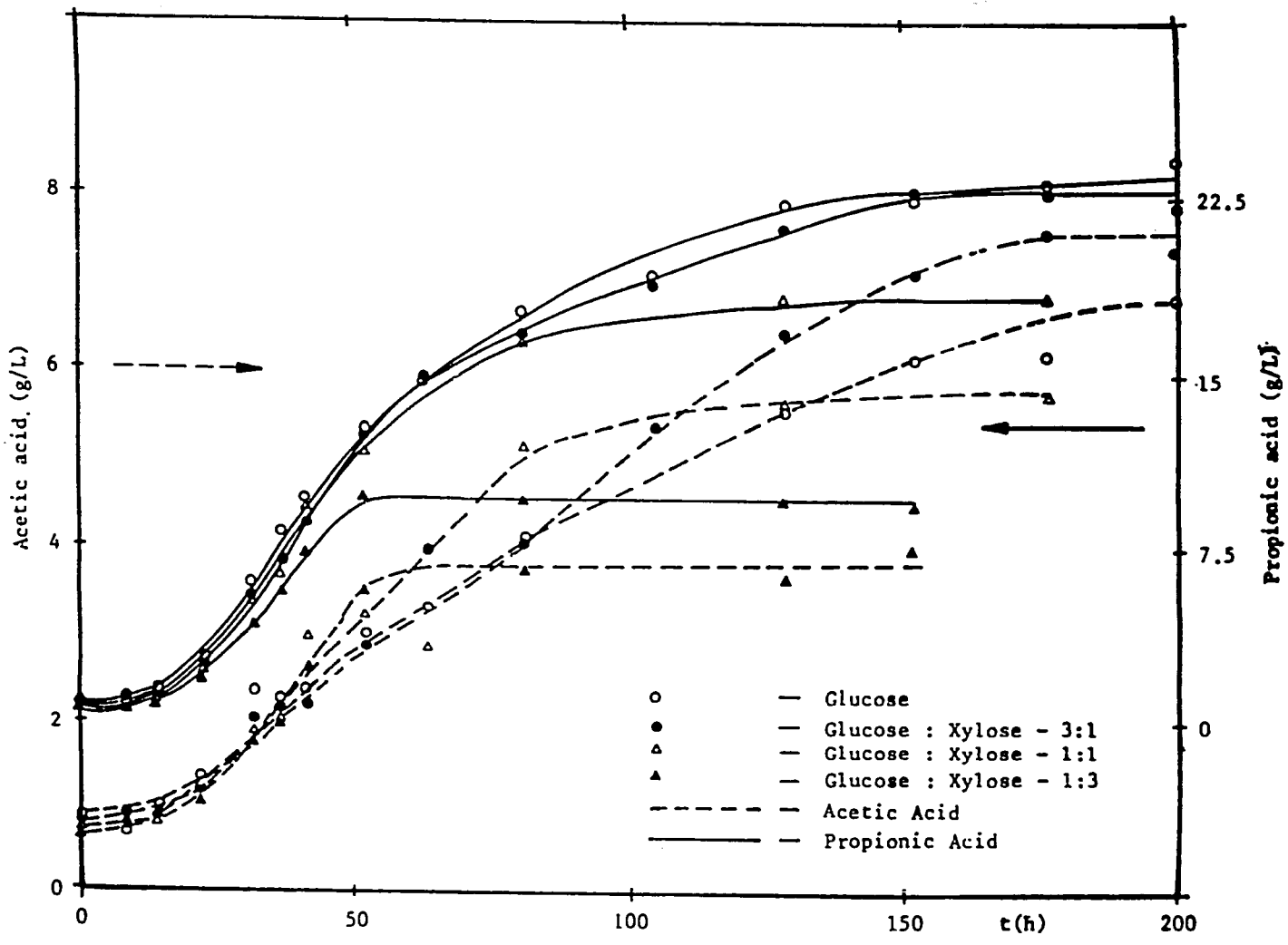
Acetic acid (g/L)
Propionic acid (g/L)
t(h)
0
2
4
6
8
0
50
100
150
200
0
7.5
15
22.5
Glucose
Glucose : Xylose - 3:1
Glucose : Xylose - 1:1
Glucose : Xylose - 1:3
Acetic Acid
Propionic Acid

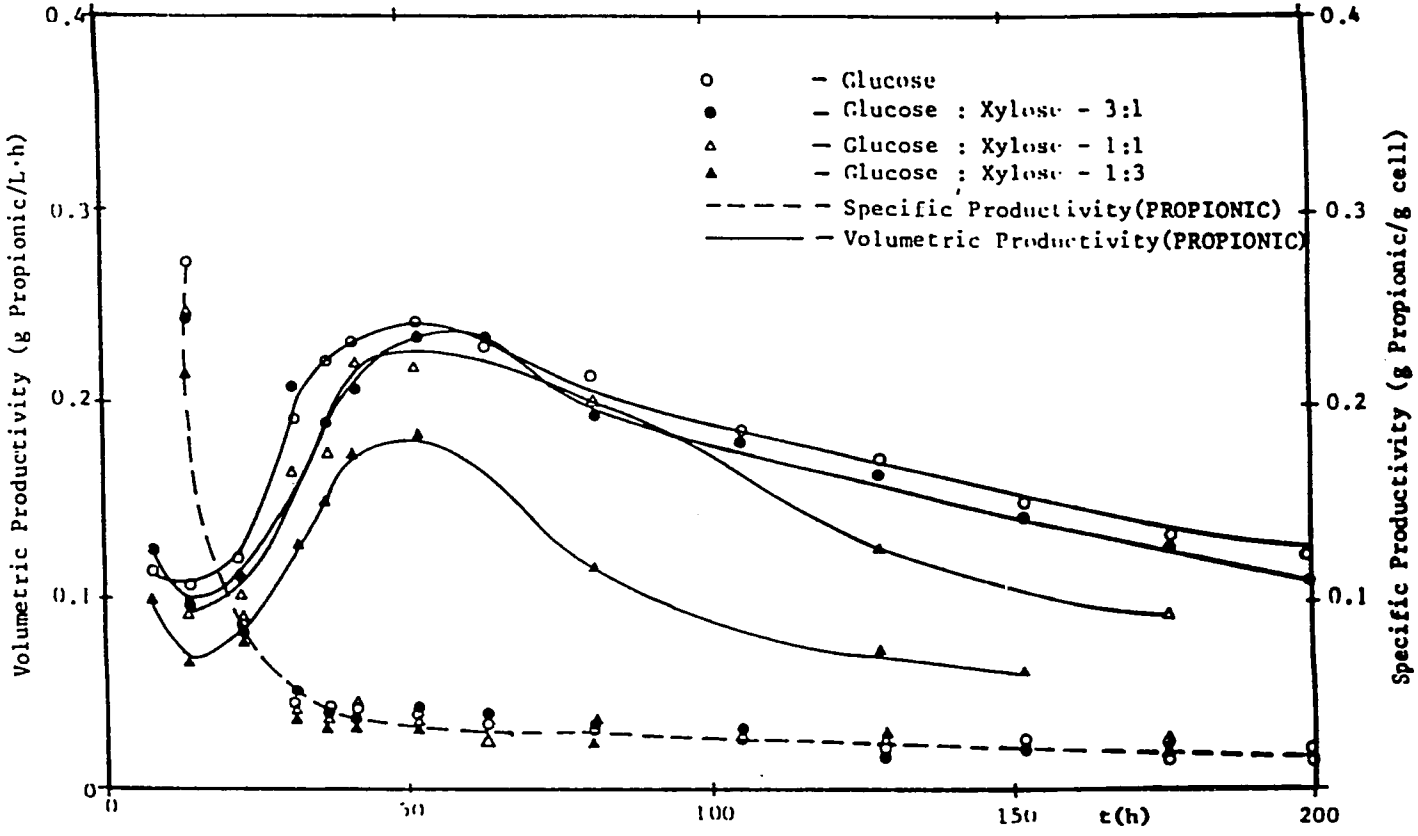
Volumetric Productivity (g Propionic/L·h)
Specific Productivity (g Propionic/g cell)
t(h)
0.4
0.3
0.2
0.1
0
50
100
150
200
○ – Glucose
● – Glucose : Xylose - 3:1
△ – Glucose : Xylose - 1:1
▲ – Glucose : Xylose - 1:3
– – – – Specific Productivity(PROPIONIC)
——— Volumetric Productivity(PROPIONIC)

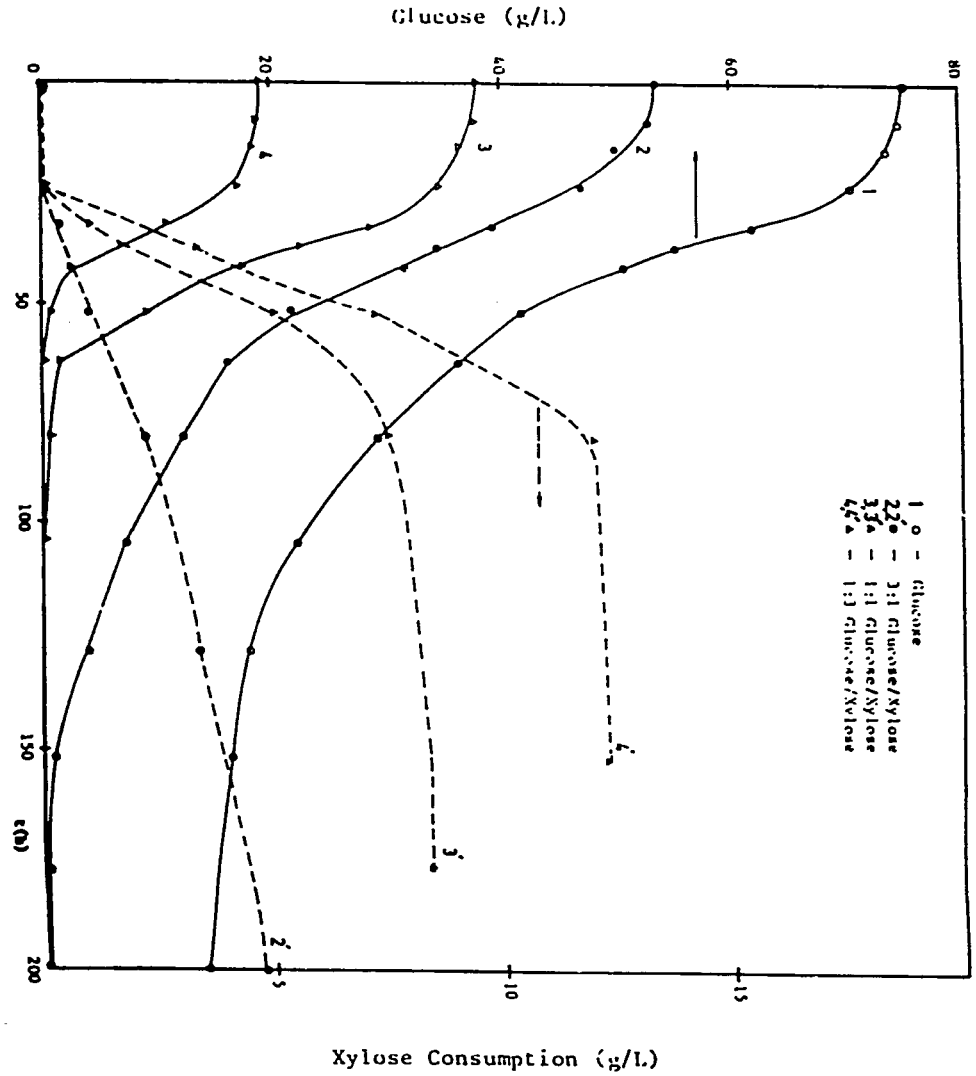
Glucose (g/L)
Xylose Consumption (g/L)
0
20
40
60
80
50
100
150
200
5
10
15
1 o - Glucose
2,2' - 3:1 Glucose/Xylose
3,3' - 1:1 Glucose/Xylose
4,4' - 1:3 Glucose/Xylose

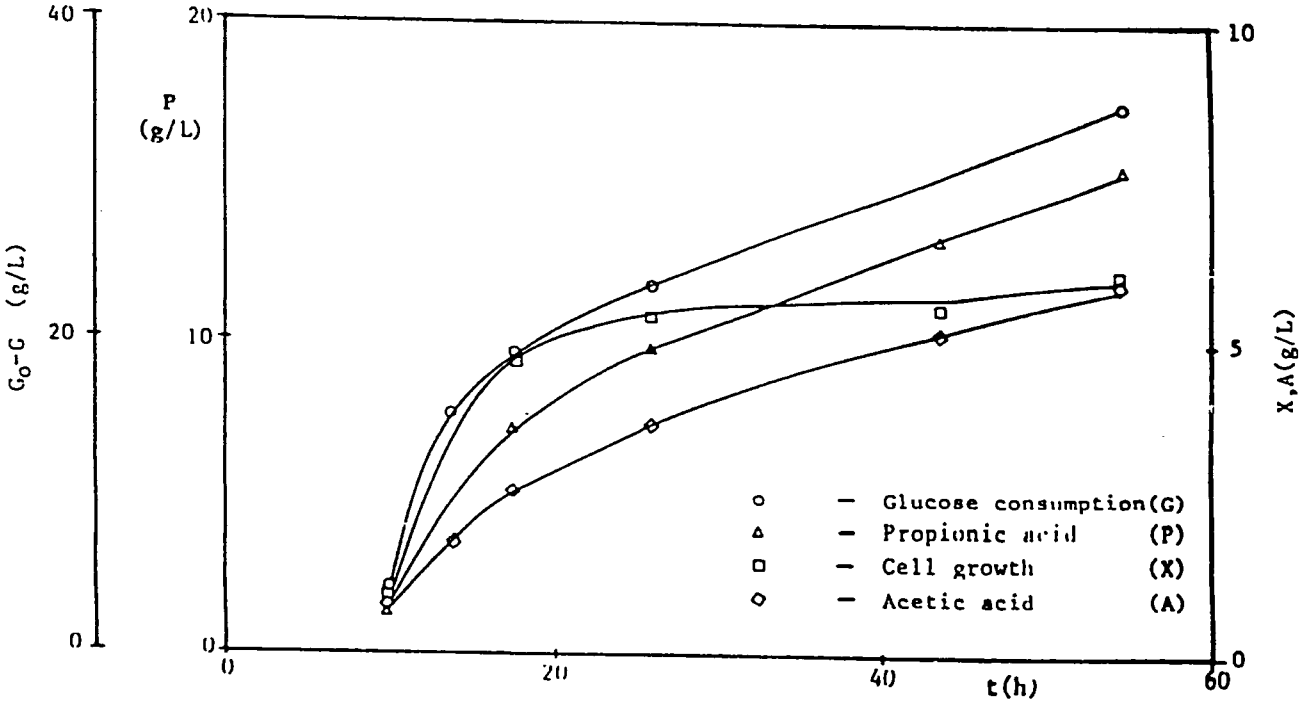
40
20
0
G_o-G (g/L)
20
10
0
P (g/L)
0
20
40
60
t(h)
10
5
0
X,A(g/L)
○ — Glucose consumption(G)
△ — Propionic acid (P)
□ — Cell growth (X)
◇ — Acetic acid (A)

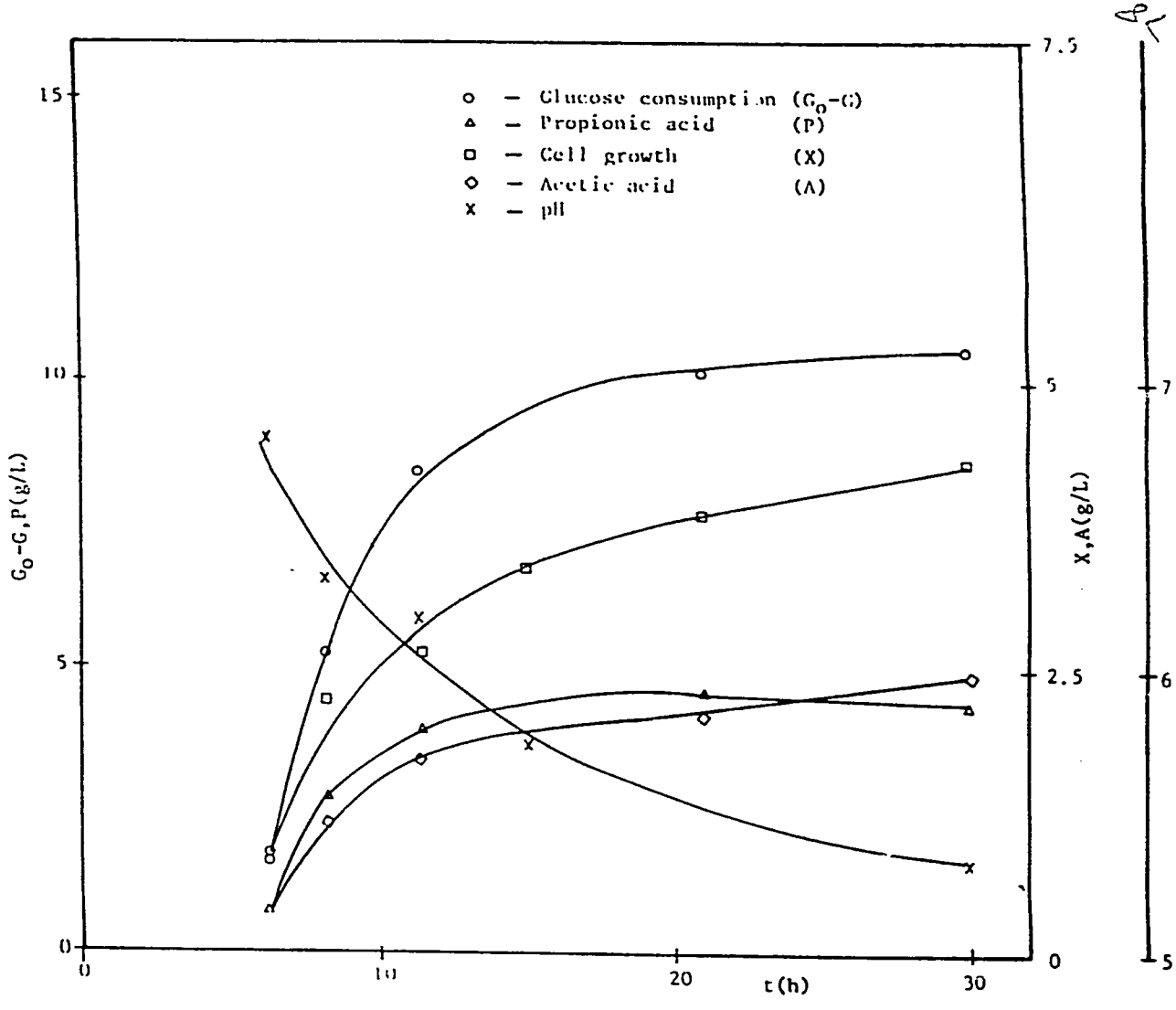
○ — Glucose consumption (G_o-G)
△ — Propionic acid (P)
□ — Cell growth (X)
◇ — Acetic acid (A)
× — pH
G_o-G, P(g/L)
X, A(g/L)
pH
t(h)
0
5
10
15
0
2.5
5
7.5
5
6
7
0
10
20
30

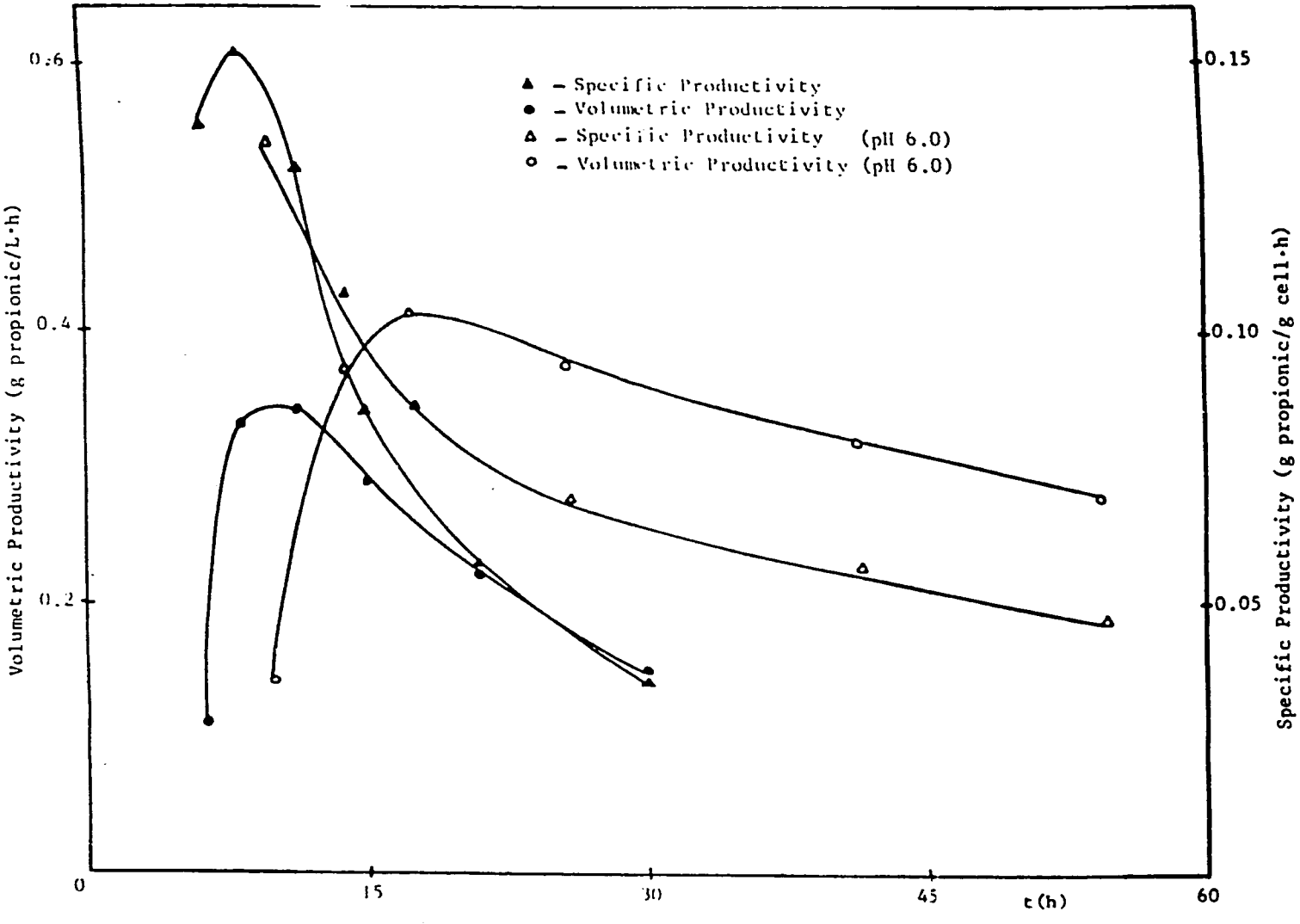
▲ – Specific Productivity
● – Volumetric Productivity
△ – Specific Productivity (pH 6.0)
○ – Volumetric Productivity (pH 6.0)
Volumetric Productivity (g propionic/L·h)
Specific Productivity (g propionic/g cell·h)
0.6
0.4
0.2
0
0.15
0.10
0.05
15
30
45
60
t(h)

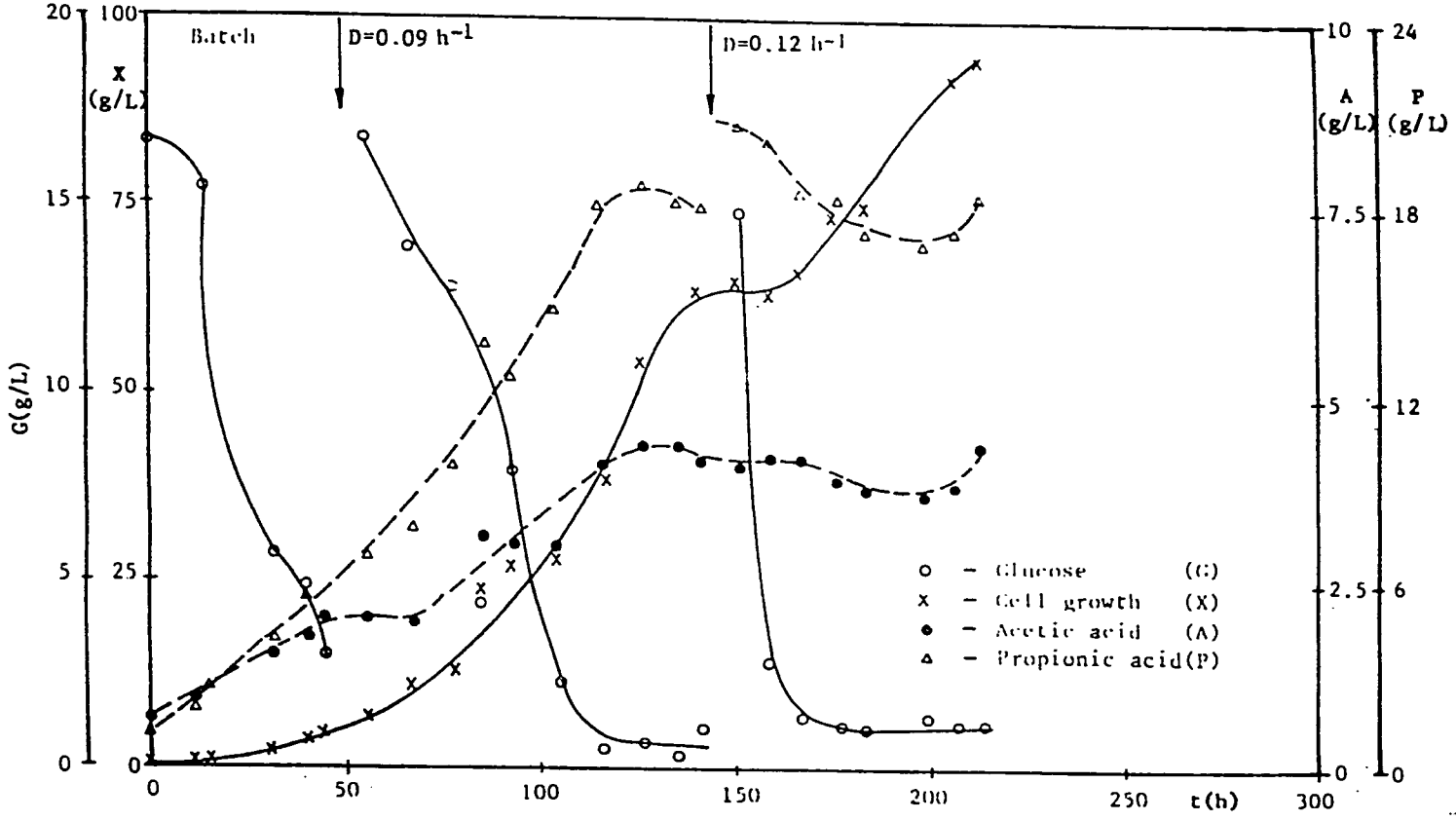
Batch
D=0.09 h-1
D=0.12 h-1
X (g/L)
G(g/L)
A (g/L)
P (g/L)
t(h)
- Glucose (G)
- Cell growth (X)
- Acetic acid (A)
- Propionic acid(P)

Apparent Viscosity (m Pa·s)
8
16
(1/S) X
50
100

SULFATE REDUCTION IN ACIDOGENIC PHASE ANAEROBIC DIGESTION

REIS, M.A.M., GONÇALVES, L.M.D., CARRONDO, M.J.T.
Laboratório de Eng.Bioquímica, Faculdade de Ciências e Tecnologia/UNL,
2825 MONTE DA CAPARICA, PORTUGAL.

ABSTRACT

Many industrial wastewaters present high sulfate contents; these may be anaerobically reduced to sulfides by sulfate reducing bacteria (SRB). The biogas produced from these wastewaters may be utilized for energy production provided it has a low sulfide content or else hydrogen sulfide may be stripped of the gas. Nevertheless if high soluble sulfide concentration exists, the methanogenic bacteria will be inhibited; further methanogenesis inhibition in the presence of SRB may result from kinetic competition for substrates (acetate and hydrogen) and thermodynamic effects.The competition between the SRB and methanogenic bacterial groups in different habitats has been studied latelly (1,2,3).

Thus, for wastewaters containing high concentrations of sulfur reduceable compounds there is a need to remove much or all of the sulfur prior to methanogenesis. The authors are thus studying the reduction of sulfate contents in the acidogenic phase of a phase separated anaerobic digestion process. The acidogenic phase is studied at different pH values in the range 5.8-6.6 and at different hidraulic retention times (HRT). At the selected pH range the acidogenic bacteria exhibit good activity whereas the SRB can be active although probably not growing at pH close to 6 (4). The soluble sulfides formed are precipitated at the outlet of the acidogenic reactor resulting in a feed to the methanogenic reactor mainly composed of organic volatile acids. The biogas produced under these conditions presents low contents of hydrogen sulfide.

The study of the acidogenic phase is done in two different reactors - an upflow fixed film fixed bed reactor and a continuous stirred reactor (CSTR). The support for the films is made up of Raschig rings of syntherised glass produced by Schott Mainz, FRG: 7 mm size, 60 to 100 μm pore size for the acidogenic phase and 12 mm size, 60:300 μm pore size for the methanogenic phase (5).

The CSTR, wich allows a better pH control, is used as reference to the former where pH control is problematic due to its plug flow characteristics. This reactor type might fail at low pH's since the SRB are probably no longer reproducing themselves and cannot attach as in the fixed film reactor.

The effluent used is cane sugar distillery molasses slops containing about 5.5 g$SO_4^{=}$/l. Preliminary results for a HRT of just under 3 days in the acidogenic reactor indicate sulfate reduction in excess of 80% was achieved at pH value of 6.6. Under these conditions the gas produced in the acidogenic reactor has a H_2S content of about 8% and the soluble sulfide concentration prior to precipitation aproximates 30 mg/l, out of the range of toxic levels for methanogenic bacteria (6); Once sulfide is removed from the gas, this still has 16% methane the rest being mainly CO_2. The acid concentrations are, aproximately, 8.5 g/l for acetic, 0.7 g/l for propionic and 7 g/l for butyric acids.

REFERENCES

1- Robinson, J.A., Tiedje, J.M. Competition between sulfate reducing and methanogenic bacteria for H_2 under resting and growing conditions. Arch. Microbiol., 137, 26, 1984.

2- Schonheil, P. Kristjansson, J.K., Thauer, R.K. Kinetic mechanism for the ability of sulfate reducers to out-compete methanogenic for acetate. Arch. Microbiol., 132, 285, 1982.

3- Koepp, H.J. Schoberth, S.M., Saham, H. Anaerobic treatment os waste water frgm citric acid production. Conservation & Recycling, 8(1/2), 211, 1985.

4- Widdell, F. Microbiology and ecology of sulfate and sulfur-reducing bacteria. Environmental Microbiology of Anaerobes. A.J.B. Zenhder,Ed., John Wiley and Sons (in press).

5- Arvasidis A. Anaerobic treatment of sulfite evaporation condensate in a fixed bed loop reactor. Wat.Sci.Tech., 17, 207, 1985.

6- Speece, R.E. Anaerobic biotechnology for industrial wastewater treatment. Environ.Sci.Technol., 17 (9), 416A, 1983.

UNIVERSITY OF CALIFORNIA, BERKELEY

BERKELEY • DAVIS • IRVINE • LOS ANGELES • RIVERSIDE • SAN DIEGO • SAN FRANCISCO

SANTA BARBARA • SANTA CRUZ

CIVIL ENGINEERING

BERKELEY, CALIFORNIA 94720

June 15, 1987

Manuel J. T. Carrondo, Ph.D.
Laboratório de Eng. Bioquímica
Faculdade de Ciéncias e Tecnologia
Universidade Nova de Lisboa
2825 Monte da Caparica
Portugal

Dear Professor Carrondo:

Your abstract entitled "Sulfate reduction in acidogenic phase anaerobic digestion" has been accepted for a platform presentation at the **IAWPRC Specialized Conference on the Microbiology of Waters and Wastewaters** in Newport Beach, California, USA, February 8-11, 1988.

Enclosed in this letter is a copy of the **Instructions for Authors and Typists**. Please follow these instructions carefully. The laysheets for typing your paper are also enclosed.

In addition to the enclosed instructions, please note the following:

1. Papers must be typed and presented in English.

2. Papers must not exceed approximately 3500 words or seven pages in length (including all tables, diagrams, etc.). Absolutely no exceptions can be made to length limitations. We have had to impose these very strict limitations because of the large number of posters and papers being presented.

3. Submit the original and two copies, together with the originals and two copies of any photographs, graphs and line drawings, etc., to, to David Jenkins, Chair, IAWPRC Scientific Program Committee, Dept. of Civil Engineering, 607 Davis Hall, University of California, Berkeley, CA 94720, USA, Telephone (415) 642-5337.

4. The **DEADLINE** for receipt of completed manuscripts is November 15, 1987. Manuscripts received after this date cannot be included in the volume of preprints that will be handed out to Conference registrants.

46

5. Authors must be present in person to present their paper and must pay for their own travel and subsistence expenses and the full Conference registration fee. You will have 20 minutes to present your paper; this will be followed by a 10 minute discussion period. Please indicate on the enclosed sheet your visual aids needs. Also, please indicate on the enclosed sheet the requested biographical information.

A Conference brochure giving details of the program, the venue, accommodation and registration will be mailed to you in the near future.

Thank you for your support and interest in what we feel will be an outstanding Conference.

Yours sincerely,

David Jenkins, Chair
Scientific Program Committee

DJ:nan
Enclosures

Vol. 141, No. 3, 1986
December 30, 1986

BIOCHEMICAL AND BIOPHYSICAL RESEARCH COMMUNICATIONS
Pages 1032-1041

LOW-SPIN SULFITE REDUCTASES: A NEW HOMOLOGOUS GROUP OF NON-HEME IRON-SIROHEME PROTEINS IN ANAEROBIC BACTERIA

I. Moura*, A.R. Lino*, J.J.G. Moura*, A.V. Xavier*, G. Fauque**+, H.D. Peck, Jr.+, and J. LeGall**+

*Centro de Quimica Estrutural, Complexo I, UNL, Av. Rovisco Pais, 1000 Lisboa, PORTUGAL

**A.R.B.S., E.C.E., CEN-Cada-rache, 13108 Saint Paul Lez Durance Cedex, FRANCE

+Department of Biochemistry, School of Chemical Sciences, University of Georgia, Athens, Ga 30602

Received October 29, 1986

SUMMARY: Two new low molecular weight proteins with sulfite reductase activity, isolated from Methanosarcina barkeri (DSM 800) and Desulfuromonas acetoxidans (strain 5071), were studied by EPR and optical spectroscopic techniques. Both proteins have visible spectra similar to that of the low-spin sulfite reductase of Desulfovibrio vulgaris strain Hildenborough and no band at 715 nm, characteristic of high-spin Fe^{3+} complexes in isobacteriochlorins is observed. EPR shows that as isolated the siroheme is in a low-spin ferric state (S=1/2) with g-values at 2.40, 2.30 and 1.88 for the Methanosarcina barkeri enzyme and g-values at 2.44, 2.33 and 1.81 for the Desulfuromonas acetoxidans enzyme. Chemical nnalysis shows that both proteins contain one siroheme and one $[Fe_4S_4]$ center per polypeptidic chain. These results suggest that the low molecular weight, low-spin non-heme iron siroheme proteins represent a new homologous class of sulfite reductases common to annerobic microorganisms.

Sulfite reductase catalyses the six-electron reduction of SO_3^{2-} to S^{2-}. This enzyme contains a novel type of iron tetrahydroporphyrin prosthetic group, termed siroheme, in addition to non-heme iron. Based on the physiological function, two types of sulfite reductase can be defined: i) the assimilatory type, which is involved in the synthesis of sulfur containing compounds and ii) the dissimilatory one, which participates in the respiratory pathway for sulfate reduction of sulfate-reducing bacteria. Enzymes resembling

0006-291X/86 $1.50

dissimilatory sulfite reductases are also found in photosynthetic bacteria (1) and Thiobacilli (2).

One characteristic of the dissimilatory sulfite reductases is the fact that under certain assay conditions, in addition to sulfide, trithionate and thiosulfate are irreversibly produced (3,4). The assimilatory type can catalyze the six electron reduction without the formation of free intermediates (5,6). Two types of dissimilatory sulfite reductases are found in Desulfovibrio species: desulfoviridin, with major absorption peaks at 580 and 628 nm (7) and desulforubidin, with major absorption peaks at 545 and 580 nm (8). In these enzymes the siroheme is in a high spin ferric state (S = 5/2) (9). A new type of dissimilatory sulfite reductase, desulfofuscidin, is present in a extreme thermophilic sulfate reducing bacteria, Thermodesulfobacterium commune (10) and in Desulfovibrio (D.) thermophilus (11).

From D. vulgaris (strain Hildenborough) both a dissimilatory as well as an assimilatory type of sulfite reductase were purified (12). The dissimilatory sulfite reductase, desulfoviridin, has a large molecular mass (226,000 Da) and is a tetramer. The assimilatory type sulfite reductase is a smaller molecular mass enzyme (27,200 Da). Its optical spectrum exhibits maxima at 590, 545 and 405 nm (12) EPR and Mossbauer studies show that in this protein as purified the siroheme is in a low-spin ferric state (13). The purification of a sulfite reductase from Methanosarcina (M.) barkeri (DSM 800) was previously reported (14). Its optical spectrum exhibits maxima at 590, 545 and 395 nm which are similar to the assimilatory sulfite reductase purified from D. vulgaris (strain Hildenborough).

This article reports the characterization of this protein by optical and EPR spectroscopies, together with its chemical

analysis. It also describes the isolation of a similar sulfite reductase from a sulfur-reducing organism Desulfuromonas (Drm.) acetoxidans. Our observations suggest that these low molecular weight, low-spin sulfite reductases represent a new class of non-heme iron-siroheme proteins common to anaerobic bacteria.

METHODS

Growth of the Microorganisms and Preparation of the Crude Extract

M. barkeri (DSM 800) - The bacteria were grown at 37°C in a methanol containing medium as previously described (15). The cells were suspended in 10 mM Tris-HCl buffer pH 7.6; DNase was added and the extract was prepared using a French press at 62 MPa under N_2 atmosphere. The extract was centrifuged at 12,000 rpm for 30 min. and the supernatant constituted the crude cell extract.

Drm. acetoxidans (strain 5071)- The bacteria were grown at 37°C in a basal salt medium containing 0.05% ethanol and 0.2% DL-sodium malate according to Pfennig and Biebl (16). The crude extract of Drm. acetoxidans was prepared in the same way as for M. barkeri (DSM 800).

Enzymes Purification

All the purification procedure was carried out at 0 - 4°C. Tris-HCl or phosphate buffers (pH 7.6) at appropriate molarities were used.

M. barkeri (DSM 800) sulfite reductase.

The sulfite reductase (P_{590}) was isolated from M.barkeri as previously described (14). An additional step of purification was performed on a DEAE-biogel column after which the protein presented a ratio A_{280}/A_{590} = 3.8.

Drm. acetoxidans (strain 5071) sulfite reductase

The crude extract was adsorbed on a DEAE-biogel A column (5 x 60 cm) equilibrated with 10 mM Tris-HCl. After elution with a continuous gradient of Tris-HCl buffer (10 mM up to 500 mM) three main fractions of the eluted proteins were obtained. The first fraction contained mainly cytochrome c_7 (17). The second fraction, also containing mainly cytochromes was applied on a DEAE-52 column (4 x 50 cm). The same gradient was performed and the fraction coming out between 0.25 M and 0.35 M presented an absorption peak in the visible spectrum at 590 nm. This fraction was dialized overnight against distilled water and readsorbed on a DEAE-biogel A column (3 x 34 cm). A continuous gradient of Tris-HCl buffer (10 mM up to 350 mM) was performed. A good separation from the cytochromes present at this stage was obtained. The eluted enzyme was concentrated on a Diaflo apparatus using a YM 10 membrane and applied on a hydroxylapatite (Bio-Rad) column (1.5 x 15 cm) equilibrated with 0.25 M Tris-HCl buffer. The column was washed with a descending gradient to bring down the Tris concentration to 0.01 M. A continuous gradient of potassium phosphate (10 mM up to 500 mM) was then applied for elution. Sulfite reductase was eluted out at about 0.25 M. The eluted enzyme was diluted

twice with distilled water and adsorbed on a DEAE-biogel A column (2x15 cm) and a linear gradient of Tris-HCl (10 mM up to 350 mM) was applied for elution. The purified protein was then concentrated in a Diaflo apparatus using a YM 10 membrane. The A_{280}/A_{590} ratio was 9.5. No further attempt of purification was done since at this stage only approximately 2 mg of protein were obtained.

Assays and Spectroscopic Measurements

Molecular masses were estimated by analytical SDS gel electrophoresis (18) on 7.5% polyacrylamide gels in the presence of mercaptoethanol, using the following molecular mass standards (Da): bovine serum albumine (66,000), ovalbumin (45,000), pepsin (34,000), trypsinogen (24,000) and α lactalbumin (14,000). Analytical gel electrophoresis was performed according to the method of Davis (19) on a 7% (v/v) gel at pH = 8.2. Protein determinations were done according to the Folin method (20). The siroheme content of P_{590} was analysed according to the method of Siegel et al. (21). Iron content was determined by plasma emission spectroscopy using a Jarrel Ash model 750 Atomcomp, and also by the 2,4,6-Tripyridyl S 1,3,5 Triazine method (22). Sulfite reductase activity of both enzymes was measured by a manometric assay as described by Schedel et al. (2). It requires the generation of reduced methyl viologen by an excess of hydrogenase activity under hydrogen atmosphere. The reduced dye then serves as electron donor to the reductase. The experimental conditions were conducted as previously described (14). [(1 unit (U) is the enzyme activity catalysing the consumption of 1 μmole H_2 per min. at 30°C)]. Colloidal sulfur reduction was followed by the Warburg respiratory method as previously described (23). Electron paramagnetic resonance spectroscopy (EPR) was carried out on a Bruker 200 tt spectrometer equiped with an ESR-9 flow cryostat (Oxford Instruments Co., Oxford, UK) equiped with a Nicolet 1180 computer. The visible/ultraviolet spectra were obtained on a spectrophotometer Beckman model 35.

RESULTS AND DISCUSSION

The purified sulfite reductase from M. barkeri was judged to be homogeneous by polyacrilamide disc electrophoresis. Due to the very small amount obtained the sulfite reductase from Drm. acetoxidans was only purified until approximately 80% (according to electrophoresis). The molecular mass was determined to be 23,000 Da for the P_{590} from M.barkeri and 23,500 Da for the P_{590} from Drm. acetoxidans. The specific sulfite reductase activity measured at pH = 8.0 using pure periplasmic hydrogenase from D. gigas was 900 mU/mg of protein for the Drm. acetoxidans enzyme and 2790 mU/mg of protein for the M. barkeri enzyme. Drm. acetoxidans P590 is not able to

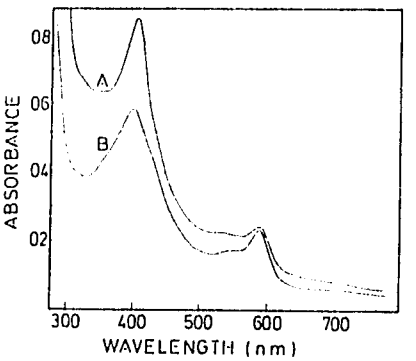

FIGURE 1

Visible absorption spectra of sulfite reductase from: (A) Drm. acetoxidans (0.25 mg/ml) (B) M.barkeri (0.24 mg/ml) in 50 mM Tris-HCl buffer, pH 7.6.

reduce colloidal sulfur to hydrogen sulfide even in presence of triheme c_7 from the same organism.

The optical spectra of both proteins are shown in Figure 1. As reported earlier the optical spectrum of M. barkeri P_{590} exhibits bands at 590, 545 and 395 nm (14). Sulfite reductase from Drm. acetoxidans exhibits bands at 587, 540 and 401 nm. The assimilatory sulfite reductase from D. vulgaris Hildenborough exhibits maxima at 590, 545 and 405 nm (12). These three sulfite reductases show very similar visible spectra. Another remarkable characteristic of these low molecular weight sulfite reductases is the fact that no band around 715 nm is present, as it is usually seen in other sulfite reductases; this band is characteristic of high-spin Fe^{3+} complexes of isobacteriochlorins (24). The lack of this band suggests that the siroheme is in a different spin state.

The ratio of total iron to siroheme was 5.2 for the M. barkeri enzyme and 5.3 for the Drm. acetoxidans one. Those results suggest the presence of a single siroheme and one $[Fe_4S_4]$ cluster in both enzymes.

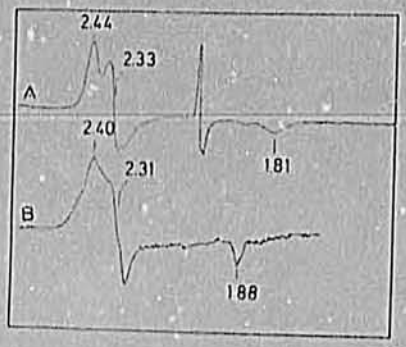

FIGURE 2

EPR spectra of sulfite reductase in the native state from: (A) Drm. acetoxidans enzyme. The protein concentration is 54 μM in 50 mM Tris-HCl buffer, pH 7.6. (A small signal at g~2 is observed, probably due to some paramagnetic impurity).
Experimental conditions: microwave power, 2 mW; modulation amplitude, 1mT; temperature, 9 K; microwave frequency, 9.530 GHz; gain, 3.2 x 10^5
(B) M.barkeri enzyme. The protein concentration is 138 μM in 50 mM Tris-HCl buffer, pH 7.6.
Experimental conditions: microwave power, 20 mW; modulation amplitude, 1 mT; temperature, 5.8 K; microwave frequency, 9.396 GHz; gain, 1.6 x 10^5.

The EPR spectra of the M.barkeri and Drm.acetoxidans sulfite reductases are shown in Figure 2. Both EPR spectra are characteristic of low-spin ferriheme. The M.barkeri protein exhibits EPR signals with g-values at 2.40, 2.30 and 1.88. Spin quantitation of this EPR signal at 9.6 K yields a value of 0.8 spins/siroheme. Upon reduction by either dithionite or reduced methyl viologen an EPR silent state is obtained. However, after reaction with cyanide under reducing conditions (in the presence of methyl viologen) it orginates an EPR spectrum characteristic of a reduced [Fe_4S_4] center (Figure 3). This signal, observable below 16K with g values at 2.05, 1.93 and 1.91, accounts only for 0.1 spins/molecule. Thus, the redox potential of the iron-sulfur center must be very negative and is affected by the sixth axial ligand of the siroheme. This effect has also been observed for the Escherichia (E.) coli sulfite reductase hemoprotein subunit (25). Mössbauer

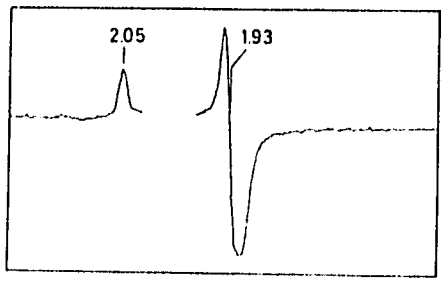

FIGURE 3

EPR spectrum of sulfite reductase from M.barkeri reacted with dithionite reduced methyl viologen in the presence of potassium cyanide (the region of g=2 is omitted due to the methyl viologen signal).
Experimental conditions: microwave power, 2 uW; modulation amplitude, 1 mT; temperature, 7.4 K; microwave frequency 9.390 GH_z; gain, 1.6 x 10^5.

studies of the E. coli enzyme (26) prove the existence of an exchange coupling between the heme and the $[Fe_4S_4]$ center. The sulfite reductase from Drm. acetoxidans also shows an EPR spectrum characteristic of low-spin ferriheme with g-values at 2.44, 2.33 and 1.81. Another low-spin species seems to be present with g-values at probably 2.42, 2.31 and 1.88. This assignment is tentative and is based on power saturation studies of the signal (not shown). Spin quantitation of the EPR signal at 9 K yields a value of 0.96 spins/siroheme. The native signal from M. barkeri enzyme seems also to contain more than one species since a shoulder in the g=2.40 signal can be detected at g=2.45, although no additional signal can be found in the high field region.

The fact that the siroheme in these two sulfite reductases is in the low-spin ferric state as was the case for the D.vulgaris Hildenborough assimilatory enzyme (13), is a unique feature. The siroheme of other sulfite reductases (25) is high-spin ferric. EPR studies on model complexes have shown that ferric isobacteriochlorins with a single axial ligand are

always high-spin while ferric isobacteriochlorins with two axial ligands are low-spin. Since in the two sulfite reductases studied here the siroheme is low-spin ferric, it could be six-coordinated.

Recently, EPR and Mössbauer studies on the low molecular weight sulfite reductase from D. vulgaris Hildenborough have shown that, as purified, the siroheme is low-spin ferric (S = 1/2) exhibiting EPR resonances at g = 2.44, 2.36 and 1.77 (13). Low-temperature Mössbauer spectra of D. vulgaris Hildenborough sulfite reductase recorded with weak and strong applied fields provided evidence for an exchange-coupled siroheme-$[Fe_4S_4]$ unit (13).

The sulfite reductases from M.barkeri and Drm.acetoxidans together with the assimilatory sulfite reductase from D.vulgaris Hildenborough belong to a new class of sulfite reductases and our results indicate that they may be common to anaerobic microorganisms. They all are small molecular weight proteins with one siroheme and one $[Fe_4S_4]$ center per polypeptide chain and in the native state their siroheme is low spin ferric. They also differ from the Desulfovibrio dissimilatory type of sulfite reductases, such as desulfoviridin, desulforubidin or desulfofuscidin by their much simpler oligomeric structure. In contrast to the E.coli type of assimilatory sulfite reductase, they do not appear to be part of a multiprotein complex. The physiological significance of this observation is not known and deserves further investigation. The term "assimilatory sulfite reductase" which is used to qualify this class of enzyme is not entirely satisfactory since these anaerobic bacteria should have sufficient sulfide at their disposal to cover their biosynthetic needs. As far as M.barkeri is concerned, it has already been suggested (14) that it could be used in a reverse

manner for the biosynthesis of coenzyme M which contains a sulfonate group. Regarding Drm. acetoxidans P590 we report in this article that it is not involved in the dissimilatory reduction of sulfur occuring in this organism.

ACKNOWLEDGEMENTS

We thank Instituto Nacional de Investigacao Cientifica e Tecnologica, Junta Nacional de Investigacao Cientifica e Tecnologica, (Portugal), Agency for International Development Grant n. 936-5542-G SS-4003-00 and NATO Grant RG 86/0172 (J.J.G.M) for financial support. We also thank Ms. I. Carvalho for skilful technical help and Mrs. M. Scandellari and Mr. R. Bourrelli for growing the bacteria which have been used in this study.

REFERENCES

1. Schedel, M, Vanselow, M. and Truper, H.G. (1979) Arch. Microbiol. 121, 29-36.
2. Schedel, M., LeGall, J and Baldensperger, J. (1975) Arch. Microbiol. 105, 339-341.
3. Akagi, J.M., (1981) Dissimilatory sulfate reduction: Mechanistic aspects in "Biology of Inorganic Nitrogen and Sulfur" Bothe, H. and Trebst, A.Eds., pp. 169-177. Berlin: Springer - Verlag
4. Lee, J.P. and Peck, Jr., H.D. (1971) Biochem. Biophys. Res. Commun. 45, 583-589.
5. Siegel, L.M. and Kamin, H. (1968) in "Flavins and Flavoproteins" (Yagi, K. ed.) pp. 15-40, Univ. Park. Press, Baltimore.
6. Prabhakararao, K. and Nicholas, D.J.D. (1969) Biochim. Biophys. Acta. 180, 253-263.
7. Lee, J.P. and Peck, Jr., H.D. (1971) Biochem. Biophys. Res. Commun. 45, 585-589.
8. Lee, J.P., Yi, C.S., LeGall, J., Peck, Jr., H.D. (1973) J. Bacteriol. 115, 453-455.
9. Liu, C.L., DerVartanian, D.V. and Peck, Jr., H.D., (1979) Biochem. Biophys.Res. Commun. 91, 962-970.
10. Hatchikian, E.C. and Zeikus, J.C. (1983), J. Bacteriol. 153, 1211-1220.
11. Pauque, G.D., Czechowski, M.H., Kang, L., DerVartanian, D.V. and LeGall, J. (1986) Abstr. Annu. Meet. Am. Soc. Microbiol., K50, p.201.
12. Lee, J.P., LeGall, J. and Peck, Jr. H.D. (1973), J. Bacteriol. 115, 529-542.
13. Huynh, B.H., Kang, L., DerVartanian, D.V., Peck, Jr., H.D. and LeGall, J. (1984) J. Biol. Chem. 259, 15373-15376.
14. Moura, J.J.G., Moura, I., Santos, H., Xavier, A.V., Scandellari, M. and LeGall, J. (1982). Biochem. Biophys. Res. Commun. 108, 1002-1009.
15. Blaylock, B.A. and Stadtman, T.C. (1966) Arch. Biochem. Biophys. 116, 138-158.
16. Pfennig, N. and Biebl, H. (1976), Arch. Microbiol. 110, 1-12.
17. Probst I, Bruschi, M., Pfennig, N., and LeGall J., (1977) Biochim. Biophys. Acta. 460, 58-64.

18. Weber, K and Osborn, M. (1969) J. Biol. Chem. 244, 4406-4412.
19. Davis, B.J. (1964) Ann. N.Y. Acad. Sci. 121, 404-427.
20. Lowry, O.H., Rosebrough, N.Y., Fan, A.L. and Randall, R.J. (1951) J. Biol. Chem. 193, 265-275.
21. Siegel, L.M., Murphy, M.J. and Kamin, H. (1978) Methods. Enzymol. 52, 436-447.
22. Fisher, D.S. and Price, D.C. (1964) Clin. Chem. 10, 21-25.
23 Fauque, G., Herve, D. and LeGall, J. (1979) Arch. Microbiol. 121, 261-264.
24. Stolzenbach, A.M., Strauss, S.H. and Holm, R.H. (1981) J.Am.Chem.Soc. 103, 4763-4778.
25. Siegel, L.M., Rueger, D.C., Barber, M.J., Krueger, R.J., Orme-Jonhson, N.R. and Orme Jonhson, W.H. (1982) J.Biol. Chem. 257, 6343-6350.
26. Christner, J.A., Munck, E., Janick, P.A. and Siegel, L.M. (1983), J.Biol.Chem. 258, 11147-11156.

THE JOURNAL OF BIOLOGICAL CHEMISTRY

Vol. 262, No. 2, Issue of January 15, pp. 795-800, 1987
Printed in U.S.A.

On the Active Sites of the [NiFe] Hydrogenase from *Desulfovibrio gigas*

MÖSSBAUER AND REDOX-TITRATION STUDIES*

(Received for publication, April 14, 1986)

Boi Hanh Huynh and Daulat S. Patil

From the Department of Physics, Emory University, Atlanta, Georgia 30322

Isabel Moura, Miguel Teixeira, and José J. G. Moura

From the Centro de Quimica Estrutural, Universidade Nova de Lisboa, 1000 Lisboa, Portugal

Daniel V. DerVartanian, Melvin H. Czechowski, Benet C. Prickril, Harry D. Peck, Jr., and Jean LeGall

From the Department of Biochemistry, School of Chemical Sciences, University of Georgia, Athens, Georgia 30602

The [NiFe] hydrogenase isolated from *Desulfovibrio gigas* was poised at different redox potentials and studied by Mössbauer spectroscopy. The data firmly establish that this hydrogenase contains four prosthetic groups: one nickel center, one [3Fe-*x*S], and two [4Fe-4S] clusters. In the native enzyme, both the nickel and the [3Fe-*x*S] cluster are EPR-active. At low temperature (4.2 K), the [3Fe-*x*S] cluster exhibits a paramagnetic Mössbauer spectrum typical for oxidized [3Fe-*x*S] clusters. At higher temperatures (>20 K), the paramagnetic spectrum collapses into a quadrupole doublet with parameters $|\Delta E_Q| = 0.7 \pm 0.06$ mm/s and $\delta = 0.36 \pm 0.06$ mm/s, typical of high-spin Fe(III). The observed isomer shift is slightly larger than those observed for the three-iron clusters in *D. gigas* ferredoxin II (Huynh, B. H., Moura, J. J. G., Moura, I., Kent, T. A., LeGall, J., Xavier, A. V., and Münck, E. (1980) *J. Biol. Chem.* 255, 3242–3244) and in *Azotobacter vinelandii* ferredoxin I (Emptage, M. H., Kent, T. A., Huynh, B. H., Rawlings, J., Orme-Johnson, W. H., and Münck, E. (1980) *J. Biol. Chem.* 255, 1793–1796) and may indicate a different iron coordination environment.

When *D. gigas* hydrogenase is poised at potentials lower than −80 mV (*versus* normal hydrogen electrode), the [3Fe-*x*S] cluster is reduced and becomes EPR-silent. The Mössbauer data indicate that the reduced [3Fe-*x*S] cluster remains intact, *i.e.* it does not interconvert into a [4Fe-4S] cluster. Also, the electronic properties of the reduced [3Fe-*x*S] cluster suggest that it is magnetically isolated from the other paramagnetic centers.

Hydrogenase catalyzes one of the most fundamental oxidation-reduction processes, namely the activation of molecular hydrogen. Over the past decade, physical and biochemical techniques have been applied extensively to the study of hydrogenase (1–17, 19–23). It is now evident that hydrogenases may be grouped into two general categories: 1) the [NiFe] hydrogenases, which contain both nickel and [Fe-S] clusters, found in *Chromatium vinosum* (DSM 185) (1), *Desulfovibrio baculatus* (ATCC 9974) (2), *Desulfovibrio desulfuricans* (ATCC 27774 and Norway strains) (3, 4), *Desulfovibrio gigas* (NCIB 9332) (5–7), *Desulfovibrio multispirans* (8), *Desulfovibrio salexigens* (9), *Methanobacterium thermoautotrophicum* (Marburg and ΔH strains) (10, 11) and *Methanosarcina barkeri* (DSM 800) (12); and 2) the [Fe] hydrogenases, which contain only [Fe-S] clusters, found in *Clostridium pasteurianum* W5 (13), *Desulfovibrio vulgaris* (Hildenborough and Miyasaki F strains) (14, 15), and *Megasphaera elsdenii* (16). Some but not all of the [NiFe] hydrogenases contain selenium stoichiometric with nickel (2, 4, 9).

Because the discovery of nickel in purified enzymes was relatively recent (6, 10, 17), many current studies are centered around the [NiFe] hydrogenases (19–23). Based on the results of a series of systematic EPR studies, a working hypothesis for the mechanism of *D. gigas* hydrogenase has been proposed (19). As isolated, the enzyme is inactive and exhibits two distinct Ni(III) EPR signals: nickel signal A ($g = 2.31, 2.23, 2.02$), and nickel signal B ($g = 2.33, 2.16, 2.00$). The isolated enzyme also exhibits an isotropic signal at $g = 2.02$ attributed to a [3Fe-*x*S] cluster. In addition to the nickel center and the [3Fe-*x*S] cluster, the isolated enzyme was found to contain two $[4Fe\text{-}4S]^{2+}$ clusters as indicated by iron and sulfur determinations and preliminary Mössbauer measurements (5, 24). During anaerobic reoxidation, the intensity of nickel signal B increases, whereas that of nickel signal A decreases, suggesting that nickel signal A may represent an oxygenated species and nickel signal B a deoxygenated species. According to the working hypothesis, the oxygenated species goes through a slow activation process (1–2 h) in order to express full activity, whereas the deoxygenated species can be rapidly activated. During the activation process, both the isotropic $g = 2.02$ signal and the nickel signals A and B disappear; thus, the active enzyme is EPR-silent. The loss of the $g = 2.02$ signal was attributed to the reduction of the [3Fe-*x*S] cluster. The disappearance of the nickel signals was tentatively explained by assuming that one of the $[4Fe\text{-}4S]^{2+}$ clusters is reduced to the 1+ state and that the spin of the reduced cluster couples to the Ni(III) center, resulting in an EPR-silent state

* This study was supported by National Science Foundation Grant DMB 8415632 (to J. L., H. D. P., Jr., and D. V. D.), by Department of Energy Grant DE-A-509-79 ER10499 (to H. D. P., Jr.), by National Institutes of Health Grants AM01135 and GM32187 (to B. H. H.), and by Junta Nacional de Investigação Cientifica and Tecnologica (to J. J. G. M.). The costs of publication of this article were defrayed in part by the payment of page charges. This article must therefore be hereby marked "*advertisement*" in accordance with 18 U.S.C. Section 1734 solely to indicate this fact.

(19). This assumption is of particular importance since it permits the proposal of a mechanism where the nickel center operates between the Ni(III) and Ni(II) states during the catalytic cycle (19) and thus avoids the alternative suggestion of a chemically less plausible mechanism that requires the nickel center to cycle from Ni(III) to Ni(0) states (20, 22). This controversy has arisen because the oxidation state of nickel cannot be unambiguously assigned by EPR or extended x-ray absorption fine structure measurements.

In this paper, we present quantitative Mössbauer evidence, in conjunction with previous EPR measurements (5, 6, 19) that *D. gigas* hydrogenase contains one nickel center, one [3Fe-*x*S] cluster, and two [4Fe-4S] clusters. The Mössbauer data also indicate that *D. gigas* hydrogenase contains a [3Fe-*x*S] cluster that does not convert into a [4Fe-4S] cluster during redox cycling.

MATERIALS AND METHODS

Isotopic Labeled ^{57}Fe Cell Growth and Enzyme Purification—D. gigas cells were grown in a lactate/sulfate medium, and the hydrogenase was purified as previously described (25). For the growth of isotopically labeled cells, 200 mg of ^{57}Fe (enrichment 95%, New England Nuclear) were first dissolved in H_2SO_4 and then in HCl, neutralized, and added to 400 liters of medium. The protein concentration was estimated by the method of Lowry *et al.* (26). The hydrogenase activity was assayed by the hydrogen evolution procedure as described by Peck and Gest (27). The hydrogenase in 50 mM Tris-HCl (pH 7.2) with a specific activity of 370–400 μM H_2 evolved min^{-1} mg^{-1} was used in the experiments. Hydrogenases isolated from cells grown in medium containing naturally abundant ^{57}Fe (2.2%) and enriched in ^{57}Fe (>95% enrichment) were analyzed for metals by plasma emission spectroscopy. They were found to contain 10.6 g atoms of iron and 0.85 g atom of nickel and 10.2 g atoms of iron and 0.8 g atom of nickel, respectively.

Redox Potential Poising of the Enzyme—The redox potentials were measured using a platinum *versus* a calomel standard electrode and a titration assembly as described by Dutton (28). The cell was calibrated by the potentials of quinhydrone at pH 4 and 7 and equimolar solutions of the ferri/ferrocyanide couple. Calibrations were performed before and after each experiment. The redox vessel was equipped with a sampling head to which a Mossbauer cell and an EPR tube were attached. The system was kept anaerobic by constant purging of argon gas previously passed over a heated copper catalyst and through a sodium dithionite solution. After equilibration, samples were withdrawn with a gas-tight syringe and transferred to a Mossbauer cell and an EPR tube which were attached to the redox vessel and immediately frozen using liquid nitrogen.

The enzyme samples poised at different redox potentials were prepared by two procedures. 1) Using a sodium dithionite solution as the reductant, samples were poised at −80, −270, and −375 mV (*versus* normal hydrogen electrode) for Mossbauer and EPR spectroscopy. 2) The enzyme was initially purged with hydrogen gas for 2 h, and the potential was stabilized at −400 mV. Samples for Mossbauer and EPR studies were withdrawn and frozen. Argon was then introduced into the system through a controlled flow meter. By properly adjusting the H_2/argon ratio, different potentials can be stabilized. After stable equilibration, samples were withdrawn at −350 and −300 mV (*versus* normal hydrogen electrode) and frozen immediately.

The mediator dyes used (100 μM) in the titration were methyl viologen, benzyl viologen, diquat (1,1′-ethylene-2,2′-dipyridylium dibromide), indigo sulfonate, safranin T, phenosafranin, anthraquinone 2-sulfonate, and methylene blue. The potentials reported above have an estimated uncertainty of ±15 mV (28).

Spectroscopy—Both the EPR and the Mossbauer spectrometers have been described elsewhere (29).

RESULTS AND DISCUSSION

Enzyme as Purified (Native State)—Fig. 1 shows Mossbauer spectra of ^{57}Fe-enriched hydrogenase purified from *D. gigas*. The data were recorded at 4.2 K with a magnetic field of 50 mT[1] applied parallel (Fig. 1*A*) and perpendicular (Fig. 1*B*) to the γ-beam. The Mössbauer spectrum of *D. gigas* hydrogenase with naturally abundant ^{57}Fe has been published; however, the statistics of the spectrum were poor, and quantitative conclusions were difficult to obtain (5). The spectra shown in Fig. 1 clearly consist of two subspectral components: 1) a magnetic component extending from −2.5 to +3.0 mm/s, and 2) a quadrupole doublet with parameters (ΔE_Q = 1.05 mm/s and δ = 0.42 mm/s) characteristic of a $[4Fe\text{-}4S]^{2+}$ cluster (30). The quadrupole doublet accounts for approximately 70% of the total iron absorption. Since metal determination yields ~11 mol of iron/mol of enzyme (see "Materials and Methods"), 70% would indicate two [4Fe-4S] clusters/molecule of hydrogenase.

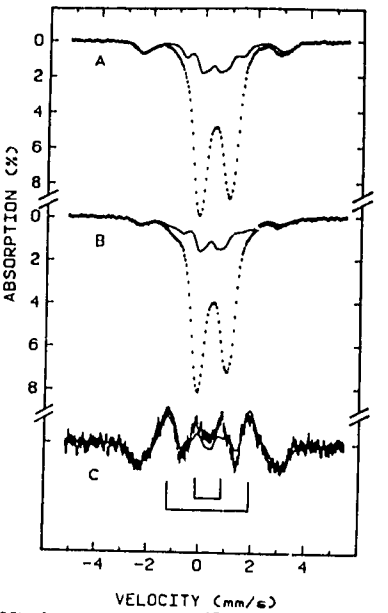

FIG. 1. **Mössbauer spectra of ^{57}Fe-enriched hydrogenase purified from *D. gigas*.** The data were recorded at 4.2 K with a magnetic field of 50 mT applied parallel (*A*) and perpendicular (*B*) to the γ-beam. The spectrum in *C* is a difference spectrum of spectra *A* and *B*. The *two brackets* indicate the two $\Delta m = 0$ nuclear transitions associated with the [3Fe-*x*S] cluster. The *solid lines* are simulated spectra using the parameters listed in Table I. Three-iron sites with different magnetic hyperfine coupling constants are assumed. The theoretical spectra in *A* and *B* are scaled to 27% of the total iron absorption.

The absorption pattern of the magnetic component depends strongly on the direction of the applied field, and a difference spectrum of spectra *A* and *B* in Fig. 1 reveals two pairs of nuclear $\Delta m = 0$ transitions (Fig. 1*C*). The observed isotropic g = 2.02 EPR signal together with the Mössbauer spectroscopic properties detected for this magnetic component, namely the total magnetic splitting (~5.5 mm/s), the absorption pattern, and the field direction dependence, are all typical for oxidized [3Fe-*x*S] clusters (31–33). At higher temperatures (>20 K), the electronic relaxation of the [3Fe-*x*S] cluster is fast and the magnetic component collapses into a sharp quadrupole doublet (full-width at half-maximum is less than 0.4 mm/s) with parameters $\Delta E_Q = 0.7 \pm 0.06$ mm/s and δ = 0.36 ± 0.06 mm/s typical of high-spin Fe(III). Consequently, the three-iron cluster in *D. gigas* hydrogenase is similar to the

[1] The abbreviations used are: T, tesla; Fd, ferredoxin.

three-iron clusters in *D. gigas* Fd II (32) and in *Azobacter vinelandii* Fd I (31) in the sense that it consists of three high-spin ferric ions which are spin-coupled to form an $S = 1/2$ system. However, the observed isomer shift for the *D. gigas* hydrogenase is somewhat larger, indicating that the iron coordination environment may be different. It is interesting to note that the isomer shift for the oxidized [3Fe-*x*S] cluster in *D. desulfuricans* hydrogenase was also found to be 0.36 mm/s (3).

In order to obtain a quantitative measure of the three-iron cluster in *D. gigas* hydrogenase, we analyzed the magnetic subspectral component using the following spin hamiltonian with $S = 1/2$.

$$\hat{H} = \beta\hat{S}\cdot\tilde{g}\cdot\hat{H} + \hat{S}\cdot\hat{A}\cdot\hat{I} + \frac{eQV_{zz}}{2}[3\hat{I}_z^2 - I(I+1) + \eta(\hat{I}_x^2 - \hat{I}_y^2)] - g_n\beta_n\hat{H}_n\cdot\hat{I} \quad (1)$$

Three-iron sites with different magnetic hyperfine coupling constants are assumed. The parameters used are listed in Table I, and the resulting theoretical spectra, scaled to 27% of the total iron absorption, are plotted in Fig. 1 (*solid lines*). The good agreement between experiment and theory indicates that *D. gigas* hydrogenase contains only one [3Fe-*x*S] cluster.

Intermediate Oxidation States—In order to follow the changes occurring in the nickel center and the iron clusters during the oxidation-reduction cycle, we poised the *D. gigas* hydrogenase at different redox potentials (see "Materials and Methods"). Samples thus prepared were then studied by Mössbauer and EPR spectroscopies. Fig. 2 shows the Mössbauer spectra of *D. gigas* hydrogenase poised at −80 mV. The data were recorded at 4.2 K in the absence of a magnetic field (Fig. 2*A*) and in the presence of a magnetic field of 50 mT applied parallel to the γ-beam (Fig. 2*B*). An EPR sample prepared simultaneously with the Mössbauer sample indicated that the intensity of the isotropic $g = 2.02$ signal had decreased to less than 10% of its initial intensity, whereas the nickel EPR signals changed little, suggesting that only the [3Fe-*x*S] cluster has been reduced. Without exception, all reduced [3Fe-*x*S] clusters studied so far (31–33) exhibit unique Mössbauer properties: in the absence of an applied field, the Mössbauer spectrum of a reduced [3Fe-*x*S] cluster consists of two sharp quadrupole doublets (labeled doublets I and II) of intensity ratio 2:1 with the more intense doublet having the larger quadrupole splitting. Both doublets are broadened substantially by the application of a magnetic field of a few tens of milli tesla. The reduced [3Fe-*x*S] cluster in *D. gigas* hydrogenase has similar properties; thus, in the absence of an applied field, only quadrupole doublets are observed (Fig. 2*A*), whereas in the presence of a weak applied field, a broad and featureless magnetic component is observed (Fig. 2*B*). This magnetic component is most apparent in the velocity regions from −2 to −1 mm/s and from +2 to +4 mm/s. To illustrate these unique properties, a difference spectrum of *spectra A* and *B* in Fig. 2 is shown in Fig. 2*C*. In such a difference spectrum, the contribution from the diamagnetic $[4Fe\text{-}4S]^{2+}$ clusters is canceled and the difference spectrum from the [3Fe-*x*S] cluster can be obtained. The two characteristic quadrupole doublets can then be identified. The observed Mössbauer parameters are listed in Table I and are compared with those of the reduced *D. gigas* Fd II (32). Again, we notice that the average isomer shift for the reduced cluster in hydrogenase is slightly larger than that in Fd II. As these two doublets can easily be broadened by a weak magnetic field, the fact that we observed them in the absence of an applied field strongly suggests that the reduced [3Fe-*x*S] cluster in *D. gigas* hydrogenase is magnetically isolated from other paramagnetic centers. By EPR, it was confirmed that the nickel center remains paramagnetic. Consequently, there is no spin-

TABLE I

Hyperfine parameters of the [3Fe-xS] cluster in hydrogenase and Fd II from D. gigas

	Oxidized					
	Hydrogenase[a]			Fd II[b]		
Iron site	1	2	3	1	2	3
δ (mm/s)	0.36 (6)[c]	0.36 (6)	0.36 (6)	0.27 (3)	0.27 (3)	0.27 (3)
ΔE_Q (mm/s)	−0.70 (6)	0.70(6)	0.70 (6)	0.54 (3)	0.54 (3)	0.54 (3)
η	0.2	0	0	1	1	1
$A_x/g_n\beta_n$ (T)	36.0	11.0	2.5	19.7	21.0	2.5
$A_y/g_n\beta_n$ (T)	28.0	11.0	2.5	32.0	11.5	2.5
$A_z/g_n\beta_n$ (T)	32.0	11.0	2.5	32.0	11.5	2.5
	Reduced[d]					
	Hydrogenase			Fd II[b]		
Iron site	I	II[e]		I	II	
δ (mm/s)	0.44 (4)	0.42 (4)		0.46 (2)	0.30 (2)	
ΔE_Q (mm/s)	1.73 (4)	0.30 (4)		1.47 (3)	0.47 (2)	
η	0.75	−2.0		0.37	−2.0	
$A_x/g_n\beta_n$ (T)	15.0	−6.8		16.0	−6.8	
$A_y/g_n\beta_n$ (T)	11.3	−12.7		12.0	−12.7	
$A_z/g_n\beta_n$ (T)	11.3	−12.7		12.0	−12.7	

[a] Due to the strong absorption of the [4Fe-4S] cluster, the spectrum of the oxidized [3Fe-*x*S] cluster in hydrogenase can not be resolved. Therefore, the magnetic hyperfine tensor A is assumed to be isotropic for iron site 2 and is undetermined for site 3. The value obtained for iron site 3 in Fd II is used for that in hydrogenase.

[b] From Ref. 31.

[c] The values in parentheses gave the uncertainties in the last significant digits.

[d] The zero-field splitting parameters ($D = -2.5$ cm^{-1} and $E/D = 0.22$) for the reduced [3Fe-*x*S] cluster and a set of Euler angles ($\alpha = 0$, $\beta = 20$, $\gamma = 0$) describing the electric field gradient tensor of doublet I relative to the electronic system were determined by a series of high-field measurements on the reduced Fd II. These parameters are assumed to be the same for the [3Fe-*x*S] cluster in hydrogenase.

[e] The magnetic hyperfine A-tensor obtained for doublet II of Fd II is used for that in hydrogenase. These parameters yield theoretical spectra in good agreement with experimental data recorded in applied magnetic fields up to 8 T.

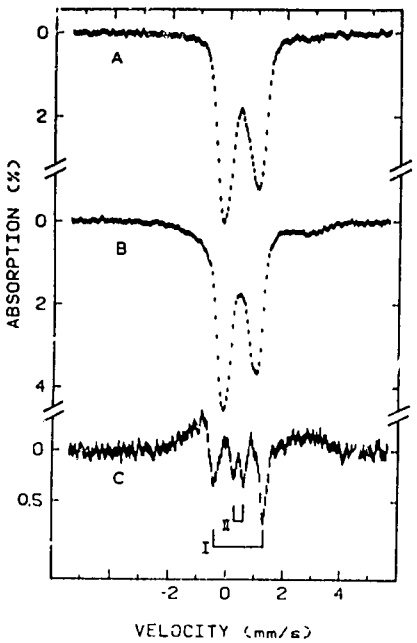

FIG. 2. **Mössbauer spectra of *D. gigas* hydrogenase poised at −80 mV.** The data were recorded at 4.2 K in the absence of a magnetic field (A) and in the presence of a field of 50 mT applied parallel to the γ-beam (*B*). The spectrum in *C* is a difference spectrum of spectra *A* and *B*. The *two brackets* mark the positions of the two quadrupole doublets I and II.

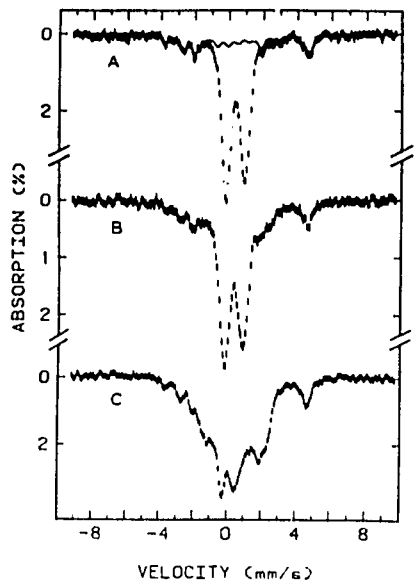

FIG. 3. **Mössbauer spectra of *D. gigas* hydrogenase poised at −80 mV (*A*), −270 mV (*B*), and −400 mV (*C*).** The data were recorded at 4.2 K with a magnetic field of 1 T applied parallel to the γ-beam. The *solid line* in *A* is a theoretical simulation of the reduced [3Fe-xS] cluster using the parameters listed in Table I. The theoretical spectrum is scaled to 27% of the total iron absorption. This distinct spectrum of the reduced [3Fe-xS] cluster is clearly recognizable in all three spectra, and its percent absorption remains constant, indicating that the [3Fe-xS] cluster does not convert into a [4Fe-4S] cluster under these reducing conditions.

spin interaction between the reduced [3Fe-xS] cluster and the Ni(III) center.

In Fig. 2 (*A* and *B*), it is shown that in zero or weak magnetic field the spectra of the reduced [3Fe-xS] and the $[4Fe\text{-}4S]^{2+}$ clusters overlap. The amount of the reduced [3Fe-xS] cluster in the sample is therefore difficult to determine; however, from previous studies (31, 32), we know that an applied field of 1 T would induce saturated magnetic hyperfine fields at the iron sites of the reduced [3Fe-xS] cluster. This would result in a spectrum with a total magnetic splitting of ~9 mm/s, whereas the spectrum arising from the diamagnetic $[4Fe\text{-}4S]^{2+}$ cluster would remain as a quadrupole doublet. These features are documented in the spectrum shown in Fig. 3*A*, which was recorded at 4.2 K with a field of 1 T. The magnetic spectrum of the [3Fe-xS] cluster is clearly discernible as three sharp peaks at the region between −4 and −2 mm/s and an intense absorption peak at +4.7 mm/s. The pattern of this magnetic spectrum is almost identical to that of the reduced *D. gigas* Fd II (32). With such a well-defined spectrum, we were able to analyze the data using a spin hamiltonian as expressed in Equation 1 with spin $S = 2$. Similar to *D. gigas* Fd II, the spectrum of the reduced [3Fe-xS] cluster in *D. gigas* hydrogenase can also be decomposed into two subcomponents with intensity ratio of 2:1. The two iron sites associated with doublet I were found to remain equivalent in magnetic fields up to 8 T. The solid curve in Fig. 3*A* is the result of a simulation. To obtain a good agreement with the experimental data, the theoretical spectrum was scaled to 27% of the total iron absorption. This suggests that the sample contains approximately one reduced [3Fe-xS] cluster/molecule of hydrogenase. The parameters used for the theoretical simulation are listed in Table I and are compared with those of *D. gigas* Fd II.

In Fig. 3 (*B* and *C*), Mössbauer spectra of *D. gigas* hydrogenase poised at −270 and −400 mV, respectively, are shown.[2] In order to resolve the subspectral components, the data were recorded at 4.2 K with an applied field of 1 T, and the characteristic spectrum of the reduced [3Fe-xS] cluster is observed in both spectra. Since the absorption peak at the velocity region around 4.7 mm/s is well-isolated from the rest of the spectrum, it can be used to quantitate the amount of reduced [3Fe-xS] cluster in the protein. We found that the contribution from the reduced [3Fe-xS] cluster is always approximately 27% of the total absorption when the sample

[2] The Mossbauer data of the −400 mV sample indicate that all the iron-sulfur clusters are reduced. At 160 K, the reduced [4Fe-4S] clusters exhibit a quadrupole doublet with parameters (ΔE_Q = 1.10 mm/s and δ = 0.47 mm/s) typical of a $[4Fe\text{-}4S]^{1+}$ cluster. A spectrum which represents the $[4Fe\text{-}4S]^{1+}$ clusters at 4.2 K can therefore be prepared by subtracting the contribution of the reduced [3Fe-xS] cluster from spectrum *C* in Fig. 3. Such a prepared spectrum can then be used to estimate the amount of absorption attributable to the reduced [4Fe-4S] cluster in protein poised at different redox potentials. In Fig. 3*B*, the paramagnetic subspectral component associated with the reduced [4Fe-4S] cluster is clearly observed at velocity region between −2 and +2 mm/s. Approximately 25% of the total absorption of spectrum *B* in Fig. 2 is attributable to the $[4Fe\text{-}4S]^{1+}$ cluster. This percentage yields an average of 0.7 $[4Fe\text{-}4S]^{1+}$ cluster/molecule in the −270 mV sample. It is interesting to note that the corresponding EPR sample exhibits a 70% reduction of the native nickel signal. No other signal is observed except a $g = 2.0$ radical signal arising from the redox mediators. Since the $[4Fe\text{-}4S]^{1+}$ cluster is a system containing an odd number of electrons, it generally yields a characteristic EPR signal. The fact that some of the [4Fe-4S] clusters are in the 1^+ state but do not exhibit a corresponding EPR signal needs further investigation. Further work is underway in order to clarify the situation.

is poised at potentials lower than −80 mV, indicating that the [3Fe-xS] cluster is present in the reduced form and does not convert into the [4Fe-4S] cluster.

The [3Fe-xS] cluster has been found in a variety of proteins including aconitase (33) and *D. gigas* Fd II (32). In *D. gigas* Fd II, the [3Fe-xS] cluster was shown to be easily converted into a [4Fe-4S] cluster under proper reducing conditions (34), whereas the activation of aconitase was shown to involve the transformation of the [3Fe-xS] cluster into a [4Fe-4S] cluster (35). Interconversion between the [3Fe-xS] cluster and the [4Fe-4S] cluster has also been suggested for hydrogenase purified from *C. vinosum* (36); however, the present Mössbauer study reveals unambiguously that the [3Fe-xS] cluster in *D. gigas* hydrogenase remains intact under reducing conditions and does not convert into the [4Fe-4S] cluster. This is the first quantitative evidence for the existence of a reduced [3Fe-xS] cluster in a catalytically active enzyme. Although the specific role of the [3Fe-xS] cluster in hydrogenase remains unknown, it is interesting to note that most of the [NiFe] hydrogenases purified from different organisms do exhibit the isotropic $g = 2.02$ EPR signal characteristic of [3Fe-xS] clusters (1-9, 12). Recently, magnetic circular dichroism studies of reconstituted succinate dehydrogenase have shown that a reduced [3Fe-xS] cluster is necessary (37). Unfortunately, it was difficult to draw a quantitative conclusion from the magnetic circular dichroism measurement.

CONCLUSIONS

The Mössbauer data of ^{57}Fe-enriched *D. gigas* hydrogenase presented in this paper together with our previous EPR studies (5, 6, 19) firmly establish that *D. gigas* hydrogenase contains one nickel center, one [3Fe-xS] cluster, and two [4Fe-4S] clusters. Similar prosthetic groups were also found in another [NiFe] hydrogenase isolated from *D. desulfuricans* (ATCC 27774) (3). Our Mössbauer studies of the *D. gigas* hydrogenase reduced under H_2 atmosphere or poised at different redox potentials demonstrate that the [3Fe-xS] cluster remains intact and does not convert into a [4Fe-4S] cluster during reduction of the enzyme. The presence of a reduced [3Fe-xS] cluster in the hydrogenase of *D. gigas* was also shown by magnetic circular dichroism studies (38). However, in the case of the [NiFe] hydrogenase from *C. vinosum*, the conversion of a [3Fe-xS] cluster into a [4Fe-4S] cluster has been correlated with the activation of this hydrogenase (18).

The reduced [3Fe-xS] cluster in *D. gigas* hydrogenase exhibits paramagnetic properties similar to that of the reduced [3Fe-xS] cluster in *D. gigas* Fd II, indicating that this cluster is not spin-coupled to another paramagnetic center. This observation suggests that the [3Fe-xS] cluster may be physically distant from the other centers.

The relatively recent discovery of nickel in purified enzymes has triggered numerous investigations aimed at revealing the function of nickel in biological systems. Since *D. gigas* hydrogenase contains both nickel and iron-sulfur clusters, it is an ideal system for studying the function and interplay between these two types of centers. Based on a series of EPR studies, we have proposed a working hypothesis for the mechanism of [NiFe] hydrogenase (19). The present studies have confirmed some of the assumptions made in this hypothesis, namely that the [3Fe-xS] cluster can be reduced, remains intact in the active enzyme, and is not magnetically interacting with other paramagnetic centers in the protein. However, many questions remain unanswered. Direct evidence for the existence of a nickel hydride species in *D. gigas* hydrogenase has not been found. The nature of the complex EPR signals of the reduced enzyme (19) remains unknown, and the role of the [3Fe-xS] cluster has not yet been clarified. A full understanding of the hydrogenase mechanism obviously cannot be reached until answers to these problems are obtained.

Acknowledgments—We thank Pat Kelly and Liesje DerVartanian for excellent technical assistance during preparation of the hydrogenase and EPR measurements, respectively. We thank Dr. Adrian Meagher for his assistance in the acquisition of Mössbauer data and the staff of the University of Georgia Fermentation Plant for growing the bacterial cells.

REFERENCES

1. Albracht, S. P. J., Van der Zwaan, J. W., and Fontijn, R. D. (1984) *Biochim. Biophys. Acta* **766**, 245-258
2. Teixeira, M., Moura, I., Xavier, A. V., Moura, J. J. G., Fauque, G., Pickril, B., and LeGall, J. (1985) *Rev. Port. Quim.* **27**, 194-195
3. Krüger, H.-J., Huynh, B. H., Ljungdahl, P. O., Xavier, A. V., DerVartanian, D. V., Moura, I., Peck, H. D., Jr., Teixeira, M., Moura, J. J. G., and LeGall, J. (1982) *J. Biol. Chem.* **257**, 14620-14623
4. Bell, S. H., Dickson, D. P. E., Rieder, R., Cammack, R., Patil, D. S., Hall, D. O., and Rao, K. K. (1984) *Eur. J. Biochem.* **145**, 645-651
5. Teixeira, M., Moura, I., Xavier, A. V., DerVartanian, D. V., LeGall, J., Peck, H. D., Jr., Huynh, B. H., and Moura, J. J. G. (1983) *Eur. J. Biochem.* **130**, 481-484
6. Moura, J. J. G., Moura, I., Huynh, B. H., Krüger, H.-J., Teixeira, M., DuVarney, R. C., DerVartanian, D. V., Xavier, A. V., Peck, H. D., Jr., and LeGall, J. (1982) *Biochem. Biophys. Res. Commun.* **108**, 1388-1393
7. Cammack, R., Patil, D. S., Aguirre, R., and Hatchikian, E. C. (1982) *FEBS Lett.* **142**, 289-292
8. Czechowski, M. H., He, S. H., Nacro, M., DerVartanian, D. V., Peck, H. D., Jr., and LeGall, J. (1984) *Biochem. Biophys. Res. Commun.* **125**, 1025-1032
9. Teixeira, M., Moura, I., Fauque, G., Czechowski, M. H., Berlier, Y., Lespinat, P. A., LeGall, J., Xavier, A. V., and Moura, J. J. G. (1986) *Biochimie (Paris)* **68**, 75-84
10. Albracht, S. P. J., Graft, E. G., and Thauer, R. K. (1982) *FEBS Lett.* **140**, 311-313
11. Kojima, N., Fox, J. A., Hausinger, R. P., Daniels, L., Orme-Johnson, W. H., and Walsh, C. (1983) *Proc. Natl. Acad. Sci. U. S. A.* **80**, 378-382
12. Fauque, G., Teixeira, M., Moura, I., Lespinat, P. A., Xavier, A. V., DerVartanian, D. V., Peck, H. D., Jr., LeGall, J., and Moura, J. J. G. (1984) *Eur. J. Biochem.* **142**, 21-28
13. Wang, G., Benecky, M. J., Huynh, B. H., Cline, J. F., Adams, M. W. W., Mortenson, L. E., Hoffman, B. M., and Münck, E. (1984) *J. Biol. Chem.* **259**, 14328-14331
14. Huynh, B. H., Czechowski, M. H., Krüger, H.-J., DerVartanian, D. V., Peck, H. D., Jr., and LeGall, J. (1984) *Proc. Natl. Acad. Sci. U. S. A.* **81**, 3728-3732
15. Yagi, T., Kimura, K., and Inokuchi, H. (1985) *J. Biochem. (Tokyo)* **97**, 181-187
16. Van Dijk, C., Grande, H. J., Mayhew, S. G., and Veeger, C. (1980) *Eur. J. Biochem* **107**, 251-261
17. Lancaster, R. (1982) *Science* **216**, 1324-1325
18. Albracht, S. P. J., Fontign, R. D., and Van der Zwaan, J. W. (1985) *Biochim. Biophys. Acta* **832**, 89-97
19. Teixeira, M., Moura, I., Xavier, A. V., Huynh, B. H., DerVartanian, D. V., Peck, H. D., Jr., LeGall, J., and Moura, J. J. G. (1985) *J. Biol. Chem.* **260**, 8942-8950
20. Cammack, R., Patil, D. S., and Fernandez, V. M. (1985) *Biochem. Soc. Trans.* **13**, 572-578
21. Mege, J.-M., and Bourdillon, C. (1985) *J. Biol. Chem.* **260**, 14701-14706
22. Van der Zwaan, J. W., Albracht, S. P. J., Fontijn, R. D., and Slater, E. C. (1985) *FEBS Lett.* **179**, 271-277
23. Lissolo, T., Pulvin, S., and Thomas, D. (1984) *J. Biol. Chem.* **259**, 11725-11729
24. Hatchikian, E. C., Bruschi, M., and LeGall, J. (1978) *Biochem. Biophys. Res. Commun.* **82**, 451-461
25. LeGall, J., Ljungdahl, P. O., Moura, I., Peck, H. D., Jr., Xavier, A. V., Moura, J. J. G., Teixeira, M., Huynh, B. H., and DerVartanian, D. V. (1982). *Biochem. Biophys. Res. Commun.* **106**, 610-616

26. Lowry, O. H., Rosebrough, N. J., Farr, A. L., and Randall, R. J. (1951) *J. Biol. Chem.* **193**, 265–275
27. Peck, H. D., Jr., and Gest, H. (1956) *J. Bacteriol.* **71**, 70–80
28. Dutton, P. L. (1978) *Methods Enzymol.* **54**, 411–434
29. Huynh, B. H., Liu, M. C., Moura, J. J. G., Moura, I., Ljungdahl, P. O., Münck, E., Payne, W. J., Peck, H. D., Jr., DerVartanian, D. V., and LeGall, J. (1982) *J. Biol. Chem.* **257**, 9576–9581
30. Middleton, P., Dickson, D. P. E., Johnson, C. E., and Rush, J. D. (1980) *Eur. J. Biochem.* **104**, 289–296
31. Emptage, M. H., Kent, T. A., Huynh, B. H., Rawlings, J., Orme-Johnson, W. H., and Münck, E. (1980) *J. Biol. Chem.* **255**, 1793–1796
32. Huynh, B. H., Moura, J. J. G., Moura, I., Kent, T. A., LeGall, J., Xavier, A. V., and Münck, E. (1980) *J. Biol. Chem.* **255**, 3242–3244
33. Kent, T. A., Dreyer, J.-L., Kennedy, M. C., Huynh, B. H., Emptage, M. H., Beinert, H., and Münck, E. (1982) *Proc. Natl. Acad. Sci. U. S. A.* **79**, 1096–1100
34. Moura, J. J. G., Moura, I., Kent, T. A., Lipscomb, J. D., Huynh, B. H., LeGall, J., Xavier, A. V., and Münck, E. (1982) *J. Biol. Chem.* **257**, 6259–6267
35. Kent, T. A., Emptage, M. H., Merkle, H., Kennedy, M. C., Beinert, H., and Münck, E. (1985) *J. Biol. Chem.* **260**, 6871–6881
36. Albracht, S. P. J., Kalkman, M. L., and Slater, E. C. (1983) *Biochim. Biophys. Acta* **724**, 309–316
37. Johnson, M. K., Moringstar, J. E., Bennett, D. E., Ackrell, B. A. C., and Kearney, E. B. (1985) *J. Biol. Chem.* **260**, 7368–7378
38. Johnson, M. K., Zambrano, I. C., Czechoski, M. H., Peck, H. D., Jr., DerVartanian, D. V., and LeGall, J. (1986) in *Frontiers in Bioinorganic Chemistry* (Xavier, A. V., ed) Vol. 6H, pp. 36–44, VCH Verlagsgesellschasd, Weinheim, Federal Republic of Germany

102

Iron-Sulfur Protein Research, eds. H. Matsubara et al., pp. 149–164 (1986).
Japan Sci. Soc. Press, Tokyo/Springer-Verlag, Berlin

Iron-Sulfur Cluster Interconversions

José J. G. MOURA

*Centro de Quimica Estrutural Complexo I, UNL**

The ferredoxin II (Fd II) from *Desulfovibrio* which contains a single [3Fe-4S] cluster serves as a model protein for quantitative studies of the three iron center and has been examined in considerable detail with a number of spectroscopic techniques (EPR, Mössbauer, EXAFS, MCD and Resonance Raman spectroscopies). The studies performed have revealed interesting properties of this structure, demonstrating the simultaneous existence of localized and delocalized valence states in the same cluster and the occurrence of facile interconversions between 3Fe and 4Fe clusters, as well as the possibility of specific isotopic labelling of a subsites of an iron-sulfur cluster.

DESULFOVIBRIO GIGAS FERREDOXINS

Desulfovibrio gigas ferredoxins (Fds) are isolated in different oligomeric forms (*6*). Ferredoxin II (Fd II) is a tetramer of four identical monomers, M_r 6.000. Each monomer consists of 57 amino acid residues, including six cysteinyl residues, of known sequence (*5*). Ferredoxin I (Fd I) is a trimer made up of the same monomers. These two forms differ drasti-

* Av. Rovisco Pais, 1000 Lisboa, Portugal.

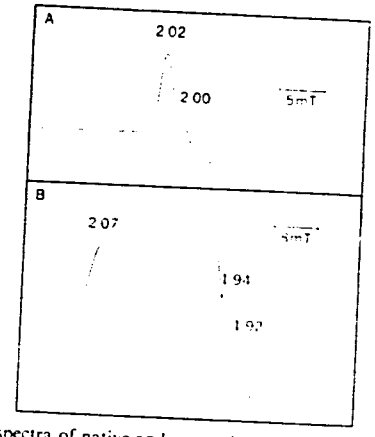

Fig. 1. X-band EPR spectra of native and reconstituted *D. gigas* Fd II.
A: native *D. gigas* Fd II (⁵⁶Fe) oxidized state recorded at 8K. B: reconstituted apoFd II (Fd_R), dithionite reduced state, recorded at 8K. Derivative of the absorption is plotted *versus* the magnetic induction.

cally in their optical, redox, and magnetic properties, and their physiological role (*6, 7, 21*).

In the oxidized state, Fd II exhibits a fairly isotropic EPR signal centered around $g = 2.02$ (*7*). A typical EPR spectrum taken at 8K is shown in Fig. 1A. The increase of the spin relaxation rate at high temperatures makes the signal too broad to be detected above 16K. This EPR spectra can be fitted with Gaussian line-shapes 1.5, 3.5, and 8.0 mT wide at g values of 2.02, 2.00, and 1.97, respectively. Quantitation against a copper-EDTA standard gave (0.93 ± 0.12) spins per 3Fe at 8K. Iron quantitation yielded an average value of 3.01 ± 0.15 irons per minimal molecular weight (*12*).

By combining EPR and Mössbauer studies we have demonstrated that Fd II is spectroscopically pure and contains a single [3Fe-4S] cluster per monomeric unit (*12*) (see also footnote*).

* The 3Fe cluster has been studied in detail in *Azotobacter vinelandii* Fd I (*8, 9*), beef heart aconitase (*14*) and *D. gigas* Fd II (*12*). A careful determination of labile sulfide in aconitase indicates that the ratio of Fe to S^{2-} is 3:4 (*3*). These results suggest the presence of a [3Fe-4S] structure that can be built by removal of one iron from the [4Fe-4S] cluster. The result is quite attractive since it explains the facile interconversion between these type of structures

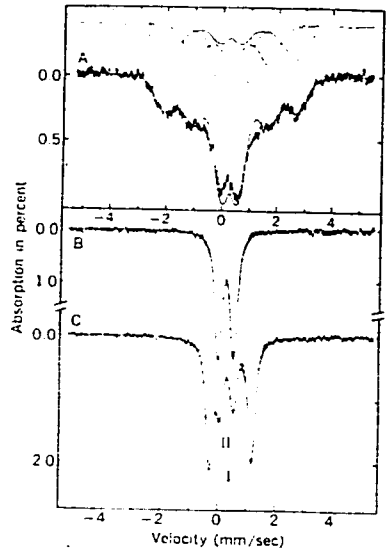

Fig. 2. Mössbauer spectra of oxidized and reduced *D. gigas* Fd II.
A: oxidized Fd II taken at 1.5K in a field of 60 mT applied parallel to the observed γ-radiation. The solid line plotted over the experimental data is the superposition of three computed subcomponents (*12*). B: oxidized Fd II taken at 77K, zero field. C: reduced Fd II taken at 4.2K zero field. In B and C the solid line is the result of fitting quadrupole doublets to the experimental data.

Figure 2A shows the Mössbauer spectrum of oxidized Fd II taken at 1.5K. At this temperature the spin fluctuates slowly and a magnetic spectrum is observed revealing three magnetic inequivalent subsites. Attempts have been made to decompose the spectrum into three subcomponents using a spin Hamiltonian with an effective $S=1/2$ (*12*). The theoretical spectrum of such a decompsition is plotted over the experimental data in Fig. 2A (for complete analysis of the oxidized

(see text). However, the structure of the cluster remains controversial. X-ray diffraction data at 2 Å resolution indicates the presence of a [3Fe-3S] cluster in *A. vinelandii* Fd I (*9*). The core was proposed to be an essential planar structure with Fe-Fe distances of 4.1 Å, different from the values proposed for *D. gigas* Fd II and aconitase (see text). To address the discrepancy between the X-ray, the extended X-ray absorption fine structure and the S^{2-} determinations, it was suggested that two substantially different structures may exist, defined as [3Fe-*n*S], with $n = 3$ or 4.

spectrum, see refs. *12* and *22*). At higher temperature, the electronic spin relaxation is fast and only one quadrupole doublet is observed (Fig. 2B). The spectral line width (0.28 mm/sec) indicates that the three subsites yield the same spectrum, at 77K, with ΔE_Q 0.54 ± 0.03 mm/sec and $\delta = 0.27 \pm 0.03$ mm/sec. These values are typical of high-spin ferric sites, suggesting tetrahedral coordination of predominantly sulfur ligation. However, the parameters do not exclude the possibility of ligands having, *O* or *N* as coordinating atoms (see also ref. *22*).

Fd II is reducible by a one electron step ($E_0' \sim -130$ mV) yielding an EPR silent state (). In the reduced state, the 4.2K zero-field Mössbauer spectrum reveals two distinct doublets (labelled I and II) with intensity ratio of 2:1 (Fig. 2C). The spectral parameters are $\Delta E_Q = 1.47 \pm 0.03$ mm/sec and $\delta = 0.46 \pm 0.02$ mm/sec (doublet I) and $\Delta E_Q = 0.47 \pm 0.02$ mm/sec and $\delta = 0.30 \pm 0.02$ mm/sec (doublet II). The values suggest that the iron atom associated with doublet II is high-spin ferric in character, similar to the iron sites in oxidized Fd II. The parameters of doublet I suggest a formal oxidation state between +2 and +3. The two iron atoms of doublet I share the electron that enters the cluster upon reduction. Hence, the reduced state represents a mixed valence state compound: $2Fe^{+2.5} + 1Fe^{3+}$.

An important observation is the fact that a weak applied magnetic field (~60 mT) can elicit a substantial broadening of both doublets observed in the reduced state, firmly indicating that the iron atoms associated with doublets I and II share a common electronic system with an integer larger than zero (*12*, *22*).

Thorough studies of the cluster were feasible by other complementary spectroscopic techniques. Magnetic circular dichroism (MCD) studies have revealed a distinct fingerprint for the [3Fe-4S] cluster and have shown that the reduced state has a spin $S = 2$ (*24*) in agreement with the Mössbauer data. Resonance Raman spectroscopy has also been used to characterize the 3Fe center, yielding a spectrum clearly distinguishable from that of a [4Fe-4S] cluster (*13*). Extended X-ray absorption fine structure (EXAFS) data on Fd II gave the following coordination distances for both oxidation states of the cluster: 2.4 Å (Fe-S) and 2.7 Å (Fe-Fe) (*2*). Similar values have been reported for beef heart aconitase (*4*). The EXAFS data suggest that the Fe-S-Fe angles are acute and very similar to those observed for [2Fe-2S] and [4Fe-4S] clusters.

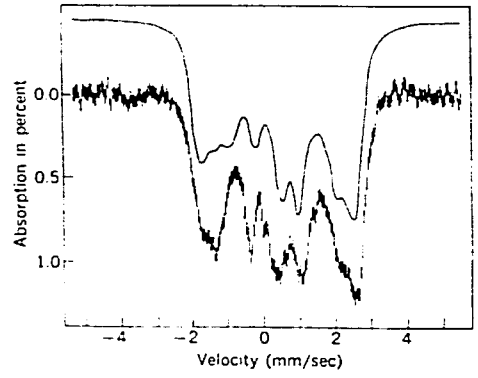

Fig. 3. Mössbauer spectrum of reduced [4Fe-4S] centers of *D. gigas* Fd I taken at 4.2K in a field of 60 mT applied parallel to the γ-radiation. The contribution of the spectral components due to the 3Fe centers was subtracted. The upper trace is the simulated Mössbauer spectrum obtained using *B. stearothermophilus* [4Fe-4S] Fd parameters for the reduced form (*17*) and ΔE_Q and δ values of reduced *D. gigas* Fd I.

In contrast to Fd II, the trimeric Fd I (*6*, *7*) shows an EPR in the reduced state ($E_0' \sim -450$ mV) with *g*-values at 1.92, 1.94, and 2.07 suggesting the presence of [4Fe-4S]$^+$ clusters. This was confirmed by Mössbauer studies (*12*, *25*). The spectrum of the reduced sample at 4.2K in a parallel applied field of 60 mT shows a magnetic spectrum very similar to that observed for the [4Fe-4S] clusters of reduced *Bacillus stearothermophilus* Fd (Fig. 3). At 90K the relaxation rate of the electronic spin is fast and the Mössbauer spectrum gives rise to two quadrupole doublets with equal intensity (similar to the hash marks of Fig. 6). These studies revealed also the presence of some 3Fe clusters in the Fd I preparations; the amount of 3Fe centers varies between 10 and 30% in the preparations examined so far (*7*, *25*). Upon oxidation, the [4Fe-4S] centers of Fd I become EPR silent and the Mössbauer spectrum at 4.2K modifies into a quadrupole pattern showing two doublets in a ratio of 3:1 (*12*, *19*).

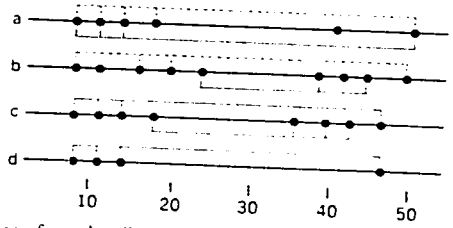

Fig. 4. Comparison of cysteine distribution for ferredoxins from *D. gigas* (a), *A. vinelandii* (b), *P. aerogenes* (c), and *B. stearothermophilus* (d).
Cluster attachments for *A. vinelandii* and *P. aerogenes* were determined by X-ray crystallography (*1*, *9*). The others are speculative.

ACCOMMODATION OF 3Fe AND 4Fe CLUSTERS BY THE SAME POLYPEPTIDE CHAIN

The differences in cluster composition between Fd I and Fd II indicate that the basic polypeptide unit can accommodate [4Fe-4S] clusters as well as [3Fe-4S] cores. Comparison of the amino acid sequences of the *D. gigas* monomer (*5*) with those of some other ferredoxins provides some insight on how the two cluster types are easily accommodated. As shown in Fig. 4, the *B. stearothermophilus* Fd (*10*) has only four cysteines. These residues are homologous with those linking one of the two [4Fe-4S] clusters of the *Peptococcus aerogenes* Fd (*1*) to the polypeptide. It is instructive to compare these sequence patterns of cysteinyl residues with that reported for Fd I from *A. vinelandii*. The latter protein contains a [3Fe-3S] and a [4Fe-4S] cluster; the points of cluster attachment deduced from X-ray crystallographic measurements by Ghosh *et al.* (*9*) are shown in Fig. 4. According to the interpretation of the X-ray data, five cysteinyl residues link the [3Fe-3S] core to the protein. Presumably a water molecule will provide a sixth ligand (oxygen). Remarkably, the *D. gigas* Fd sequence is constructed such that both cluster types can be fitted into the protein matrix: cysteinyl residues 8, 11, 14, 18, and 51 (or 41) could ligate to a 3Fe core whereas residues 8, 11, 14, and 51 (or 41) could form linkages to the [4Fe-4S] cluster.

PHYSIOLOGICAL ROLE OF *D. GIGAS* FERREDOXINS

Desulfovibrio gigas Fd have been tested individually in two important metabolic reactions of sulfate reducing bacteria: the phosphoroclastic reaction and the sulfite reductase system (*4*, *21*). Fd II is more efficient than Fd I in the sulfite reductase system. Fd I is active in the phosphoroclastic reaction in conditions where Fd II is not active. Fd II only participates in this reaction after a long lag phase. The activation step of Fd II in the phosphoroclastic reaction was monitored by EPR in a time course experiment (*18*). The development of "$g=1.94$" EPR signal, concomitant with the disappearance of $g=2.02$ signal, showed that after the lag phase [4Fe-4S] centers were being formed. Integration of the EPR features indicates that the newly formed [4Fe-4S] clusters represent an almost quantitative interconversion of the centers under these experimental conditions.

INTERCONVERSIONS BETWEEN 3Fe AND 4Fe CLUSTERS IN *D. GIGAS* FERREDOXIN II, A MODEL SYSTEM

Desulfovibrio gigas Fd have allowed us to probe in detail the interconversion process in iron-sulfur clusters. The possibility for accommodation of either a 3Fe or a 4Fe cluster by the same polypeptide chain, as anticipated by comparison of Fd I and Fd II spectroscopic data, led to the design of a set of experiments to study the possibility of cluster interconversion. Also, the physiological activation of Fd II described before suggests the occurrence of an interconversion step.

These studies were complemented by reconstitution experiments of *D. gigas* apoFd which demonstrated the rebuilding of both [3Fe-4S] and [4Fe-4S] centers (*19*). A proper combination of the techniques can be used for specific labelling of subsites of these iron-sulfur clusters (*19*). Such labelling with ^{57}Fe provides enhanced spectral resolution of the Mössbauer experiments.

Reconstitution of ApoFd II

The procedure for removing the [3Fe-4S] center from Fd II and rebuilding of an iron-sulfur center in the resulting monomeric apoprotein was

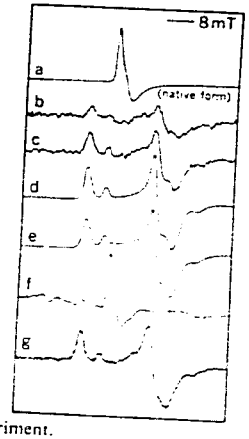

Fig. 5. EPR time course experiment.
Incubation of native Fd II (spectra a) with stoichiometric amounts of Fe^{2+} and S^{2-} and dithiothreitol for the following times: b, 1 hr; c, 2.5 hr; and d 10 hr. Spectrum e was taken after 1 hr incubation with a 5-fold excess of iron. Spectrum f represents reoxidation of the sample shown in e. Spectrum g represents an incubation of Fd II in the presence of mercaptoethanol.

adapted from that proposed by Hong and Rabinowitz (*11*). Samples reconstituted with an excess amount of ^{57}Fe, termed Fd_R were EPR-silent in the oxidized state (*19*, *25*). Upon reduction with dithionite the samples developed an EPR-spectrum (Fig. 1B) identical with the one observed for reduced Fd I. The principal g-values at 1.92, 1.94, and 2.07 are typical of a reduced $[4Fe\text{-}4S]^{+1}$ cluster. This conclusion was emphasized by the Mössbauer data.

The Mössbauer spectrum of oxidized reconstituted ferredoxin (Fd_R) measured at 4.2K, zero field, consists of two sharp quadrupole doublets (I and II), with an intensity ratio of approximately 3:1, and with the following Mössbauer parameters: doublet II, ΔE_Q 1.32 mm/sec and δ=0.45 mm/sec and doublet I, ΔE_Q=0.55 mm/sec and δ=0.41 mm/sec. Mössbauer studies in applied fields of 6T show that both doublets result from diamagnetic (S=0) sites. The spectral parameters taken together with the observed diamagnetism and the intensity ratio of both doublets indicate that the subsites observed in the Mössbauer spectrum of the reconstituted cluster represent a [4Fe-4S] cluster in the +2 oxidation state.

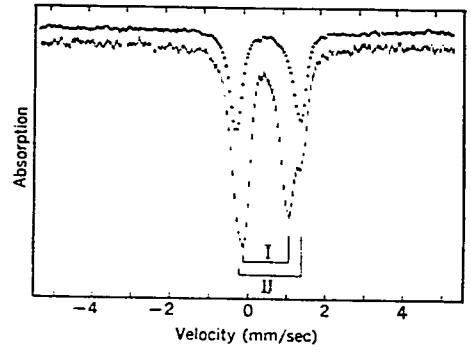

Fig. 6. Mössbauer spectrum of reduced [4Fe-4S] cluster in zero-field at 90K. Spectra of reduced Fd_R (reconstituted ^{57}Fe apoFd II) (hash marks) and of reduced *D. gigas* Fd II incubated with a 4-fold excess of ^{57}Fe in the presence of dithiothreitol (●). Doublets I and II are indicated in brackets referring to reduced Fd_R.

As anticipated from the EPR data the Mössbauer spectrum of reduced Fd_R measured at 4.2K in a 60 mT parallel applied magnetic field exhibits hyperfine structure. The magnetic features are identical with those of the reduced [4Fe-4S] centers of Fd I (Fig. 3) (*19*, *25*), and again very similar to those observed for the [4Fe-4S] Fd from *B. stearothermophilus* (*17*).

At 90K the relaxation of the electronic spin S=1/2 is fast and two quadrupole doublets (termed I and II) of equal intensity are observed (*19*) (Fig. 6). Again, the data are very similar to those reported at high temperature for reduced [4Fe-4S] centers of Fd I (*16*, *19*).

2. Conversion of 3Fe to 4Fe Cluster-isotopic Labelling Experiments

Incubation of dithionite-reduced Fd II, with Fe^{2+} and S^{2-} under anaerobic conditions and in the presence of dithiothreitol, was performed in order to convert the native [3Fe-4S] core into a [4Fe-4S] one. For aconitase it was also shown that the presence of dithiothreitol accelerates the interconversion kinetics (*15*). As indicated previously, the [3Fe-4S] cluster of Fd II yields an EPR signal at g=2.02 in the oxidized state; the reduced cluster is EPR silent (*7*, *19*, *25*). The spectra in Fig. 5 show a typical time course experiment in which Fd II (spectrum a) was incu-

bated with one equivalent of iron and sulfide per protein monomer in the presence of a slight excess of dithionite. The appearance of a g 1.94 EPR spectrum shows that [4Fe-4S] centers are formed. Quantitation of spectrum d shows that 36% of the 3Fe clusters were converted into 4Fe clusters after 10 hr incubation. When a 5-fold excess of iron and sulfide were used, 70% of 3Fe clusters were converted after 1 hr incubation time (*19*). Reoxidation of the sample enables the observation of the unconverted 3Fe clusters (Fig. 5f). When dithiothreitol is replaced by mercaptoethanol the yield of conversion is much lower (after 1 hr of incubation, only 5% of conversion was observed, Fig. 5g).

We have studied these cluster interconversions with ^{57}Fe Mössbauer spectroscopy by incubating Fd II with iron isotopically enriched in either ^{57}Fe or ^{56}Fe. When ^{57}Fe is added to the incubation medium the Mössbauer techniques give information about the sites into which the externally provided iron is incorporated, whereas the global effect of iron incorporation in the cluster is observed by the incorporation of ^{57}Fe (99.9%).

Mössbauer spectrum of Fd II incubated anaerobically for 6 hr with a 4-fold excess of ^{57}Fe and S^{2-} and purified in aerobic conditions, (oxidized state) yields a single quadrupole doublet with parameters identical to doublet II in Fd_R (*19*). So, the externally added iron is incorporated in site II. As indicated before, site II contains three indistinguishable iron atoms. So this result does not allow differentiation between specific site occupancy or a distribution between three sites.

It is noteworthy that, when beef heart aconitase is submitted to similar treatment, the iron atom is incorporated into a site (with a single iron atom) which yields doublet I (*15*), the $[4Fe\text{-}4S]^{2+}$ cluster of Fd_R and aconitase yield virtually the same Mössbauer spectra, suggesting a 3:1 site occupancy.

When the ^{57}Fe incubated Fd II sample is reduced, the 90K spectrum clearly indicates that only one quadrupole doublet (site II) is observed ($\Delta E_Q = 1.67$ and $\delta = 0.60$ mm sec) (Fig. 6). The $[4Fe\text{-}4S]^{1+}$ cluster of Fd_R, it is remembered, shows a 2:2 site occupancy. This technique allowed for the first time the correlation of spectral components in different oxidation states of a [4Fe-4S] cluster. The site that gives origin to doublet II (oxidized state) is the same that contributes to doublet II (reduced state).

This leaves open the question of whether the ^{57}Fe has been incorporated into one site or two equivalent sites. Spectral simulation of low temperature Mössbauer spectra of incubated ^{57}Fe sample (*19*), as well as our recent unpublished data using the conjunction of EPR spin quantitation and measurement of absolute iron concentration, and determination of ^{57}Fe/^{56}Fe ratios seem to indicate a single occupancy. Our data also exclude the possibility of isotopic scrambling between sites I and II.

3. *Conversion of 4Fe to 3Fe Cluster: Ferricyanide Treatment*

Thomson and coworkers (*23*) have reported that the low temperature MCD of ferricyanide oxidized 2×[4Fe-4S] Fd from *C. pasteurianum* are very similar to those of Fd II. Using the [4Fe-4S] cluster of reconstituted apoFd II (Fd_R) we have extended the ferricyanide oxidation studies to *D. gigas* Fd II. The Mössbauer and EPR data shows unambiguously that a [4Fe-4S] to [3Fe-4S] cluster conversion can indeed be achieved by the oxidative procedure. The general features of the Mössbauer spectrum of the native Fd II and ferricyanide treated Fd_R at 4.2K with an applied field of 60 mT are identical and confirm that all the [4Fe-4S] clusters are converted into [3Fe-3S] cores (*19*, *25*).

4. *Conversion of 4Fe into 3Fe Clusters under Reducing Conditions: Ionic Strength Effects*

Fd_P contains after reconstitution a single [4Fe-4S] cluster. No [3Fe-4S] cores are present in the oxidized state (a characteristic Mössbauer spectrum (*12*) and a $g = 2.02$ EPR signal would be detected). However, dithionite-reduced Fd_R contains variable amounts of 3Fe clusters. Furthermore, the amount of these clusters observed upon reduction increases with the ionic strength of the buffer (the experiments were conducted using dithionite as reductant). We found that in 0.8 M buffer about 50% of the clusters present in reduced Fd_R were converted to 3Fe clusters (*19*) (see also footnote**).

** The interconversion between 3Fe and 4Fe centers has also been probed extensively in beef heart aconitase (*14*, and references therein). Under conditions of partial unfolding of the protein, at alkaline pH, a linear form of the $[3Fe\text{-}4S]^{+1}$ cluster was proposed based on spectroscopic measurements and on the comparison with synthetic [Fe-S] compounds. Also, a substantial fraction of [2Fe-2S] was shown to be accommodated.

Together with the discussion in the previous section, we have shown that 4Fe clusters can be converted to 3Fe clusters in oxidative conditions, but that the conversion also takes place under reducing conditions. The reduced [4Fe-4S] clusters of Fd_R are unstable under high ionic strength conditions.

SYNTHESIS OF MIXED METAL CLUSTERS: COBALT DERIVATIVE (20)

Using the techniques and procedures described for the interconversion of 3Fe into 4Fe cores, we recently attempted to produce cubane-like structures containing three iron atoms and one extra metal atom: [3Fe,M-4S]. *Desulfovibrio gigas* Fd II containing a single [3Fe-4S] cluster (enriched and unenriched in ^{57}Fe) was used as starting material. Cobalt ion was successfully introduced into a mixed metal cluster, assuming a paramagnetic configuration into the fourth site of the cubane structure. Our preliminary data show that the cobalt derivative (typical yield of conversion, 70%) was prepared after anaerobic incubation of the native

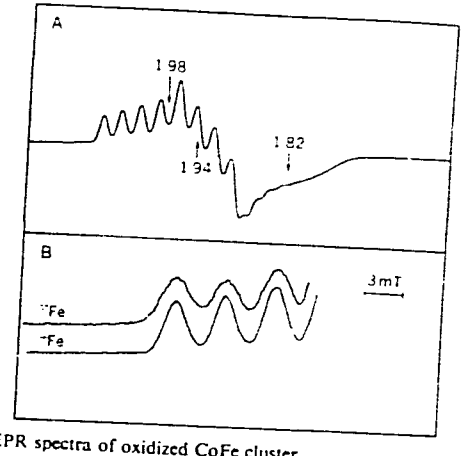

Fig. 7. X-band EPR spectra of oxidized CoFe cluster.
A: CoFe cluster containing the ^{56}Fe isotope, T = 40K, microwave power 1 mW, modulation amplitude 0.5 mT. B: expanded view of low field position of 40K spectra using samples containing ^{56}Fe ($I=0$) and ^{57}Fe ($I=1/2$).

3Fe cluster (^{57}Fe and ^{56}Fe *D. gigas* Fd II samples) for 6–10 hr in the presence of dithionite, dithiothreitol, cobalt (II) (sulfide was not required), followed by chromatographic purification steps. The combination of metal analysis, EPR and Mössbauer measurements clearly indicates that a cubane-like structure is formed: [3Fe,Co-4S]. Metal analysis of different preparations yields Fe: Co; (3.0±0.10): 1. The newly formed cluster was studied in the oxidized and reduced states. In the oxidized state the cluster exhibits a $S=1/2$ EPR signal with g-values at 1.82, 1.94, and 1.98 (g_z) (Fig. 7A). The g_z feature shows eight well resolved ^{59}Co hyperfine lines ($^{59}A_z=4.4$ mT); the ^{59}Co hyperfine structure is broadened by ^{57}Fe (~0.6 mT) (Fig. 7B), showing that Fe and Co reside in the same complex. Quantitation of the EPR spectra at 40K yields 1 spin/Co. EPR studies at low temperature (~8K) enabled the quantification of unconverted 3Fe centers.

The Mössbauer spectrum of the oxidized cluster exhibits at 4.2K two distinct spectral sites with an intensity ratio of 2:1, suggesting that three iron atoms reside in the cluster. The spectrum of the dithionite-reduced sample shows a quadrupole doublet at 4.2K ($\Delta E_Q=1.28$ mm/sec δ = 0.53 mm/sec). However, in strong applied fields the spectrum exhibits magnetic hyperfine structure, indicating that the complex is paramagnetic with an integer spin, $S>0$.

CONCLUSION

Desulfovibrio gigas Fd II provides a unique opportunity for the study of the chemistry involved in the cluster interconversion process. The protein has a low molecular weight and contains only one type of cluster, and the quality of the protein preparations are excellent: EPR integrations are quantitative and no iron impurities have been detected by Mössbauer spectroscopy. The concept of interconversion between iron-sulfur clusters introduces a new dynamic approach to the understanding of the role of iron-sulfur proteins. Also, it was shown that this chemical pathway can be used in more diversified ways to explore the possibility of introducing an extra-metal in a [Fe-S] core.

A brief summary of the interconversion pathways as well as the potentialities of the method for specific labelling of iron-sulfur clusters is indicated in Fig. 8. Combination of isotopic enrichment and specific

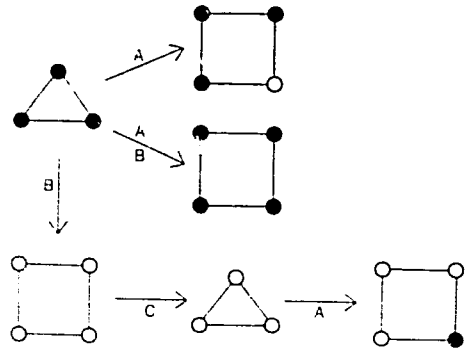

Fig. 8. Iron-sulfur cluster interconversion: isotopic labelling.
A, incubation of Fd II with Fe^{2+} (^{57}Fe or ^{56}Fe isotopes) in the presence of dithionite, dithiothreitol, and sulfide. B, reconstitution of apoFd II, in the presence of Fe^{2+} (^{57}Fe or ^{56}Fe isotopes) and S^{2-}. C, ferricyanide oxidation step.

labelling techniques has enabled us to produce different isotopic labelled clusters (see Fig. 8).

The interconversion studies clearly indicate that [4Fe-4S] clusters can be converted to [3Fe-4S] cores either by ferricyanide oxidation (*8, 19, 23*) or by reduction with dithionite in high ionic strength medium (*16, 19*). Using the method described it seems feasible to rebuild [4Fe-4S] centers, using specific ^{57}Fe markers. If the technique could be applied to the modification of a single cluster in a complex enzyme, enhanced spectral analysis could be achieved.

The formation of mixed metal clusters of the type [3Fe,M-4S] in Fd II shows that the [3Fe-4S] cluster incorporated in the protein matrix can serve as a precursor for the formation of novel metal clusters. This new synthetic route could facilitate the formation of relevant model compounds. It will be interesting to explore the possibility of formation of cubane-like structures containing molybdenum and nickel with obvious relevance for nitrogenase research and nickel biochemistry. The method is also potentially interesting for specifically modifying a [Fe-S] core in a complex enzyme.

Acknowledgments

I am indebted to my colleagues who have contributed with enthusiasm to the work described here, Drs. I. Moura, A.V. Xavier, B.H. Huynh, T.A. Kent, V. Papaefthymiou, J. LeGall, J.D. Lipscomb, and E. Münck, and to Ms. I. Ribeiro for carefully typing this manuscript. This work was supported by AID, NATO, INIC, and JNICT.

REFERENCES

1. Adman, E. T., Sieker, L. C., and Jensen, L. H. *J. Biol. Chem.*, **248**, 3987 (1973).
2. Antonio, M. R., Averill, B. A., Moura, I., Moura, J. J. G., Orme-Johnson, W. H., Teo, B. K., and Xavier, A. V. *J. Biol. Chem.*, **257**, 664 (1982).
3. Beinert, H. *Anal. Biochem.*, **131**, 373 (1983).
4. Beinert, H., Emptage, M. H., Dreyer, J. L., Scott, R. A., Hahn, J. E., Hodgson, K. D., and Thomson, A. J. *Proc. Natl. Acad. Sci. U.S.A.*, **80**, 393 (1983).
5. Bruschi, M. *Biochem. Biophys. Res. Commun.*, **91**, 623 (1979).
6. Bruschi, M., Hatchikian, E. C., LeGall, J., Moura, J. J. G., and Xavier, A. V. *Biochim. Biophys. Acta*, **449**, 275 (1976).
7. Cammack, R., Rao, K. K., Hall, D. O., Moura, J. J. G., Xavier, A. V., Bruschi, M., LeGall, J., Deville, A., and Gayda, J. P. *Biochim. Biophys. Acta*, **490**, 311 (1977).
8. Emptage, M. H., Kent, T. A., Huynh, B. H., Rawlings, J., Orme-Johnson, W. H., and Münck, E. *J. Biol. Chem.*, **255**, 1793 (1980).
9. Ghosh, D., Furey, W., Jr., O'Donnell, S., and Stout, C. D. *J. Biol. Chem.*, **256**, 4185 (1981).
10. Hase, T., Ohmiya, N., Matsubara, H., Mullinger, R., Rao, K. K., and Hall, D. O. *Biochem. J.*, **159**, 55 (1976).
11. Hong, J. S. and Rabinowitz, J. C. *J. Biol. Chem.*, **245**, 6574 (1970).
12. Huynh, B. H., Moura, J. J. G., Moura, I., Kent, T. A., LeGall, J., Xavier, A. V., and Münck, E. *J. Biol. Chem.*, **255**, 3242 (1980).
13. Johnson, M. K., Hare, J. W., Spiro, T. G., Moura, J. J. G., Xavier, A. V., and LeGall, J. *J. Biol. Chem.*, **256**, 9806 (1981).
14. Kennedy, M. C., Kent, T. A., Emptage, M., Merkle, H., Beinert, H., and Münck, E. *J. Biol. Chem.*, **259**, 14463 (1984).
15. Kent, T. A., Dreyer, J. L., Kennedy, M. C., Huynh, B. H., Emptage, M. H., Beinert, H., and Münck, E. *Proc. Natl. Acad. Sci. U.S.A.*, **79**, 1096 (1982).
16. Kent, T. A., Moura, I., Moura, J. J. G., Lipscomb, J. D., Huynh, B. H., LeGall, J., Xavier, A. V., and Münck, E. *FEBS Lett.*, **139**, 55 (1982).
17. Middleton, P., Dickson, D. P. E., Johnson, C. E., and Rush, J. D. *Eur. J. Biochem.*, **88**, 135 (1978).
18. Moura, J. J. G., LeGall, J., and Xavier, A. V. *Eur. J. Biochem.*, **141**, 319 (1984).
19. Moura, J. J. G., Moura, I., Kent, T. A., Lipscomb, J. D., Huynh, B. H., LeGall, J., Xavier, A. V., and Münck, E. *J. Biol. Chem.*, **257**, 6259 (1982).
20. Moura, J. J. G., Moura, I., Münck, E., Papaefthymiou, V., and LeGall, J. *J. Biol. Chem.*, **260**, 8942 (1985).
21. Moura, J. J. G., Xavier, A. V., Hatchikian, E. C., and LeGall, J. *FEBS Lett.*, **141**, 319 (1977).

22. Münck, E. *In* "Iron-Sulfur Proteins," ed. T. G. Spiro, p. 147 (1982). Academic Press, New York.
23. Thomson, A. J., Robison, A. E., Johnson, M. K., Cammack, R., Rao, K. K., and Hall, D. O. *Biochim. Biophys. Acta*, **637**, 423 (1981).
24. Thomson, A. J., Robison, A. E., Johnson, M. K., Moura, J. J. G., Moura, I., Xavier, A. V., and LeGall, J. *Biochim. Biophys. Acta*, **670**, 93 (1981).
25. Xavier, A. V., Moura, J. J. G., and Moura, I. *Struct. Bond.*, **43**, 187 (1981).

Evidence for the Formation of a $ZnFe_3S_4$ Cluster in *Desulfovibrio gigas* Ferredoxin II

Kristene K. Surerus and Eckard Münck*

Gray Freshwater Biological Institute
University of Minnesota, Navarre, Minnesota 55392

Isabel Moura and José J. G. Moura

Centro de Química Estrutural, UNL
1000 Lisboa, Portugal

Jean LeGall

Center for Biological Resource Recovery
Department of Biochemistry, University of Georgia
Athens, Georgia 30602

Received December 22, 1986

The electron-transport protein ferredoxin II (Fd II) from *Desulfovibrio gigas* contains an Fe_3S_4 cluster[1] which reacts readily with Fe^{2+} to form the cubane Fe_4S_4 complex.[2] This conversion suggested that the Fe_3S_4 core of Fd II can serve as a precursor for the formation of novel clusters of the MFe_3S_4 type. Indeed, we have demonstrated[3] the formation of $[CoFe_3S_4]^{1+,2+}$. The Fe_3S_4

(1) Huynh, B. H.; Moura, J. J. G., Moura, I.; Kent, T. A.; LeGall, J.; Xavier, A. V.; Munck, E. *J. Biol. Chem.* **1980**, *255*, 3242–3244.
(2) Moura, J. J. G.; Moura, I.; Kent, T. A.; Lipscomb, J. D.; Huynh, B. H.; LeGall, J.; Xavier, A. V.; Munck, E. *J. Biol. Chem.* **1982**, *257*, 6259–6267.
(3) Moura, I.; Moura, J. J. G., Munck, E.; Papaefthymiou, V.; LeGall, J. *J. Am. Chem. Soc.* **1986**, *108*, 349–351.

0002-7863/87/1509-3805$01.50/0

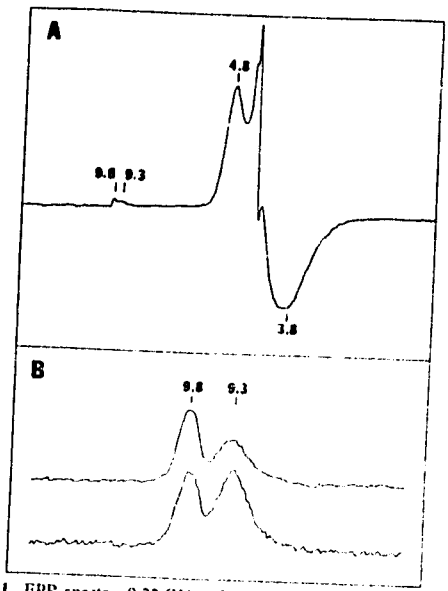

Figure 1. EPR spectra, 9.22 GHz, of I. (A) Spectrum recorded at $T \approx 8$ K; microwave power, 0.1 mW; modulation amplitude, 10 G. (B) Expanded region around $g = 9$–10. Upper trace: $T = 8$ K, 1 mW, 10-G modulation amplitude. Lower trace: $T = 15$ K, 1 mW, 10-G modulation amplitude.

cluster is also interesting from a standpoint of magnetism because the reduced cluster (spin $S = 2$) is a mixed-valence system with one localized Fe^{3+} and one delocalized $Fe^{2.5+}/Fe^{2+}$ pair. Thus, Fd II has features (delocalization) typical of Fe_4S_4 cubanes. We have recently described the spin coupling in reduced Fd II with a Hamiltonian which takes into account Heisenberg exchange as well as electron delocalization.[4] This Hamiltonian holds promise for the description of Fe_4S_4 clusters. Since spin coupling in the latter is exceedingly complex, it is desirable to incorporate a diamagnetic metal, rather than Co^{2+}, into the Fe_4S_4 core and thus produce a cubane with only three paramagnetic sites. Here we report evidence for the formation of a cluster with novel features, most probably $ZnFe_3S_4$.

Fd II was purified as described.[2] Typically 0.5 mL of dithionite-reduced Fd II, 0.5 mM in Fe_4S_4, was anaerobically incubated for 2 h with 15 mM $Zn(NO_3)_2$ and 7 mM dithiothreitol. Excess reagents were removed with an anaerobic Sephadex G-25 column. Plasma emission spectroscopy yielded 4.2 Zn, 3.0 Zn, and 1.3 Zn per 3 Fe for three preparations;[5] the latter sample was enriched in ^{57}Fe. Except for ^{57}Fe hyperfine broadening for the 1.3 Zn per 3 Fe sample, the EPR spectra of the three samples were the same. We refer to the dithionite-reduced cluster as I.

Figure 1 shows X-band EPR spectra of I. Prominent resonances are observed at $g = 4.8$ and 3.8 and at $g = 9.8$ and 9.3. These signals are typical of an $S = {}^5/_2$ system described by the Hamiltonian

$$\hat{H}_e = D[S_z^2 - {}^{35}/_{12} + (E/D)(S_x^2 - S_y^2)] + g_0\beta\vec{H}\cdot\vec{S} \quad (1)$$

for $\beta H \ll |D|$ and $g_0 \approx 2$. In fact, for $D < 0$ and $E/D = 0.25$, eq 1 predicts three Kramers doublets with the following sets of g values: $g_{x,y,z} = (0.5, 0.4, 9.8)$ for the ground doublet, $g_{x,y,z}$ (4.1, 3.8, 4.8) for the middle doublet, and $g_{x,y,z} = (1.4, 9.4, 0.9)$ for the upper doublet. Variable temperature (8–15 K) studies showed that the $g_z = 9.8$ resonance belongs to the ground state (see Figure 1B) and that $D = (-2.7 \pm 0.5)$ cm^{-1}. Upon mild oxidation with gallocyanin ($E_m \approx 30$ mV vs. NHE) the EPR signals dissappeared; they reappeared quantitatively upon rereduction with dithionite.

Figure 2B shows a 4.2 K Mössbauer spectrum of I. The spectral pattern observed is typical for a Kramers doublet with $g_z \gg g_x, g_y$ (the middle doublet is only $\approx 3\%$ populated at 4.2 K). At 50 K the electronic spin relaxes fast, and the Mössbauer spectrum consists of two doublets with an area ratio $\simeq 2{:}1$. The values for ΔE_Q and δ (Table I) for site 1 (one Fe) suggest Fe^{2+} with tetrahedral sulfur coordination whereas those of site 2 remind us of the delocalized $Fe^{2.5+}/Fe^{3+}$ pairs of $[Fe_4S_4]^{1+}$; see ref 6.

The spectrum of Figure 2B can be decomposed into essentially two components (the two Fe of site 2 are only slightly inequivalent; sites 2a and 2b). The rightmost absorption line in Figure 2B belongs entirely to sites 2a and 2b. By matching the theory to this line, we found that $\approx 60\%$ of total Fe belongs to site 2 and about 30% to site 1; the remaining absorption is as yet unidentified. Six preparations gave identical spectra; none had detectable levels of adventitious Fe^{3+} or Fe^{2+}.

The spectrum of Figure 2B was analyzed by augmenting eq 1 with the hyperfine terms (i = 1, 2a, 2b).

$$\hat{H}_{hf} = \sum_i \vec{S}\cdot\vec{A}(i)\cdot\vec{I}(i) - g_n\beta_n\vec{H}\cdot\vec{I}(i) + \hat{H}_{quad}(i) \quad (2)$$

The spectral simulations are not perfect; however, the essential features of the data are well represented by the theory. Because of the uniaxial nature of the electronic ground doublet, the spectrum of Figure 2B is only sensitive to the z-components of the magnetic hyperfine tensors, $A_z(i)$. From studies in applied

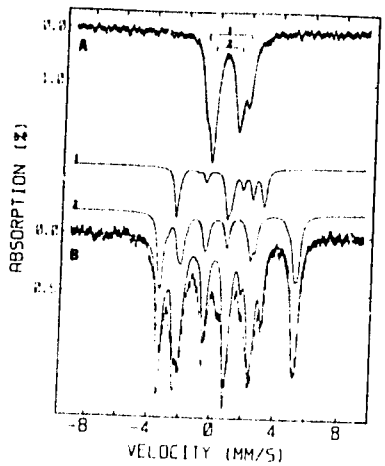

Figure 2. Mössbauer spectra of ^{57}Fe-enriched cluster I. (A) Spectrum recorded at 50 K. Solid line is the result of a least-squares fitting the spectrum to two doublets. The fit yielded an area ratio of 1.97:1 for sites 1 and 2. (B) 4.2 K spectrum recorded in a magnetic field of 0.05 T applied parallel to the γ-radiation. Solid lines are spectral simulations using the parameters of Table I. Spectral decomposition into components 1 and 2 is shown above the data; vertical scale of curves 1 and 2 is compressed by a factor of 2.

Table I. Hyperfine Parameters of I Used To Simulate the Spectrum of Figure 2B[a]

site	A_z, MHz	δ, mm/s	ΔE_Q, mm/s	η	β, deg
1	+6.6	0.62	−2.7	0.8	30
2a	−14.0	0.51	+1.6	0.5	33
2b	−14.8	0.54	+1.6	−2	15

[a] Zero-field splitting parameters used were $D = -2.7$ cm^{-1} and $E/D = 0.25$. The z-axes of the electric field gradient tensors (V_{xx}, V_{yy}, V_{zz}; $\eta = (V_{xx} - V_{yy})/V_{zz}$) are tilted by an angle β relative to the z-axis of the zero field splitting tensor. For the electronic system at hand, the values of η and β are not unique; see ref 7.

(4) Papaefthymiou, V.; Girerd, J. J.; Moura, I.; Moura, J. J. G.; Munck, E. *J. Am. Chem. Soc.*, in press.

(5) The protein seems to bind Zn^{2+} in variable amounts. In a related project, we have observed with EPR binding of two–three Cu^{2+} in sites other than the "vacant" site of Fe_4S_4.

(6) Munck, E.; Kent, T. A. *Hyperfine Interact.* **1986**, *27*, 161–172.

(7) Van Dongen, T.; Jagannathan, R.; Trooster, J. M. *Hyperfine Interact.* **1975**, *1*, 135–144.

fields up to 6.0 T we found that $A_z(1) > 0$, $A_z(2a) < 0$, and $A_z(2b) < 0$.

Cluster I has unique spectroscopic features. Formally, it contains two Fe^{2+} and one Fe^{3+}; thus the three iron sites accommodate one more electron than those of reduced Fd II. Since we have no spectroscopic data on the Zn, our spectra could indicate the formation of a superreduced Fe_3S_4 cluster, the reduction being achieved, however, only in the presence of Zn (but not with Fe, Co, Cu, or V); Zn^{2+} would bind to the protein in the vicinity of the cluster stabilizing the superreduced state. The oxidized/reduced Fd II couple has $E_m = -130$ mV (vs. NHE); in the absence of Zn^{2+} we have never observed, even at ~600 mV, any EPR feature indicative of the $S = {}^5/_2$ state (3% $S = {}^5/_2$ clusters would have been detected). A superreduced state has never been indicated for any protein containing an Fe_3S_4 cluster. More plausibly, therefore, Zn has been incorporated into the vacant site of the Fe_3S_4 cluster to form $ZnFe_3S_4$. This interpretation is suggested by our earlier work which has demonstrated facile formation of $[Fe_4S_4]^{1+}$ and $[CoFe_3S_4]^{1+}$ under similar incubation conditions. Since I has half integer spin, the incorporated Zn must be Zn^{2+}, suggesting that I is $[ZnFe_3S_4]^{1+}$ and thus the analogue of $[Fe_4S_4]^{1+}$. In order to prove incorporation of Zn directly, EXAFS and ENDOR experiments are in preparation.

$[Fe_4S_4]^{1+}$ cores seem to consist of two spin-coupled pairs; see ref 8. For the postulated $[ZnFe_3S_4]^{1+}$ the replacement of one Fe^{2+} by Zn^{2+} has disrupted one pair and created the trapped Fe^{2+} of site 1. In order to exploit the cluster for the study of spin coupling of cubanes, $A_x(i)$ and $A_y(i)$ need to be determined. Such efforts are in progress.

Acknowledgment. This work was supported by the National Science Foundation, the National Institutes of Health, the Instituto de Investigação Cientifica Technologica, the Junta Nacional de Investigação Cientifica Tecnologica, the Agency for International Development, and a NATO Collaborator Research Grant.

(8) (a) Aizman, A.; Case, D. A. *J. Am. Chem. Soc.* **1982**, *104*, 3269–3279. (b) Dickson, D. P. E.; Johnson, C. E.; Thompson, C. L.; Cammack, R.; Evans, M. C. W.; Hall, D. O.; Rao, K. K.; Weser, U. *J. Phys. (Paris)* **1974**, *35*, C6–343.

Volume 215, number 1, 63–67 FEB 04630 May 1987

Isolation and characterization of a rubredoxin and a flavodoxin from *Desulfovibrio desulfuricans* Berre-Eau

Guy D. Fauque[a]*, Isabel Moura[b], José J.G. Moura[b], António V. Xavier[b] Nicole Galliano[c] and Jean LeGall[c]*

[a]*Department of Biochemistry, University of Georgia, School of Chemical Sciences, Athens, GA 30602, USA,* [b]*Centro de Química Estrutural, Complexo I, UNL, Av. Rovisco Pais, 1000 Lisboa, Portugal* and [c]*ARBS, ECE, CEN Cadarache, 13108 Saint-Paul-lez-Durance Cédex, France*

Received 20 January 1987; revised version received 19 February 1987

A rubredoxin and a flavodoxin have been purified and characterized from soluble extracts of a sulfate-reducing bacterium able to grow with N_2 as the only nitrogen source: *Desulfovibrio desulfuricans* strain Berre-Eau. These two electron carriers have characteristics similar to homologous proteins found in other *Desulfovibrio* species (molecular mass, absorption spectrum, extinction coefficient and amino acid composition). In contrast to rubredoxin, flavodoxin mediates electron transfer in the reduction of sulfite to sulfide and in hydrogen evolution from pyruvate, when in the presence of hydrogenase

Rubredoxin; Flavodoxin; Electron transfer; Sulfate reduction; (*Desulfovibrio*)

1. INTRODUCTION

The sulfate-reducing bacteria are strict anaerobic microorganisms with an oxidative metabolism based on the utilization of sulfate and other sulfur anions as terminal electron acceptors [1,2]. The dissimilatory sulfate-reducers *Desulfovibrio desulfuricans* strains Berre-Eau and Berre-Sol have been isolated from enrichment cultures with N_2 as sole nitrogen source [3]. Recently, several strains and species of sulfate-reducing bacteria of genera *Desulfovibrio* and *Desulfotomaculum* were shown to be able to grow while fixing N_2 [4–6].

Correspondence address: G.D. Fauque, Department of Biochemistry, University of Georgia, School of Chemical Sciences, Athens, GA 30602, USA

Abbreviations: FMN, flavin adenine mononucleotide; HPLC, high-pressure liquid chromatography; PITC, phenylisothiocyanate; ϵ_M, molar extinction coefficient

A rubredoxin and a ferredoxin with one [4Fe-4S] center have been isolated from *D. desulfuricans* Berre-Sol [7,8], but no study has been reported on the electron carrier system of *D. desulfuricans* Berre-Eau. Rubredoxins are the simplest and the smallest iron-sulfur proteins and have been isolated from 7 *Desulfovibrio* species [7,9–14] and one strain of sulfur-reducing bacteria *Desulfuromonas acetoxidans* [15]. Flavodoxins are a class of low-M_r proteins containing FMN as prosthetic group which are not found in all of the *Desulfovibrio* species [13,16,17].

Here, we report on the purification and characterization of a rubredoxin and a flavodoxin from *D. desulfuricans* Berre-Eau.

2. MATERIALS AND METHODS

D. desulfuricans Berre-Eau (NCIB 8387) was grown at 37°C on the lactate-sulfate medium of Starkey [18], under non-nitrogen-fixing conditions. Wet cells (600 g) were suspended in 10 mM

Published by Elsevier Science Publishers B.V. (Biomedical Division)
00145793/87/$3.50

Tris-HCl buffer (pH 7.6) and ruptured by passing twice through a French press at 7000 lb/inch^2. The extract was centrifuged at 20000 × g for 45 min and the supernatant constituted the crude cell extract. Purification of proteins was performed from the soluble fraction by conventional chromatographic procedures; the rubredoxin was purified in four steps (DEAE-cellulose, DEAE-Biogel A, hydroxyapatite and DEAE-cellulose) and the flavodoxin in three (DEAE-cellulose, DEAE-Biogel A, and hydroxyapatite).

Protein homogeneities were checked by electrophoresis on 7% polyacrylamide gels with Tris-HCl glycine buffer at pH 8.9 [19]. The molecular masses of rubredoxin and flavodoxin were estimated by gel filtration on a Sephadex G-50 column (1.5 × 105 cm) according to Whitaker [20]. UV-visible absorption spectra were recorded using a Beckman model 35 spectrophotometer. EPR spectra were carried out on a Bruker ER-200 tt spectrometer equipped with an Oxford Instruments continuous helium flow cryostat interfaced to a Nicolett 1180 computer. Protein concentrations were determined by the method of Lowry et al. [21] with bovine serum albumin as standard.

Amino acid analyses were performed on an LKB amino acid analyzer. The protein samples were hydrolyzed under vacuum in 6 N HCl at 113°C for 24 h. The analysis of amino acid hydrolysates was performed after PITC derivatization and HPLC separation on a reversed-phase column C_{18}. The values of the molar extinction coefficients were calculated using protein concentrations determined from amino acid analysis of an aliquot of a protein solution for which the absorbance had been previously determined. As described in [22], manometric assays were utilized to determine the physiological activity of the two proteins following respectively at 37°C the reduction of fresh sodium

Table 1

Amino acid composition of rubredoxins isolated from 8 *Desulfovibrio* species

	D. salexigens	*D. gigas*	*D. vulgaris* Hildenborough	*D. africanus*	*D. desulfuricans* Norway 4	*D. desulfuricans* ATCC 27774	*D. desulfuricans* Berre-Sol	*D. desulfuricans* Berre-Eau
Lys	3	6	4	4	5	2	4	3
His	0	0	0	0	0	1	0	0
Arg	0	0	0	0	0	0	0	0
Trp	n.d.	1	1	3	n.d.	1	1	1
Asp	8	8	7	9	13	8	7	6
Thr	2	2	3	1	4	0	2	2
Ser	1	2	2	2	0	2	2	3
Glu	7	4	3	5	5	5	8	5
Pro	5	5	6	6	5	5	6–7	7
Gly	6	5	6	5	7	2	6	5
Ala	3	4	4	2	5	2	6	5
Cys (half)	4	4	4	4	4	5	4	4
Val	2	3	5	6	6	5	5	4
Met	1	1	1	1	1	1	1	1
Ile	0	2	0	1	0	0	2	2
Leu	2–3	1	1	0	1	1	0	0
Tyr	2	3	3	3	4	3	3	3
Phe	2	2	2	2	2	2	3	2
Total	48–49	53	52	54	62	45	60–61	53
References	[13]	[25]	[10]	[12]	[11]	[28]	[7]	this work

n.d., not determined

sulfite (4 μmol) by hydrogen and H_2 production from sodium pyruvate (30 μmol). Pure periplasmic *D. gigas* hydrogenase was added in all cases to the enzymatic systems to ensure excess of this activity.

3. RESULTS AND DISCUSSION

The molecular mass of the rubredoxin from *D. desulfuricans* Berre-Eau was estimated to be 5700 Da by gel filtration. The nearest minimum molecular mass as determined by amino acid analysis was found to be 5691 Da for a total of 53 residues. The calculation of this value is based on the presence of one methionine residue and by adding one tryptophan. These two residues are present in such an amount in all the rubredoxins for which the amino acid sequences have been determined. The amino acid composition of this rubredoxin is shown in table 1 and compared with seven other rubredoxins from *Desulfovibrio* species. Acidic amino acids are predominant in these proteins and all the rubredoxins isolated so far lack arginine. The absorption spectrum of the oxidized *D. desulfuricans* Berre-Eau rubredoxin, shown in fig.1, is similar to the optical spectra

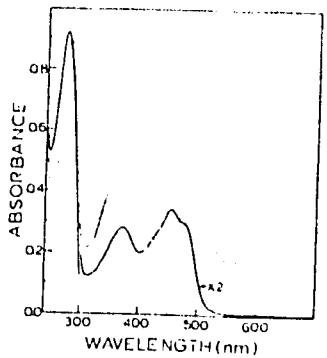

Fig.1. Absorption spectra of oxidized *D. desulfuricans* Berre-Eau flavodoxin (——) and rubredoxin (···). The protein concentrations for rubredoxin and flavodoxin were 50.8 and 34.9 μM, respectively.

Table 2

Amino acid composition of 4 flavodoxins from *Desulfovibrio* species

	D. gigas	*D. vulgaris* Hildenborough	*D. salexigens*	*D. desulfuricans* Berre-Eau
Lys	8	4	10	6
His	0	1	0	0
Arg	3	7	2	4
Trp	1	2	n.d.	n.d.
Asp	17	19	20	20
Thr	9	7	8	8
Ser	8	8	9	9
Glu	18	16	19	18
Pro	6	3	4	5
Gly	14–15	18	13	19
Ala	15	17	9	15
Cys(half)	5	4	3	7
Val	16	9	10	10
Met	2	1	1–2	2
Ile	5	9	9	6
Leu	14	12	10	14
Tyr	5	5	5	4
Phe	3	6	5	4
Total	149–150	148	137–138	151
References	[17]	[17]	[13]	this work

n.d., not determined

reported for rubredoxins from different *Desulfovibrio* species. The absorption maxima were at 278, 378 and 491 nm with molar extinction coefficients of 18521, 8396 and 6976 $M^{-1} \cdot cm^{-1}$, respectively (an error of ± 9% is estimated). Again, these values are similar to those obtained with other rubredoxins from *Desulfovibrio* and *Dm. acetoxidans* [9–15]. As for the *D. gigas* rubredoxin, the protein from *D. desulfuricans* Berre-Eau is completely reduced by ascorbate at pH 7.6. In contrast, the rubredoxins from *D. salexigens* British Guiana [13] and *D. vulgaris* Hildenborough (unpublished) are only partly reduced under the same conditions.

The oxidized form of rubredoxin shows an EPR spectrum which does not differ from that reported for other sulfate- and sulfur-reducing organisms [23]. High-spin ferric resonances were observed at g values 4.3 and 9.4 (below 20 K).

The amino acid composition of *D. desulfuricans* Berre-Eau flavodoxin is presented in table 2. The protein contains 151 residues, with a rather large proportion of acidic amino acids and is devoid of histidine, like almost all the flavodoxins (table 2). The minimum molecular mass was calculated to be 15801 Da and the value estimated by gel filtration was 15400 Da.

The absorption spectrum of *D. desulfuricans* Berre-Eau oxidized flavodoxin is shown in fig.1. The absorption maxima were at 274, 374 and 456 nm with molar extinction coefficients of 45835, 8460 and 10035 (an error of ± 10% is estimated) respectively and a shoulder is noticeable at 480 nm, identical to that obtained for *D. gigas* flavodoxin [16].

The results of the coupling effect of *D. desulfuricans* Berre-Eau rubredoxin and flavodoxin on sulfite reductase and pyruvate dehydrogenase activities are reported in table 3. Rubredoxin was inactive both in the coupling between hydrogenase and sulfite reductase and in the phosphoroclastic reaction. When compared with the endogenous activity of the control using acidic electron carrier-free extracts, the system containing the *D. desulfuricans* Berre-Eau flavodoxin exhibited significant stimulations for both sulfite reduction and H_2 evolution from pyruvate (table 3). There is an evident lack of specificity of *D. desulfuricans* Berre-Eau extract for the electron carrier isolated from the same strain mainly in the phosphoroclastic reaction. However, *D. vulgaris* Hildenborough and *Clostridium pasteurianum* flavodoxins are also active in the coupling between the pyruvate dehydrogenase and the hydrogenase (table 3).

Table 3

Coupling activity of *D. desulfuricans* Berre-Eau flavodoxin in the sulfite reductase activity and in the phosphoroclastic reaction

Enzymatic extract	Sulfite reductase activity[a]	Phosphoroclastic reaction[b]
Crude extract	9.30	7.90
DEAE-cellulose extract	1.10	1.35
+ *D. desulfuricans* Berre-Eau flavodoxin	6.45	6.70
+ *D. vulgaris* Hildenborough flavodoxin	4.95	6.10
+ *C. pasteurianum* flavodoxin	n.d.	5.45
+ methyl viologen	10.2	n.d.

[a] H_2 consumed in 20 min under the assay conditions
[b] H_2 evolved in 12 min under the assay conditions

Enzymatic activities were determined as described [22]. The crude extract and DEAE-cellulose-treated extract, prepared as in [22], contained 23 mg protein. Flavodoxins, 30 nmol (saturation conditions); methyl viologen, 100 nmol; n.d., not determined

The function of electron transfer proteins from *Desulfovibrio* species is far from being understood [24]. Here, we have reported the purification and characterization of a rubredoxin and a flavodoxin from *D. desulfuricans* Berre-Eau grown on a lactate-sulfate medium under non-nitrogen-fixing conditions. We have also isolated other proteins from this strain: two ferredoxins, a molybdenum-containing iron-sulfur protein, a low redox potential tetraheme cytochrome c_3 and a monohemic cytochrome c-553 [25]. As for other rubredoxins from strict anaerobic bacteria the physiological function of *D. desulfuricans* Berre-Eau rubredoxin is still unknown. The relatively high redox potential of *Desulfovibrio* rubredoxins (around 0 mV) [26] makes it difficult to place this electron carrier in the frame of the physiological reactions occurring during the metabolism of sulfate-reducing bacteria.

In the sulfate reducers of the genus *Desulfovibrio* flavodoxin may replace ferredoxin as electron carrier in both the pyruvate dehydrogenase system and sulfite reductase reaction [27]. The flavodoxin from *D. desulfuricans* Berre-Eau is also able, in the presence of hydrogenase, to mediate electron transport in the reduction of sulfite and in H_2 evolution from pyruvate. It will be interesting to test the specificity of the two ferredoxins from *D. desulfuricans* Berre-Eau in these two metabolic pathways.

ACKNOWLEDGEMENTS

We are indebted to Mrs I Carvalho for her skillful technical help and to Dr M. Scandellari and Mr R. Bourelli for growing the bacteria which have been used in this study. We thank B.C. Prickril for interesting discussions and I. Ribeiro for preparing the manuscript. This work was supported by INIC, JNICT and AID (J.J.G.M.) and National Science Foundation no. DMB-8602789 (J.L.).

REFERENCES

[1] Postgate, J.R. (1984) The Sulphate-Reducing Bacteria, 2nd edn, Cambridge University Press, Cambridge.
[2] Widdel, F. (1987) in: Biology of Anaerobic Organisms (Zehnder, A.J.B. ed.) Wiley, New York, in press.
[3] LeGall, J., Senez, J. and Pichinoty, F. (1959) Ann. Inst. Pasteur 96, 223–230.
[4] Nazina, T.N., Rozanova, E.P. and Kaulininskaya, T.A. (1979) Mikrobiologiya 48, 133–136.
[5] Lespinat, P.A., Denariaz, G., Fauque, G., Toci, R., Berlier, Y. and LeGall, J. (1985) CR Acad. Sci. Paris 301, 707–710.
[6] Postgate, J.R. and Kent, H.M. (1985) J. Gen. Microbiol. 131, 2119–2122.
[7] Newman, D.J. and Postgate, J.R. (1968) Eur. J. Biochem. 7, 45–50.
[8] Zubieta, J.A., Mason, R. and Postgate, J.R. (1973) Biochem. J. 133, 851–854.
[9] LeGall, J. and Dragoni, N. (1966) Biochem. Biophys. Res. Commun. 23, 145–149.
[10] Bruschi, M. and LeGall, J. (1972) Biochim. Biophys. Acta 263, 279–282.
[11] Bruschi, M., Hatchikian, C.E., Golovleva, L.A. and LeGall, J. (1977) J. Bacteriol. 129, 30–38.
[12] Hatchikian, C.E., Jones, H.E. and Bruschi, M. (1979) Biochim. Biophys. Acta 548, 471–483.
[13] Moura, I., Moura, J.J.G., Bruschi, M. and LeGall, J. (1980) Biochim. Biophys. Acta 591, 1–8.
[14] Sieker, L.C., Jensen, L.H., Prickril, B.C. and LeGall, J. (1983) J. Mol. Biol. 171, 101–103.
[15] Probst, I., Moura, J.J.G., Moura, I., Bruschi, M. and LeGall, J. (1978) Biochim. Biophys. Acta 502, 38–44.
[16] LeGall, J. and Hatchikian, E.C. (1967) CR Acad. Sci. Paris 264, 2580–2583.
[17] Dubourdieu, M. and LeGall, J. (1970) Biochem. Biophys. Res. Commun. 38, 965–972.
[18] Starkey, R.L. (1938) Arkv. Mikrobiol. 9, 268–304.
[19] Davis, B.J. (1964) Ann. NY Acad. Sci. 21, 404–427.
[20] Whitaker, J.R. (1963) Anal. Chem. 35, 1950–1953.
[21] Lowry, O.H., Rosebrough, N.J., Farr, A.L. and Randall, R.J. (1951) J. Biol. Chem. 193, 265–275.
[22] Fauque, G. (1985) Doctorat d'Etat Thesis, University of Technology of Compiegne, France.
[23] LeGall, J., Moura, J.J.G., Peck, H.D. jr and Xavier, A.V. (1982) in: Iron-Sulfur Proteins (Spiro, T.G. ed.) pp.177–248, Wiley, New York.
[24] LeGall, J. and Fauque, G. (1987) in: Biology of Anaerobic Organisms (Zehnder, A.J.B. ed.) Wiley, New York, in press.
[25] Moura, I., Fauque, G., LeGall, J., Xavier, A.V. and Moura, J.J.G. (1987) Eur. J. Biochem., in press.
[26] Moura, I., Moura, J.J.G., Santos, M.H., Xavier, A.V. and LeGall, J. (1979) FEBS Lett. 107, 419–421.
[27] LeGall, J., DerVartanian, D.V. and Peck, H.D. jr (1979) Curr. Top. Bioenerg. 9, 237–265.
[28] Hormel, S., Walsh, K.A., Prickril, B.C., Titani, K., LeGall, J. and Sieker, L.C. (1986) FEBS Lett. 201, 147–150.

D-03

SYNTHESIS OF MIXED METAL CLUSTERS FROM A [Fe$_3$S$_4$] CORE.

J.J.G.Moura(*), I.Moura(*),K.Surerus(**) V. Papaefthymiou (**), E.Münck (**) and J.LeGall (***).

(*)Centro de Quimica Estrutural, Complexo I, UNL, Av. Rovisco Pais, 1096 Lisboa, Portugal.
(**) Gray Freshwater Biological Institute, Univ. of Minnesota, P.O.Box 100, Navarre, MN 55392, U.S.A.
(***)Department of Biochemistry, Univ. of Georgia, Athens, GA 30602, U.S.A.

Ferredoxin II (FdII) isolated from Desulfovibrio gigas, a sulfate reducer, contains a single [Fe$_3$S$_4$] core. It was previously shown that this cluster can be interconverted into a [Fe$_4$S$_4$] cluster upon incubation of reduced FdII with Fe^{2+}, in the presence of dithiothreitol [1]. The facility of the conversion [Fe$_3$S$_4$] $\leftrightharpoons$ [Fe$_4$S$_4$] has suggested a way of incorporating other metals into the vacant site of a [Fe$_3$S$_4$] core and thus generate a series of novel metal clusters, [MFe$_3$S$_4$], using the native structure of FdII as a synthetic precursor. The formation of a [CoFe$_3$S$_4$]$^{1+,2+}$ cluster was fully demonstrated by chemical analysis, EPR and Mössbauer measurements. In the oxidized state the cluster exhibits an S=1/2 EPR signal with g-values at g_x=1.82, g_y=1.92 and g_z=1.98. The well-resolved ^{59}Co hyperfine lines at the g_z line (A_z ~4.4 mT) are also broadened by ^{57}Fe isotopic substitution indicating that Fe and Co share a common unpaired electron. Upon one electron reduction (E_0 ~-220 mV) the cluster becomes EPR silent. Mössbauer studies in strong applied fields shows that the reduced state has an integer electron spin, with $S > 0$. The formation of a [ZnFe$_3$S$_4$]$^{+1}$ core by incubation of FeII with excess Zn^{2+} under reducing conditions, transforms the native FeS cluster into a structure with unique spectroscopic properties. The reduced ZnFe cluster exhibits well resolved EPR signals typical of an S=5/2 spin system. The associated Mössbauer spectrum has features quite different from other FeS clusters. The spectra reveal two types of iron sites: one site is typical of Fe^{2+} while the other contains a Fe^{3+}/Fe^{2+} delocalized pair. The described protein - matrix - assisted inorganic synthesis provides an interesting pathway for the formation of novel mixed-metal clusters. A renewed interest in this field arises from: i) possibility of forming new bio-catalysts with unexpected properties; ii) introduction of a site into a cubane structure with different magnetic properties enabling the exploration of magnetism in valence - delocalized systems as well as simplifying the spectral analysis; iii) synthesis of relevant model compounds via the formation of mixed metal cubane structures containing other metals like molybdenum, vanadium and nickel. This synthesis is also potentially interesting for specifically modifying a [FeS] core in a complex enzyme.

1. J.J.G. Moura (1986), in "Iron-sulfur Protein Research", eds.H.Matsubara et al pp.149-164.
2. I. Moura , J.J.G. Moura , E. Münck , V. Papaefthymiou, and J. LeGall, (1986) J. Am. Chem. Soc. 108, 349-351.
3. K. Surerus , E. Münck , I. Moura , J.J.G. Moura and J. LeGall (1987) submitted to J. Am. Chem. Soc.

We thank Dr. A.V. Xavier for valuable discussions. This worked was supported by AID, JNICT, INIC and NATO.

120

B-24

G-19

A COMPARATIVE STUDY OF TWO DISSIMILATORY SULFITE REDUCTASES FROM SULFATE-REDUCING BACTERIA

I.Moura (*), A.R.Lino(*),J.J.G.Moura(*), A.V. Xavier (*), G. Fauque (**), D.V. DerVartanian (**), H.D. Peck Jr. (**), J. LeGall (**) and B.H. Huynh (***).

(*) Centro de Quimica Estrutural, Complexo I, UNL, Av.Rovisco Pais, 1096 Lisboa, Portugal
(**) Department of Biochemistry, Univ. of Georgia, Athens, GA 30602, U.S.A.
(***) Department of Physics, Emory Univ. Atlanta, GA 30322, U.S.A.

Sulfite reductase catalyses the six-electron reduction of sulfite to sulfide, a key step in the biological sulfate-reduction pathway. Based on their physiological function, sulfite reductase can be grouped into two general categories: i) assimilatory sulfite reductase which are involved in the synthesis of sulfur containing cell constituents and ii) dissimilatory sulfite reductase which participate in the terminal respiration. Extensive physical and biochemical methods have been applied to the study of the assimilatory sulfite reductase from E.coli and a wealth of information has been obtained for its functional subunit an exchange coupled siroheme-[4Fe-4S] unit [1]. A variety of dissimilatory sulfite reductases have been purified from several sulfate reducing bacteria: desulfoviridin, desulforubidin, P582 and desulfofuscidin [2]. We have undertaken a study of desulfoviridin isolated from Desulfovibrio gigas and desulforubidin from Desulfovibrio baculatus (9974). These two proteins show very different spectroscopic characteristics. The visible spectra of both proteins show drastic differences. In conditions where a siroheme is extracted from desulforubidin, a spectrum characteristic of siroporphyrin is obtained from desulfoviridin. So, a question arises whether in the native desulfoviridin a siroheme or a siroporphyrin is present. Both proteins show in the native state EPR spectra characteristic of the siroheme in a high-spin state (S=5/2) with g values at 6.97, 4.72 and 1.93 for desulfoviridin and at 6.43, 5.33 and 1.97 for desulforubidin. The comparison of signal intensities show that only 26% of a heme signal is observed for desulfoviridin. The total iron content of desulfoviridin and desulforubidin is respectively 18 ± 1 and 21 ± 1 moles per mole of protein. The siroporphyrin/siroheme quantitation in both proteins accounts for nearly 2 of these groups per mole of protein. Mössbauer studies were performed on both proteins purified from ^{57}Fe enriched cells. Again, some interesting differences in the siroheme content were observed. The Mössbauer spectrum of desulforubidin shows a central doublet with Mössbauer parameters characteristic of [4Fe-4S]$^{2+}$ clusters. Besides this doublet there is a magnetic spectral component extending from -4.2 mm/s to +4.0 mm/s due to the high-spin ferric siroheme and signals at - 1.1 mm/s and +2.0 mm/s indicative of a [4Fe-4S] cluster coupled to the paramagnetic siroheme. The intensities of the Mössbauer absorptions for the uncoupled [4Fe-4S] cluster and the coupled siroheme-[4Fe-4S] unit are similar indicating that the siroheme-[4Fe-4S] unit ratio is about 1 to 2 of the total [4Fe-4S] clusters. This ratio is in agreement with the chemical analysis that shows that the ratio [4Fe-4S]/siroheme is 2.2. The Mössbauer spectrum of ^{57}Fe enriched desulfoviridin obtained in the same experimental conditions shows a very small amount of coupled siroheme-[4Fe-4S] unit (only 12% of this unity is observed). This means that the ratio of siroheme-[4Fe-4S] to uncoupled [4Fe-4S] is 0.5 to 3.5 clusters per mole of protein. This ratio is in agreement with the EPR quantitation. The present data clearly show that the active center composition of both proteins are different. Desulforubidin contains 2 siro-heme-[4Fe-4S] coupled unities and 2 [4Fe,4S] per mole of protein in contrast with desulfoviridin where the amount of coupled center is only 25% suggesting the presence of 0.5 siroheme-[4Fe-4S] coupled unities, 1.5 siroporphyrin and 3.5 [4Fe-4S] clusters per mole of protein. The physiological significance of this difference is still not fully understood.

1. E. Münck, in "Iron-Sulfur proteins", ed. T.G. Spiro, pp.147-175, (1982) (and references there in).
2. J. LeGall and G. Fauque, in "Environmental Microbiology of Anaerobes", ed. A.J.B. Zehnder (1987) in press.

ACKNOWLEDGMENTS
We thank INIC, JNICT, AID and NATO for financial support.

121

B-25

H-15

THE ALDEHYDE OXIDASE ACTIVITY OF DESULFOVIBRIO GIGAS Mo(Fe,S) PROTEIN

B.A.S.Barata (*), N.Turner(**), R.C.Bray(**), A.V.Xavier(*), J.LeGall(***) and J. G.Moura(*)

(*) Centro de Quimica Estrutural, Av.Rovisco Pais, 1096 Lisboa, Portugal.
(**) School of Chemistry and Molecular Sciences, University of Sussex, Falmer, Brighton BN1 9QJ, U.K.
(***) Department of Biochemistry, University of Georgia, Athens, GA 30602

The Mo-protein isolated from Desulfovibrio gigas (NCIB 9332) is a non-heme iron protein containing no FAD and a Mo atom per 120 KDa (no subunits).The UV/Visible spectrum of this protein is rather similar to those observed for the deflavo forms of the xanthine and aldehyde oxidases(1). CD and EPR identified a [2Fe-2S] arrangement of the iron-sulfur cores(1,2). Besides the molybdenum "Resting" and "Slow" type EPR signals previously described(2), it was recently shown to be possible to develop a Mo(V) "Rapid type 2" EPR signal centered at g_{av}=1.9742 similar to those observed for the xanthine and aldehyde oxidases (3). These "Rapid" type EPR signals have been shown, in these proteins, to be physiologically significant as they develop within enzyme turnover time scale. The observed "Rapid" signals were not only obtained after a short reduction time with dithionite but also with some substrates. Actually, the search of these "Rapid" signal-producing-substrates was initiated after the detection and isolation of the dithionite generated one. These Mo-"Rapid" signals were visualized by spectral subtraction, since they were obtained in a complex mixture of different Mo(V) EPR active species. Several aldehydes (e.g., benzaldehyde, salicylaldehyde) were capable of not only to generate the "Rapid" signal but also to have their electrons mediated by the protein to a suitable electron acceptor (DCPIP=2.6-dichlorophenolindophenol). This DCPIP dependent aldehyde oxidase activity was followed in a wide range of substrate concentrations and the kinetic parameters were estimated. The best activities correspond to acetaldehyde and benzaldehyde turnovers. It is interesting to notice the following facts: i) rather low Km values were obtained with some substates in terms of standard aldehyde oxidase activities; ii) a simple Michaelis-Menten model is suitable, as a first approximation,to account for the kinetic data; iii) xanthine, purines and N'methylnicotinamide could not be utilised by the protein as substrates. Although the physiological role of D.gigas Mo-protein is still unknown this capability to hydroxilate without FAD (as compared to xanthine/aldehyde oxidases) or heme (as in sulfite oxidase models) is consistent with the fact that these domains are related, in these proteins, to the oxidation with O_2. The Mo protein from this sulfate-respiring anaerobic bacterium is not capable to operate with molecular oxygen as an electron acceptor.

ACKNOWLEDGMENTS
We would like to thank INIC, JNICT, USAID and the British Council for financial support.

1. J.J.G.Moura, A.V.Xavier, M.Bruschi, J.LeGall, D.O.Hall and R.Cammack.(1976), Biochem.Biophys.Res.Commun, 72, 782-789.
2. J.J.G.Moura, A.V.Xavier, R.Cammack, D.O.Hall, M.Bruschi and J.LeGall. (1978), Biochem.J.173, 419-425.
3. N.Turner, B.Barata, R.C.Bray, J.Deistung, J.LeGall, and J.J.G.Moura. (1987), Biochem.J., 243,(in press.)

H-16

THE ROLE IN AZOTOBACTER VINELANDII OF THE IRON PROTEIN OF NITROGENASE IN IRON-MOLYBDENUM COFACTOR BIOSYNTHESIS

Jai-Ge Li (*), Amy C. Robinson (**), Dennis R. Dean (***) and Barbara K. Burgess (**)

(*) Institute of Botany, Academia Sinica, Beijing China, present address (**)
(**) Department of Molecular Biology and Biochemistry, University of California-Irvine, Irvine California 92717 USA
(***) Department of Anaerobic Microbiology, Virginia Polytechnic Institute and State University, Blacksburg, Virginia 24061 USA

The enzyme nitrogenase is the catalytic component of the biological nitrogen fixation system. It is composed of two separately purified oxygen-sensitive proteins called the iron protein (Fe-protein) and the molybdenum-iron protein (MoFe-protein). The Fe protein has two identical subunits, a native molecular weight of ca. 60,000 daltons, and contains a single [4Fe-4S] cluster. The MoFe protein is a two-alpha two-beta tetramer, with a native molecular weight of ca. 220,000 daltons, containing two Mo atoms, 32+3 Fe atoms and a similar number of S atoms per tetramer. The metals are believed to be arranged in four [4Fe-4S] clusters, two uncharacterized iron clusters (S-centers), and two iron-molybdenum cofactors (FeMo-co) centers. The FeMoco is thought to be the actual site of N_2 binding and reduction [1]. It is not known where the electrons enter or reside in the MoFe protein prior to reduction of substrate at the FeMoco center. The genetics of biological nitrogen fixation are quite complex. In the obligately aerobic, free living, nitrogen fixing organism, Azotobacter vinelandii, there are at least 16 nitrogen fixation genes, which are clustered in one area on the genome. The three genes coding for the structural proteins of nitrogenase are in one operon. This operon is arranged as: promotor, nifJ(Fe protein), nifD (MoFe protein alpha subunit), nifK (MoFe protein beta subunit) and nifY (a gene of unknown function). The structural genes have been isolated and the complete nucleotide sequence determined [2].

B-26

J-16

GLUCOSEISOMERASE, OBVIOUSLY THE FIRST NATIVE COBALT ENZYME

Jörg Hemker, Ludger Kleinschmitdt and Herbert Witzel

Department of Biochemistry, University of Münster, Wilhelm-Klemm-Straße 2, 4400 Münster

Glucoseisomerase of several streptomyces strains is a tetrameric enzyme [1,2] . It contains one non-corrinoid Co(II) ion in the native form. Beside this central Co(II) there are two further sites for Co(II) interactions at the enzyme. The central cobalt ion forms a low spin Co(II) complex as indicated by EPR-spectroscopy (with Gersonde, Aachen) seen in Fig. 1

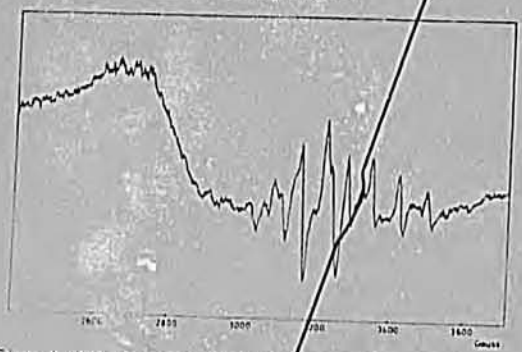

Fig. 1 EPR spectrum of the one-cobalt(II) Glucoseisomerase

The $g_\perp$ signal at 2.36 and the $g_\parallel$ signal at 2.02 show rhombic symmetry with hyperfine splitting expected for low spin complexes. No signal is detected in the range for high spin complexes. Compared with vitamine B12 no superhyperfine splitting is seen as caused there by the benzimidazol ligand in axial position.
EXAFS measurements (see Nolting et al. - this conference) indicate a distorted octahedral symmetry of the cobalt center and a ligation to N or O ligands. S-ligands can be excluded.
ENDOR measurements (with Hüttermann, Homburg-Saar) as seen in Fig. 2 indicate only one type of nitrogen ligands with a coupling constant of 16 MHz. These nitrogen ligands probably are imidazoles from histidines.
The visible spectrum of the enzyme shows only a shoulder at 410 nm and a slight maximum at 735 nm. The weak absorbance bands indicate also a distorted octahedral co-ordination of the Co(II) ion. Addition of cyanide in presence of dithionite shifts the absorption from 410 nm to a maximum at 385 nm. The dithionite does not reduce the Co(II) ion. We suggest that one of the axial ligands not belonging to the enzyme is replaced by the cyanide ligand. The cyanide derivate of Co(II) substituted carboanhydrase which also is a low spin complex shows a similar VIS-spectrum [3] .

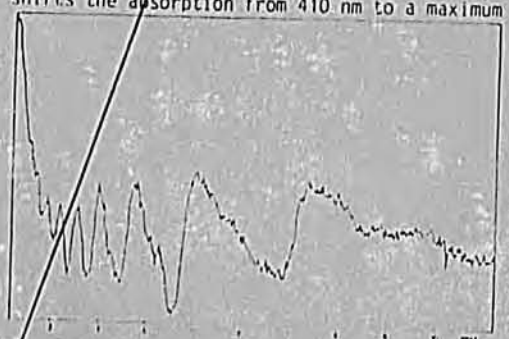

Fig. 2 ENDOR spectrum of the one-cobalt(II) Glucoseisomerase [in a plot]

The cobalt ion can be removed with loss of activity at pH 9 at higher temperature (half-life time at 80°C is 70 min), at pH 4,5 (half-life time at 25°C is 60 min), or at pH 7 and low temperature (25°C) in presence of EDTA after several days. HPLC analysis shows, that heat treatment of the enzyme leads to a dissociation into the monomers, which aggregate if the temperature or pH is lowered or salts are added. Reconstitution is not possible. Small reactivation effects are only found in low temperature experiments.

Addition of four equivalents of Co(II) to the enzyme increase the heat stability for a further 10°C and stabilizes the enzyme at lower pH values. Compared with the one Co(II) enzyme the activity is increased up to 250% when the Co(II) concentration is 0.01 mM. The EPR-spectrum shows a rhombic signal at g = 4,2 indicating that this peripheral cobalt is bound as a high spin Co(II). The visible spectrum at pH above 8 indicates a tetrahedral symmetry, at lower pH values a pentacoordinated structure might be formed.
Paramagnetic proton NMR measurements (with Bertini, Florence) cannot be applied at the mono-Co(II) enzyme because of the slow relaxation of the Co nucleus in the low spin complex.
Studies on the high spin four-Co(II) enzyme with this method indicates that there are four identical and specific binding sites for Co(II). This Co(II) does not interact with the substrate.
The enzyme requires Mg(II) ions for its activity and is saturated at a concentration of 5 mM. Saturation with Co(II) in presence of Mg(II) is reached at a concentration of 0.1 mM. 15% activity at 40°C and 50% activity at 70°C is obtained. This indicates that Cobalt interacts also at the Mg(II) binding site and still catalyzes the reaction, however with lower efficiency. The Mg(II) binding site can be titrated with Cd(II), a very strong competitive inhibitor for Mg(II). A Scatchard plot indicates that there are four binding sites at the tetrameric enzyme

1. R.A. Hogue-Angeletti, J. Biol. Chem. 250, 7814 (1975)
2. W.P. Chen, Process Biochem. 15, 36 (1980)
3. S.A. Cockle, Biochem. J. 137, 587 (1974)

J-17

EVIDENCE FOR THE PRESENCE OF A NATIVE METHYLATED B_{12} PROTEIN IN A THERMOPHILIC METHANOGENIC BACTERIUM

Ana R.Lino (*), José J.G.Moura (*), Jean LeGall (**), António V.Xavier (*) and Isabel Moura (*)

(*) Centro de Química Estrutural, Complexo I, UNL, Av.Rovisco Pais, 1096 Lisboa, Portugal
(**) Department of Biochemistry, Univ. of Georgia, Athens, GA 30602, U.S.A

We have previously characterized two B_{12} proteins from Methanosarcina barkeri (DSM 800 and 804) [1]. The proteins were shown by visible spectroscopy to contain

the corrinoid in the aquocobalamine form. In addition the corrinoids were extracted and purified from cell extracts and also from the purified proteins in their cyano form. Visible, NMR and EPR spectroscopies were used in order to identify factor III (5-hydroxibenzimidazole cobalamine) as the corrinoid present in the purified proteins. Also, this is the major corrinoid component in the cell extracts [1]. Here we report the isolation of a B_{12} containing protein from a thermophilic methanogenic bacterium Methanosarcina MST. The protein was isolated from the soluble extract of cells grown on a methanol containing medium. Several chromatographic steps (DEAE-Biogel, DEAE-52, gel filtration on a HPLC with a column of Spherogel TSK-G-3000) were used in order to obtain a homogeneous protein fraction. The UV/visible spectrum of this protein on the native form shows absorption maxima at 538 nm, 358 nm and 277 nm typical of a methylated corrinoid (Figure 1-A).

Fig.1-(A) Absorption spectrum of B_{12} containing protein from Methanosarcina MST in the native form
(B) EPR spectrum of B_{12} containing protein from Methanosarcina MST after photolysis under reducing conditions.
EPR conditions:
Microwave frequency: 9.52 GHz
Temperature: 40 K; Microwave power: 2 mW
Field Modulation: 1 mT

An EPR active Co(II) species could be obtained from this protein by photolysis under reducing conditions of the already present CH_3-Co bond, not requiring a methylating step [1]. The EPR spectrum at 40 K obtained under the described conditions show typical signals of a stable Co(II) complex (Figure 1-B). Triplets are observed from the N-hyperfine interaction of the coordinated benzimidazole base. Thus, the nucleotide base is coordinated to the cobalt corrinoid in its protein bound form. To our knowledge this is the first evidence for the purification of a B_{12} containing protein in a methylated form.

1. A. R. Lino, A. V. Xavier, I. Moura, J. LeGall and L. G. Ljungdahl, Rev. Port. Quim., 27, 175 (1985).

ACKOWLEDGMENTS
We thank INIC, JNICT, AID and NATO for financial support

^{13}C-NMR STUDIES OF THE BASE-ON-BASE-OFF EQUILIBRIUM OF METHYLCOBALAMIN

Kenneth L. Brown and Sherri Peck

Department of Chemistry, Box 19065, The University of Texas at Arlington, Arlington, Texas 76019

The thermodynamics of the base-on-base-off reaction of methylcobalamin have been studied, at several ionic strengths, by measurement of the difference in chemical shift between ^{13}C enriched methylcobalamin ($^{13}CH_3Cbl$) and methylcobinamide ($^{13}CH_3Cbi$) as a function of temperature. Analysis of the results via an equation which takes into account both the (apparently linear) temperature dependence of the chemical shifts of the base-on and base-off forms and the temperature dependence of the base-on/base-off equilibrium allows calculation of the apparent pK_a of the pendent, protonated dimethylbenzimidazole moiety at 25°C. The values obtained (pK_{Bz}) and the relevant values of the pK_a of free α-ribazole at various ionic strengths are listed in Table I. The values of pK_{Bz} are significantly lower than the pK_a's

Table I:

I, M	pK_{Bz}	pK_a (α-ribazole)
0.0	4.39	5.38
0.1	4.57	5.47
1.0	4.85	5.56

of α-ribazole at all ionic strengths suggesting a substantial interaction of the pendent nucleotide with the remainder of the structure in the base-off form. Such an interaction has recently been demonstrated [1] by comparison of the natural abundance ^{13}C NMR spectrum of dicyanocobalamin with that of dicyanocobinamide, and characterized as a hydrogen bonding interaction of the pendent, free base benzimidazole N-3 with an amide proton on the e side chain. Reinterpretation of these results using a scheme for the base-on/base-off equilibrium which includes this hydrogen bonded complex allows calculation (at 25°) of the equilibrium constant for formation of this complex from the base-off,deprotonated specier (K_H) and the equilibrium constant for formation of the base-on species from the base-off, deprotonated species (K_{Co}). As seen in Table II,

Table II:

I, M	K_H	K_{Co}
0.0	8.7	480
0.1	6.8	505
1.0	4.2	452

K_H is ionic strength dependent but K_{Co} is independent of ionic strength, and the average value of K_{Co} (472 ± 26) is nearly identical to the value previously calculated (467 [2]) from the simpler scheme omitting the hydrogen bonded species. By use of the values of the base-on/base-off pK_a ($pK_{base\text{-}off}$) for methylcobalamin and α-ribazole previously determined at various temperatures [2] K_{Co} and K_H may also be calculated at several temperatures (at I = 1.0 M). The results (Table III) lead

Table III:

T(°C)	$pK_{base\text{-}off}$	pK_{Bz}	K_H	K_{Co}
5.2	2.84	5.90	4.18	1140
15.1	2.86	5.68	3.79	656
25.0	2.90	5.56	4.16	452
34.9	2.92	5.40	4.14	297

to values of ΔH_H = 0.1 kcal mol^{-1} and ΔS_H = 3.1 eu for formation of the hydrogen bonded complex and ΔH_{Co} = -7.6 kcal mol^{-1} and ΔS_{Co} = -13.4 eu for formation of the base-on species. The latter values compare favorably with those previously determined [2] using the simpler scheme without the hydrogen bonded complex (ΔH_{Co} = -7.1 kcal mol^{-1}, ΔS_{Co} = -17.4 eu).

1. K.L. Brown, *J. Am. Chem. Soc.*, in press.
2. K.L. Brown, J.M. Hakimi, D.M. Nuss, Y.D. Montejano, and D.W. Jacobsen, *Inorg. Chem.* 23, 1463 (1984).

124

O-27

SPECTROSCOPIC STUDIES OF COBALT AND NICKEL SUBSTITUTED RUBREDOXIN

I.Moura(*), M.Teixeira(*), A.V.Xavier(*), J.J.G.Moura(*), P.A. Lespinat(**), J. LeGall(**), Y. M. Berlier (**), P. Saint-Martin(**) and G.Fauque(**)

(*) Centro de Quimica Estrutural, Complexo I, UNL, Av.Rovisco Pais, 1096 Lisboa, Portugal
(**) A.R.B.S., C.E.N., Cadarache, Saint-Paul-lez-Durance, France

Rubredoxins are the simplest iron-sulfur proteins. The active center is characterized by the absence of labile S and the presence of one iron atom linked in a tetrahedral arrangement to the S atoms of four cysteinyl residues. This protein has been isolated from several sulfate and sulfur reducing organisms [1]. The very simple constitution of the active center and the low molecular mass (≈6 KDa) makes rubredoxin suitable for the synthesis of metal substituted derivatives. It was previously shown that substitution of the native iron by ^{57}Fe [2] or ^{54}Fe [3] isotopes could produce an isomorphous replacement of the native center being amenable for the application of Mössbauer spectroscopy and assignment of Fe-S stretching modes observed in the Resonance Raman spectrum. The obtention of derivatives with other metals is of high spectroscopic interest and can be useful as simple enzyme models. Replacement of iron by cobalt was already reported for the rubredoxin of Pseudomonas oleovorans (molecular mass ≈19 KDa) [4]. Here we report the replacement of iron by cobalt and nickel in rubredoxins isolated from several Desulfovibrio sp. Apo-rubredoxin (iron free), obtained after precipitation of the native protein with TCA in the presence of mercaptoethanol, was then redissolved in Tris-base containing mercaptoethanol (under Argon). Stoichiometric amounts of cobalt (II) nitrate and nickel (II) nitrate were added. The reconstituted materials where subsequently purified by gel chromatography. A stoichiometric amount of Ni and Co was shown to be present in the metal substituted rubredoxins. In Figure 1 we compare the visible spectra of the native rubredoxin with those for the Co and Ni substituted ones.

Fig.1. Visible/U.V. absorption spectra of Co (A), Ni (B) and Fe (C) rubredoxins (from D.gigas)

Both the d-d and the charge transfer spectral regions closely resemble those of simple tetrathiolate complexes. The ^{1}HNMR spectra of the nickel and cobalt substituted rubredoxins reveal extremely low-field shifted resonances. The spectrum of the nickel-rubredoxin (Fig.2) shows eight low-field resonances of one proton intensity with a Curie law temperature dependence at 349.9, 344.7, 274.8, 261.2, 194.5, 185.2, 160.0, 155.6 ppm (at 308 K).

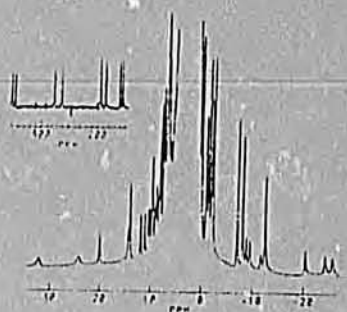

Fig.2. ^{1}HNMR spectrum of Ni-rubredoxin from D.gigas.

These resonances can be assigned to protons of the cysteinyl ligands. Other well resolved low-field and high-field resonances (probably of pseudo-contact origin) can be observed outside the main spectrum of the protein envelope in contrast to the native protein. Several resonances are also resolved in the low and high field spectral regions of the cobalt-rubredoxin. At least five resonances are detected in the very low field region (120.6, 110.6, 88.9, 56.5, 48.6, 43.2 ppm, at 308 K) which are tentatively assigned to cysteinyl protons. The present data is very promising in terms of structural analysis of the coordination sphere and environment of the metal core. The nickel substituted rubredoxins were shown to be active in both the D_2/H^+ exchange reaction and in H_2 production (from dithionite reduced methylviologen). The values of D_2/H^+ exchange rates are comparable with those observed for Pt catalysts. The H_2 evolution is competitively inhibited by carbon monoxide. The nickel substituted rubredoxins, providing a sulfur environment for the metal center, mimic, in many respects, the bacterial hydrogenase activity and may prove to be a useful model for nickel containing enzymes.

1 I.Moura, J.J.G.Moura, M.H.Santos, A.V.Xavier and J.LeGall, FEBS Lett. 107, 419 (1979)
2 I.Moura, B.H.Huynh, R.P.Hausinger, J.LeGall, A.V Xavier and E Münck, J Biol Chem 255, 2493 (1980)
3 R.S Czenuszewicz, J LeGall, I Moura and T.G.Spiro, Inorg.Chem 25, 696 (1986)
4 S.W.May and J.Y.Kuo, Biochem 17, 3333 (1978)

This work was supported by INIC, JNICT, AIP and NATO

B·28
(622/135

Characterization of electron transfer proteins from the nitrogen-fixing sulfate-reducing bacterium Desulfovibrio desulfuricans Berre-Eau

Guy FAUQUE[*], Isabel MOURA[±], Antonio V. XAVIER[±], Nicole GALLIANO[*], José J.G. MOURA[±] and Jean LE GALL[*‡]

[*] Section Enzymologie et Biochimie Bactérienne, A.R.B.S., C.E.N. Cadarache, 13108 Saint-Paul-Lez-Durance Cédex, France;

[±] Centro de Quimica Estrutural, Complexo I, UNL, 1096 Lisbon Codex, Portugal, and

[‡] School of Chemical Sciences, Department of Biochemistry, University of Georgia, Athens, GA 30602, U.S.A.

Fixation of molecular nitrogen has been observed with different sulfate-reducing bacteria of the genera Desulfovibrio (Le Gall et al., 1959 ; Postgate, 1984 ; Postgate and Kent, 1984 ; Postgate and Kent, 1985 ; Lespinat et al., 1987), Desulfotomaculum (Postgate, 1970 ; Lespinat et al., 1985 ; Fauque, 1985), Desulfobacter and Desulfobulbus (Widdel, 1987). Desulfovibrio (D.) desulfuricans strain Berre-Eau (NCIB 8387) is able to grow while fixing nitrogen (Le Gall, 1967).

Several electron carriers have been purified from D. desulfuricans Berre-Eau grown on lactate/sulfate medium with combined nitrogen. The rubredoxin and the flavodoxin present similar characteristics to homologous proteins found in other Desulfovibrio species (absorption spectrum, molecular mass, amino-acid composition, molar extinction coefficient) (Fauque et al., 1987). In contrast to rubredoxin, flavodoxin is able, in the presence of hydrogenase, to mediate electron transfer in the reduction of sulfite and in the hydrogen evolution from pyruvate.

A tetrahemic and a monohemic c-type cytochromes have been isolated and characterized from D. desulfuricans Berre-Eau by electron paramagnetic resonance (~~EPR~~ e.p.r.) and nuclear magnetic resonance (~~NMR~~ n.m.r.) spectroscopic techniques (Moura et al., 1987). The multiheme cytochrome c has a molecular mass of 13.5 kDa and an isoelectric point of 8.6. It presents visible, ~~NMR~~ n.m.r. and ~~EPR~~ e.p.r. spectra similar to the class of tetraheme cytochrome c3, the low-potential bis-histidinyl axially bound hemoprotein found in all Desulfovibrio species (Le Gall and Fauque, 1987), in Thermodesulfobacterium commune (Hatchikian et al. 1984) and in Desulfobulbus elongatus (Samain et al., 1986). The amino-acid

Rec'd in SCI. AUG 7 1987

Abbreviations used : e.p.r., electron paramagnetic resonance

composition of D. desulfuricans Berre-Eau tetraheme cytochrome c3 is the following : lysine (16 residues), histidine (9), arginine (0), tryptophane (0), aspartic acid (20), threonine (7), serine (11), glutamic acid (2), proline (6), glycine (10), alanine (25), cysteine (8), valine (2), methionine (0), isoleucine (2), leucine (3), tyrosine (1) and phenylalanine (2). This protein, devoid of arginine, tryptophane and methionine, contains 124 residues and possesses the required number of cysteine (8 residues) to bind four hemes per molecule. The main characteristics of this hemoprotein are a high number of alanine residues and a low content of valine residues.

The monohemic cytochrome c553 from D. desulfuricans Berre-Eau is completely reduced by ascorbate and its EPR and NMR data are characteristic of a cytochrome with methionine-histidine ligation (Moura et al., 1987). This protein has an isoelectric point of 9.2, a molecular mass of 9 kDa and its amino-acid composition is : lysine (10 residues), histidine (1-2), arginine (1), tryptophane (0), aspartic acid (7), threonine (2), serine (7), glutamic acid (8), proline (1), glycine (18), alanine (16), cysteine (2), valine (1), methionine (1), isoleucine (1), leucine (5), tyrosine (3) and phenylalanine (0). The presence of two cysteinyl residues is just sufficient to link a single heme group to the apoprotein. This amino-acid composition is very close to that reported for D. vulgaris Hildenborough cytochrome c553 (Bruschi and Le Gall, 1972) except for the glycine and tyrosine content. The D. desulfuricans Berre-Eau cytochrome c553 is more closely related to the cytochrome c553 from D. vulgaris Hildenborough than to the cytochrome c553(550) from D. baculatus strains Norway 4 (Fauque et al., 1979b) and DSM 1743 (Fauque, 1979a). These data confirm that two different types of monohemic cytochrome c are present in Desulfovibrio species.

We have also isolated from D. desulfuricans Berre-Eau other electron carriers and enzymes such as, two ferredoxins, a molybdenum-containing iron-sulfur protein, the adenylyl sulfate (APS) reductase and a dissimilatory sulfite-reductase of the desulfoviridin type.

This work was supported by grants from NIH (GM 34903) to JLG and from INIC, JNICT and AID to JJGM.

(3) (PNΣ - bold only where indicated)

REFERENCES

Bruschi, M. and Le Gall, J. (1972) Biochim. Biophys. Acta 271, 48-60

Fauque, G. (1979a). Thèse de Doctorat de Spécialité, University of Aix-Marseille I, 121 p.

Fauque, G. (1985). Thèse de Doctorat d'Etat, University of Technology of Compiègne, 222 p.

Fauque, G., Bruschi M. and Le Gall, J. (1979b) Biochem. Biophys. Res. Comm. 86, 1020-1029

Fauque, G.D., Moura, I., Moura, J.J.G., Xavier, A.V., Galliano, N. and Le Gall, J. (1987) FEBS Lett., in the press (?) No

Hatchikian, E.C., Papavassiliou, P., Bianco, P. and Haladjian, J. (1984) J. Bacteriol. 159, 1040-1046

Le Gall, J. (1967) Thèse de Doctorat d'Etat, University of Aix-Marseille, 135 p.

Le Gall, J. and Fauque, G. (1987) in Biology of Anaerobic Microorganisms (Zehnder, A.J.B., ed), John Wiley and Sons, in the press (?) No

Le Gall, J., Senez, J.C. and Pichinoty, F. (1959) Ann. Inst. Pasteur, Paris 96, 223-230

Lespinat, P.A., Denariaz, G., Fauque, G., Toci, R., Berlier, Y. and Le Gall, J. (1985) C.R. Acad. Sc. Paris, Sciences 301, 707-710 o.k.

Lespinat, P.A., Berlier, Y.M., Fauque, G.D., Toci, R., Denariaz, G. and Le Gall, J. (1987) J. Ind. Microbiol., ~~in the press~~ (?) 1, 383 - 388

Moura, I., Fauque, G., Le Gall, J., Xavier, A.V. and Moura, J.J.G. (1987) Eur. J. Biohem. 162, 547-554

Postgate, J.R. (1970) J. Gen. Microbiol. 63, 137-139

– Postgate, J.R. (1984) in the Sulphate-Reducing Bacteria, 2nd ed., 208 p., Cambridge University Press

Postgate, J.R. and Kent, M.H. (1984) J. Gen. Microbiol. 130, 2825-2831

– Postgate, J.R. and Kent, M.H. (1985) J. Gen. Microbiol. 131, 2119-2122

– Samain, E., Albagnac, G. and Le Gall, J. (1986) FEBS Lett. 204, 247-250

– Widdel, F. (1987) in Biology of Anaerobic Microorganisms (Zehnder, A.J.B., ed.), John Wiley and Sons, in the press

No

Received 27 March 1987

Eur. J. Biochem. ●, ●–● (1987)

B-29 (73)

Nickel-[iron-sulfur]-selenium-containing hydrogenases from *Desulfovibrio baculatus* (DSM 1743)

Redox centers and catalytic properties

Miguel TEIXEIRA[1], Guy FAUQUE[2,3], Isabel MOURA[1,3], Paul A. LESPINAT[2], Yves BERLIER[2], Ben PRICKRIL[3], Harry D. PECK Jr[3], António V. XAVIER[1], Jean Le GALL[2,3] and José J. G. MOURA[1,3]

[1] Centro de Química Estrutural, Universidade Nova de Lisboa
[2] A■ R■ B■ S■, Centre d'Etudes Nucleaires, Cadarache
[3] Department of Biochemistry, University of Georgia, Athens

(Received February 13/April 10, 1987) – EJB 87 0193

The hydrogenase from *Desulfovibrio baculatus* (DSM 1743) was purified from each of three different fractions: soluble periplasmic (wash), soluble cytoplasmic (cell disruption) and membrane-bound (detergent solubilization). Plasma-emission metal analysis detected in all three fractions the presence of iron plus nickel and selenium in equimolecular amounts. These hydrogenases were shown to be composed of two non-identical subunits and were distinct with respect to their spectroscopic properties. The EPR spectra of the native (as isolated) enzymes showed very weak isotropic signals centered around $g \approx 2.0$ when observed at low temperature (below 20 K). The periplasmic and membrane-bound enzymes also presented additional EPR signals, observable up to 77 K, with g greater than 2.0 and assigned to nickel(III). The periplasmic hydrogenase exhibited EPR features at 2.20, 2.06 and 2.0. The signals observed in the membrane-bound preparations could be decomposed into two sets with g at 2.34, 2.16 and ≈ 2.0 (component I) and at 2.33, 2.24, and ≈ 2.0 (component II). In the reduced state, after exposure to an H_2 atmosphere, all the hydrogenase fractions gave identical EPR spectra.

EPR studies, performed at different temperatures and microwave powers, and in samples partially and fully reduced (under hydrogen or dithionite), allowed the identification of two different iron-sulfur centers: center I (2.03, 1.89 and 1.86) detectable below 10 K, and center II (2.06, 1.95 and 1.88) which was easily saturated at low temperatures. Additional EPR signals due to transient nickel species were detected with g greater than 2.0, and a rhombic EPR signal at 77 K developed at g 2.20, 2.16 and 2.0. This EPR signal is reminiscent of the Ni-signal C (g at 2.19, 2.14 and 2.02) observed in intermediate redox states of the well characterized *Desulfovibrio gigas* hydrogenase (Teixeira et al. (1985) *J. Biol. Chem. 260*, 8942]. During the course of a redox titration at pH 7.6 using H_2 gas as reductant, this signal attained a maximal intensity around −320 mV. Low-temperature studies of samples at redox states where this rhombic signal develops (or lower) revealed the presence of a fast-relaxing complex EPR signal with g at 2.25, 2.22, 2.15, 2.12, 2.10 and broad components at higher field. The soluble hydrogenase fractions did not show a time-dependent activation but the membrane-bound form required such a step in order to express full activity. This indicates that the redox state of the isolated enzyme is important for the full expression of enzymatic activity. The catalytic properties were also followed by the proton-deuterium exchange reaction. The isolated hydrogenases produced H_2/HD ratios higher than those observed for non-selenium-containing hydrogenases.

The enzyme responsible for the biological activation of H_2, termed hydrogenase [1, 2], has a central role in many relevant anaerobic processes where molecular hydrogen is oxidized or evolved. Also, molecular hydrogen, via the hydrogenase system, is a link between different bacterial consortia which carry out complex fermentations. A striking example of this interspecies hydrogen transfer is the symbiotic relationship between sulfate-reducing bacteria and methane-forming organisms involved in the final steps of the conversion of cellulose and other organic substrates to methane and carbon dioxide [2]. The oxidation/reduction of molecular hydrogen is considered as one of the simplest redox processes known; however, the biological activation of H_2 is catalyzed by enzymes which appear to differ in their molecular properties and redox center composition. The metabolism of hydrogen in the sulfate-reducing bacteria is regulated by reversible hydrogenases, and the microcosmos represented by the *Desulfovibrio* world is clearly representative of the complexity involved in this process. At least three different hydrogenases are now recognized within this bacterial group: (a) [Fe] hydrogenases, containing only iron-sulfur centers, purified from *Desulfovibrio vulgaris* (Hildenborough) [3, 4] and *D. desulfuricans* (NCR 43001) [5]; (b) [NiFe] hydrogenases, containing nickel and iron-sulfur centers, generally arranged as one [3Fe-*x*S] and two [4Fe-4S] clusters, purified from *D. gigas* [6–9], *D. desulfuricans* (ATCC 27774) [10] and *D. multispirans* n. sp. [11]; (c) [NiFeSe] hydrogenases, which contain iron-sulfur centers and equimolecular amounts of nickel and selenium, purified from *D. desulfuricans* (Norway 4) [12] and *D. salexigens* (British Guiana) [13]. No definitive proof has been presented for the quantitative pres-

Correspondence to J. J. G. Moura, Centro de Química Estrutural, Universidade Nova de Lisboa, Complexo I, Avenida Rovisco Pais, P-1000 Lisboa, Portugal

Abbreviations. EXAFS, extended X-ray absorption fine structure; MCD, magnetic circular dichroism.

Rec'd in SCI. AUG 7 1987
FEBS Eur. J. Biochem. Ms.-No. 929/870193 Teixeira Ms. 1-51 Pages 1-12
Springer-Verlag, 6900 Heidelberg 1 / Wiesbadener Graphische Betriebe GmbH, 6200 Wiesbaden
Provisorische Seitenzahl / Provisional page number 1. Korr. Date 2.6.87

ence of 3Fe clusters, but two [4Fe-4S] clusters were shown to be present in the latter species.

The picture is further complicated by the presence of multiple forms of hydrogenases occurring within a single bacterium as reported in *D. desulfuricans* (ATCC 27774) [10], *D. desulfuricans* (Norway 4) [12, 14] and *D. vulgaris* (Hildenborough and Miyazaki) [15–17]. More recently, the presence of [NiFe] and [NiFeSe] hydrogenases in the membrane fractions of *D. vulgaris* (Hildenborough) has been demonstrated [17]. This emerging complexity contrasts with the more simple idea that in sulfate-reducing bacteria of the genus *Desulfovibrio*, one enzyme is responsible both for the utilization and production of molecular hydrogen, and is coupled to low-molecular-mass electron carriers such as ferredoxin, flavodoxin and rubredoxin through the tetraheme cytochrome c_3 [18]. Genetic analysis may be decisive in establishing more accurate relationships among the different molecular forms of hydrogenases in a single microorganism as well as between the different types of hydrogenase. Over the past ten years, there has been a renewed interest in the physiology and biochemistry of hydrogenases, with emphasis on the catalytic properties and mechanisms involved, and on possible applications of the enzyme to bioconversion [19] as well as to other interesting biotechnological processes [20]. These enzymes have been purified to homogeneity from strict and facultative aerobic and anaerobic organisms, and in particular from sulfate-reducing, methanogenic and photosynthetic bacteria [1]. It is generally believed that they represent a diverse group of proteins differing not only with respect to their metal content and subunit structure, but also to their electron donor/acceptor specificity, the effect of denaturants (detergents, urea) and the reactivity toward CO or O_2.

This report describes the purification, characterization and catalytic activity of three selenium-containing hydrogenases from *D. baculatus* (DSM 1743), screened for the function of their cellular localization: periplasmic, cytoplasmic and membrane-bound. Important differences exist in their physico-chemical properties, particularly with respect to the nickel redox states as detected in the native state, which may be relevant to the discussion of the role of nickel in hydrogen metabolism. Their activity in hydrogen evolution and in the D_2/H^+ exchange in conjunction with the reported spectroscopic data clearly demonstrates that the [NiFeSe] hydrogenases are a new class of nickel-containing hydrogenases; however the relationships among the three [NiFeSe] hydrogenases purified from different cellular compartments of *D. baculatus* and their relationships with the [NiFe] hydrogenases must await further structural studies. The results are compared with those for other nickel-[iron-sulfur]-selenium-containing hydrogenases isolated from *D. salexigens* (British Guiana) [13] and *D. desulfuricans* (Norway 4) [12].

MATERIALS AND METHODS

All chemicals and reagents were of analytical grade. DEAE-Bio-Gel and hydroxyapatite were purchased from Bio-Rad.

Assays

Hydrogenase was assayed by the rate of H_2 evolution with sodium dithionite (15 mM) as electron donor and methylviologen (1 mM) as mediator [21], at 32 °C and pH 7.6. Hydrogen was determined by gas chromatography using an Aerograph A-90 P3 chromatograph. One activity unit is defined as the amount catalyzing the evolution of 1 μmol H_2/min at 32 °C. The D_2/H^+ exchange reaction was performed as previously described [22] using a VG-80 mass spectrometer equipped with an Apple-II-based data acquisition system. Total iron was determined by the 2,4,6-tripyridyl-1,3,5-triazine method [23]. Metals were screened and quantified by plasma-emission spectroscopy using a Mark II Jarrell-Ash model 965 Atom Comp. Nickel was also determined by atomic absorption spectroscopy. Protein was determined by Lowry's method [24] using as standard a bovine serum albumin, purchased from Sigma, or purified *D. gigas* periplasmic hydrogenase ($\varepsilon_{400} = 48000\ M^{-1}\ cm^{-1}$) [25]. The homogeneity of the proteins was established by polyacrylamide disc electrophoresis [26] and subunit structure and molecular masses were estimated by analytical SDS/polyacrylamide (7.5%) gel electrophoresis [27] in the presence of urea and 2-mercaptoethanol using the following molecular mass markers (kDa): α-lactalbumin (14.4), trypsin inhibitor (20.1), carbonic anhydrase (30.0), ovalbumin (43.0), bovine serum albumin (67.0) and phosphorylase *b* (94.0). Molecular masses of native samples were estimated on an LKB high-pressure liquid chromatographic system, using a TSK-3000 gel filtration column and the following molecular mass markers (kDa): chymotrypsin (23.0), ovalbumin (43.0), aldolase (158), catalase (240) and ferritin (450).

EPR samples were buffered in Tris/HCl, pH 7.6. Reduction of samples for the EPR was accomplished by exposure to hydrogen atmosphere or adding sodium dithionite under an argon atmosphere.

Spectroscopic instrumentation

Electron paramagnetic resonance spectroscopy (EPR) was carried out on a Bruker 200-tt spectrometer, equipped with an ESR-9 flow cryostat (Oxford Instruments Co., Oxford, UK) and a Nicolett 1180 computer. The visible/ultraviolet spectra were recorded on a Shimadzu model 260 spectrophotometer.

Oxidation-reduction potentiometric titrations

Oxidation-reduction titrations were carried out in an apparatus similar to that described by Dutton [28], equilibrating the enzyme under different partial pressures of hydrogen (using different proportions of argon plus hydrogen) at 30 °C and pH 7.6 (100 mM Tris/HCl), in the presence of redox mediators as given in [7]. The system was calibrated with quinhydrone at pH 4.0 and 7.0. All the redox potentials, measured using a platinum-saturated calomel electrode system, are quoted relatively to the standard hydrogen electrode (pH = 0). The system was kept anaerobic by a constant purging with argon gas previously bubbled through a buffered dithionite solution. The protein concentration in the titration vessel was 60 μM. Typically, the sample was first reduced under purified H_2 (atmospheric pressure) and left to equilibrate for 2 h, after which the potential stabilized at around −450 mV. Sample reoxidation was accomplished by varying the partial pressure of H_2 gas, using the hydrogen and argon mixture. After equilibration at a fixed redox potential a sample was transferred into an EPR tube under a slight gas pressure and immediately frozen at 77 K for further quantification.

Organism and growth conditions

D. baculatus (DSM 1743), isolated from the mixed culture originally called '*Chloropseudomonas ethylica* (strain N_2)' is also able to use elemental sulfur as an electron acceptor for growth [29] and contains a tetraheme cytochrome c_3 which acts as sulfur reductase [30–32]. Cells of *D. baculatus* (previously referred to as *Desulfovibrio* strain 9974 [29]) were grown on a lactate/sulfate medium at 37°C and harvested as previously described [33].

Spheroplast preparation

For spheroplast preparation, approximately 2 g cells of *D. baculatus* were grown [33] and centrifuged for 30 min at 8000 × *g*. 1 g wet-packed cells was diluted to 10 ml with an argon-equilibrated solution containing 0.5 M sucrose, 0.05 M Na_4EDTA, lysozyme (0.2 mg/ml) and 0.1 M Tris/HCl pH 7.6. The cell suspension was gently agitated at 37°C in a sealed flask and continuously flushed with argon. Spheroplasts were formed after 2 h and then centrifuged at 8000 × *g* for 20 min. The supernatants was reserved and the pellet was resuspended in an equal volume of spheroplast-inducing solution without lysozyme and recentrifuged. The second supernatant contained less than 10% of the hydrogenase activity of the previous one, and they combined to give the periplasmic fraction. The washed pellet containing intact spheroplasts was again resuspended in the lysozyme-free solution and sonicated for 3 min using a Branson cell disruptor 200 equipped with a micro-tip to completely lyse the spheroplasts. The lysed suspension was subjected to ultracentrifugation at 185000 × *g* for 1 h and the resulting supernatant was called the cytoplasmic fraction. The pellet from this solution was called the membrane fraction, and was washed twice with the lysozyme-free solution to remove any residual soluble hydrogenase activity. The membrane fraction was assayed for hydrogenase activity and protein content after resuspension in the lysozyme-free solution using a glass tissue homogenizer.

Purification of hydrogenases

All steps of purification were performed at 4°C. Tris/HCl and phosphate buffers at pH 7.6 at appropriate concentrations were used.

Preparation of the periplasmic fraction. 700 g cells were carefully suspended in 500 ml 50 mM Tris/HCl buffer and the mixture was frozen at −80°C for 60 h. After thawing, the cells were separated from the buffer by centrifugation at 20000 rpm for 1 h and the reddish-brown supernatant containing mostly the periplasmic proteins was collected. The pellet was resuspended in an equal volume of buffer, recentrifuged, and the resulting pellet was frozen. The washed fraction obtained by the combination of the two supernatants was utilized as starting material for the purification of the periplasmic hydrogenase after concentration to 420 ml in an Amicon Diaflo apparatus using a YM-30 membrane.

First DEAE-Bio-Gel column. The periplasmic fraction was applied on a DEAE-Bio-Gel column (5 × 28 cm) previously equilibrated with 10 mM Tris/HCl. The proteins were eluted with a Tris HCl linear gradient (750 ml of 10 mM Tris/HCl and 750 ml of 400 mM Tris/HCl). The hydrogenase fraction was collected in a total volume of 300 ml and dialyzed overnight against distilled water.

Second DEAE-Bio-Gel column. The periplasmic hydrogenase was laid on a DEAE-Bio-Gel column (3.5 × 32 cm) and a linear gradient (500 ml of 10 mM Tris/HCl and 500 ml of 400 mM Tris/HCl) was performed. The hydrogenase was collected in a total volume of 190 ml.

First hydroxyapatite column. An hydroxyapatite column (3.5 × 15 cm) was prepared and washed with 0.25 M Tris/HCl. The periplasmic hydrogenase in a total volume of 190 ml was adsorbed and the column was washed successively with 100 ml of the following buffers: Tris/HCl 0.25 M, 0.20 M, 0.10 M, 0.01 M. A linear phosphate gradient was then used (500 ml of 1 mM and 500 ml of 500 mM). The hydrogenase was eluted in a final volume of 150 ml.

Third DEAE-Bio-Gel column. The hydrogenase fraction was dialyzed and adsorbed on a DEAE-Bio-Gel column (3.5 × 40 cm), and a linear gradient of Tris/HCl was then applied (500 ml of 10 mM Tris/HCl and 500 ml of 400 mM Tris/HCl). The main fraction of hydrogenase presented an $A_{390}/A_{280} = 0.28$ and a specific activity of 527 μmol H_2 mg^{-1} min^{-1}.

Preparation of the cytoplasmic and membrane-bound hydrogenases

The previous washed cells were resuspended in 500 ml of 50 mM Tris/HCl buffer and broken by passing twice through a Gaulin homogenizer at 62 MPa. A few milligrams of DNAse were added to lower the viscocity. A cell-free extract was obtained by centrifugation at 4°C and 12000 rpm for 40 min in a Beckman centrifuge model J21C rotor JA-14. The crude extract was centrifuged 1 h at 20000 rpm (Beckman Rotor JA-20) and the pellets were suspended in 50 mM Tris/HCl to a final volume of 60 ml. At this stage a soluble hydrogenase fraction and a membrane-bound hydrogenase fraction were obtained.

Solubilization of the membrane-bound hydrogenase

The pellet suspension (60 ml) was sonicated twice for 3 min in the presence of sodium deoxycholate (1.5% w/v). The sonicated material was centrifuged for 1.5 h at 20000 rpm. The solubilized fraction was dialyzed and centrifuged once more for 1.5 h at 20000 rpm. To the solubilized hydrogenase in a total volume of 70 ml, pancreatin was added (1 mg/10 mg protein) and the mixture was incubated 50 min in a water bath at 50°C. The mixture was centrifuged for 1 h at 20000 rpm and the solubilized membrane-bound hydrogenase was obtained in a total volume of 75 ml.

Purification of the membrane-bound hydrogenase

First DEAE-Bio-Gel column. The solubilized hydrogenase fraction was diluted to 100 ml and adsorbed on a DEAE-Bio-Gel column (3.5 × 32 cm) equilibrated with 10 mM Tris/HCl. The hydrogenase was eluted with a linear gradient of Tris/HCl (500 ml of 10 mM and 500 ml of 300 mM). A fraction containing mostly hydrogenase and cytochrome in a total volume of 200 ml was obtained.

Second DEAE-Bio-Gel column. The hydrogenase fraction from the the first Bio-Gel column was diluted twice with water and adsorbed on another DEAE-Bio-Gel column (3.5 × 35 cm) equilibrated with 10 mM Tris/HCl buffer.

A linear gradient in Tris/HCl was used (500 ml of 10 mM and 500 ml of 400 mM). Two bands of hydrogenase were resolved. Membrane-bound hydrogenase I (the less acidic fraction) was obtained with an $A_{390}/A_{280} = 0.1$ and a specific activity of 47 μmol H_2 mg^{-1} min^{-1}. This fraction was not

47 μmol

further studied. Membrane-bound hydrogenase II (the more acidic fraction) was obtained with an $A_{390}/A_{280} = 0.14$ and a specific activity of 121 μmol H_2 mg^{-1} min^{-1}.

Purification of the cytoplasmic hydrogenase fraction

First DEAE-cellulose column. The soluble crude extract fraction ($V = 1560$ ml) was adsorbed on a column (5 × 38 cm) of DEAE-cellulose (DE-52) equilibrated with 10 mM Tris/HCl. A linear gradient of Tris/HCl was performed (1000 ml of 10 mM and 1000 ml of 500 mM). The hydrogenase fraction was obtained in a volume of 300 ml.

First DEAE-Bio-Gel column. The hydrogenase was dialyzed and applied on a DEAE-Bio-Gel column (3.5 × 32 cm) equilibrated with 10 mM Tris/HCl. A linear gradient was then applied (500 ml of 10 mM Tris/HCl and 500 ml of 400 mM Tris/HCl) and the hydrogenase fraction was obtained in a volume of 200 ml.

Second DEAE-Bio-Gel column. The hydrogenase fraction was dialyzed against distilled water and adsorbed on a DEAE-Bio-Gel column (3.5 × 40 cm) equilibrated with 10 mM Tris/HCl. The column was eluted with a linear gradient of Tris/HCl (10 – 400 mM; total volume 1000 ml). The active hydrogenase fraction was collected in a volume of 125 ml and dialyzed against distilled water.

Third DEAE-Bio-Gel column. The dialyzed hydrogenase fraction was loaded on a DEAE-Bio-Gel column (3.5 × 30 cm) equilibrated with 10 mM Tris/HCl. A linear gradient of Tris/HCl (500 ml of 10 mM and 500 ml of 400 mM) was applied and the main hydrogenase fraction was eluted with an $A_{390}/A_{280} = 0.25$ and specific activity of 466 μmol H_2 $(mg^{-1} min^{-1})$.

Yields

The recovery yield of the three enzymes was 37% for the periplasmic, 32% for the cytoplasmic and 28% for the membrane-bound hydrogenase.

RESULTS

Cellular localization of hydrogenase activities

One of the goals of the present study was to establish the presence of multiple forms of hydrogenase in *D. baculatus* (DSM 1743). Enzyme localization is a difficult task since artifacts may occur, such as cell lysis and proteolytic effects. The periplasmic origin of one of the hydrogenases was established by the preparation of spheroplasts. Treatment of intact freshly grown cells with lysozyme, Tris/HCl and EDTA resulted in 90 – 95% spheroplast formation; after centrifugation at 8000 × *g* for 30 min, 47% of the hydrogenase activity was found in the supernatant (Table 1). After disruption of the prepared spheroplasts it was found that 23% of the total hydrogenase activity was in the cytoplasmic fraction, and that 30% of the activity resided in the membrane fraction, confirming the localization of these enzymes. The screening of cytoplasmic enzyme markers, e.g. dissimilatory bisulfite reductase, desulforubidin and APS reductase, was used to establish the extent of cell lysis [18].

Molecular masses and metal content

Table 2 indicates the results of metal analysis and subunit structure determinations of the three hydrogenases isolated from different cellular compartments of *D. baculatus*. All three hydrogenase fractions were found to be composed of two non-identical subunits with the following molecular masses: 49 and 26 kDa for the periplasmic hydrogenase; 54 and 27 kDa for the cytoplasmic hydrogenase; and 62 and 27 kDa for the membrane-bound hydrogenase. Within experimental error, the molecular mass of the heavier subunit was definitely smaller in the periplasmic preparation but the molecular masses of the three smaller subunits appeared to be similar. The molecular masses of the native preparations, determined under non-dissociating conditions by HPLC on a gel filtration column, confirmed that each fraction contained one subunit of each type. The molecular masses used in the subsequent calculations were derived by adding the molecular masses of the subunits as estimated in the presence of SDS.

Plasma-emission metal analysis showed the presence of iron and equimolar amounts of nickel and selenium in the three hydrogenases. The metal content varied for each hydrogenase, and there was no obvious correlation of this parameter with catalytic activity. This suggests the presence of inactive protein in the hydrogenase preparations. For comparison, see Table 2; the metal contents were calculated on a basis of 1 nickel atom per molecule.

Ultraviolet visible spectroscopy

The three hydrogenase fractions had a golden-brown color with very similar electronic spectra. Broad absorption bands were detected in the 270-nm and 390 – 400-nm regions, typical

Table 1. *Cellular localization of hydrogenase in* D. baculatus
Mass of protein is given as wet-packed weight. Specific activity was measured for H_2 evolution

Fraction	Protein	Hydrogenase	Specific activity
	mg/g cells (%)	U g cells (%)	μmol min^{-1} $(mg\ protein)^{-1}$
Periplasm	24.3 (48)	431 (47)	17.7
Membrane	10.2 (20)	284 (30)	27.8
Cytoplasm	16.6 (32)	210 (23)	12.7

Table 2. *Molecular masses and metal content of* D. baculatus *hydrogenases*
Values of metal content in parentheses are calculated on the basis of 1 mol nickel/mol enzyme

Parameter	Value for hydrogenase		
	cytoplasmic	periplasmic	membrane-bound
Molecular mass (kDa) by HPLC	100	100	100
SDS gel electrophoresis	81 [54, 27]	75 [49, 26]	89 [62, 27]
Metal content (mol/mol)			
Fe	7.7 (14.1)	9.25 (13.5)	10.3 (11.4)
Ni	0.54 (1.0)	0.69 (1.0)	0.9 (1.0)
Se	0.56 (1.03)	0.66 (0.96)	0.86 (0.95)
Absorbance ratio A_{390}/A_{280}	0.28	0.25	0.10

Table 3. *Catalytic activity of* D. baculatus *hydrogenases: comparison with other bacterial hydrogenase activities*
Specific activity is measured as rate of H_2 evolved per mass of sample at 32 °C. The optimal pH is the pH of observed maximal activity. n.d. = not determined

Organism	Sample	Specific activity	H_2/HD ratio	Optimal pH	Reference
		μmol min^{-1} mg^{-1}			
Proteus vulgaris	whole cells	–	0.2	7	[72]
Cl. pasteurianum	crude extracts	–	0.45	8.3	[72]
D. vulgaris (Hildenborough)	crude extracts	–	0.4	5.5	[71]
D. gigas	pure proteins	440	~~0.55~~ (0.22-0.4)	8.0	[34]
D. vulgaris (Hildenborough)	pure proteins	4800	~~0.5~~ (0.4-0.6)	5.5	[34]
D. desulfuricans (ATCC 27774)	pure proteins	152	(0.2–0.4)	n.d.	our unpublished
D. multipirans n.sp.	pure proteins	790	(0.3–0.5)	7	[34]
M. barkeri (DSM 800)	pure proteins	270	0.42	n.d.	[24, 25]
D. salexigens	pure proteins	1830	>1	n.d.	[74]
D. baculatus (DSM 1743)	membrane-bound (*)	122	1.36	n.d.	this work and [34]
	periplasmic (*)	526	1.51	~~4.0~~	
	cytoplasmic (*)	467	1.35	4.5	

(*) pure proteins

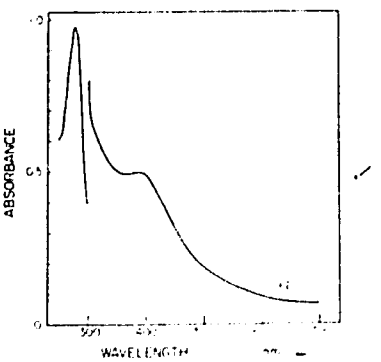

Fig. 1. *Ultraviolet and visible spectrum of native cytoplasmic* D. baculatus *hydrogenase.* Protein concentration 11 μM, 50 mM Tris HCl buffer pH 7.6

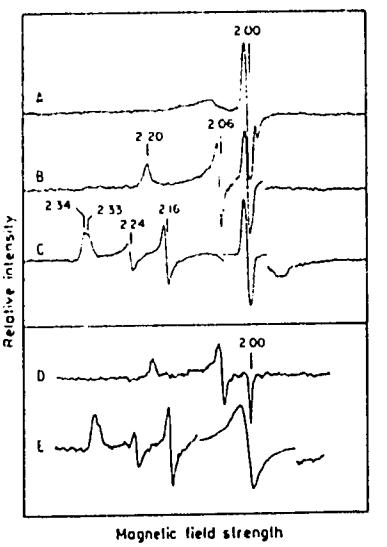

Fig. 2. *EPR spectra of* D. baculatus *as isolated hydrogenases.* (A) Cytoplasmic fraction; (B, D) periplasmic fraction; (C, E) membrane-bound fraction. Experimental conditions: microwave power 2 mW; modulation amplitude 1 mT; (A, B, C) temperature 8 K, microwave frequency 9.410 GHz, gain 6.3×10^4; (D, E) temperature 40 K, microwave frequency 9.525 GHz, gain 10^3

of iron-sulfur-containing proteins. Fig. 1 shows the spectrum of the native cytoplasmic enzyme.

Catalytic activity

The catalytic activity of the three hydrogenase fractions was tested in H_2 production and in the D_2/H^+ exchange reaction. The periplasmic and cytoplasmic hydrogenases were found to have comparable high specific activities in H_2 evolution assay (Table 3). These fractions did not show a lag phase or an activation-dependent step, hydrogen evolution being linear from time zero. The membrane-bound hydrogenase required an activation step (approx. 15–20 min) under reducing conditions. H_2 production by the periplasmic and cytoplasmic hydrogenase fractions was maximal at pH 4.0 and was strongly dependent on the buffer used (the activity was higher in Tris/HCl than in phosphate buffers). Maximal H_2 consumption was previously determined to occur at pH 7.5 [34]. The isotopic D_2-H^+ exchange activity of the soluble hydrogenases was extensively studied. Maximal activities occurred at acidic pH values (see Table 3) but there was a major difference between these hydrogenases containing selenium and other hydrogenases in the formation of the exchange products HD and H_2. The maximal HD production took place at pH 3.0, while the maximal H_2 production was attained at pH 5.0. Above pH 4.5 the ratio of H_2/HD detected for the three fractions was ~~slightly~~ higher than one. At lower pH values (< 4.5) this ratio decreased and might attain values close to those reported for the *D. gigas* periplasmic enzyme (Table 3), which consistently shows H_2/HD ratios much less than one in the pH range 5–10 [34].

Native (as isolated) hydrogenases: EPR studies

The EPR spectra of *D. baculatus* hydrogenases (as isolated) had different characteristics (Fig. 2). The cytoplas-

mic enzyme was almost EPR silent, showing a weak isotropic signal (less than 0.01 spin/mole) in the $g = 2.02$ region, detectable below 35 K. The EPR spectra of the membrane-bound hydrogenase was dominated at low temperature by an identical isotropic signal (0.1 spin/mole). Additional signals were observed at lower field (easily detected above 30 K), with g at 2.34, 2.33, 2.24, 2.16 and around 2.0 (this last feature was superimposed on the isotropic signal when measured at low temperature). These signals might be decomposed into two spectral components of a nickel(III) rhombic signal by comparison with other [NiFe] hydrogenases, e.g. *D. gigas* hydrogenase [7, 8]; the signals associated with g values at 2.34, 2.16 and 2.0 closely resemble the *D. gigas* hydrogenase Ni-signals B, and the component with g values at 2.33, 2.2 and 2.0 the *D. gigas* hydrogenase Ni-signal A [8]. In addition to the weak isotropic signal, the periplasmic hydrogenase also exhibited a rhombic signal with g values at 2.20, 2.06 and 2.0, detectable at high temperature. Theses g values are different from the values usually reported for the nickel(III) center in bacterial hydrogenases [35]; however, as was previously discussed, native hydrogenases from different species yield different EPR signals, suggesting differences in the nickel(III) coordination. As the metal analysis detects only nickel and iron, the $S = {}^1/_2$ system associated with this signal must correspond to a paramagnetic nickel(III) center. The intensities of the EPR signals were small and the double-integrated intensities yielded 10–15% of the chemically detectable nickel in the membrane-bound fractions, so it is likely that some of the nickel centers were EPR-silent at this oxidation state.

The EPR characteristics of the detected isotropic signal and the metal analysis are consistent with the presence of a partially reduced 3Fe center (assuming that the extra two 4Fe centers, silent in the native state, are observable in the reduced state; see below). However, EPR spectroscopy by itself cannot unequivocally identify or refute the presence of this type of center.

Reduced states

Upon reduction under an H_2 atmosphere or with sodium dithionite, the EPR signals observed in the native state disappeared. An EPR-silent state was attained on partial reduction, and complex EPR signals were observed in further reduced states of the enzymes. Temperature and microwave power dependence studies were useful for analyzing these complex signals assigned to nickel and iron-sulfur centers. Although spectroscopically different in the native state, upon reduction the three hydrogenase fractions showed very similar EPR signals, irrespective of the origin of the hydrogenase. Figs 3 and 4 shows the EPR spectra of the periplasmic and cytoplasmic hydrogenases reduced under an H_2 atmosphere. At low temperature, the EPR spectrum was dominated by a slightly rhombic signal at 2.03, 1.89 and 1.86. This fast-relaxing signal was not observable above 15 K, and was assigned to an iron-sulfur center in the +1 oxidation state (center I). At temperatures above 8 K, another rhombic EPR signal, detectable only up to 30 K due to line broadening, appeared with g values at 2.06, 1.95 and 1.88, well defined in the periplasmic (Fig. 3) and membrane-bound (Fig. 5) fractions. This signal was assigned to a second $[4Fe\text{-}4S]^{1+}$ cluster (center II), which relaxes more slowly than center I. The spectra observed at intermediate temperatures represent a superimposition of both center signals (Fig. 5). It should be noted that in further reduced states of the enzyme the intensity of the $g = 2.06$ component increased, suggesting a slight

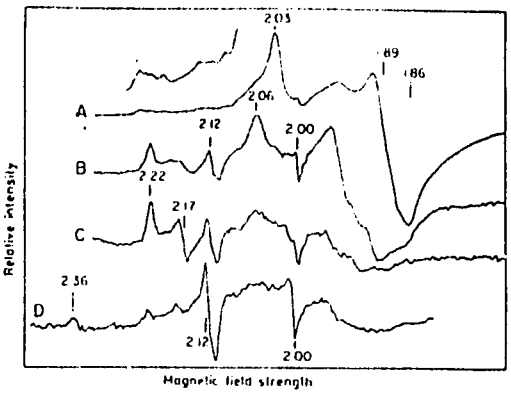

Fig. 3. *Temperature dependence of the EPR spectra of H_2-reduced (A, B and C) and dithionite-reduced (D)* D. baculatus *hydrogenase (periplasmic).* Experimental conditions as in Fig. 2. Temperature: (A) 4.2 K, (B) 15 K, (C) 37 K and (D) 27 K

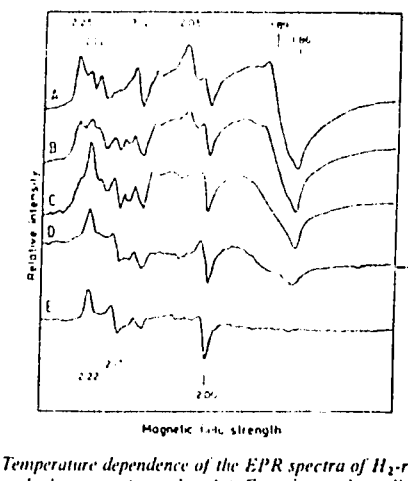

Fig. 4. *Temperature dependence of the EPR spectra of H_2-reduced* D. baculatus *hydrogenase (cytoplasmic).* Experimental conditions as in Fig. 2. Temperature: (A) 4.2 K, (B) 8 K, (C) 11 K, (D) 17 K and (E) 36 K

difference in redox potentials between the two centers. In the most reduced states, the integrated EPR intensities of the iron-sulfur centers corresponded to 0.42 (cytoplasmic) and 0.93 (periplasmic) spin/mole.

The temperature dependence of the EPR signals of the H_2-reduced periplasmic and cytoplasmic fractions is shown in Figs 3 and 4. At lower magnetic fields, complex EPR signals were observed with g at 2.25, 2.22, 2.15, 2.12 and 2.10 (and components around 2.0), better developed in the cytoplasmic fractions. This complex signal relaxes rapidly, being hardly detectable at 10 K. At higher temperatures this spectral region was dominated by a well-resolved rhombic signal with g at 2.22, 2.17 and 2.0. These two sets of signals are reminiscent of the '$g = 2.21$' and Ni-signal C (2.19, 2.14 and 2.02) (compare Figs 3C and 4E) studied in detail in H_2-reduced *D. gigas* [NiFe] hydrogenase [8, 35]. The '$g = 2.22$' signals have g values, relaxation properties (slow relaxing being saturated below 10 K and 2 mW microwave power) and redox behavior (see

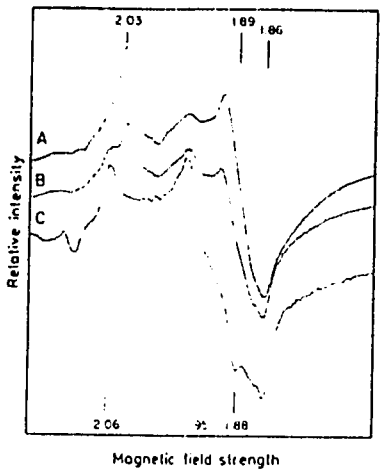

Fig. 5. *Details of the EPR spectra of* D. baculatus *hydrogenase (membrane-bound) in the 'iron-sulfur' region.* Experimental conditions as in Fig. 2. Temperature: (A) 4.2 K, (B) 9 K, and (C) 15 K

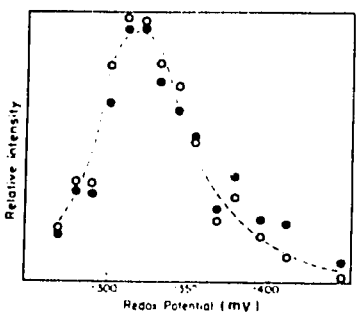

Fig. 6. *EPR signal intensities (arbitrary units) of the* g = 2.22 *nickel signal of* D. baculatus *hydrogenase (cytoplasmic).* The redox potential was controlled by varying the partial pressure of H_2 gas, as indicated in Material and Methods. EPR signals were measured at 20 K, at g = 2.22 (●) and g = 2.17 (○). No attempts were made to fit the results to a Nernst profile. Other experimental conditions as in Fig. 2

below) very similar to the transient species observed in other [NiFe] hydrogenases upon reduction by molecular hydrogen.

Redox titration of the intermediate redox species

A redox titration of the *D. baculatus* cytoplasmic hydrogenase was carried out and the intensity of the signals followed by EPR measurements, as a function of the poised solution redox potential at pH 7.6 in the range −250 mV to −450 mV. The redox potential was adjusted by controlling the H_2 partial pressure (see Material and Methods). The intensities of the rhombic 'g = 2.22' signals were monitored at 20 K; the data obtained are plotted in Fig. 6. Relative intensities are indicated since the maximal intensity was not evaluated. The transient species appeared at redox potentials below −250 mV, attained a maximal intensity around −320 mV and was not detectable below −430 mV. When the enzyme was poised at redox potentials more negative than −400 mV, low-temperature EPR studies revealed the presence of a complex fast-relaxing g = 2.25 component.

DISCUSSION

The present studies carried out on the hydrogenase activity in *D. baculatus* (DSM 1743) indicate that this activity is distributed throughout the periplasmic, cytoplasmic and membrane fractions. The hydrogenase activity isolated from sulfate-reducing bacteria of the genus *Desulfovibrio* most often has been found to be located in the periplasmic space [2] although membrane-localized enzymes have also been reported [14–17]. The presence of a cytoplasmic hydrogenase has been postulated based on dye permeability and activity measurements using whole and lysed cells [36]. More recently a careful study on cell localization was reported on the [NiFe] hydrogenase from *D. multispirans* n. sp. in which the cytoplasmic location of the enzyme was confirmed [11]. Furthermore, multiple forms of hydrogenase have been reported within a single organism. For example, two soluble forms of hydrogenase were found in *D. desulfuricans* (ATCC 27774) [10]. A soluble and a membrane-bound hydrogenase were reported in *D. desulfuricans* (Norway 4) [12, 14] and the treatment of the cells with EDTA released a minor fraction with hydrogenase activity which was taken as an indication of the presence of a periplasmic enzyme. Recently, a membrane-bound hydrogenase was identified in *D. vulgaris* (Hildenborough) [15] and in an independent study three new hydrogenases were isolated from the membranes of the same organism [17]. Two of them can react with antibodies to the [NiFe] periplasmic hydrogenase of *D. gigas*, and the third one reacts with antibodies to the [NiFeSe] periplasmic hydrogenase of *D. baculatus*.

The genes encoding for the large and small subunits of the periplasmic hydrogenases of *D. gigas* and *D. baculatus* have been cloned and partially sequenced (C. Li, M. Menon, J. LeGall, H. D. Peck Jr and A. Przybyla, unpublished data). As suggested by immunological studies, there appears to be little sequence homology between the two types of nickel-containing hydrogenases.

The relationship among these multiple forms of hydrogenase within the same bacterium is not yet clear. From a physiological point of view, multiple forms of hydrogenase with different molecular properties may be required to provide regulatory mechanisms for the various metabolic pathways involving the production and utilization of hydrogen.

In addition to the intrinsic physiological significance of the existence of multiple forms of hydrogenase within the same organism, the hydrogenase fractions isolated from *D. baculatus* show unusual spectroscopic properties relevant to our understanding of EPR-detectable nickel in hydrogenase.

The native state (as isolated)

In the native state, the membrane-bound hydrogenase from *D. baculatus* shows rhombic EPR signals similar to the ones observed in *D. gigas* [7–9], *D. desulfuricans* (Norway 4) (membrane-bound form) [14], and *D. multispirans* n. sp. [11]. The EPR g values at 2.30, 2.23 and 2.0 are also related to the ones observed in *Methanobacterium thermoautotrophicum* (Marburg [37] and H [38]) and *Mb. bryantii* membranes [39]. These signals are easily detectable up to 100 K. By isotopic ^{61}Ni (I = 3/2) replacement, hyperfine lines were observed in the EPR signals of the enzymes isolated from *D. gigas* [40].

D. desulfuricans (ATCC 27774) [10] and *Mb. thermoautotrophicum* [37, 38], providing direct evidence that nickel was at the origin of the observed paramagnet. This species was identified as nickel(III) in the presence of a strong ligand field with a tetragonally distored octahedral symmetry, resulting in an $S = 1/2$ system with one unpaired electron in a d_{z^2} orbital. The coordination sphere was proposed to be dominated by sulfur atoms based on model compound data [41] and EXAFS studies [42–44]. The involvement of sulfur as a ligand to nickel has been independently confirmed by EPR studies of the hydrogenase from *Wolinella succinogens* enriched in ^{33}S [45]. The optical transitions associated with the nickel(III) center have been identified by MCD spectroscopy [46].

The hydrogenases isolated from *D. gigas*, *D. baculatus* (membrane-bound form) and *D. desulfuricans* (Norway 4) (membrane-bound form) show two distinct rhombic EPR signals with g values at 2.31, 2.23, and 2.0 (Ni signal A) and at 2.33, 2.16 and $\approx$2.0 (Ni-signal B). Ni-signal B is the predominant nickel species observed in *D. desulfuricans* (ATCC 27774) hydrogenase. It was observed that Ni signals A and B could be interconverted by anaerobic redox cycling of *D. gigas* hydrogenase [8]; during the reoxidation process Ni signal B appears prior to Ni signal A. The latter signal was proposed to represent an oxygenated form of Ni-signal B. The intensity of the nickel EPR signals of native *D. baculatus* and *D. desulfuricans* (Norway 4) membrane-bound hydrogenases are very weak, i.e. less than 10% of the chemically detectable nickel, indicating that most of the nickel centers are EPR-silent. The intensity of the nickel EPR signals of native *D. gigas*, *D. desulfuricans* (ATCC 27774) and *D. multispirans* n. sp. hydrogenases vary from 0.2 up to 0.9 spin/mole depending on the enzyme preparation. As isolated, *D. desulfuricans* (Norway 4) (soluble form) and *D. baculatus* (periplasmic) hydrogenases gave rise to different rhombic EPR signals (also of low intensity) with g values at 2.20, 2.06 and 2.0. These species may represent variations of the coordination sphere and/or geometry of the nickel(III) site, as compared to Ni-signals A and B. *D. baculatus* (cytoplasmic) and *D. salexigens* hydrogenases do not reveal rhombic EPR nickel signals and are practically spectroscopically silent as isolated. The low intensity of nickel signals A and B in [NiFeSe] hydrogenases is consistent with the general observation that activation of these hydrogenases is either not required or proceeds very rapidly [47].

At temperatures below 30 K the EPR spectra of *D. gigas*, *D. desulfuricans* (ATCC 27774) and *D. multispirans* n. sp. hydrogenases are dominated by an intense isotropic $g = 2.02$ signal. Detailed spectroscopic studies of the native state of the enzyme clearly indicate the presence of an oxidized [3Fe-*x*S] center ($S = 1/2$). Mössbauer spectroscopic studies of ^{57}Fe-enriched samples indicate that the isomer shift ($\delta = 0.36$ mm/s) of this cluster [8, 48] is higher than the one reported for other 3Fe clusters ($\delta = 0.30$ mm/s), e.g. *D. gigas* ferredoxin II, [49] aconitase [50] and *Azotobacter vinelandii* ferredoxin I [51] suggesting that the iron cluster may be coordinated by oxygen and/or nitrogen ligands [7, 8]. *D. baculatus* membrane and periplasmic hydrogenases and *D. desulfuricans* (Norway 4) (membrane-bound and soluble) hydrogenases show very low-intensity isotropic EPR signals at $g = 2.02$ (less than 0.05 spin/mole).

In order to determine if these hydrogenases contain a 3Fe center in significant amounts or whether these signals may result from partially degraded 4Fe centers, it is necessary to carry out a thorough study using Mössbauer spectroscopy. Mössbauer and MCD studies on the soluble hydrogenase isolated from *D. desulfuricans* (Norway 4) were unable to detect the presence of 3Fe centers in the oxidized and reduced states [52], although resonance Raman spectroscopic studies detected the presence of 3Fe centers [53], in agreement with the weak EPR signal observed at $g = 2.01$ [52]. The Mössbauer studies performed with *D. gigas* [7, 48], *D. desulfuricans* (ATCC 27774) [10] and *D. desulfuricans* (Norway 4; soluble) [52] hydrogenases show that the native enzymes contain two [4Fe-4S] clusters in the +2 oxidation state.

In conclusion, the nickel-containing hydrogenases show a certain diversity in the native or 'as isolated' state with respect to the EPR characteristics of the nickel, perhaps reflecting differences in the oxidation or coordination of the nickel; however, all the hydrogenases seem to contain two 4Fe clusters. The unambiguous presence of a 3Fe cluster has only been demonstrated in the *D. gigas* [7, 48] and *D. desulfuricans* (ATCC 27774) [10] enzymes. Selenium and nickel may also be present in equimolar amounts in nickel-containing hydrogenases.

The intermediate species and redox behavior under H_2

It is a common aspect of the redox pattern of nickel-containing hydrogenases that, upon exposure to an H_2 atmosphere, an EPR-silent state is attained followed by the development of new EPR signals of a more transient nature. A well-defined rhombic EPR signal assigned to nickel by isotopic replacement [40] seems to be a common intermediate in the hydrogenase reaction mechanism (see Table 4). This signal, termed Ni-signal C [8], was readily observable in intermediate redox states of the following hydrogenases from the sulfate-reducing bacteria: *D. gigas* [8, 40] *D. desulfuricans* (ATCC 27774) [10], *D. multispirans* n. sp. [11], *D. salexigens* [13], and *D. baculatus* [54] (and this work). EPR studies conducted at low temperature (generally below 10 K), at redox levels below which Ni-signal C develops, reveal complex EPR signals that can be essentially decomposed into two groups. First, signals at $g_{av} \approx 1.94$ typical of $[4Fe\text{-}4S]^{1+}$ clusters; temperature and microwave power dependence studies reveal the presence of two types of clusters in *D. gigas* [8], *D. baculatus* and *D. salexigens* [13] enzymes. Mössbauer studies fully support the presence of two [4Fe-4S] clusters in *D. gigas* [7, 48] and *D. desulfuricans* (ATCC 27774) [10] hydrogenases. The presence of two [4Fe-4S] clusters was also revealed by Mössbauer studies of ^{57}Fe-enriched *D. desulfuricans* (Norway 4) soluble hydrogenase, but upon H_2 reduction a 50% reduced state was attained showing a single fast-relaxing rhombic EPR signal assigned to an iron-sulfur center with g values at 2.03 and 1.89 [52]. Second, signals with g values higher than 2.0, termed Ni-signal C ('$g = 2.19$') and a '$g = 2.21$' signal. The Ni-signal C was assigned in *D. gigas* hydrogenase to nickel by isotopic replacement with ^{61}Ni [40], and had a slowly relaxing behavior. The $g = 2.21$ signal is only observable at low temperature (below 10 K) and with a high microwave power (fast-relaxing species). Because of the heterolytic mechanism deduced from H^+/D_2 isotopic exchange experiments [54], the Ni-signal C was proposed to represent a nickel hydride [8, 35], since the development of the '2.19' EPR signal under hydrogen is concomitant with the activation of the enzyme [8]. Also, it was observed that this signal, originated in the *Chromatium* [55] and *D. gigas* [56] enzymes, is reversibly modified by ilumination with visible light in the frozen state. The rate of conversion was found to show a kinetic isotopic effect (slower in D_2O than in H_2O).

Table 4. *EPR characteristics of the native and H_2-reduced intermediate states in sulfate-reducers* Desulfovibrio *[NiFe] and [NiFeSe] hydrogenases*
n.r. = not reported; + = present

Organism	Localization	Oxidized state				H_2-reduced state			
		g_1	g_2	g_3	[3Fe-xS]	g_1	g_2	g_3	[4Fe-4S]
D. gigas	periplasm	2.31	2.23	2.02	+	2.19*	2.14	2.02	+(2)
		2.33	2.16	≈2.02		–			
D. desulfuricans (ATCC 27774)	periplasm	2.32	2.16	2.01	+	2.19	2.14	2.02	+
D. desulfuricans Norway 4	soluble	2.22	2.07	2.016	weak	2.20	2.15	(≈2.0)	
	membrane	2.32	2.23	2.014	weak	2.19	2.15	(≈2.0)	n.r.
D. salexigens (NCIB 8403)	periplasm	EPR silent				2.22*	2.10	≈2.0	+(2)
D. multispirans n.sp.	cytoplasm	2.31	2.22	≈2.01	+	2.19*	2.14	2.01	n.r.
D. baculatus (DSM 1743)	cytoplasm	EPR silent			weak	2.20*	2.16	≈2.0	+(2)
	periplasm	2.20	2.06	≈2.0	weak	2.20*	2.16	≈2.0	+(2)
	membrane	2.34	2.16	≈2.0	weak	2.20	2.16	≈2.0	+(2)
		2.33	2.24	≈2.0					
D. africanus	soluble	EPR silent			weak	2.21	2.17	2.01	+

* A fast relaxing component ('g = 2.21' type signal) is observed below 10 K.

The nature of the $g = 2.21$ signal is still unresolved, but its relaxation behavior may indicate that this signal represents a spin-spin interacting species, and not a simple $S = 1/2$ paramagnet. The appearance of this $g = 2.21$ signal has also been interpreted as a splitting of Ni-signal C ('$g = 2.19$') by spin-spin interaction with a $[4Fe\text{-}4S]^{1+}$ cluster [56]. However, the relative intensities of the Ni-signal C and of the '$g = 2.21$' signal vary with the redox potential and may have different origins. Redox states have been observed in [NiFe] hydrogenases where the $g = 2.21$ signal is observable at low temperature without showing the $g = 2.19$ counterpart (our unpublished results). The same applies for *D. baculatus* hydrogenases.

Although different in the oxidized (native) state, upon H_2 reduction most of the [NiFe] and [NiFeSe] hydrogenases share identical intermediates, suggesting that a common mechanism is operative. Detailed studies have been performed in intermediate redox states only for *D. gigas* hydrogenase [48] using both Mössbauer and EPR techniques. In the reduced state (below −270 mV) the 3Fe center is paramagnetic ($S > 1$, integer spin), and is not converted into a 4Fe center [48]. Below −400 mV the two [4Fe-4S] clusters are in the +1 oxidation state.

In order to characterize the intermediate redox species and place it in a catalytic framework, the redox potential value is a necessary parameter. Redox titrations (performed under partial pressures of hydrogen or with dithionite as chemical reductant) were conducted with the hydrogenases isolated from *D. gigas* [7, 8], *D. salexigens* [13] (periplasmic) and *D. baculatus* (cytoplasmic). The results are summarized as follows. First, the isotropic signal at $g = 2.02$ has a pH-independent midpoint redox potential of −70 mV [7, 58]. Second, Ni-signal A disappears in a pH-dependent manner (60 mV/Δ pH) by a one-electron process at around −220 mV at pH = 8.5 [7, 58]. The interpretation of this redox process has been questioned [8]. Although a similar value was reported for the *Chromatium vinosum* enzyme [58], the nickel center in the *Mb. formicicum* enzyme is reduced at −400 mV [40]. Third, Ni-signal C shows a bell-shaped redox titration curve and appears at around −300 mV, attains maximal intensity around −350 mV to −400 mV and disappears below −450 mV in a process which is also pH-dependent [8, 56]. Fourth, the $g = 2.21$ signal as observed in *D. gigas* [56] and *D. salexigens* [13] hydrogenases appears at slightly more negative potentials than Ni-signal C, and is still observable around −450 mV.

The catalytic properties

The previously described observations can now be correlated with the catalytic properties of the enzyme. It is known that the nickel-containing hydrogenases are reversibly inactivated by oxygen. For example, *D. gigas* hydrogenase is in an inactive [8, 60] or unready [47] state and the catalytically competent form of the enzyme is only attained after a lag phase consisting of two steps: a deoxygenation step demonstrated by the use of oxygen scavengers such as glucose plus glucose oxidase or tetrahaem cytochrome c_3, and a reductive step under H_2 or D_2 [60, 62]. Lissolo et al. showed that for *D. gigas* periplasmic hydrogenase the activation step is a redox- and pH-dependent process (60 mV/ΔpH, E_o = −350 mV at pH 8.0) [62]. The enzyme is also deactivated by another redox-linked step (E_o = −220 mV) which is also pH-dependent [62]. These values are closely related to the redox transitions involved with Ni-signals A and C. The activation of *D. desulfuricans* (ATCC 27774) hydrogenase is faster than that of the *D. gigas* enzyme, a phenomenon possibly associated with a reductive step [63]. This was rationalized in terms of an hypothetical activation mechanism [8, 47]. Ni-signal A is associated with an inactive or unready form of the enzyme (oxygenated). Ni-signal B represents a ready state of the enzyme, in the sense that the active state of the enzyme can rapidly be attained starting from this form [8]. *D. baculatus* membrane-bound enzyme shows both Ni-signals A and B and a catalytic behavior similar to that of the enzyme from *D. gigas*. *D. salexigens*, *D. baculatus* (soluble forms), *D. desulfuricans* (Norway 4; soluble), and *D. africanus* [63] hydrogenases are almost EPR-silent as isolated and do not require a lag phase during the activation step, as maximal activity is observed from time zero. The soluble hydrogenase isolated from *D. desulfuricans* strain Norway 4 requires an activation step only when its activity is measured at 0 °C [66]. A correlation can thus be established between the EPR spectral characteristics of the hydrogenases in the native state and their need for an activation: (a) enzymes showing EPR nickel(III) signals require an activation step and are not correlated directly with

catalytically relevant sites; (b) enzymes that are almost EPR-silent in the native state are generally in a catalytically competent state.

The understanding of the mechanisms involved requires a sensitive probe for the study of catalytic processes. The first step to be considered in this process is the activation of the hydrogen molecule. The role of transition metals has been studied in detail with respect to the hydrogenation reactions of unsaturated hydrocarbons [66]. The active species is considered to be a hydride-metal complex, but the intermediate species has rarely been isolated. Most of the evidence relies on kinetic analyses and on the study of the reactional mechanisms involved [68]. It has been proposed that the activation of the H_2 molecule may occur by three main processes [68]

Oxidative addition: $M^{n+} + H_2 \rightarrow M^{n+2}H_2$
Homolytic cleavage: $2M^{n+} + H_2 \rightarrow 2M^{n+1}H$
Heterolytic cleavage: $M^{n+} + H_2 \rightarrow M^{n}H^{-} + H^{+}$

Thermodynamic considerations favor the heterolytic cleavage (155 kJ mol^{-1}) rather than the homolytic process (418 kJ mol^{-1}) [68]. However, the nature of the metal center may play an important role in determining the actual mechanism. The activation of the hydrogen molecule by hydrogenase has been studied using reactions where the net electronic balance is zero. These include the isotopic exchange between D_2 and H^+ and the *ortho/para* hydrogen conversion. The data obtained with both method are consistent with the heterolytic cleavage of the hydrogen molecule [54, 68]. The heterolytic cleavage requires the presence of a metal-hydride complex and of a proton acceptor site. The stabilization of the proton by a base (external or a metal ligand) is considered to be a necessary requirements:

$$M + H_2 + B \rightarrow \overline{MH} + H^+ - B \qquad M-H^-$$
$$M - X + H_2 \rightarrow M-H^- \overline{X}H^+ \qquad M-H^- \; X-H^+$$

The exchange reaction with D_2/H^+ or H_2/D^+ has been studied using whole cells, crude extracts and purified enzymes (see Table 3); the first product of the reaction is generally HD. This result has been used in support of the heterolytic cleavage mechanism, assuming that one of the enzyme-bound H or D atoms exchanges more rapidly with the solvent than the other. Thus HD is the initial product, but D_2 (or H_2) is none the less the final product of the total exchange process, since there occurs a secondary exchange step of the HD molecule. On the basis of the heterolytic mechanism, the initial production of H_2 (or D_2) should theoretically be zero, but depending on the organism different ratios for initial rates of H_2 and HD formation have been found (Table 3).

Assuming that the hydride and proton acceptor sites can exchange independently with the solvent, the amount of HD and D_2 produced depends on the relative exchange rates of both sites. According to this assumption, the ratio of products should be pH-dependent; the available experimental data indicate, that this is indeed the case [32, 69, 70]. A change in the pK_a of the proton acceptor or active site can be viewed as responsible for attaining these isotope ratios. Comparing the experimental data on the exchange reaction measured with different purified enzymes (see Table 3) it is clear that only the [NiFeSe] hydrogenases have H_2/HD ratios greater than 1. The [NiFe] hydrogenases isolated from *D. gigas*, *D. multispirans* n. sp. and *D. desulfuricans* (ATCC 27774) show a ratio of H_2/HD smaller than 1 (0.3) ~~at pH 7.6, but maximal activity is generally attained at intermediate pH values~~. This trend has been cited as further evidence that a heterolytic process is operative by analogy with inorganic models such as the (Pd-salen) complex [71]. Excluding extreme pH values where enzymatic denaturation may occur, the rate-limiting step for the cleavage process at acidic pH values is the protonation of the proton-accepting site. At basic pH values, the limiting step is the reformation of the hydrogen molecule since the proton-accepting site has been deprotonated. *D. baculatus* and *D. gigas* hydrogenases show pH-dependent H_2/HD ratios [34]; in Fig. 7 these ratios have been recalculated using previously reported experimental data on the evolution of HD and H_2 as a function of the pH of the medium [34]. In the pH range 5–11, the H_2/HD ratio is always smaller than 1 for the *D. gigas* enzyme. The same ratio calculated for *D. baculatus* cytoplasmic hydrogenase is greater than 1 at pH > 5. The curve evidently follows the profile of a normal titration curve and thus may indicate the protonation of the proton acceptor site.

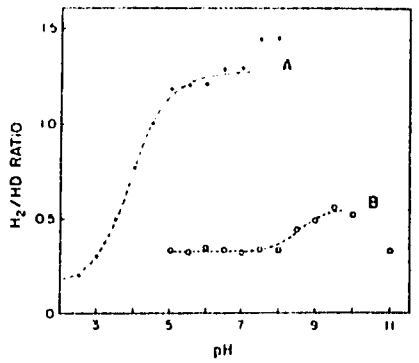

Fig. 7. *Variation of the experimental ratios H_2/HD (as measured by mass spectrometry) as a function of pH.* The plotted data were recalculated from H_2 and HD measurements previously determined (see [34]), obtained by varying the solution pH in the presence of buffers. (A) [NiFeSe] hydrogenase from *D. baculatus* (cytoplasmic); (B) [NiFe] periplasmic hydrogenase from *D. gigas*

The different exchange kinetics of the hydrogen binding sites may reflect differences in the active centers. Selenium and nickel are present in equimolecular amounts in the [NiFeSe] hydrogenases, suggesting that selenium is a ligand to the nickel site, thereby replacing a sulfur in the first coordination sphere of nickel:

$(X)_n - Ni - S$	$(X)_n - Ni - Se$
[NiFe] hydrogenases	[NiFeSe] hydrogenases
$H_2/HD < 1$	$H_2/HD > 1$.

Substitution of one of the sulfur ligands to the nickel by the less electronegative selenium may serve to destabilize the hydride form of this hydrogenase. Experiments using cells of ^{77}Se-enriched *D. baculatus* are under way in order to determine the involvement of selenium in the nickel-binding site.

In conclusion, among the nickel-containing hydrogenases isolated from the sulfate-reducing and methanogenic bacteria, multiple molecular forms of hydrogenase exist which exhibit different spectral properties in the 'as-isolated' state; however, under reducing conditions, several common spectral features emerge which are considered to reflect a common mechanism.

The [NiFeSe] hydrogenases clearly emerge as a distinct group of enzymes in terms of catalytic and active-site composition, but the degree of structural homology between the [NiFe]

Instituto Nacional de Investigação Científica,

and [NiFeSe] hydrogenases and among the three [NiFeSe] hydrogenases is yet to be determined. Selenium may play a role in modulating or fine-tuning the catalytic properties through an acid-base equilibrium at the proton acceptor site or at the hydride site.

We are indebted to M. Scandellari and R. Bourrelli for growing the bacteria used in the present study, and to I. Carvalho for skilful technical assistance. This research work was supported in part by grants from (*Instituto Nacional de Investigação/Junta Nacional de Investigação Científica e Tecnológica* and AID-936-5542 G-SS-4003-00 (J. M.), National Science Foundation (NSF) grant DMB-841-5632 (J. L., H. P.), a grant to G. F. from the NSF/*Centre National de la Recherche Scientifique* fellowship program and by the US Department of Energy under contract DEAS09-80-ER-10499 (H. P.).

REFERENCES

1. Adams, M. W. W., Mortenson, L. E. & Chen, J.-S. (1981) *Biochim. Biophys. Acta 594*, 105–176.
2. LeGall, J., Moura, J. J. G., Peck, H. D. Jr & Xavier, A. V. (1982) in *Iron-sulfur proteins* (Spiro, T. G., ed.) pp. 177–245, Wiley, New York.
3. Huynh, B. H., Czechowski, M. H., Kruger, H. J., DerVartanian, D. V., Peck, H. D. Jr & LeGall, J. (1984) *Proc. Natl Acad. Sci. USA 81*, 3728–3732.
4. Van der Westen, H. M., Mayhew, S. G. & Veeger, C. (1978) *FEBS Lett. 86*, 122–126.
5. Glick, B. R., Martin, W. G. & Martin, S. M. (1980) *Can. J. Microbiol. 26*, 1214–1223.
6. LeGall, J., Ljungdahl, P. O., Moura, I., Peck, H. D. Jr, Xavier, A. V., Moura, J. J. G., Teixeira, M., Huynh, B. H. & DerVartanian, D. V. (1982) *Biochem. Biophys. Res. Commun. 106*, 810–816.
7. Teixeira, M., Moura, I., Xavier, A. V., DerVartanian, D. V., LeGall, J., Peck, H. D. Jr, Huynh, B. H. & Moura, J. J. G. (1983) *Eur. J. Biochem. 130*, 481–484.
8. Teixeira, M., Moura, I., Xavier, A. V., Huynh, B. H., DerVartanian, D. V., Peck, H. D. Jr, LeGall, J. & Moura, J. J. G. (1985) *J. Biol. Chem. 260*, 8942–8956.
9. Moura, J. J. G., Teixeira, M., Moura, I., Xavier, A. V. & LeGall, J. (1986) in *Frontiers in bioinorganic chemistry* (Xavier, A. V., ed.) pp. 3–11, VCH Publishers, ●—● Weinheim (FRG).
10. Krüger, H. J., Huynh, B. H., Ljungdahl, P. O., Xavier, A. V., DerVartanian, D. V., Moura, I., Peck, H. D. Jr, Teixeira, M., Moura, J. J. G. & LeGall, J. (1982) *J. Biol. Chem. 257*, 14620–14622.
11. Czechowski, M. H., Huynh, B. H., Nacro, M., DerVartanian, D. V., Peck, H. D. Jr & LeGall, J. (1985) *Biochem. Biophys. Res. Commun. 125*, 1025–1032.
12. Rieder, R., Cammack, R. & Hall, D. O. (1984) *Eur. J. Biochem. 145*, 637–643.
13. Teixeira, M., Moura, I., Fauque, G., Czechowski, M. H., Berlier, Y., Lespinat, P. A., LeGall, J., Xavier, A. V. & Moura, J. J. G. (1986) *Biochimie (Paris) 68*, 75–84.
14. Lalla-Maharajah, W. V., Hall, D. O., Cammack, R., Rao, K. K. & LeGall, J. (1983) *Biochem. J. 209*, 445–454.
15. Gow, L. A., Pankhania, I. P., Ballantine, S. P., Boxer, D. H. & Hamilton, W. A. (1986) *Biochim. Biophys. Acta 851*, 57–64.
16. Yagi, T., Kimura, K. & Inokuchi, H. (1985) *J. Biochem. (Tokyo) 97*, 181–187.
17. Lissolo, T., Choi, E. S., LeGall, J. & Peck, H. D. Jr (1986) *Biochem. Biophys. Res. Commun. 139*, 701–708.
18. Bell, G. R., LeGall, J. & Peck, H. D. Jr (1974) *J. Bacteriol. 120*, 994–997.
19. Voordouw, G. & Brenner, S. (1985) *Eur. J. Biochem. 148*, 515–520.
20. Hilhorst, R., Laane, C. & Veeger, C. (1983) *FEBS Lett. 159*, 225–228.
21. Peck, H. D. Jr & Gest, H. (1956) *J. Bacteriol. 71*, 70–80.
22. Berlier, Y. M., Dimon, B., Fauque, G. & Lespinat, P. A. (1985) in *Gas enzymology* (Degn, H., Cox, R. P. & Toftlund, H., eds) pp. 17–35, Reidel, Dordrecht.
23. Fisher, D. S. & Price, D. C. (1984) *Clin. Chem.*
24. Lowry, O. H., Rosebrough, N. J., Farr, [illegible] (1951) *J. Biol. Chem. 193*, 265–275.
25. Hatchikian, E. C. [illegible] *Biophys. Res. Commun.*
26. Davis, B. J. (1964) *Ann. N. Y. Acad.*
27. Weber, K. & Osborn, M. J. (1969) [illegible] 4412.
28. Dutton, D. L. (1971) *Biochim. Biophys. Acta*
29. Biebl, H. & Pfennig, N. (1977) *Arch. Microbiol.* [illegible] 19.
30. Fauque, G., Herve, D. & LeGall, J. (1979) *Arch. Microbiol. 121*, 261–264.
31. Cammack, R., Fauque, G., Moura, J. J. G. [illegible] (1984) *Biochim. Biophys. Acta 784*, 68–74.
32. Fauque, G. D., Barton, L. L. & LeGall, J. (1[illegible] *Symp. 72*, 71–86.
33. Starkey, R. L. (1938) *Arch. Mikrobiol. 9*, 268–[illegible]
34. Lespinat, P. A., Berlier, Y., Fauque, G., [illegible] H., Dimon, B. & LeGall, J. (1986) *Biochimie (Paris) 68*, 55–61.
35. Moura, J. J. G., Teixeira, M., Moura, I., Xavier, A. V. & LeGall, J. (1984) *J. Mol. Catal. 23*, 303–314.
36. Odom, J. M. & Peck, H. D. Jr (1981) *FEMS Lett. 12*, 47–50.
37. Albracht, S. P. J., Graf, E. G. & Thauer, R. K. (1982) *FEBS Lett. 140*, 311–313.
38. Kojima, N., Fox, J. A., Hausinger, R. P., Daniels, L., Orme-Johnson, W. J. & Walsh, C. (1983) *Proc. Natl Acad. Sci. USA 80*, 378–382.
39. Lancaster, J. R. (1980) *FEBS Lett. 536*, 165–169.
40. Moura, J. J. G., Moura, I., Huynh, B. H., Kruger, H. J., Teixeira, M., DuVarney, R. C., DerVartanian, D. V., Xavier, A. V., Peck, H. D. Jr & LeGall, J. (1982) *Biochem. Biophys. Res. Commun. 108*, 1388–1393.
41. Sugiura, Y., Kawashara, J. & Suzuki, T. (1983) *Biochem. Biophys. Res. Commun. 115*, 878–881.
42. Scott, A., Wallin, S., Czechowski, M., DerVartanian, D. V., LeGall, J., Peck, H. D. Jr & Moura, I. (1984) *J. Am. Chem. Soc. 106*, 6864–6865.
43. Scott, R. A., Czechowski, M. H., DerVartanian, D. V., LeGall, J., Peck, H. D. Jr & Moura, I. (1985) *Rev. Port. Quim. 74*, 67–70.
44. Lindahl, P. A., Kojima, M., Hausinger, R. P., Fox, J. A., Teo, B. K., Walsh, C. T. & Orme-Johnson, W. H. (1984) *J. Am. Chem. Soc. 106*, 3062–3064.
45. Albracht, S. P. J., Kroger, A., Van der Zwaan, J. W., Unden, G., Bocher, R., Mell, H. & Fontijn, R. D. (1986) *Biochim. Biophys. Acta 874*, 116–127.
46. Johnson, M. K., Zambrano, I., Czechowski, M. H., Peck, H. D. Jr, DerVartanian, D. V. & LeGall, J. (1986) in *Frontiers in bioinorganic chemistry* (Xavier, A. V., ed.) pp. 36–44, VCH Publishers, ●—● Weinheim (FRG).
47. Cammack, R., Fernandez, V. M. & Schneider, K. (1986) *Biochimie (Paris) 68*, 85–91.
48. Huynh, B. H., Patil, D. S., Moura, I., Teixeira, M., Moura, J. J. G., DerVartanian, D. V., Czechowski, M. H., Prickril, B. C., Peck, H. D. Jr & LeGall, J. (1987) *J. Biol. Chem. 262*, 795–800.
49. Huynh, B. H., Moura, J. J. G., Moura, I., Kent, T. A., LeGall, J., Xavier, A. V. & Munck, E. (1980) *J. Biol. Chem. 255*, 3242–3244.
50. Emptage, M. H., Kent, T. A., Huynh, B. H., Rawlings, J., Orme-Johnson, W. H. & Munck, E. (1980) *J. Biol. Chem. 255*, 1793–1796.
51. Kent, T. A., Dreyer, J. L., Kennedy, M. C., Huynh, B. H., Emptage, M. H., Beinert, H. & Munck, E. (1982) *Proc. Natl Acad. Sci. USA 79*, 1096–1100.
52. Bell, S. H., Dickson, D. P. E., Rieder, R., Cammack, R., Patil, D. S., Hall, D. O. & Rao, K. K. (1984) *Eur. J. Biochem. 145*, 645–651.

53. Johnson, M. K., Czernuszewicz, R. S., Spiro, T., Ramsay, R., Singer, T. P. & Rao, K. K. (1983) *J. Biol. Chem. 258*, 12771–12774.

54. Krasna, A. I. & Rittenberg, D. (1954) *J. Am. Chem. Soc. 76*, 3015–3020.

55. Johnson, M. K., Zamboni, I. C., Czechowski, M. H., Peck, H. D. Jr, DerVartanian, D. V. & LeGall, J. (1985) in *Frontiers in bioinorganic chemistry* (Xavier, A. V., ed.) pp. 36–44, VCH Publishers, Weinheim (FRG).

56. Van der Zwaan, J. W., Albracht, S. P. J., Fontijn, R. D. & Slater, E. C. (1985) *FEBS Lett. 179*, 275–277.

57. Cammack, R., Fernandez, V. M. & Schneider, K. (1986) *Biochimie (Paris) 68*, 85–91.

58. Cammack, R., Patil, D. S. & Hatchikian, E. C. (1982) *FEBS Lett. 142*, 289–292.

59. Van der Zwaan, J. W., Albracht, S. P. J., Fontijn, R. D. & Slater, E. C. (1985) *FEBS Lett. 179*, 271–277.

60. Adams, M. W. W., Jin, S. L. C., Chen, J. S. & Mortenson, L. E. (1986) *Biochim. Biophys. Acta 869*, 37–42.

61. Berlier, Y. M., Fauque, G., Lespinat, P. A. & LeGall, J. (1982) *FEBS Lett. 140*, 185–188.

62. Lissolo, T., Pulvin, S. & Thomas, D. (1984) *J. Biol. Chem. 259*, 11725–11729.

63. Mege, R. M. & Bourdillon, C. (1985) *J. Biol. Chem. 260*, 14701–14706.

64. Kruger, H. J. (1983) Master Thesis, University of Georgia.

65. Niviere, N., Forget, N., Gayda, J. P. & Hatchikian, E. C. (1986) *Biochem. Biophys. Res. Commun. 139*, 658–665.

66. Fernandez, V. M., Rao, K. K., Fernandez, M. A. & Cammack, R. (1986) *Biochimie (Paris) 68*, 43–48.

67. James, B. R. (1982) in *Comprehensive organometallic chemistry*, vol. VIII, chap. 51 (Wilkinson, G., ed.) Pergamon Press, New York.

68. Brother, P. (1981) *Prog. Inorg. Chem. 28*, 1–61.

69. James, B. R. (1972) *Homogeneous hydrogenation*, Wiley, New York.

70. Fischer, H. F., Krasna, A. I. & Rittenberg, D. (1954) *J. Biol. Chem. 209*, 569–578.

71. Yagi, T., Truda, M. & Inokuchi, H. (1973) *J. Biochem. (Tokyo) 73*, 1069–1081.

72. Olive, H. & Olive, S. (1975) *J. Mol. Catal. 1*, 121–125, 1069–1081.

73. Tamiya, N. & Miller, S. (1963) *J. Biol. Chem. 238*, 2194–2198.

74. Fauque, G. D., Berlier, Y. M., Czechowski, M. H., Dimon, B., Lespinat, P. A. & LeGall, J. (1987) *J. Ind. Microbiol.*, in the press.

75. Fauque, G., Teixeira, M., Moura, I., Lespinat, P. A., Xavier, A. V., DerVartanian, D. V., Peck, H. D. Jr, LeGall, J. & Moura, J. J. G. (1984) *Eur. J. Biochem. 142*, 21–28.

B-31

CHARACTERIZATION OF TWO DISSIMILATORY SULFITE REDUCTASES (DESULFORUBIDIN AND DESULFOVIRIDIN) FROM THE SULFATE-REDUCING BACTERIA. MÖSSBAUER AND EPR STUDIES

I. Moura[†], J. LeGall[‡], A. R. Lino[†], H. D. Peck, Jr.[‡], G. Fauque[‡¶], A. V. Xavier[†], D. V. DerVartanian[‡], J. J. G. Moura[†], and B.H. Huynh[§]*

Contribution from the Department of Physics, Emory University, Atlanta, GA 30322, Centro de Quimica Estrutural, Universidade Nova de Lisboa, Complexo I, IST,AV. Rovisco Pais, 1000 Lisboa, Portugal, and Department of Biochemistry, University of Georgia, Athens, GA 30602.

[†]Universidade Nova de Lisboa

[‡]University of Georgia

[§]Emory University

[¶]Present address: ARBS, St. Paul-Lez-Durance, BP1, 13115, France.

142

ABSTRACT

Mössbauer, EPR, optical and biochemical techniques were used to characterize the prosthetic groups of two dissimilatory sulfite reductases: desulforubidin from Desulfovibrio baculatus strain DSM 1743 and desulfoviridin from Desulfovibrio gigas. For each molecule of desulforubidin, which has a $\alpha_2\beta_2$ configuration, there are two sirohemes and four [4Fe-4S] clusters. The [4Fe-4S] clusters are in the diamagnetic 2+ oxidation state and exhibit Mössbauer spectral properties similar to those of the oxidized Bacillus stearothermophilus ferredoxin. The sirohemes are high-spin ferric (S = 5/2) and exhibit characteristic ferric heme EPR resonances at g = 6.43, 5.34 and 1.97. The Mössbauer parameters for the sirohemes (ΔE_Q = 1.94 ± 0.03 mm/s and δ = 0.42 ± 0.02 mm/s at 195 K) are consistent with a high-spin ferric heme assignment. The Mössbauer measurements further demonstrate that each siroheme is exchange-coupled to a $[4Fe\text{-}4S]^{2+}$ cluster. Such an exchange-coupled siroheme-[4Fe-4S] unit has also been found in the assimilatory sulfite reductase from Escherichia coli (J.A. Christner et al., J. Biol. Chem. 1981, 256, 2098-2101) and in a low-molecular weight sulfite reductase from Desulfovibrio vulgaris (B. H. Huynh et al., J. Biol. Chem. 1984, 259, 15373-15376). Detailed data analysis suggests that eventhough the siroheme and the exchange-coupled [4Fe-4S] cluster in desulforubidin have spectral properties distinctively different from those of E. coli sulfite reductase, the exchange-coupling mechanism appears to be the same in both enzymes. Desulforubidin can be reduced under hydrogen atmosphere in the presence of trace amounts of hydrogenase and methyl viologen. The reducing electron was found to reside on the siroheme. The Mössbauer parmeters for the reduced siroheme (ΔE_Q = 2.72 ± 0.05 mm/s and δ = 0.92 ± 0.03 mm/s at 4.2 K) indicate that it is in a high-spin ferrous (S = 2) state. The electronic states of the exchange-coupled and the uncoupled [4Fe-4S] clusters are unaltered under this reducing condition.

.17

The most exciting and curious results were obtained from the studies of desulfoviridin. We found that for each molecule of desulfoviridin there are two tetrahydroporphyrin groups and four $[4Fe\text{-}4S]^{2+}$ clusters. Most surprisingly, about 80 % of the tetrahydroporphyrin groups do not bind iron. Assuming that each molecule can have upto two tetrapyrrolic groups, our finding suggests that 60 to 80 % of the purified desulfoviridin molecules may contain only metal free tetrahydroporphyrins while only 40 to 20 % of the molecules may contain one to two sirohemes. Interestingly, the sirohemes are also exchange-coupled to $[4Fe\text{-}4S]^{2+}$ clusters. Implications for the existence of metal free tetrahydroporphyrins in the purified enzymes are discussed. Spectroscopic properties for the iron containing prosthetic groups in desulfoviridin are essentially the same as those reported for desulforubidin.

In addition to the tetrapyrrolic groups and the [4Fe-4S] clusters, a solitary iron center was also found in both dissimilatory sulfite reductases. In the as-purified reductases, this solitary iron is high-spin ferric. In the reduced enzymes, it is high-spin ferrous. The Mössbauer parameters for the reduced iron (ΔE_Q = 3.2 mm/s and δ = 1.25 mm/s at 4.2 K) are consistent with octahedrally coordinated Fe(II) compounds with oxygenous and/or nitrogenous ligands. Whether this iron is adventitiously bound to the protein or has any physiological role is presently unclear.

144

INTRODUCTION

A variety of bisulfite reductases has been purified from the sulfate reducing bacteria: (1) desulfoviridins from Desulfovibrio (D.) gigas, D. Salexigens, and D. vulgaris [1-3], (2) desulforubidins from D. baculatus strains Norway 4 and DSM 1743[4], (3) P-582 from Desulfotomaculum (Dt.) ruminis and Dt. nigrificans[5,6], and (4) desulfofuscidins from D. thermophilus[7] and Thermodesulfobacterium Commune[8]. These bisulfite reductases are involved in the pathway of respiratory sulfate reduction, and are termed "dissimilatory" sulfite reductases. Another class of sulfite reductase is called "assimilatory" sulfite reductase whose function is to provide reduced sulfur for the synthesis of sulfur-containing cell constituents. A third class of sulfite reductase is found in several strictly anaerobic bacteria and has been termed "assimilatory-type" sulfite reductase[2]. This class of enzymes is characterized by the presence of a ferric low-spin siroheme exchange-coupled to a [4Fe-4S] cluster in a relatively small (@ 25 kDaltons) polypetide chain[9,10]. The physical properties of the dissimilatory sulfite reductases are quite similar in general, but different in details. They are large oligomers with molecular mass in the order of 200 kDaltons and are composed of two different types of subunits organized in a $\alpha_2\beta_2$ configuration. Each enzyme was reported to contain approximately 14-16 non-heme iron atoms and comparable amounts of labile sulfide[11]. Their optical spectra show typical siroheme bands in the region 540-580 nm and around 400 nm. Additional absorption maximum at 628 nm was observed for desulfoviridin[8,12,13]. Curiously, the non-heme iron does not contribute significantly to the optical spectrum and is difficult to reduce. The EPR spectra of these reductases show characteristic high-spin-ferric-heme-type EPR signals in the g ~ 6 and 2 regions; however, significant differences in their g values were observed[11,14]. Upon treatment of acetone/HCl, heme chromophore can be extracted from desulforubidin, desulfofuscidine, and P-582 with spectral properties identical to those of the extracted siroheme from Escherichia (E.)

145

coli sulfite reductase[8,12,15] and approximately two sirohemes were found for each enzyme molecule. However, under the same condition the chromophore extracted from desulfoviridin showed spectral properties of sirohydrochlorin (tetrahydroprophyrin; demetallized siroheme)[12,13]. Approximately two sirohydrochlorins were extracted from each reductase.

The mechanism of sulfite reductase is not yet perfectly understood; in particular, the functional roles of the sirohemes and the iron-sulfur clusters. The latter are not essential for the reduction of sulfite, since it has been demonstrated that isolated sirohydrochlorin plus iron, or siroheme is capable of reducing sulfite[16,17]. In the case of siroheme, the reduced product is exclusively trithionate. The amount of sulfite reduced is proportional to the amount of siroheme present in the reaction mixture and each molecule of siroheme performs only 300 catalytic cycles[18]. These observations point to a possible regulatory role of the iron-sulfur clusters to insure proper internal electron transfer in the enzyme molecule.

In this paper, we report a detailed Mössbauer investigation of two different bisulfite reductases, namely, desulforubidin from _D. baculatus_ and desulfoviridin from _D. gigas_. In order to better characterize the prosthetic groups, we have also studied the EPR spectra and determined the iron and heme contents of the ^{57}Fe-enriched enzymes. We found that desulforubidin contains exchange-coupled siroheme-[4Fe-4S] units which are similar to those found in the hemoprotein subunit of _E. coli_ sulfite reductase[19]. To our surprise, we discovered that the majority of the purified desulfoviridin contains demetallized sirohydrochlorin with only a minor portion of the sample containing siroheme. The siroheme in desulfoviridin was also found to be coupled with a [4Fe-4S] cluster.

1146

METHODS

Growth of Organisms and Preparation of Crude Extracts. ^{57}Fe-enriched cells of D. gigas NCIB 9332 and D. baculatus DSM 1943 were grown in lactate-sulfate media as previously described[20]. The medium contains 0.5 mg of ^{57}Fe (95% enrichment, New England Nuclear) per liter. Cells from 400 liters were harvested by centrifugation at the end of the growth phase and stored at -80 °C. Approximately 300 g wet weight of D. gigas or D. baculatus cells were suspended in 300 ml of 10 mM pH 7.6 Tris-HCl buffer, DNase added and the cells ruptured in a French press at 62 MPa. The extract was then centrifuged at 12,000 rpm for 30 min and a total volume of 500 ml of crude cell extract was obtained.

Purification of Desulfoviridin from D. gigas. All purification procedures were carried out in air, at 5 °C and the pH of the buffers was 7.6 (measured at 20 °C for Tris-HCl)

The crude cell extract was adsorbed on a DEAE-cellulose (DE52) column (5x36 cm) and the proteins were eluted with a continuous gradient of 10-500 mM Tris-HCl buffer (2 liters). A green solution containing the desulfoviridin fraction was recovered between 250 mM and 300 mM Tris-HCl. This green fraction was dialyzed overnight against 20 liters of distilled water and adsorbed on a DEAE-Biogel A column (4x25 cm). After elution with a continuous gradient of 10-300 mM Tris-HCl buffer (1.5 liter), a protein solution containing desulfoviridin was collected in a volume of 600 ml. This protein solution yielded an absorption ratio of A_{280}/A_{628} = 7.5. After dialysis the proteins were again placed on a second DEAE-Biogel A column identical to the previous one. The same gradient was performed and the protein solution collected at this stage had an A_{280}/A_{628} ratio of 4.8. A final step of purification was performed on a hydroxylapatite column (2.5x20 cm) equilibrated with 300 mM Tris-HCl. A linear Tris-HCl gradient from 300 mM to 10 mM (0.5 liter) was applied to the column and the protein desulfoviridin was eluted with a continuous potassium phosphate gradient

147

of 1 mM-100 mM (1 liter). The purified desulfoviridin had an A_{280}/A_{628} ratio of 4.0.

Purification of Desulforubidin from D. baculatus. The crude cell extract was adsorbed on a DEAE-Biogel A column (5x50 cm) and a continuous gradient of Tris-HCl buffer from 10 mM-400 mM (2 liters) was applied. A red protein solution of 500 ml containing desulforubidin was collected between 250 mM and 300 mM Tris-HCl. This red fraction was dialyzed against distilled water for overnight and was adsorbed on a second DEAE-Biogel A column (5x50 cm). The same gradient of Tris-HCl was applied and a desulforubidin fraction collected at this stage had an A_{280}/A_{543} of 9.6. The fraction was concentrated in an Amicon diaflo ultrafilter with a YM 30 membrane. The concentrated solution was passed on a Spherogel TSK-G-3000 preparative column in a H.P.L.C. apparatus and the protein was eluted with a 0.1 M phosphate buffer pH 7.0 containing 0.1 M NaCl. The purified desulforubidin had an A_{280}/A_{543} ratio of 7.1.

Protein Determination. The protein concentration was determined by the method of Lowry et al.[21] with the Folin-ciocalteau phenol reagent. Bovine serum albumin was used as standard.

Iron Determination. The total iron content was determined by plasma emission spectroscopy using a Jarrel-Ash model 750, and by forming a ferrous complex with 2,4,6-tripyridyl-s-triazine using the method described by Fisher and Price[22].

Determination of Siroheme or Sirohydrochlorin Content. The classical method of Siegel et al[23] was used to extract siroheme or sirohydrochlorin from the sulfite reductases. To each volume of enzyme solution, nine volumes of ice-cold acetone/HCl (15 mM in acetone) were added. After vigorous mixing, the mixture was allowed to stand for 5 min at 0 °C and was then centrifuged at high speed to remove the protein precipitate. To stabilize the extracted chromophore, 0.5 volume of pyridine was added to each volume of the extracted solution. The pyridine chromophore solution was centrifuged and its absorption spectrum measured.

14

Optical, EPR, and Mössbauer Methods. Optical absorption spectra were recorded on a Shimadzu model 260 spectrophotometer. EPR spectra were recorded on a Bruker ER-200 tt spectrometer equipped with an Oxford Instruments continuous flow cryostat. Both the low- and high-field Mössbauer spectrometers are of the constant acceleration types and have been described previously[24]. The zero velocity was referred to the centroid of the room-temperature Mössbauer spectrum of a metallic iron foil.

RESULTS

Iron Content. Four preparations of each bisulfite reductase were used for iron determinations. Applying plasma-emission spectroscopy and chemical methods, the total iron contents were found to be 21 ± 2 moles of iron per mole of desulforubidin and 18 ± 2 moles of iron per mole of desulfoviridin. The lower value for desulfoviridin is consistent with the following EPR and Mössbauer data which show that a majority of the desulfoviridin molecules contains metal free sirohydrochlorin. The EPR and Mössbauer data also indicate that the purified desulfoviridin and desulforubidin contain approximately 5-6 % solitary non-heme high-spin ferric iron.

Siroheme and Sirohydrochlorin Determinations. Four preparations of each sulfite reductase were used for chromophore extractions (see methods). The extracted chromophores were allowed to complex with pyridines and their concentrations were determined by optical spectroscopy. The extinction coefficients $\epsilon_{557} = 1.57 \times 10^4\ M^{-1}\ cm^{-1}$ and $\epsilon_{588} = 2.4 \times 10^4\ M^{-1}\ cm^{-1}$ were used for siroheme and porphin methyl ester in pyridine, respectively[13]. A value of 2.2 ± 0.3 moles of siroheme were extracted per each mole of desulforubidin, and 2.0 ± 0.2 moles of sirohydrochlorin were found for each mole of desulfoviridin. The following Mössbauer and EPR data indicate that 75-80 % of the tetrapyrrolic chromophores in the purified desulfoviridin contains metal-free sirohydrochlorin while 20-25% contain iron atoms. To examine whether this finding is compatible with the

optical data, the spectra of the extracted chromophores were studied in more detail. Figure 1 shows the optical spectrum of the extracted desulfoviridin chromophore (trace A). Characteristic absorption maxima for sirohydrochlorin at 378, 510, 545, 588 and 638 nm are observed. Trace C is a spectrum of the extracted desulforubidin chromophore (siroheme) normalized to 25 % of the sirohydrochlorin concentration of the sample which yielded spectrum A. This 25 % siroheme contribution is then subtracted from spectrum A, and the resulting spectrum is shown as trace B. Comparing traces A and B, it becomes obvious that the extracted desulfoviridin chromophore could have contained a minor amount of siroheme, and it would be difficult to detect using optical spectroscopy.

EPR. In the earlier preparations, multiple EPR-active species were reported for dissimilatory sulfite reductases[11,14]. The recently purified ^{57}Fe-enriched enzymes yielded much cleaner EPR spectra, even though multiple species remain visible. In figure 2, a low-temperature EPR spectrum of the purified desulforubidin from D. baculatus is compared with a spectrum of D. gigas desulfoviridin. High-spin-ferric-heme-type EPR signals are observed for both enzymes. For desulforubidin (spectrum 2A) resonances of the major component are detected at g = 6.43, 5.34 and 1.97 and a minor component is detected at g = 6.94, ~5.0 and ~1.9. The minor component is quantitated to be less than 10 % of the major component. For desulfoviridin (spectrum 2B), two EPR-active species are observed. The major resonances at g = 7.20, 4.95 and 1.93 are attributed to the siroheme. The small signal at g = 5.8 is most probably originating from the excited state of the siroheme, since its intensity relative to the g = 7.20 signal declines with decreasing temperature. The identity of the species with resonance at g = 9.7 is presently unclear. The large g-value indicates that it is not originating from a heme species, and is consistent with a rhombic (E/D = 0.33) S = 5/2 system. From the following Mössbauer data, we believe that the signal at g = 9.7 may represent a high-spin Fe(III) species. This same Fe(III) signal with comparable intensity is also detected for

desulforubidin (see Figure 2A). In comparison with the EPR spectrum of E. coli sulfite reductase[25], the heme spectra show different rhombicities indicating different conformational states for the sirohemes in these enzymes.

Since spectrum 2B was recorded with a gain of 5 times larger than that in spectrum 2A, it followed then that the EPR intensity of desulfoviridin should be approximately 5 times weaker than that of desulforubidin. After normalizing the EPR intensities with respect to protein concentrations and correcting for the Assa and Vängård factor[26], we found that the concentration of EPR-active siroheme in desulfoviridin was only 25 % of that in desulforubidin. This finding is in good agreement with the Mössbauer data presented below.

Low-Temperature Mössbauer Studies of Native Proteins. Figure 3A shows a Mössbauer spectrum of the as-purified desulforubidin from D. baculatus. The spectrum was recorded at 4.2 K with a magnetic field of 50 mT applied parallel to the γ-rays. The magnetic subspectral component extending from -4 mm/s to +4 mm/s arises from the high-spin ferric siroheme and the peaks at -1.1 mm/s and +2.0 mm/s are indicative of $[4Fe\text{-}4S]^{2+}$ cluster exchange-coupled to the paramagnetic siroheme. (Detailed analysis of the spectra of the exchange-coupled siroheme - [4Fe-4S] unit will be given in a following section). Similar spectra have been reported for the siroheme - [4Fe-4S] unit in the hemoprotein subunit of E. coli sulfite reductase[19]. The broad central doublet has parameters (apparent quadrupole splitting ΔE_Q = 1.1 mm/s and isomer shift δ = 0.43 mm/s) characteristic of a $[4Fe\text{-}4S]^{2+}$ cluster. Spectra recorded at strong applied fields (see Figure 4A) indicates that this [4Fe-4S] cluster is diamagnetic and therefore not coupled to the siroheme. The relative absorption intensities for the coupled [4Fe-4S] cluster and the uncoupled [4Fe-4S] cluster are about 1 : 1. From the EPR studies, we realize that there exists also a rhombic high-spin Fe(III) species. The existence of this Fe(III) species can be detected in spectra recorded at strong applied fields (e.g. See Figure 4), but is not obvious in weak-field spectra (e.g. Figure 3A). With so many species

present, a precise quantitation obviously cannot be achieved from spectrum 3A alone. However, by analysing data of the native enzyme recorded at different temperatures and applied fields, and by correlating with data of the reduced enzyme (see below), we were able to obtain quantitative results. We found that the relative Mössbauer absorption for the siroheme is (10 ± 2) %, for the coupled [4Fe-4S] cluster (42 ± 3) %, for the uncoupled [4Fe-4S] cluster (42 ± 3) %, and for the rhombic Fe(III) species (6 ± 1) %. Combining these quantitative data with the results of iron content determination, we concluded that each molecule of desulforubidin contains 2 exchange-coupled siroheme [4Fe-4S] units, 2 uncoupled $[4Fe\text{-}4S]^{2+}$ clusters and approximately one rhombic high-spin Fe(III) species.

Figure 3B shows a Mössbauer spectrum of desulfoviridin from D. gigas recorded under the same experimental conditions as in spectrum 3A. The majority of the absorptions appears to be originating from uncoupled $[4Fe\text{-}4S]^{2+}$ cluster. Most surprisingly, the spectrum corresponding to a siroheme - [4Fe-4S] unit is not observable, indicating that either the coupled unit has a fast electronic relaxation rate and therefore exhibits quadrupole doublets or the presence of such a unit in desulfoviridin is minor! In order to exclude the possiblility of fast relaxation, we recorded spectra at strong applied fields. (Regardless of electronic relaxation rate, the internal field of a paramagnetic species will reach its saturation value when a strong magnetic field is applied, resulting in a magnetic spectrum that is easily distinguishable from a diamagnetic system). Figure 4 shows the Mössbauer spectra of desulforubidin (4A) and desulfoviridin (4B) recorded at 4.2 K in a parallel applied field of 8 T. A close examination of the spectrum of desulforubidin reveals that the subspectral components corresponding to the four different iron species in the enzyme are partially resolved: The siroheme has absorption peaks at velocities -4.4 mm/s and +4.5 mm/s, the coupled [4Fe-4S] cluster at -2.3 and +3.4 mm/s, the uncoupled [4Fe-4S] cluster at -1, +0.5 and +2 mm/s, and the rhombic high-spin Fe(III) species at

-5.6 and +5.8 mm/s. Comparing spectrum 4B with spectrum 4A and with simulated diamagnetic spectrum (see below), it becomes evident that the majority of the Mössbauer absorption of desulfoviridin can be attributed to diamagnetic uncoupled [4Fe-4S] clusters, and the siroheme content is very minor. Since the spectrum of the siroheme is magnetically split in the native enzyme, it is not surprising that we could not detect the presence of a small quantity of siroheme in spectrum 3B or 4B. Nevertheless, the existence of siroheme in desulfoviridin is evident from the EPR measurements and from the Mössbauer measurements of the reduced enzyme reported in the following section. An accurate quantitation of the siroheme absorption is derived from the spectra of the reduced enzyme which indicates 2 % absorption. Most interestingly, in spectrum 4B there are shoulders appearing at around -2.3 and +3.4 mm/s. Since only the coupled [4Fe-4S] cluster exhibits absorptions at these velocity regions, the observation of these shoulders indicates that the sirohemes in desulfoviridin, regardless of the small quantity, are also exchange-coupled to [4Fe-4S] clusters. Similar to desulforubidin, desulfoviridin also contains the rhombic high-spin Fe(III) species which exhibits absorptions at -5.6 mm/s and +5.8 mm/s. Approximately equal amounts of this Fe(III) species (5 - 6 % of total iron absorption) is observed for both sulfite reductases.

From the above discussions, we realize that over 90 % of the Mössbauer absorptions of native desulfoviridin arise from $[4Fe\text{-}4S]^{2+}$ clusters. In order to better characterize the $[4Fe\text{-}4S]^{2+}$ cluster the desulfoviridin spectra were analysed in detail. We first performed least-squares fit to the 4.2 K weak-field spectrum of native desulfoviridin (Figure 3B). For simplicity it was assumed that the contributions from the minor species would not effect the spectrum significantly and fit the data with four quadrupole doublets of equal intensity and linewidth. The parameters obtained (listed in Table 1) are very similar to those reported for $[4Fe\text{-}4S]^{2+}$ clusters in reduced HiPIP[27] and oxidized ferredoxin[28]. In order to prove that the majority of the [4Fe-4S]

clusters in desulfoviridin is diamagnetic, we used the results obtained from the least-squares fit and simulated the corresponding strong-field spectra assuming diamagnetism for the iron sites. The solid line in Figure 4B is the result of such a simulation. The good agreement between theory and experiment indicates that the majority of the $[4Fe\text{-}4S]^{2+}$ clusters in desulfoviridin is indeed diamagnetic.

The same theoretical spectrum is also plotted in Figure 4A to compare with the spectrum of the uncoupled [4Fe-4S] clusters in desulforubidin. The theoretical spectrum is normalized to 42 % of the total Mössbauer absorption. From such a comparison, it becomes obvious that the spectrum of the uncoupled [4Fe-4S] cluster in desulforubidin may be approximated by the theoretical simulation using parameters obtained from the desulfoviridin analysis. This finding enables us to prepare spectra representing the coupled siroheme - [4Fe-4S] unit by subtracting the contributions of the uncoupled [4Fe-4S] cluster from the raw data using these simulated spectra. Some of the prepared spectra are shown in Figure 5. (Contributions from the rhombic Fe(III) species has not been removed). To further characterize the siroheme - [4Fe-4S] unit, we analyzed these prepared spectra with the following S = 5/2 spin Hamiltonian,

$$\hat{H} = D\left[S_z^2 - S(S+1)/3 + \frac{E}{D}\left(S_x^2 - S_y^2\right)\right] + \beta \vec{S}\cdot\tilde{g}\cdot\vec{H} + \vec{S}\cdot\tilde{A}\cdot\vec{I} + \frac{eQV_{zz}}{12}\left[3I_z^2 - I(I+1) + \eta\left(I_x^2 - I_y^2\right)\right] - g_n\beta_n\vec{H}\cdot\vec{I} \qquad (1)$$

For our analysis, we assumed that the coupled [4Fe-4S] cluster consisted of two pairs of equivalent iron sites and that the magnetic hyperfine coupling tensors, $\tilde{A}$, for the iron sites are isotropic. The assumption of two pairwise equivalent sites is supported by previous studies on iron-sulfur clusters[27,28], and isotropic A was reported for the cluster in E. coli sulfite reductase[19] With these assumptions, analysis of the data was possible and the hyperfine parameters were determined with certainty. The value for E/D was obtained by

the EPR measurements, the zero-field splitting D was determined from the strong-field Mössbauer spectra, the magnetic hyperfine coupling constants, A, were estimated from the total splitting of the weak-field spectra, the quadrupole splitting of the siroheme were inferred from the high-temperature data (see below), and the quadrupole splittings for the two pairwise iron sites were taken from the averaged values of the results of the least-squares fit for the uncoupled [4Fe-4S] cluster. The rest of the parameters were determined through a series of theoretical simulations and visually comparing the simulations with experiments. The set of hyperfine parameters which yields theoretical spectra (solid lines in Figure 5) that best resemble the experimental data are listed in Table 2. A particularly interesting result of this analysis is that the magnetic hyperfine coupling constants obtained for the coupled [4Fe-4S] cluster are strikingly similar to those found for the siroheme - [4Fe-4S] unit in E. coli sulfite reductase[19]. In order to explain the magnetic coupling constants observed in an intrinsically diamagnetic [4Fe-4S] cluster, Christner et al.[19] proposed a spin-coupling model in which the heme iron was coupled to each individual cluster iron. According to the model, the hyperfine coupling constants for the cluster irons depend on the exchange coupling constants between the heme iron and the cluster irons. The fact that the A's for the clusters in desulforubidin and in E. coli sulfite reductase are almost identical suggest strongly that the exchange-coupling mechanism of the siroheme - [4Fe-4S] units in both reductases must be very similar. The differences observed in EPR measurements may reflect only variations in the immediate heme iron environment. These variations are further substantiated by the observation that the hyperfine coupling constant (16 T) obtained for the siroheme in desulforubidin is significantly smaller than the constant 20 T reported for E. coli sulfite reductase[19]. In fact, the magnitude 16 T is the smallest value ever reported for a high-spin ferric heme.

High-Temperature Mössbauer Studies of Native Proteins. At high temperatures

(above 80 K), the electronic relaxation for biological molecules is generally fast in comparison with the ^{57}Fe nuclear precession time. The Mössbauer spectra recorded at these temperatures consist of only quadrupole doublets. Consequently, the high-temperature Mössbauer spectrum is very useful for quantitative analysis in the case that the doublets are resolved. Figure 6 shows the 195 K spectra of desulforubidin (6A) and desulfoviridin (6B). Unfortunately, a broad and unresolved doublet is observed. However, in addition to the intense central doublet, desulforubidin exhibits shoulders at -0.5 mm/s and +1.4 mm/s. From the low-temperature studies reported above and from the measurements of the reduced enzymes presented below, we realized that the difference between these two reductases is the lack of siroheme in desulfoviridin. The extra shoulders observed for desulforubidin must be therefore originating from the siroheme. The central doublet are attributed to the [4Fe-4S] clusters, and the absorptions arising from the rhombic Fe(III) species are unresolved. For a detailed analysis, the desulfoviridin spectrum (6B) was fitted with four quadrupole doublets of equal intensity. The desulforubidin spectrum (6A) was fitted with five quadrupole doublets. The heme iron was assumed to have a different intensity from those of the cluster irons. For this analysis, the contribution of the Fe(III) species was neglected. The solid lines in Figure 6 represent the least-squares fit spectra and the calculated parameters are listed in Table 1. The percent absorption for the siroheme in desulforubidin was found to be (8 ± 2) %, which is in agreement with the results obtained from the reduced enzyme (see below). The absorptions for the siroheme in desulfoviridin and for the Fe(III) species were not determined in this analysis.

The EPR measurements indicate that the siroheme is high-spin ferric. The isomer shift obtained from the least-squares fit agrees with this assignment. The quadrupole splitting (1.94 mm/s) appears to be unusually large for high-spin ferric hemes and is twice as large as the value 1 mm/s found for the siroheme in

E. coli sulfite reductase[19] This observation again indicates dissimilarities between the hemes in the dissimilatory and the assimilatory sulfite reductases. Although high-spin ferric compounds generally yields small ΔE_Q, quadrupole splittings larger than 1.5 mm/s have been reported for quite a few high-spin ferric hemoproteins[29-31].

In our analysis of the low-temperature data, we assumed that the $[4Fe\text{-}4S]^{2+}$ cluster spectra for both reductases were identical. The Mössbauer parameters obtained at high-temperatures indicate that within experimental uncertainties, the doublets originating from these clusters are practically the same and therefore support our assumption. The parameters listed in Table 1 also suggest that the [4Fe-4S] clusters in these two dissimilatory sulfite reductases are similar to the $[4Fe\text{-}4S]^{2+}$ clusters in Chromatium HiPIP[27] and Bacillus stearothermophilus ferredoxin[28]. i.e., The cluster spectrum can be decomposed into four quadrupole doublets with different splittings and is strongly temperature dependent. The spectrum for the iron-sulfur cluster in an exchange-coupled siroheme - [4Fe-4S] unit has also been reported for E. coli sulfite reductase[19] and for an assimilatory-type sulfite reductase from D. vulgaris[9]. In both cases, the cluster exhibits a single, temperature independent quadrupole doublet, suggesting that all four iron sites in the cluster are equivalent. In order to examine whether or not the coupled [4Fe-4S] cluster in desulforubidin is similar to those in E. coli and D. vulgaris sulfite reductase, we attempted to fit the central doublet of the desulforubidin spectrum with five doublets. One of the doublets was assumed to have intensity equal to the sum of the other four. No satisfactory fit could be obtained with such an assumption. Consequently, the evidence suggests that the coupled [4Fe-4S] cluster in desulforubidin in similar to the uncoupled cluster and is ferredoxin-like.

Mössbauer Studies of Reduced Reductases. Under hydrogen atmosphere and in the presence of trace quantities of hydrogenase and methyl viologen, desulforubidin and desulfoviridin can be reduced and become EPR silent. In the absence of an

external applied field, the Mossbauer spectra consist of only quadrupole doublets. In the presence of a strong applied field, large internal fields are induced at the iron sites of the reduced siroheme - [4Fe-4S] unit. These observations indicate that the reduced siroheme - [4Fe-4S] unit is an integer spin system with S > 0. (Detailed analysis of the strong-field spectra and identification of the spin state for the reduced siroheme - [4Fe-4S] unit will be the subjects of future reports). Figure 7 shows the 150 K spectra of reduced desulforubidin and desulfoviridin. Three distinct quadrupole doublets are observed and the high-energy lines of the doublets are resolved. A major difference between these two spectra is that the absorption peak at +2.1 mm/s is more intense for desulforubidin than for desulfoviridin. From the following analysis, we realized that this peak belongs to a doublet whose parameters are consistent with high-spin ferrous heme (S=2), and is therefore attributed to the siroheme. The central doublet originate from the [4Fe-4S] cluster. The right-most line is assigned to a high-spin Fe(II) species which should be the reduced state of the high-spin Fe(III) species found in the native enzymes. Each spectrum was fitted with six quadrupole doublets. Four of the doublets belonging to the [4Fe-4S] cluster were assumed to have equal intensity. The solid lines in Figure 6 are results of the least-squares fits. The parameters obtained are listed in Table 3 including results obtained for different temperatures.

A most interesting and important result of the above analysis is the discovery of different siroheme contents in these two reductases. Since the siroheme spectrum is well resolved from the rest of the spectrum, its percent absorption can be determined with certainty. The percent absorption of the siroheme was found to be (10 ± 2) % for desulforubidin and only (2 ± 1) % for desulfoviridin. This result indicates unambiguously that desulforubidin contains approximately five times more siroheme in comparison with desulfoviridin, a result that is supported by the EPR studies and is consistent

with the Mossbauer measurements of the native proteins. Correlating with the result of iron-content determination (21 irons/molecule of desulforubidin), ten percent siroheme absorption yields ~ 2 sirohemes per molecule. This value is in good agreement with the chromophore content obtained by chemical determination. On the other hand, the 2 % siroheme absorption for desulfoviridin yields only an average of 0.4 siroheme per molecule. Since about 2 sirohydrochlorins were extracted from each molecule, we concluded that 80 % of the tetrahydroporphyrin chromophores in the purified desulfoviridin do not ~~contain~~ bind iron. Implications of this conclusion will be discussed in the following section.

The Mössbauer parameters obtained for the [4Fe-4S] clusters are almost indistinguishable from those of the clusters in the native enzymes, suggesting that the oxidation state of the cluster in the reduced enzymes remains at 2+. The siroheme parameters indicate that the heme is reduced into a high-spin ferrous state (S=2). Consequently, under the above mentioned reducing conditions, the siroheme - [4Fe-4S] unit in both dissimilatory sulfite reductases is reduced by one electron, and the electron is localized on the heme. Mössbauer measurements of the one-electron reduced state of E. coli sulfite reductase have been reported[32]. It was also found that the state of the [4Fe-4S] cluster was unaltered when compared with the native enzyme, and the electron was also localized on the siroheme. However, in E. coli sulfite reductase the reduced siroheme was in an intermediate spin state (S=1). Its spectrum is distinctively different from that of the reduced siroheme in desulforubidin or desulfoviridin. From the studies of the native enzymes, the siroheme environments of the two dissimilatory sulfite reductases were found to be different from the assimilatory sulfite reductase. The above results indicate further that the heme environments remain distinct in the one-electron reduced enzymes.

The Mossbauer parameters of the high-spin Fe(II) species are consistent with adventitiously bound impurity irons found in protein samples. In fact, the 4.2

160

K values (ΔE_Q = 3.2 mm/s and δ = 1.25 mm/s) are identical to those reported for Fe(II) in buffer solution[33]. However, these values are common for octahedrally coordinated Fe(II) compounds[34] and are not unique for adventitous iron. Presently, we are perplexed by the facts that this species exists in both dissimilatory sulfite reductases, and quantitates to approximately one iron per molecule.

DISCUSSION

In the previous section, we have presented some chemical, optical, EPR and Mössbauer data of two dissimilatory sulfite reductases isolated from sulfate reducing bacteria, namely, desulforubidin from D. baculatus and desulfoviridin from D. gigas. The data indicate that both reductases contain equal amount of [4Fe-4S] clusters (4 clusters per molecule) but have different contents of siroheme. Desulforubidin contains 2 sirohemes per molecule, and each siroheme is exchange-coupled to a [4Fe-4S] clusters. (i.e., two of the four clusters are uncoupled). For desulfoviridin an average of 0.4 siroheme per molecule was found. Taking into consideration all the experimental evidence, we reach the conclusion that 80 % of the tetrapyrrolic ~~tetrahydroporphyrin~~ chromophores in desulfoviridin do not contain iron. Our data suggest that the purified desulfoviridin is inhomogeneous with respect to the distribution of the prosthetic groups. Depending on the distribution of the sirohemes, 60 to 80 % of the desulfoviridin molecules contain only metal free tetrahydroporphyrins while 20 to 40 % of the enzyme molecules contain two to one siroheme per molecule. In the earlier studies[12,13], investigators were puzzled by the observation that metal free tetrahydroporphyrins were extracted from desulfoviridin while sirohemes were extracted from E. coli sulfite reductase, from desulforubidins and from P-582. The present finding not only can explain this puzzling observation, but is also consistent with the distinct optical spectrum observed for desulfoviridin. In Table 4, we compare the relative intensities and wavelengths of the absorption

maxima of D. gigas desulfoviridin with those of the E. coli sulfite reductase and of the demetallized siroheme esters in methanol - H_2SO_4[12]. It is obvious from this comparison that the optical spectrum of desulfoviridin resembles the metal free tetrahydroporphyrin methyl ester and is distinct from the E. Coli sulfite reductase.

The exchange-coupled siroheme - [4Fe-4S] unit was first reported in E. coli sulfite reductase[19], and extensive spectroscopic studies have been performed to characterize this unit[32,36-39]. The coupling between the siroheme and the cluster was found to be retained in all the oxidation and ligation states examined. A recent x-ray crystallographic study indicates that the two prosthetic groups are bridged by a common ligand, probably a cysteine $S\gamma$[40]. This work shows that the siroheme - [4Fe-4S] unit in desulforubidin exhibits properties that are both similar and dissimilar to the coupled unit in E. coli sulfite reductase. In the native enzymes, both units are composed of a high-spin ferric S = 5/2 siroheme exchange-coupled to an intrinsically diamagnetic S = 0 $[4Fe\text{-}4S]^{2+}$ cluster. The magnetic hyperfine coupling constants, A, of the cluster irons obtained for both enzymes are almost identical. Since the A's of the cluster irons are inferred from the paramagnetic siroheme through the exchange interaction, the observation of identical hyperfine constants indicates similar exchange coupling mechanism. The bridging ligand and the geometrical arrangement between the siroheme and the cluster may be the same in both units; however, the local environments surrounding the iron sites were found to be different. These variations are reflected in the differences observed in the EPR spectra, in the quadrupole splittings and the A values of the sirohemes, and in the ΔE_Q's of the cluster irons.

Under reducing condition, the siroheme - [4Fe-4S] unit in desulforubidin can be reduced by one electron. The electron is localized in the siroheme and the ferric siroheme is reduced into a ferrous state. The [4Fe-4S] cluster remains in the 2+ state. Similar behavior was also reported for the one-electron

reduced E. coli sulfite reductase[35]; however, the electronic spin states of the ferrous sirohemes are different: S = 2 for desulforubidin and S = 1 for E. coli sulfite reductase. In E. coli sulfite reductase, the mid-point oxidation-reduction potentials for the siroheme and the cluster differ only by 65 mV[39]. Consequently, coexistence of 1e and $2e^-$ - reduced states are obtained under reducing conditions. Fully reduced ($2e^-$ - reduced) enzymes can be prepared under Ar atmosphere in the presence of deazaflavin, EDTA and light[38]. In the case of desulforubidin, we were not successful in producing the corresponding 2e - reduced state. The reduced desulforubidin reported in this work is in a pure 1e - reduced state. For this to occur the redox potentials of the siroheme and the coupled cluster in desulforubidin must be differ by at least 100 mV. Since the $1e^-$ - reduced state is the active state of the enzyme, detailed Mössbauer studies of the reduced desulforubidin should yield information of physiological significance, and are the subjects of a future publication. We are also exploring different reduction methods in order to attain the $2e^-$ - reduced state, and we are attempting to determine the redox potentials of the siroheme and the clusters using redox-titration technique.

After the discovery of the exchange-coupled siroheme - [4Fe-4S] unit in E. coli sulfite reductase[19], spectroscopic evidence for the existence of a siroheme - [4Fe-4S] unit was reported for spinach sulfite reductase[41] and for spinach nitrite reductase[42], which possesses sulfite-reductase activity[43]. More recently, an assimilatory-type sulfite reductase isolated from D. vulgaris was also found to contain a coupled siroheme - [4Fe-4S] unit[9]. The present studies further indicate that desulforubidin, a dissimilatory sulfite reductase, also contains similar siroheme - [4Fe-4S] unit. These observations strongly suggest that the siroheme - [4Fe-4S] unit is a common prosthetic group and is the active site for sulfite and nitrite reduction. The discovery of metal-free tetrahydroporphyrin in the majority of the purified desulfoviridin indicates that nature may be more perverse. Interestingly, we found evidence that a minor

portion of the purified desulfoviridins contains sirohemes and that the sirohemes are also coupled to [4Fe-4S] clusters. Consequently, an important question to ask is could the existence of sirohydrochlorin be a result of damage caused by protein purification and have no physiological significance? Perhaps the observed enzymatic activity results from those proteins containing the coupled siroheme - [4Fe-4S] unit. Due to the following consideration we believe that this is not the case. Small molecules, such as CN^- or CO, form complexes with desulforubidin and with E. coli sulfite reductase. They were shown to coordinate to the siroheme group and inhibit the sulfite reduction activity[37,39]; however, these ligands do not inhibit the sulfite reduction activity of desulfoviridin[44]. As the siroheme - [4Fe-4S] cluster unit in desulfoviridin is similar to that in desulforubidin or in E. coli sulfite reductase, it is expected to complex with CO or CN^-. The fact that neither CO nor CN^- inhibit desulfoviridin suggested that the enzymatic activity originates from the enzyme molecules containing sirohydrochlorins. We have also performed preliminary Mössbauer studies on other dissimilatory sulfite reductases, namely, desulforubidin from D. baculatus strain Norway 4 and desulfoviridin from D. desulfuricans strain ATCC 27774. These preliminary investigations indicate that metal-free tetrahydroporphyrins are commonly present in desulfoviridin. Furthermore, if the sirohemes were solely responsible for activity, one would expect desulfoviridin to exhibit about 20 % of the activity found with desulforubidin. In fact, D. gigas desulfoviridin was reported to be more active than D. baculatus desulforubidin[3]. A survey of the specific activities of both types of reductases shows that there is no correlation with the nature of the prosthetic group. Finally, the 628 nm absorption peak, as we have noted appears to be related to the presence of sirohydrochlorin in desulfoviridin, is seen in bacterial crude extracts and its intensity does not increase in the course of protein purification. Observation of the 628 nm peak has also been reported for whole bacterial cells[45].

ACKNOWLEDGMENTS. We thank Mr. Jeffrey Levy for writing the program to plot the Mossbauer Figures, and we also thank the National Institutes of Health for a research career development award (Grant AM01135) to B.H.H. and a Grant from the NSF/CNRS fellowship program to G.F. This work was supported by the National Science Foundation (Grants PCM-8305995 and DMB-8614290 to B.H.H., DMB-8602789 to J.L.G., and PCM-8213874 to D.V.D.), by the U.S. Department of Energy (Grant DE-A509-80ER 10499 to H.D.P.), and by Instituto National de Investigação Cientifica, Junta Nacional de Investigação, Cientifica e Tecnologica and Agency for International Development (I.M.)

REFERENCES

(1) Lee, J.P.; Peck, H.D., Jr. Biochem. Biophys. Res. Commun. 1971, 45, 583-586.

(2) Lee, J.P.; LeGall, J.; Peck, H.D., Jr. J. Bacteriol. 1973, 115, 529-542.

(3) Czechowski, M.; Fauque, G.; Galliano, N.; Dimon, B.; Moura, I.; Moura, J.J.G.; Xavier, A.V.; Barata, B.A.S.; Lino, A.R.; LeGall, J. J. Ind. Microbiol. 1986, 1, 139-147.

(4) Lee, J.P.; Yi, C.; LeGall, J.; Peck, H.D., Jr. J. Bacteriol. 1973, 115, 453-455.

(5) Trudinger, P.A. J. Bacteriol. 1970, 104, 158-170.

(6) Akagi, J.M.; Adams, V. J. Bacteriol. 1973, 116, 392-396.

(7) LeGall, J.; Fauque, G. Biology of Anaerobic Microorganisms; Zehnder, A.J.B., Ed.; John Wiley & Sons: New York, 1987; in press.

(8) Hatchikian, E.C.; Zeikus, J.G. J. Bacteriol. 1983, 153, 1211-1220.

(9) Huynh, B.H.; Kang, L.; DerVartanian, D.V.; Peck, H.D., Jr.; LeGall, J. J. Biol. Chem. 1984, 259, 15373-15376.

(10) Moura, I.; Lino, A.R.; Moura, J.J.G.; Xavier, A.V.; Fauque, G.; Peck, H.D., Jr.; LeGall, J. Biochem. Biophys. Res. Commun. 1986, 141, 1032-1041

(11) Liu, C.L.; DerVartanian, D.V. Peck, H.D., Jr. Biochem. Biophys. Res. Commun. 1979, 91, 962-970.

(12) Murphy, M.J.; Siegel, L.M. J. Biol. Chem. 1973, 248, 6911-6919.

(13) Murphy, M.J.; Siegel, L.M.; Kamin, H.; DerVartanian, D.V.; Lee, J.P.; LeGall, J.; Peck, H.D., Jr. Biochem. Biophys. Res. Commun. 1973, 54, 82-83.

(14) Hall, M.H.; Prince, R.H.; Cammack, R. Biochim. Biophys. Acta 1979, 581, 27-33.

(15) Murphy, M.J.; Siegel, L.M.; Kamin, H.; Rosenthal, D. J. Biol. Chem. 197 248, 2801-2814

(16) Seki, Y.; Sogawa, N.; Ishimoto, M. J. Biochem. (Tokyo) 1981, 90, 1487-1492.

(17) Seki, Y.; Ishimoto, M. J. Biochem. (Tokyo) 1979, 86, 273-276.

(18) Kang, L.; LeGall, J.; Kowal, A.T.; Johnson, M.K. J. Inorg. Chem. 1987, i press.

(19) Christner, J.A.; Münck, E.; Janick, P.A.; Siegel, L.M. J. Biol. Chem. 1981, 256, 2098-2101.

(20) Huynh, B.H.; Czechowski, M.H.; Krüger, H.J.; DerVartanian, D.V.; Peck, H.D., Jr.; LeGall, J. Proc. Natl. Acad. Sci, U.S.A. 1984, 81, 3728-3732.

(21) Lowry, O.H.; Rosebrough, N.J.; Fan, A.L.; Randall, R.J. J. Biol. Chem. 1951, 193, 265-275.

(22) Fisher, D.S.; Price, D.C. Clin. Chem. 1964, 10, 21-25.

(23) Siegel, L.M.; Murphy, M.J.; Kamin, H. Methods of Enzymology 1978, 52, 436-447.

(24) Yang, C.Y.; Meagher, A.; Huynh, B.H.; Sayers, D.E.; Thiel, E.C. Biochemistry 1987, 26, 497-503.

(25) Rueger, D.C.; Siegel, L.M. in Flavins and Flavoproteins; Singer, T. P., Ed.; Elsevier: Amsterdam, 1976; pp. 610-620.

(26) Aasa, R., Vänngård, T. J. Magn. Reson. 1975, 19, 308-315.

(27) Middleton, P.; Dickson, D.P.E., Johnson, C.E.; Rush, J.D. Eur. J. Biochem. 1980, 104, 289-296.

(28) Middleton, P.; Dickson, D.P.E.; Johnson, C.E.; Rush, J.D. Eur. J. Biochem. 1978, 88, 135-141.

(29) Münck, E.; Champion, P.M. J. Physique 1974, 35(C6), 33-46.

(30) Emptage, M.H.; Zimmermann, R.; Que, L., Jr.; Münck, E.; Hamilton, W. D.; Orme-Johnson, W.H. Biochim. Biophys. Acta 1977, 495, 12-23.

(31) Lang, G. Quart. Rev. Biophys. 1970, 3, 1-60.

(32) Christner, J.A.; Münck, E.; Janick, P.A.; Siegel, L.M. J. Biol. Chem. 1983, 258, 11147-11156.

(33) Kent, T.A.; Dreyer, J.L.; Kennedy, M.C.; Huynh, B.H.; Emptage, M.H.; Beinert, H.; Münck, E. Proc. Natl. Acad. Sci, U.S.A. 1982, 79, 1096-1100.

(34) Menil, F. J. Phys. Chem. Solids 1985, 46, 763-789.

(35) Christner, J.A.; Janick, P.A.; Siegel, L.M.; Münck, E. J. Biol. Chem. 1983, 258, 11157-11164.

(36) Janick, P.A.; Siegel, L.M. Biochemistry 1982, 21, 3538-3547.

(37) Janick, P.A.; Siegel, L.M. Biochemistry 1983, 22, 504-515.

(38) Christner, J.A.; Münck, E.; Kent, T.A.; Janick, P.A.; Salerno, J. C.; Siegel, L.M. J. Am. Chem. Soc. 1984, 106, 6786-6794.

(39) Siegel, L.M.; Rueger, D.C.; Barber, M.J.; Krueger, R.J.; Orme-Johnson, N.R.; Orme-Johnson, W.H. J. Biol. Chem. 1982, 257, 6343-6350.

(40) McRee, D.E.; Richardson, D.C.; Richardson, J.S.; Siegel, L.M. J. Biol. Chem. 1986, 261, 10277-10281.

(41) Krueger, R.J.; Siegel, L.M. Biochemistry 1982, 21, 2905-2909.

(42) Wilkerson, J.O., Janick, P.A., and Siegel, L.M. Biochemistry 1983, 22, 5048-5054.

(43) Krueger, R.J.; Siegel, L.M. Biochemistry 1982, 21, 2892-2904.

(44) Ishimoto, M.; Yagi, T. J. Biochem. (Tokyo) 1961, 49, 103-109

(45) Postgate, J.R. J. Gen. Microbiol. 1956, 14, 545-572.

170

Table 1. Mössbauer parameters for the $[4Fe\text{-}4S]^{2+}$ clusters in the as purified *D. baculatus* desulforubidin and *D. gigas* desulfoviridin.

T(K)		desulfoviridin		desulforubidin	
		ΔE_Q (mm/s)	δ (mm/s)	ΔE_Q (mm/s)	δ (mm/s)
195	Siroheme	———	———	1.94 ± 0.03	0.42 ± 0.02
	[4Fe-4S]:				
	Site 1	1.13 ± 0.04	0.36 ± 0.02	1.10 ± 0.04	0.36 ± 0.02
	Site 2	0.91 ± 0.04	0.35 ± 0.02	0.98 ± 0.04	0.37 ± 0.02
	Site 3	0.80 ± 0.04	0.37 ± 0.02	0.83 ± 0.04	0.37 ± 0.02
	Site 4	0.50 ± 0.04	0.35 ± 0.02	0.51 ± 0.04	0.36 ± 0.02
4.2	[4Fe-4S]:				
	Site 1	1.45 ± 0.04	0.45 ± 0.02		
	Site 2	1.10 ± 0.04	0.45 ± 0.02		
	Site 3	1.10 ± 0.04	0.45 ± 0.02		
	Site 4	0.72 ± 0.04	0.41 ± 0.02		

Table 2. Spin-Hamiltonian parameters for the exchange-coupled siroheme-[4Fe-4S] unit in the native desulforubidin from D. baculatus[a].

		[4Fe-4S]	
	Siroheme	Site 1	Site 2
D (cm^{-1})	13.5 ± 1.5	13.5 ± 1.5	13.5 ± 1.5
E/D	0.02 ± 0.01	0.02 ± 0.01	0.02 ± 0.01
$A_{xx}/g_n\beta_n$ (T)[b]	-15.8 ± 0.5	5.2 ± 0.5	-5.2 ± 0.7
$A_{yy}/g_n\beta_n$ (T)	-16.5 ± 0.5	5.2 ± 0.5	-5.2 ± 0.7
$A_{zz}/g_n\beta_n$ (T)	-16.2 ± 1.0	5.2 ± 0.5	-5.2 ± 0.7
ΔE_Q (mm/s)	2.0 ± 0.2	-0.9 ± 0.2	1.2 ± 0.2
δ (mm/s)	0.47 ± 0.05	0.45 ± 0.02	0.45 ± 0.02
η[c]	0 ± 0.2	-2.0 ± 0.5	-3 ± 1

[a] The uncertainities were estimated by visually comparing the theoretical simulations with the experimental data.

[b] The symbol β_n represents the nuclear magneton and g_n has the values 0.1806 and -0.1033 for the ground and excited states of the ^{57}Fe nucleus.

[c] $\eta = (V_{xx} - V_{yy}) / V_{zz}$, where V_{ii} are the principal components of the electric field gradient tensor.

Table 3. Mossbauer parameters for the reduced desulforubidin from D.baculatus and the reduced desulfoviridin from D. gigus.

T(K)		reduced desulforubidin		reduced desulfoviridin	
		ΔE_Q (mm/s)	δ (mm/s)	ΔE_Q (mm/s)	δ (mm/s)
195	Siroheme	2.47 ± 0.05	0.83 ± 0.03	2.3 ± 0.1	0.80 ± 0.06
	[4Fe-4S]:				
	Site 1	1.11 ± 0.04	0.36 ± 0.03	1.17 ± 0.04	0.38 ± 0.03
	Site 2	0.93 ± 0.04	0.36 ± 0.03	0.96 ± 0.04	0.37 ± 0.03
	Site 3	0.87 ± 0.04	0.38 ± 0.03	0.88 ± 0.04	0.40 ± 0.03
	Site 4	0.54 ± 0.04	0.37 ± 0.03	0.58 ± 0.04	0.37 ± 0.03
	Fe(II)	2.76 ± 0.07	1.20 ± 0.04	2.69 ± 0.07	1.19 ± 0.04
150	Siroheme	2.56 ± 0.05	0.84 ± 0.03	2.4 ± 0.1	0.84 ± 0.06
	[4Fe-4S]:				
	Site 1	1.15 ± 0.04	0.37 ± 0.03	1.20 ± 0.04	0.35 ± 0.03
	Site 2	0.96 ± 0.04	0.39 ± 0.03	0.97 ± 0.04	0.40 ± 0.03
	Site 3	0.94 ± 0.04	0.40 ± 0.03	0.93 ± 0.04	0.42 ± 0.03
	Site 4	0.60 ± 0.04	0.40 ± 0.03	0.64 ± 0.04	0.40 ± 0.03
	Fe(II)	2.90 ± 0.07	1.20 ± 0.04	2.93 ± 0.07	1.21 ± 0.04
4.2	Siroheme	2.72 ± 0.05	0.92 ± 0.03	2.7 ± 0.1	0.99 ± 0.06
	[4Fe-4S]:				
	Site 1	1.38 ± 0.04	0.45 ± 0.03	1.44 ± 0.04	0.45 ± 0.03
	Site 2	1.10 ± 0.04	0.45 ± 0.03	1.16 ± 0.04	0.43 ± 0.03
	Site 3	1.02 ± 0.04	0.45 ± 0.03	1.04 ± 0.04	0.45 ± 0.03
	Site 4	0.71 ± 0.04	0.44 ± 0.03	0.73 ± 0.04	0.43 ± 0.03
	Fe(II)	3.22 ± 0.07	1.25 ± 0.04	3.25 ± 0.07	1.24 ± 0.04

Table 4. Wavelengths and relative intensities of the absorption maxima for *D. gigas* desulfoviridin, *E. coli* sulfite reductase and metal free tetrahydroporphyrin methyl easter[a].

D. gigas desulfoviridin	*E. coli* sulfite reductase	metal free chromophore
380 nm (0.86)	386 nm (1.00)	375 nm (0.89)
390 nm (0.91)		385 nm (0.39)
408 nm (1.00)	455 nm (0.57)	403 nm (1.00)
583 nm (0.21)	587 nm (0.23)	570 nm (0.15)
628 nm (0.42)	714 nm (0.07)	617 nm (0.20)

[a] The data are taken from reference 12. Relative intensities are given in values inside parentheses.

FIGURE CAPTIONS

Figure 1. Absorption spectra of the tetrapyrrolic chromophores extracted from *D. gigas* desulfoviridin (Trace A) and from *D. baculatus* desulforubidin (Trace C). Spectrum C is normalized to 25% of the chromophore concentration of the sample in A. Trace B is the difference spectrum of spectra A and C.

Figure 2. EPR spectra of dissimilatory sulfite reductases isolated from *D. baculatus* (desulforubidin, trace A) and *D. gigas* (desulfoviridin, trace B). Experimental conditions: microwave power, 2 milliwatts; modulation amplitude, 1 mT; temperature, 8 K; microwave frequency, 9.43 GHz; receiver gain, 2×10^4 for A and 1×10^5 for B.

Figure 3. Mössbauer spectra of the as isolated desulforubidin from *D. baculatus* (A) and desulfoviridin from *D. gigas* (B). The data were recorded at 4.2 K in a magnetic field of 50 mT applied parallel to the γ- beam. The three resolved spectral subcomponents are indicated by the brackets. The spectrum of the rhombic Fe(III) species is not resolved. The *solid line* in (B) is the result of a least-squares fit of four quadrupole doublets with equal intensity. Parameters resulted from the fit are listed in table 1.

Figure 4. Strong-field Mossbauer spectra of the as isolated desulforubidin from *D. baculatus* (A), and desulfoviridin from *D. gigas* (B). The data were recorded at 4.2 K in a parallel applied field of 8 T. The spectral components of the four different iron centers are resolved under these experimental conditions, and are marked by the brackets. The *solid lines* are theoretical simulations of the diamagnetic, uncoupled $[4Fe\text{-}4S]^{2+}$ clusters. Parameters obtained from the least-squares fit of the weak-field spectrum (Figure 3B) were used in the simulations. The theoretical spectrum in A is normalized to 42 % of the total Iron absorption and it is normalized to 80 % in B.

Figure 5. Mössbauer spectra of the exchange-coupled siroheme-[4Fe-4S] unit in desulforubidin from D. baculatus recorded at 4.2 K in parallel applied fields of the indicated strengths. These spectra were prepared by subtracting the 42 % contribution of the diamagnetic $[4Fe\text{-}4S]^{2+}$ cluster from the raw data (see Text). The contribution from the Fe(III) species has not been removed and is indicated by the arrows in (C). The solid lines plotted over the data are theoretical simulations using the parameters listed in Table 2. Theoretical spectra of the individual iron sites are also shown: siroheme, (----); site 1 of the [4Fe-4S] cluster, (— —); site 2 of the [4Fe-4S] cluster, (——).

Figure 6. 195 K Mössbauer spectra of the as isolated desulforubidin from D. baculatus (A) and desulfoviridin from D. gigas (B). The solid lines are least-squares fits of the data. Absorptions originating from the siroheme and the [4Fe-4S] cluster are indicated.

Figure 7. 150 K Mössbauer spectra of the reduced desulforubidin from D. baculatus (A) and desulfoviridin from D. gigas (B). The solid lines are least-squares fits of the data. Positions of the quadrupole doublets originating from different iron centers are indicated.

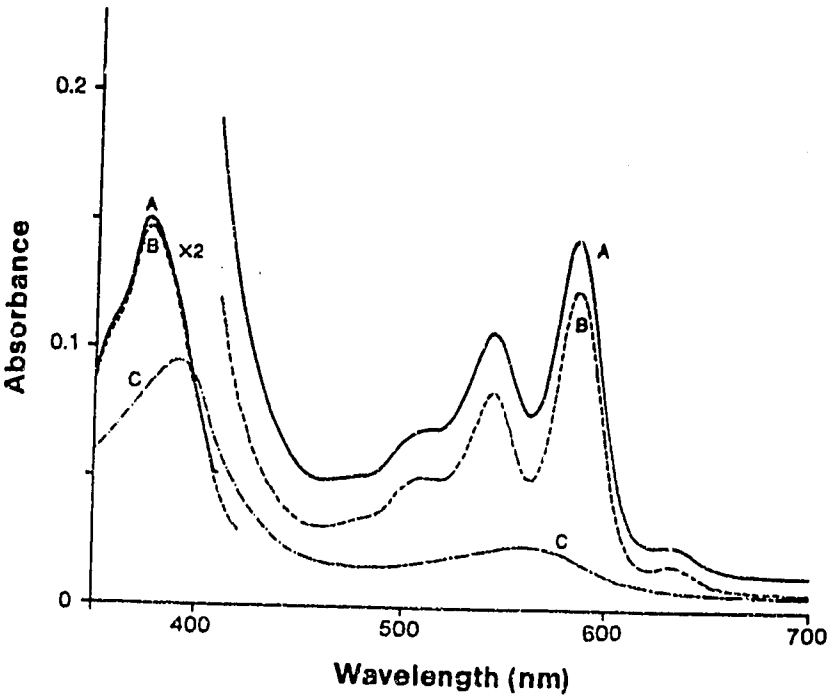

Figure 1

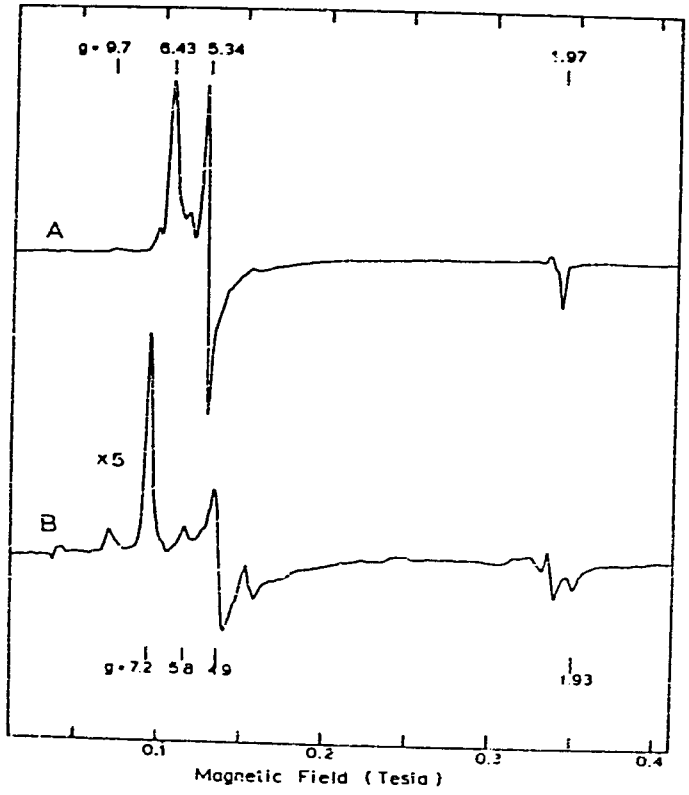

Figure 2

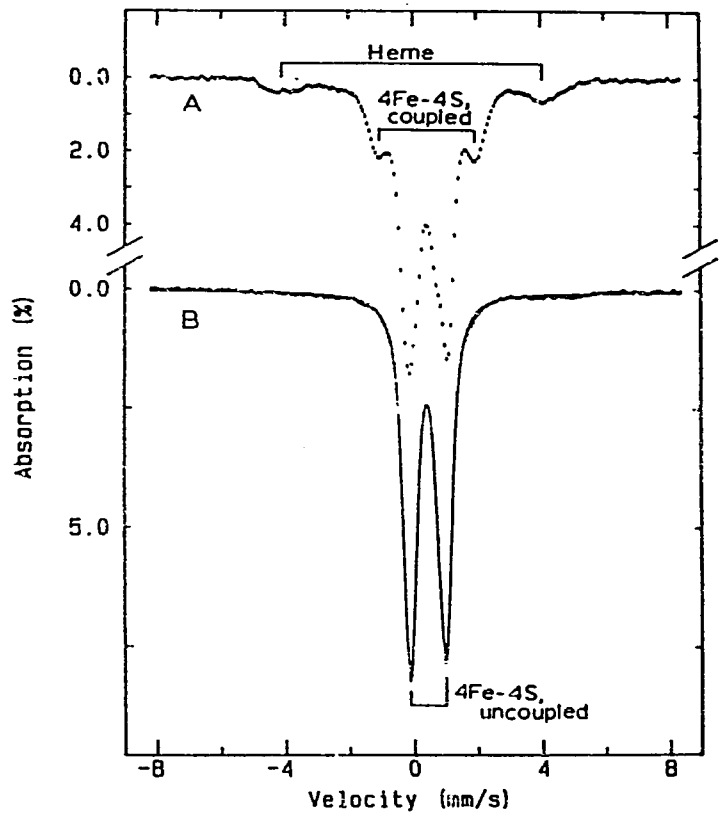

Figure 3

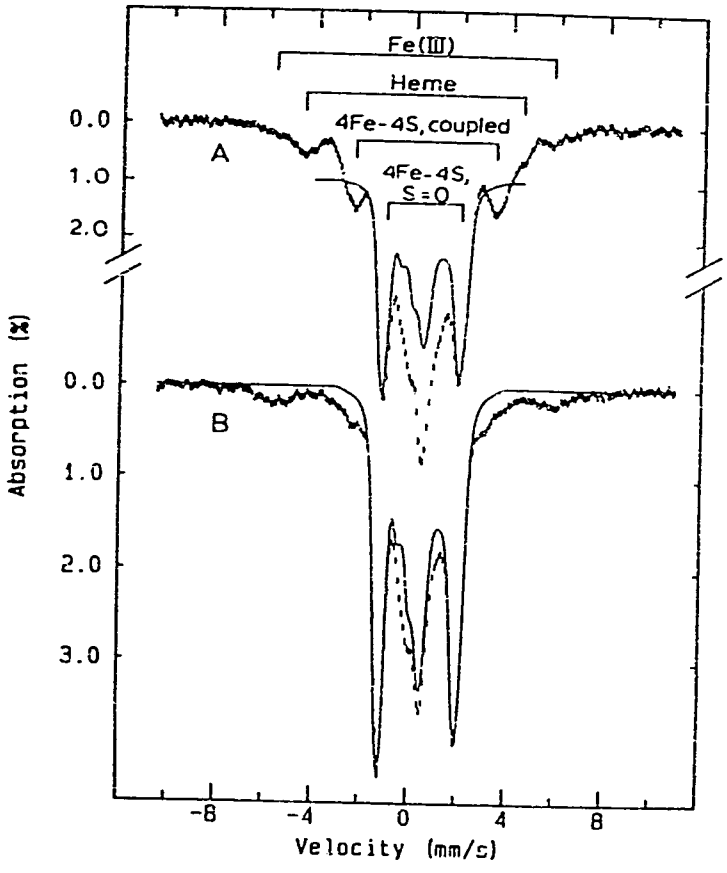

Figure 4

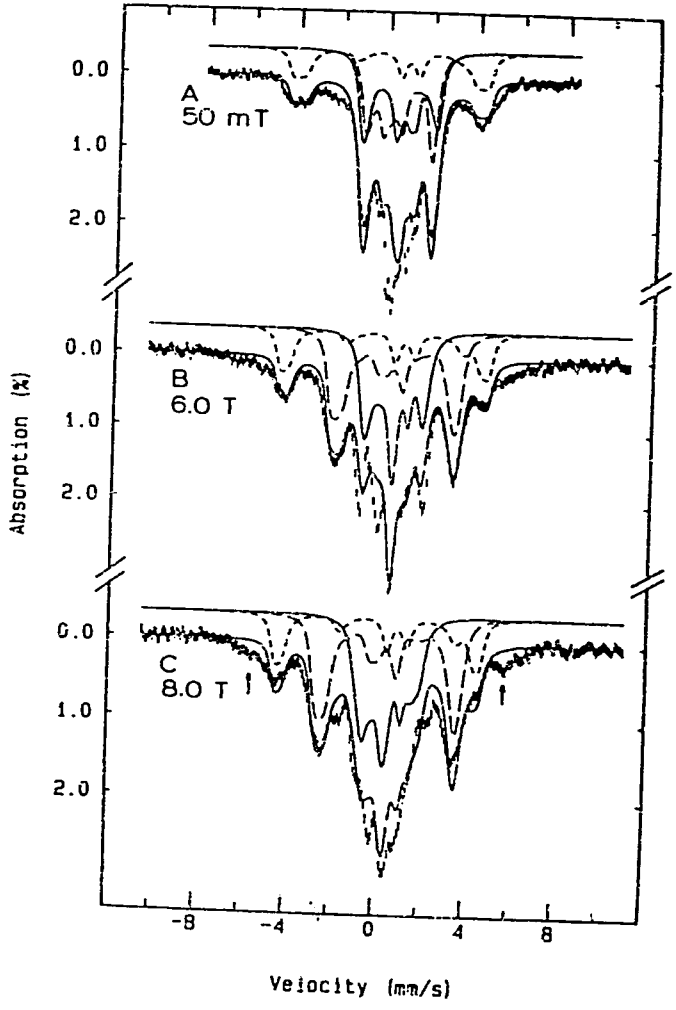

Figure 5

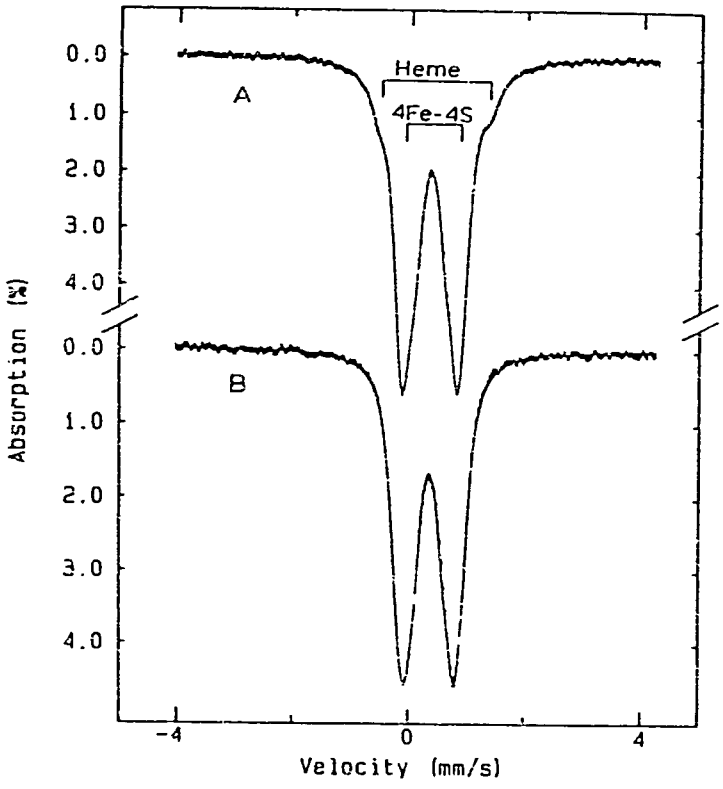

Figure 6

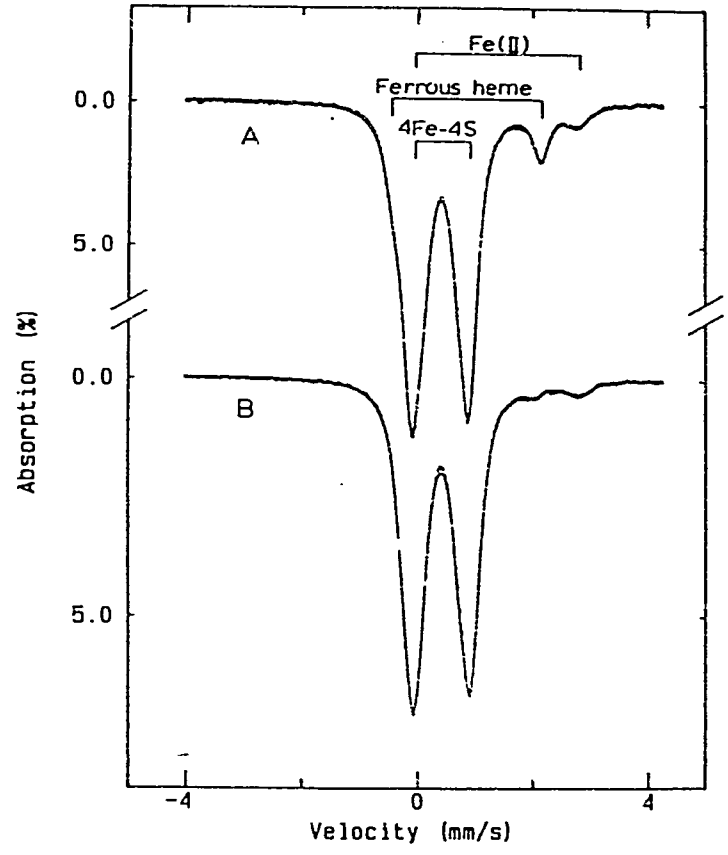

Figure 7

THE JOURNAL OF BIOLOGICAL CHEMISTRY
© 1985 by The American Society of Biological Chemists, Inc.

Electron Paramagnetic Resonance Studies on the Mechanism of Activation and the Catalytic Cycle of the Nickel-containing Hydrogenase from *Desulfovibrio gigas**

(Received for publication, December 12, 1984)

Miguel Teixeira‡, Isabel Moura‡, António V. Xavier‡, Boi H. Huynh§, Daniel V. DerVartanian¶, Harry D. Peck, Jr.¶, Jean LeGall¶‖, and José J. G. Moura‡

From the ‡Centro de Química Estrutural, UNL, Complexo I, IST, Av. Rovisco Pais, 1000 Lisboa, Portugal, the §Department of Physics, Emory University, Atlanta, Georgia 30322, and the ¶Department of Biochemistry, University of Georgia, Athens, Georgia 30602

Desulfovibrio gigas **hydrogenase (EC 1.12.2.1) is a complex enzyme containing one nickel, one 3Fe, and two [Fe_4S_4] clusters (Teixeira, M., Moura, I., Xavier, A. V., DerVartanian, D. V., LeGall, J., Peck, H. D., Jr., Huynh, B. H., and Moura, J. J. G. (1983) *Eur. J. Biochem.* 130, 481–484). This hydrogenase belongs to a class of enzymes that are inactive "as isolated" (the so-called "oxygen-stable hydrogenases") and must go through an activation process in order to express full activity. The state of characterization of the active centers of the enzyme as isolated prompted us to do a detailed analysis of the redox patterns, activation profile, and catalytic redox cycle of the enzyme in the presence of either the natural substrate (H_2) or chemical reductants. The effect of natural cofactors, as cytochrome c_3, was also studied. Special focus was given to the intermediate redox species generated during the catalytic cycle of the enzyme and to the midpoint redox potentials associated.**

The available information is discussed in terms of a "working hypothesis" for the mechanism of the [NiFe] hydrogenases from sulfate reducing organisms in the context of activation process and catalytic cycle.

The metabolism of molecular hydrogen and the study of hydrogenases have figured centrally in the development of the present concepts regarding the biochemistry and the physiology of dissimilatory sulfate reduction (1, 2). Two types of periplasmic hydrogenase have been well characterized from *Desulfovibrio* species: one type containing nickel as well as iron-sulfur clusters, termed the [NiFe] hydrogenase and another type containing only iron-sulfur clusters, termed the [Fe] hydrogenase. The first type has been most extensively studied in *Desulfovibrio gigas* (3–7) and the second one in *Desulfovibrio vulgaris* (8, 9).

The *D. gigas* [NiFe] hydrogenase has a molecular mass of 89 kDa with two subunits of molecular mass 63 and 26 kDa, respectively. It contains approximately 1 g atom of nickel, 11 g atoms of iron, and 11–12 g atoms of sulfide/molecule of 89 kDa. Mössbauer and EPR spectroscopic studies established that in the purified enzyme the iron-sulfur clusters are organized into a $[Fe_3S_X]_{ox}$ cluster (EPR active) and two $[Fe_4S_4]^{2+}$ clusters ("EPR silent").[1] The $[Fe_3S_X]_{ox}$ cluster is the origin of an almost isotropic EPR signal centered around $g = 2.02$ observable below 30 K. A rhombic EPR signal with g values at 2.31, 2.23, and 2.02 (Ni-signal A) was also observed (3). It was definitively assigned to nickel(III) and accounts for 50–100% of the chemically detectable nickel, depending on preparation. This assignment was confirmed by the observation of hyperfine coupling in ^{61}Ni isotopic labeled hydrogenase and by comparison with model nickel compounds (6, 10). A minor species can also be detected at g values 2.33, 2.16, and around 2.0 (Ni-signal B), but its intensity varies with the preparations (3). Redox titrations at pH 8.5 indicate redox transitions at −70 mV measured by the disappearance of the 2.02 signal and at −220 mV measured by the disappearance of the Ni-signal A (4, 5). The midpoint redox potential associated with the disappearance of Ni-signal A was shown to be pH dependent with a slope of −60 mV/pH unit (5).

* This research was supported by grants from the Instituto Nacional de Investigação Científica, Junta Nacional de Investigação Científica e Tecnológica, NID Grant 936-5542-G-SS-4003-00 and North Atlantic Treaty Organization Grant 0341/83 (J. J. G. M.), National Science Foundation Grant PCM 8111325 (J. L., D. V. D., and H. D. P.), Solar Energy Research Institute Subcontract XD-1-1155-1 (J. L.), National Institutes of Health Grants AM01135 and GM32187, and in part by the United States Department of Energy under Contract DE AS03-80-ER10499. The costs of publication of this article were defrayed in part by the payment of page charges. This article must therefore be hereby marked "*advertisement*" in accordance with 18 U.S.C. Section 1734 solely to indicate this fact.

‖ Association pour la Recherche en Biosynergie Solaire, Equipe Commune d'Enzymologie, Centre d'Energie Nucleaire de Cadarache, B. P. no. 1, 13115 Saint-Paul-Lez-Durance, France.

[1] First found in *Azotobacter vinelandii* ferredoxin I (41), the $[Fe_3S_X]$ cluster has since been found in beef heart aconitase (43), *D. gigas* ferredoxin II (37), and hydrogenases from *D. gigas* (44) and *Desulfovibrio desulfuricans* (45).

Although x-ray diffraction data of 20-nm resolution has been obtained for the 3Fe cluster present in *A. vinelandii* ferredoxin I (41), the structure of these clusters remains controversial. X-ray data on *A. vinelandii* ferredoxin I indicates that the 3Fe cluster is an essentially planar core with Fe-Fe distances of 41 nm. However, EXAFS studies on the 3Fe cluster present in *D. gigas* (42) and in aconitase (43) indicate a shorter Fe-Fe distance (~27 nm), in closer agreement with those found for $[Fe_4S_4]$ cubane-type structures. Also a careful determination of labile sulfide in aconitase indicates that the ratio Fe to S^{2-} is 3:4 (43). These results suggest the presence of a $[Fe_3S_4]$ structure that can be built by removal of one iron from the $[Fe_4S_4]$ cluster, which is quite attractive since it explains the facile interconversion between these type of centers (43, 44). To address the discrepancy between the x-ray, the extended x-ray absorption fine structure, and the S^{2-} chemical determinations it was suggested that either two substantially different structures for $[Fe_3S_X]$ exist or some of the structural studies are in error (42). So, since formal charge of the core depends on the number of labile sulfide assumed to be present, throughout this text these clusters will be represented as $[Fe_3S_X]$, with a subscript denoting the oxidation state described (ox or red).

Further reduction of hydrogenase results in the appearance of a new EPR signal with g values at 2.19, 2.16, and 2.02 (Ni-signal C), which subsequently disappears upon a long exposure to hydrogen gas or in the presence of excess dithionite (3, 6, 11). This last signal was assigned to nickel since hyperfine structure is also induced by ^{61}Ni isotope substitution (6). The oxidation state of the nickel center giving origin to Ni-signal C has been tentatively assigned to Ni(III), although the hypothesis that the signal originates from a Ni(I) species has not yet been eliminated (11).

In the presence of a chemical reductant (dithionite) the center associated with the $g = 2.02$ EPR signal is reduced prior to the disappearance of the Ni-signal A; however, in the presence of hydrogen both redox centers disappear almost simultaneously (4).

Most of the so-called "oxygen-stable" hydrogenases, such as *D. gigas* hydrogenase, appear to be reversibly inactivated by oxygen. They are fully active under anaerobic conditions after exposure to activators such as H_2, dithionite, reduced viologens, or tetraheme cytochrome c_3 (13 kDa). The function of activation was thought to be associated with the removal of oxygen bound to an essential redox center; however, recent reports have shown that the process is more complex (7, 12). Hydrogen evolution, hydrogen consumption, and hydrogen-deuterium exchange experiments carried out on the native preparations, which are catalytically inactive enzymes, always show a lag phase and an activation phase before full expression of activity is achieved. The disappearance of the lag phase, with concomitant increase of specific activity of the enzyme, was observed under proper reducing conditions. However, oxygen scavengers (such as glucose oxidase) could only reduce the lag phase, the activation step still being required. Berlier *et al.* (12) and Lissolo *et al.* (7) have proposed that a two-step process takes place: removal of oxygen bound to a catalytic site followed by reduction of the involved redox centers.

In this communication we describe: 1) the possible intermediate species and redox states occurring during the activation and catalytic cycle of the enzyme; 2) the activation phenomenon which is necessary in order to transform the enzyme into a fully active state; 3) the conditions for the appearance of the transient Ni-signal C and the estimation of the midpoint redox potential associated with the development of this signal; 4) the interaction between the redox centers; 5) the properties of the $[Fe_4S_4]$ clusters; 6) the possible role of cytochrome c_3 in the redox cycling of the enzyme.

Sufficient information was now accumulated in order to propose a "working hypothesis" for the mechanism of the [NiFe] hydrogenase from the sulfate-reducing bacteria, in the context of activation and catalytic cycles.

MATERIALS AND METHODS

Growth of the Organisms and Purification of Hydrogenase and Cytochrome c_3—*D. gigas* was grown on a medium as described by Le Gall *et al.* (13). The periplasmic hydrogenase was purified using DEAE-Bio-Gel and hydroxylapatite chromatographic procedures as described in Ref. 3 with the difference that the crude cell extract, obtained by pressure disruption of the cells, was applied to the column instead of the cell washings. Precautions were taken against oxygen by flushing buffers with purified argon and maintaining all fractions under the same atmosphere. The purification method outlined gave a high protein yield, approximately 800 mg of pure enzyme from 4 kg of wet cells. The preparations used showed a single electrophoretic band and a specific activity between 400 and 440 μmol H_2 min^{-1} mg^{-1} of protein (unit of activity used throughout this text).

D. gigas tetraheme cytochrome c_3 (13 kDa) was purified as previously described (14).

Assays and Metal Determinations—Hydrogenase activity was measured by the hydrogen evolution assay in the presence of an electron donor (dithionite-reduced methyl viologen) employing a Varian 4600 gas chromatograph (3). Iron was determined by the 2,4,6-tripyridyl-*S*-1,3,5-triazine method (15), and nickel was determined by plasma emission spectroscopy, using a Jarrell Ash model 750 Atomcomp. Protein was determined by the Bradford method (16), but hydrogenase concentrations were calculated based on the extinction coefficient $\epsilon_{280} = 43$ mM^{-1} cm^{-1} (17). Purity of the enzyme was checked by polyacrylamide gel electrophoresis (18).

EPR Spectroscopy—EPR spectra were recorded on a Bruker ER-200 tt spectrometer equipped with an Oxford Instruments continuous flow cryostat interfaced with a Nicolett 1180 computer where mathematical manipulations were performed. Signal intensities were determined by double integration with base-line corrections. Cu-EDTA (1 mM) or *D. gigas* ferredoxin (II) were used as reference standards. Concentrations of ferredoxin (II) samples were calculated using the extinction coefficient $\epsilon_{400} = 16$ mM^{-1} cm^{-1} (19).

Midpoint Redox Potential Determinations—Midpoint redox potentials were measured by poising the enzyme at different redox potentials in the presence of oxidation/reduction mediators, all at 80 μM (20). The potential (platinum calomel electrode) was adjusted by addition of dithionite (0.2 M in Tris-HCl, pH 9.0) or ferricyanide (0.2 M) solutions. The protein concentration in the titration vessel was 80 μM, as estimated by the extinction coefficient. After equilibration at a fixed redox potential a sample was transferred into an EPR tube under argon pressure and immediately frozen at 77 K for further quantification.

Generation of Intermediate Redox States of Hydrogenase—All experiments were conducted anaerobically in EPR tubes sealed with serum caps. Additions of reductants and gases were performed through metal needles and gas-tight Hamilton syringes. Intermediate redox states of hydrogenase were obtained by incubation under a hydrogen atmosphere for different lengths of time or by addition of substoichiometric or excess amounts of dithionite. The effect of equimolecular amounts of cytochrome c_3 in the redox pattern of hydrogenase was studied in different experimental conditions. Sample reoxidations were accomplished by replacing hydrogen atmosphere by argon.

RESULTS AND DISCUSSION

Activity Profile of the Enzyme (Hydrogen Evolution)—The profile for the hydrogen evolution activity as well as the correspondent changes of specific activities measured as a function of time are shown in Fig. 1. A typical lag phase phenomenon is observed. The time elapsed represents a true incubation time in reducing media (dithionite-reduced methyl viologen). A linear response of the system is obtained after 25–30 min at 32 °C, pH 7.6 (Tris-HCl buffer). Different preparations of hydrogenase always show a similar profile

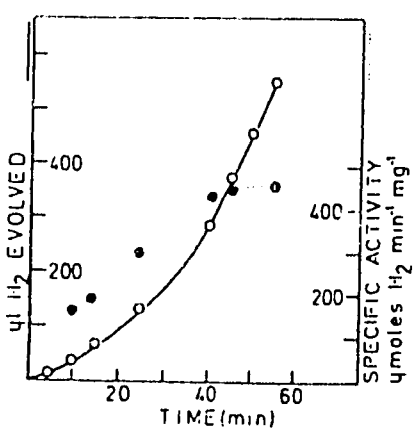

FIG. 1. Typical profile of hydrogen evolution by *D. gigas* hydrogenase assayed in the presence of dithionite-reduced methyl viologen, $t = 32$ °C, pH 7.6. Conditions are indicated under "Materials and Methods." Also indicated is the variation of specific activity calculated at different assay times.

although the lag phase may vary. The maximal specific activity reported for the enzyme was taken from the linear part of the hydrogen evolution profile and is 440. Both hydrogen evolution and hydrogen uptake (7) require an activation step in order to express full activity.

Ni EPR Signals of Oxidized Hydrogenases—Fig. 2 shows the EPR spectra of different preparations of native *D. gigas* hydrogenase as well as a comparison with other bacterial [NiFe] hydrogenases. The data were recorded at 77 K, a temperature at which the $g = 2.02$ signal of the $[Fe_4S_4]$ cluster was broadened beyond detection, and only the Ni signals were observable. As purified, *D. gigas* hydrogenase exhibits a rhombic EPR signal, $g = 2.31$, 2.23, and 2.02 (Ni-signal A, Fig. 2*A*). The quantitation of Ni-signal A varies from 0.5–1.0 spin/molecule depending on the preparation. In correlation with the activation profile of the enzyme we notice that in all cases the Ni-signal A is associated with an inactive form of the enzyme. In addition to the Ni-signal A, a minor component with g values at 2.33, 2.16, and 2.02 (Ni-signal B) is observed in some preparations (Fig. 2*B*). The relative intensity of Ni-signals A and B varies from preparation to preparation and can be altered by redox cycling of the enzyme. When *D. gigas* hydrogenase reduced under H_2 is allowed to reoxidize slowly by replacing the hydrogen atmosphere with argon, an increase in the intensity of Ni-signal B relative to the Ni-signal A is observed (Fig. 2*C*, also see below), indicating that there exists different Ni(III) environments in the anaerobically oxidized enzyme. It should be noted that the nickel(III) signal intensities (Ni-signals A and B) are recovered. The fact that Ni-signal B relative intensity increases upon anaerobic reoxidation and that anaerobic reoxidation results in the drastic decrease of the lag phase suggest that this Ni-signal B represents an environment resulting from the first step of the activation process, namely the removal of oxygen from the enzyme (see below).

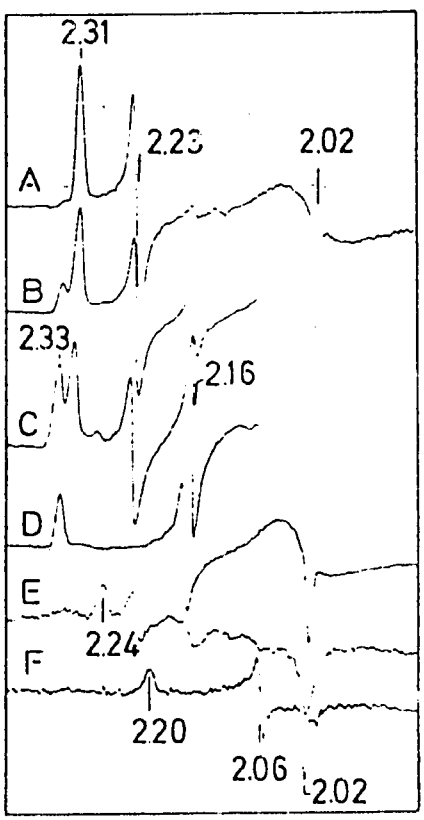

FIG. 2. Nickel EPR signals of oxidized forms of [Ni-Fe] hydrogenases. *A* and *b*, different preparations of *D. gigas* hydrogenase; *C*, reoxidized H_2-reduced *D. gigas* hydrogenase; *D*, *D. desulfuricans* (ATCC 27774) hydrogenase; *E*, *M. barkeri* hydrogenase; *F*, *D. baculatus* strain 9974 (DSM 1743) hydrogenase (periplasm). Experimental conditions: temperature 77 K; variable gain; modulation amplitude, 1 millitesla; microwave power, 2 milliwatts; frequency, 9.41 GHz.

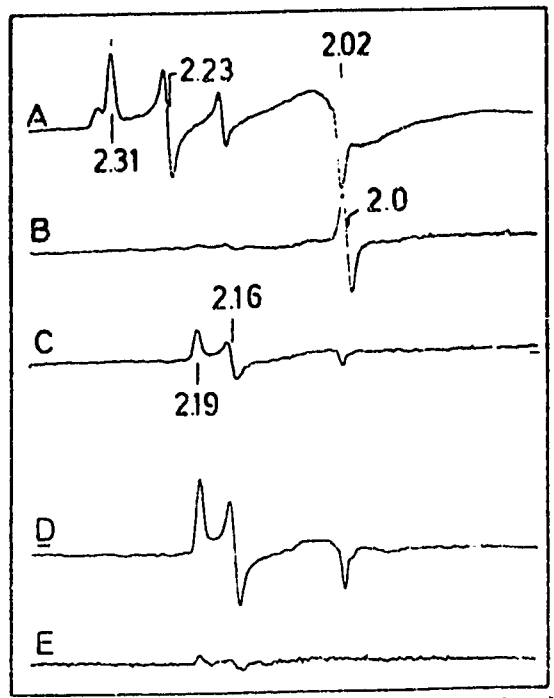

FIG. 3. EPR spectra of *D. gigas* hydrogenase monitored during different periods of exposure to hydrogen at 77 K. *A*, native enzyme; *B–E*, evolution of the EPR spectra upon increasing time of incubation under hydrogen atmosphere. Other experimental conditions were as follows. *A–E*: modulation amplitude, 1 millitesla; microwave power, 1 milliwatt; and frequency, 9.28 GHz. The gains of the different spectra shown were: *A*, 4×10^4; *B*, 8×10^4; *C–E*, 2×10^5.

In Fig. 2, we have also shown the high temperature EPR spectra of [NiFe] hydrogenases isolated from various bacterial sources (Fig. 2, *D–F*). It is interesting to notice that native hydrogenases from different species yield different EPR signals. The periplasmic hydrogenase from *Desulfovibrio desulfuricans* (ATCC 27774) exhibits an EPR signal similar to the Ni-signal B (Fig. 2*D*) (21) while *Methanosarcina barkeri* (DSM 800) (22) shows a nickel signal with g values at 2.24, 2.20, and 2.02 and a minor component at 2.30, 2.12, and ~2.0 (Fig. 2*E*). Yet another nickel signal with g values at 2.20, 2.06, and 2.0 is observed for the periplasmic [NiFe] hydrogenase isolated from *Desulfovibrio baculatus* (ATCC 9974) (Fig. 2*F*).[2]

Intermediate Oxidation States Generated by Hydrogenase Reduction—Fig. 3 shows EPR spectra representing a typical sequence of events during the anaerobic reduction of *D. gigas* hydrogenase with H_2. The spectra were recorded at 77 K. EPR signals of the iron-sulfur clusters are not observable at

[2] M. Teixeira, I. Moura, G. Fauque, A. V. Xavier, B. H. Huynh, D. V. DerVartanian, H. D. Peck, Jr., J. LeGall, and J. J. G. Moura, unpublished data.

this temperature. The first step of events is the concomitant disappearance of the Ni-signal A, Ni-signal B, and the isotropic $g = 2.02$ signal of the $[Fe_xS_x]$ cluster (as observed at 10 K). A radical-type signal with very low intensity and of unknown origin is observed next (Fig. 3*B*). The disappearance of this radical-type signal is accompanied by the development of a new rhombic EPR signal with g values at 2.19, 2.16, and 2.02 (Ni-signal C) (Fig. 3*C*). During the course of a few hours, this Ni-signal C develops through a maximum of intensity which quantitates to 40–60% of the chemically detectable nickel (Fig. 3*D*). After a long incubation (36–48 h) under hydrogen, an EPR silent state is obtained when measured at 77 K (Fig. 3*E*). At low temperature (below 15 K), EPR signals typical of $[Fe_4S_4]^{1+}$ clusters are now observed. This sequence of events can be reproducibly reversed by anaerobically oxidizing the reduced sample under argon and completely repeated by exposing the reoxidized sample to hydrogen.

At redox states of the enzyme such that Ni-signal C has developed, low temperature studies reveal the presence of another EPR active species. Fig. 4 shows the EPR spectra of such a sample recorded at different temperatures. Below 15 K, the shape of the EPR spectra changes drastically, and a new set of signals at $g = 2.21$, 2.10, and broad components at higher field are clearly discernible in the 4 K spectrum (Fig. 4*A*). This new set of EPR signals also exhibits power dependence different from that of Ni-signal C. Fig. 5 shows a power study performed at 10 K. The Ni-signal C is readily saturated at low microwave power (Fig. 5*A*), indicating slow electronic relaxation. The origin of the new set of signals is not yet understood. Since these signals are only observable at low temperature and show fast electronic relaxation, they may originate from an iron-sulfur cluster; however, the observed g values appear to be too high. Another possible explanation is that they originate from a Ni center that is weakly interacting with another paramagnetic center nearby, resulting in the fast relaxation behavior.

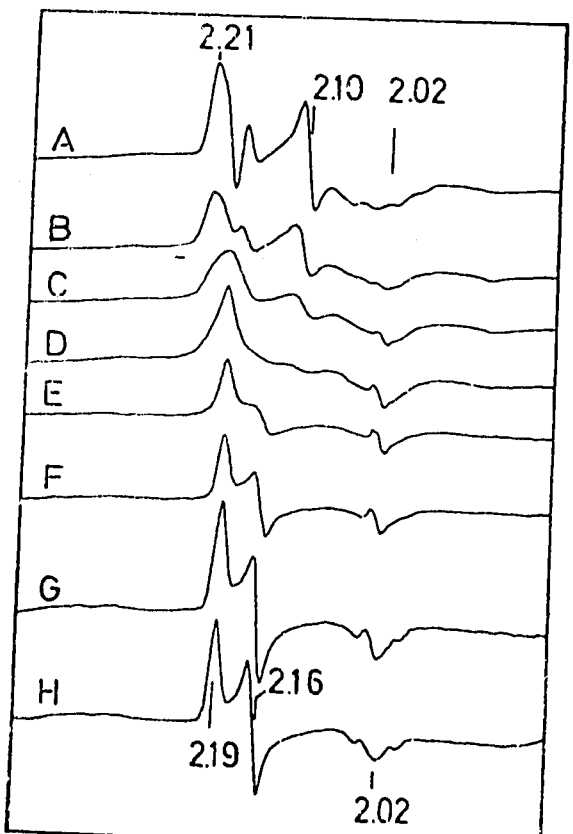

FIG. 4. Temperature dependence of the intermediate hydrogen reduced state of ^{61}Ni-enriched *D. gigas* hydrogenase. Experimental conditions of the EPR spectra as follows. Temperature and gain: *A*, 4 K, 3.2×10^4; *B*, 7 K, 5×10^4; *C*, 9 K, 6.3×10^4; *D*, 11 K, 8×10^4; *E*, 15 K, 6.3×10^4; *F*, 27 K, 10×10^4; *G*, 38 K, 2×10^5; *H*, 63 K, 2×10^5; microwave power, 2 milliwatts, except for H (5 milliwatts); modulation amplitude, 0.4 millitesla, except for H (1 millitesla); microwave frequency, 9.41 GHz.

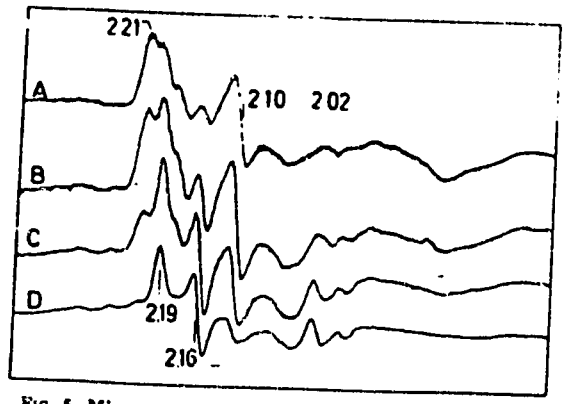

FIG. 5. Microwave power dependence of the intermediate hydrogen reduced state. *A*: microwave power, 104 milliwatts; gain, 2.5×10^4; *B*: microwave power, 2 milliwatts; gain, 4×10^4; *C*: microwave power, 1.2 milliwatts; gain, 2.5×10^4; *D*: microwave power, 200 microwatts; gain, 2.5×10^4. Other experimental conditions: temperature, 10 K; microwave frequency, 9.52 GHz.

The Ni-signal C has been reported previously and was attributed to a nickel species since hyperfine structure was induced by ^{61}Ni isotopic substitution (6). Ni-signal C is different from Ni-signal A and Ni-signal B in both g values and in hyperfine coupling constants. These differences have been proposed to reflect a replacement of ligands in the nickel coordination sphere or a different coordination number (11). It was also proposed that this transient signal might be due to a hydride-bound species by analogy with nickel catalysts involved in hydrogenation processes (23). Because of the midpoint redox potential studies reported below, we favor the later proposal. It is quite tempting to speculate that Ni-signal C may represent a Ni(I) oxidation state. However, such a proposal would imply a Ni(0) state upon further reduction. Taking into consideration the g values, the transient nature of Ni-signal C, the reductive power of H_2, and the extreme negative midpoint redox potential of the redox transition Ni(I)/Ni(0) observed in model compounds, Ni-signal C is more compatible with a Ni(III) species (see also discussion below).

Studies of Midpoint Redox Potentials Associated with Ni-Signal C—Titrimetric determinations of the oxidation-reduction potentials associated with the appearance and disappearance of the Ni-signal C were followed by EPR. Since Ni-signal C is slow to equilibrate with the electrode in the presence of dye mediators and due to the transient nature of this signal, there is a large scattering of the experimental data. The redox titration was independently determined from three different experiments, and the data is superimposed and plotted in Fig. 6. Ni-signal C develops at a potential below −270 mV, reaches maximum intensity at about −350 mV, and

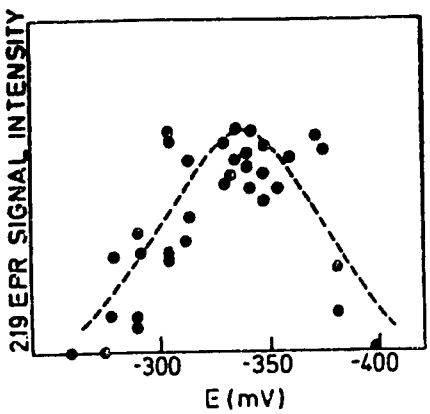

FIG. 6. EPR redox titration curve of the EPR active species detected in the hydrogen-reduced state of *D. gigas* hydrogenase. EPR signal intensity (arbitrary units) of the "2.19" EPR signals detected upon redox titration of the enzyme at 25 °C and pH 8.5 in the presence of redox mediators under conditions as described under "Materials and Methods." The EPR signals were measured at 77 K. No attempt was made to fit the experimental points to a Nernst equation.

completely disappears below −400 mV. These observations place the redox potential for the appearance of Ni-signal C between −300 mV and −350 mV. Lissolo *et al.* (7) have determined the activity of *D. gigas* hydrogenase as a function of redox potential imposed by varying the partial pressure of H_2. Their study indicated that the hydrogenase activation phenomenon is a 1-electron process with a midpoint redox potential at approximately −340 mV. This potential correlates very well with the potential at which Ni-signal C appears, strongly suggesting that this signal may represent an activated state of the enzyme.

The Reduced [Fe₄S₄] Clusters—In addition to the [Fe_2S_x] centers, *D. gigas* hydrogenase was shown to contain two [Fe_4S_4] clusters by Mössbauer spectroscopy (4). These [Fe_4S_4] clusters were previously reported to be EPR silent (4). However, reduction by either excess dithionite or by incubation under H_2 over a period of 24 h or more shows distinct EPR signals typical of $[Fe_4S_4]^{1+}$ clusters. Fig. 7 shows EPR spectra of dithionite-reduced hydrogenase. The spectra shown in Fig. 7, *A* to *E*, depict a temperature study of a hydrogenase sample reduced with substoichiometric amounts of dithionite. Ni-signal C is observed at a high temperature (Fig. 7*E*), and the $g = 2.21$ signal appears at a low temperature (Fig. 7*A*).

The isotropic signal at $g = 2.00$ may be due to dithionite oxidation products; however, as we have already pointed out, a radical species is observed during the reductive pattern of the enzyme (Figs. 3 and 8).

In addition to the Ni-signal C and the $g = 2.21$ signal, EPR signals of a $[Fe_4S_4]^{1+}$ cluster are clearly resolved at $g = 2.05$, 1.94, and 1.88. Spin quantitation of this $[Fe_4S_4]^{1+}$ signal yields approximately 0.1 spin/molecule. It is interesting to note that neither the electronic relaxation behavior of the Ni-signal C nor that of the $g = 2.21$ signal is affected by the presence of this paramagnetic $[Fe_4S_4]^{1+}$ cluster. When hydrogenase is reduced with excess amounts of dithionite, the Ni-signal C and the $g = 2.21$ signal disappear, and, at low temperature, EPR signals corresponding to two types of $[Fe_4S_4]^{1+}$ clusters integrating up to 0.5 spin/molecule are observed (Fig. 7*F*). The spectrum is complex and may have origin in interacting paramagnetic centers.

Redox Cycling of Hydrogenase in the Presence of Ferricytochrome c₃—The effects of cytochrome c_3 on the redox pattern of hydrogenase were examined since cytochrome c_3 is the natural electron donor and acceptor for this enzyme (1, 2). Cytochrome c_3 contains four low-spin hemes, and the EPR spectrum of the oxidized state is quite complex. The g_z region (not shown) exhibits several superimposed signals originating from the nonequivalent hemes ($g_z = 3.3 - 2.8$), and a large derivative peak is observed around $g_z = 2.28$ (24).

EPR spectra representing the time course of redox cycling of native hydrogenase in the presence of ferricytochrome c_3 were recorded at 77 K. In order to visualize the EPR signals originating from nickel, the contribution of cytochrome c_3 was subtracted from the spectra, when necessary. The EPR spectrum of the native hydrogenase is shown in Fig. 8*A*. Ni-signals A and B are observed. A stoichiometric amount of ferricytochrome c_3 was mixed into the native hydrogenase sample (Fig.

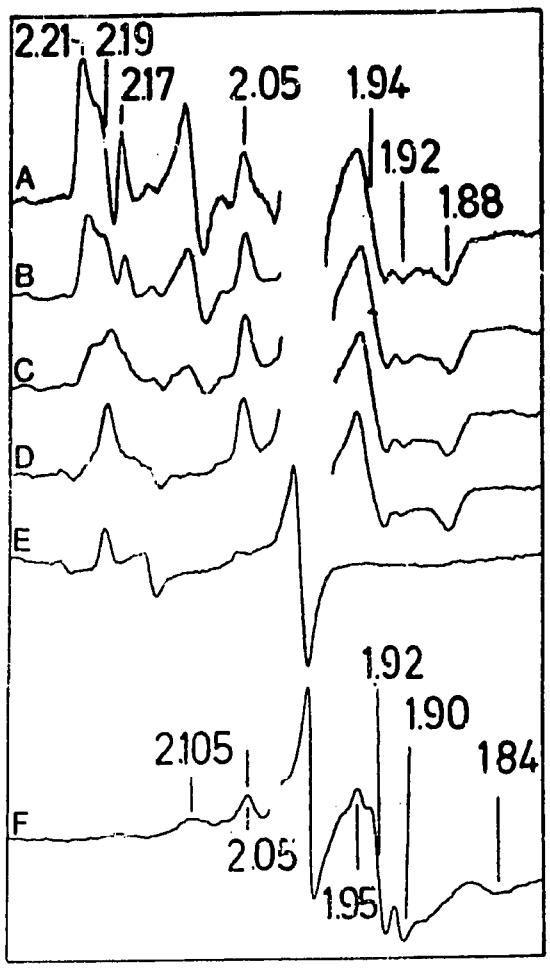

FIG. 7. EPR spectra of *D. gigas* hydrogenase in different levels of reduction, using hydrogen or sodium dithionite as reductants. *A-E*, temperature dependence of an intermediate reduced state of *D. gigas* hydrogenase obtained by reduction with substoichiometric amounts of dithionite. At 77 K this sample is equivalent to the redox state shown in *D*, *i.e.* development of "2.19" signal. Spectral gain, 1×10^5. Temperatures: *A*, 4 K; *B*, 6.7 K; *C*, 10 K; *D*, 12 K, and *E*, 40 K. *F*, reduced enzyme with a 3-fold excess of dithionite; temperature, 12 K. Other experimental conditions: modulation amplitude, 1 millitesla; microwave power, 2 milliwatts; microwave frequency, 9.41 GHz.

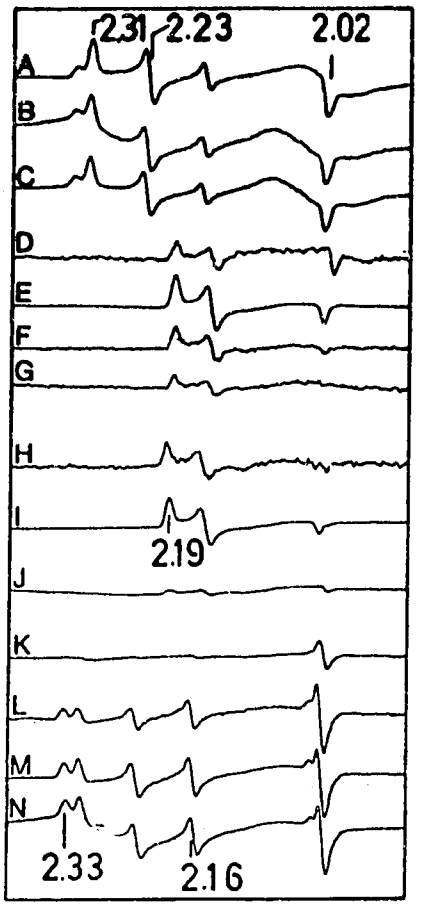

FIG. 8 Pattern for the redox cycling of *D. gigas* hydrogenase in the presence of *D. gigas* cytochrome c_3 (complex 1:1). Proteins were mixed under argon in the native state (oxidized). *A*, native *D. gigas* hydrogenase; *B*, complex 1:1 cytochrome c_3:hydrogenase; *C*, same as *B* subtracted from cytochrome c_3 spectral contribution; *D–G*, reduction of the protein complex under hydrogen; *E*, *F*, and *G* show no contribution from cytochrome c_3, already in the reduced state. Other experimental conditions: temperature, 77 K; microwave power, 2 milliwatts; modulation amplitude, 1 millitesla; microwave frequency, 9.41 GHz, variable gain.

8*B*), and the protein mixture was incubated under an H_2 atmosphere, the reductive process being monitored by EPR (Fig. 8, *C–G*). Reoxidation of the proteins was achieved by replacing the H_2 atmosphere by argon (Fig. 8, *H–N*). The sequence of events during this redox cycling followed closely the redox pattern reported previously in the absence of cytochrome c_3. However, the initial reduction of hydrogenase occurred more rapidly. In order to further investigate the effect of ferricytochrome c_3 upon the redox cycle of hydrogenase reduced by H_2 the following experiment was also carried out. Native hydrogenase was reduced by H_2 until the Ni-signal C was fully developed. Then an argon-saturated cytochrome c_3 solution was added to the sample, and the H_2 atmosphere was replaced by argon. The hydrogenase was reoxidized, and the sequence of redox events was similar to that indicated in Fig. 8. The redox cycle was shown to be reversible by exposing the samples to an hydrogen atmosphere and performing the reoxidation in the presence of argon. The intensity of the 2.02 EPR signal was recovered after the redox cycling of the enzyme.

CONCLUSIONS

A large effort has been put forward in order to understand hydrogen metabolism in sulfate-reducing bacteria (1, 2). This includes the study of the mechanism of hydrogen activation, the type and structure of different hydrogenases, as well as their compartmentalization and role in the cellular bioenergetics.

A comprehension of the mechanism of action of hydrogenase can only be achieved by a full characterization of the structure and physicochemical properties of the redox centers as well as their interaction and behavior during the catalytic cycle. A reasonable understanding of the enzyme metal centers in the "as isolated" state has already emerged from spectroscopic studies (3, 4).

Nickel Chemistry in the Context of Its Biological Role

One of the major unresolved questions concerning the [NiFe] hydrogenase is the role of the nickel during redox cycling, namely the oxidation states involved, its mode of ligation, as well as its interaction with other metal centers. Two possible schemes may be considered. One scheme involves redox cycling between Ni(III) and Ni(II) (hypothesis A), and the other requires the transition from Ni(III) to Ni(0) (hypothesis B) (see Table I).

Nickel can exist in oxidation states ranging from Ni(0) to Ni(IV). Generally, the Ni(II) state is favorably found, in agreement with the decrease in stability of higher oxidation states along the first series of transition metals (25, 26). However, Ni(III) and Ni(IV) states can be stabilized by electronegative ligands and are found to coordinate N, O, F, and anionic ligands. The lower oxidation states Ni(0) and Ni(I) are also not common, except with electron acceptor ligands (*e.g.* carboniles, phosphines, and thiolates). Restriction on the commonly available biological ligands favors a scheme involving fewer oxidation states (such as hypothesis A which involves only Ni(II) and Ni(III) states) rather than undergoing a redox transition (hypothesis B) from Ni(III) to Ni(0).

Nickel chemistry indicates that nickel can occur with different coordination numbers 4, 5, and 6, using structures ranging from square planar to tetrahedral, trigonal bipyramidal, square pyramidal, and octahedral geometries. The octahedral coordination is commonly found for Ni(II) ($S = 1$). A

TABLE I

Possible oxidation states of nickel in D. gigas hydrogenase

Redox states of hydrogenase and Ni EPR signals[a]	Hypothesis A	Hypothesis B
Oxidized (EPR active) $g = 2.31, 2.23, 2.02$ $g = 2.33, 2.16, \sim 2.0$ Forms 1 and 2[b]	Ni(III)	Ni(III)
Active state (EPR silent) Form 3[b]	Ni(III) (coupled)	Ni(II)
Hydride intermediate $g = 2.19, 2.16, 2.02$ Form 4[b]	Ni(III)- hydride	Ni(I)
Reduced state (EPR silent) Forms 5 and 6[b]	Ni(II)	Ni(0)

[a] Observable at 77 K.
[b] Forms are defined in Diagram 1.

Tetragonal distortion may result in an intermediate geometry, and a spin equilibrium between $S = 1$ and $S = 0$ species may be observed (27, 28). The pentacoordinate Ni(II) may result in different spin states ($S = 0$ or $S = 1$) depending on the geometry and ligand field strength. Ni(II) complexes with coordination number 4 are also found in a tetrahedral ($S = 1$) or square planar ($S = 0$) arrangement. Ni(0) and Ni(I) oxidation states are rarely found as pentacoordinated complexes, and the coordination number 4 is preferred. Ni(III) and Ni(IV) oxidation states are frequently found in an octahedral arrangement, Ni(III) also being found in pentacoordinated complexes. Consequently, the Ni(III)/Ni(II) redox transition offers a wide range of opportunities: rearrangement of ligands through different preferred parameters, possibility for conformational and spin equilibrium, and a capability of altering the number and type of ligands in the vicinity of the center (29). The redox transitions involved are a reflex of (and/or controlled by) the peculiar chemistry of nickel. The very high and very low oxidation states are not stable, and a consequence is the very negative and very positive redox potentials at which model compounds undergo oxidation-reduction transitions (Ni(I)/Ni(0) and Ni(III)/Ni(II)) as indicated schematically in Table II. This table compiles data on nickel compounds thought relevant for this discussion. The examples were chosen in respect to their relevance to biological systems (*i.e.* macrocycles, peptides, Schiff bases, and dithiolenes). Also, only compounds where the oxidation states +3 and +1 were unequivocally assigned (namely by EPR) were included. Many of the nickel(I) compounds generate EPR radical-type spectra due to the delocalization of the electron density toward the ligand (30).

Nickel was shown to have a primary role in very different biological situations, being a constituent of several enzymes: urease (31), CO dehydrogenase (32), coenzyme M methyl reductase (33), and some hydrogenases (11). The biological occurrence of nickel includes active sites identified as containing macrocycles (F_{430}) and amino acids using N (urease) and S (hydrogenase) coordinating atoms. So far only the nickel redox transitions occurring in *D. gigas* hydrogenase have been studied in detail. The span of redox values associated with the nickel EPR active species is narrow and in the limiting region for the Ni(III)/Ni(II) transition (Table III). However, modulation of redox potential by the biological ligands involved in metal coordination is known to be a determining parameter for the redox potential (34).

The preliminary extended x-ray absorption fine structure results of the *D. gigas* hydrogenase (35) suggest sulfur coordination around the nickel center. A comparison of Ni(III) EPR g values of hydrogenases purified from different bacterial sources and Ni(III) complexes with S and N containing peptides (Table III) showed that these complexes mimic the enzyme active center (36). Although these results are obtained by solution chemistry, the EPR spectra of the complexes show a high rhombicity, and an increase in sulfur coordination tends to cause a shift of the observable g values to higher field.

TABLE II

Redox transitions of nickel compounds

Redox transition (*versus* SHE)	Ligand (coordinating atom)	$E(V)$ (*versus* SHE)	References
Ni(III)/Ni(II)	Macrocycles (N)	0.1/1.77	29, 30, 47
	Peptides N, O)	0.62/1.13	10, 48
	Dithiolenes (S)	1.15	49
	Schiff base (N, O)	0.38/0.76	50
Ni(II)/Ni(I)	Macrocycles (N)		
	Neutral	0/0.8	
	Monoanionic	−1.4/−1.5	29, 30, 47, 51
	Dianionic	1.0	
	Dithiolenes (S)	−0.8/−1.67	49, 52
	Phosphines (P, dithiolenes (S)	−0.78/−0.89	53
	Schiff base (N, O)	−1.68/−1.77	50
Ni(I)/Ni(0)	Schiff base (N, O)	−2.31/−2.50	50

Working Hypothesis

As stated earlier, it is now well established that the so called "oxygen-stable" [NiFe] hydrogenases (*e.g. D. gigas* hydrogenase) are not fully active in the "as isolated" state. Studies of the hydrogenase activity (7, 12) indicate that the enzyme must go through a lag phase as well as an activation one in order to be able to express full activity. This complex phenomenon seems to involve the removal of oxygen (lag phase) followed by a reduction step (activation phase). This complex process is illustrated in Fig. 1. When hydrogenase is incubated with dithionite-reduced methyl viologen, the amount of H_2 evolved by the system is not linear during the first few minutes of the assay. The hydrogen evolution becomes linear with time after 25-30 min under the assay conditions. The exact time lag for the full activity to appear depends on the hydrogenase preparation as well as on the incubation conditions.

Taking into consideration the hydrogenase activity studies, the preferred Ni(III)/Ni(II) redox cycling scheme, and the sequence of events observed by EPR, a working hypothesis is proposed for the mechanism of the [NiFe] hydrogenases from the sulfate-reducing bacteria in the context of both an activation and a catalytic scheme (see Diagram 1).

A. The Activation Cycle—The [NiFe] hydrogenase as isolated in the oxidized form is composed of variable amounts of at least three different species: 1) inactive oxygenated hydrogenase (Form 1); 2) inactive but deoxygenated hydrogenase (Form 2); and 3) a trace of active hydrogenase. In Forms 1 and 2 the $[Fe_4S_4]$ clusters are in the 2+ state and are EPR silent. The $[Fe_3S_X]_{ox}$ cluster is EPR active and exhibits an isotropic $g = 2.02$ signal observed at temperatures below 30 K. The oxidation state of the nickel is Ni(III) which is EPR active. In the oxygenated form (Form 1) the nickel center exhibits Ni-signal A. In the deoxygenated form (Form 2) it exhibits Ni-signal B. As shown above, the amount of Form 2 can be increased drastically through anaerobic reoxidation (Fig. 2). EPR and Mossbauer studies in the enzyme "as isolated" (4) indicate that there is no magnetic interaction between these four redox centers.

The active state of the enzyme (Form 3) is EPR silent. It can be attained either from Form 1 through a complex and slow activation process (removal of oxygen followed by a reduction step), or it can be reached directly from Form 2 (without a lag phase). When O_2 is admitted a lag phase is required. During this activation process, both the isotropic $g = 2.02$ and the nickel signal disappear. The loss of the $g = 2.02$ signal is attributed to the reduction of the $[Fe_3S_X]$ cluster from an EPR active $[Fe_3S_X]_{ox}$ state to an EPR silent $[Fe_3S_X]_{red}$ state ($E_0 = -70$ mV). Mossbauer studies[3] of this redox state enable the recognition of the typical "signature" of the reduced 3Fe cluster. In order to retain the Ni(III)/Ni(II) redox scheme (hypothesis A), the disappearance of Ni-signal A and/or Ni-signal B requires a more complicated mechanism. We propose that one of the $[Fe_4S_4]$ clusters is reduced into a

[3] M. Teixeira, I. Moura, A. V. Xavier, B. H. Huynh, D. V. DerVartanian, H. D. Peck, Jr., J. LeGall, and J. J. G. Moura, unpublished results.

TABLE III

EPR values of hydrogenases and peptide-Ni(III) complexes

This material was adapted from Ref. 36.

		g_1	g_2	g_3	Donor set
*Methanobacterium thermoautotrophicum** hydrogenase	Native	2.305	2.231	2.015	
D. desulfuricans (27774) hydrogenase	Native	2.32	2.16	2.02	
M. barkeri hydrogenase	Native	2.24	2.20	2.02	
D. gigas hydrogenase	Native	2.31	2.23	2.02	
	Under H_2	2.19	2.16	2.02	
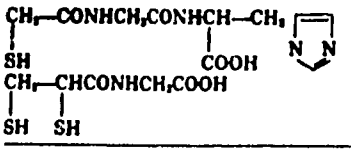		2.274	2.206	2.017	$S(N_P)_2N_{im}$
			2.163 $g_\perp$	2.015 $g_\parallel$	$(S_{cy})_2$

* *M. thermoautotrophicum* (strain ΔH) hydrogenase reduced under H_2 and exposed to an argon atmosphere also reveals a well defined rhombic "2.19" EPR type of signal (54).

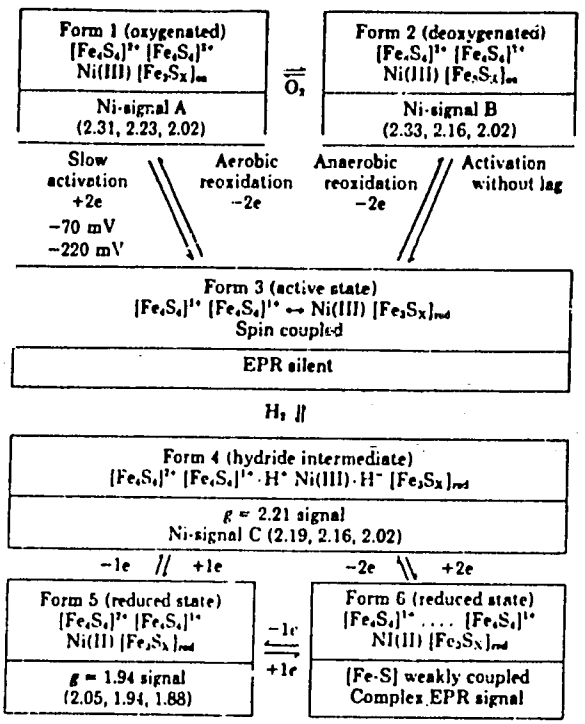

DIAGRAM 1

$[Fe_4S_4]^{1+}$ state ($S = 1/2$), and the reduced cluster is spin-coupled with the Ni(III) center resulting in an EPR silent state. This proposal implies that the previously determined redox potential, −220 mV, for the disappearance of Ni-signal A (4, 5) is actually the midpoint redox potential for one of the $[Fe_4S_4]$ clusters. Such a mechanism is supported by the optical studies which indicate that the activation process involves the reduction of iron-sulfur clusters (12). Preliminary Mössbauer data[3] also show that approximately one $[Fe_4S_4]$ cluster is reduced in the EPR silent state. A similar mechanism has been observed in the sulfide complex of *Escherichia coli* sulfite reductase (38); in the oxidized form the sulfide complex exhibits a low-spin ferric heme EPR signal. Upon reduction the EPR signal disappears; however, Mössbauer measurements (39) reveal that in the reduced sulfide-enzyme complex the siroheme remains in the ferric state and the electron is in the $[Fe_4S_4]$ cluster. The disappearance of the heme signal is a result of a spin coupling between the oxidized heme and the reduced $[Fe_4S_4]$ cluster. Also, in the case of the hydrogenase from *Chromatium vinosum* an EPR "silent state" was attributed to a magnetic interaction between Ni(III) and a $[Fe_4S_4]$ cluster (40). Evidence was presented that this state was the active form of the enzyme.

B. The Catalytic Cycle—The events which follow the EPR silent state (Form 3) are the appearance of both the Ni-signal C and the $g = 2.21$ type signal. This last signal is only observable at temperatures below 10 K, with high microwave power. In accordance with the heterolytic mechanism of hydrogen activation derived from studies of the exchange reaction (12), we propose that in the presence of the natural substrate a hydride intermediate state (Form 4) is obtained. In terms of our working hypothesis, the nickel center is assigned as the hydride-binding site and the $[Fe_4S_4]^{1+}$ cluster as the proton-binding site. The spin coupling between the Ni(III) and the $[Fe_4S_4]^{1+}$ cluster is broken in this hydride intermediate, originating Ni-signal C. Thus this signal is assumed to represent the hydride-bound Ni(III) center, and the $g = 2.21$ signal is attributed to the proton-bound $[Fe_4S_4]^{1+}$ cluster. (Alternatively, the $g = 2.19$ EPR signal could be due to a transient Ni(III) state in a different coordination, resulting from the breaking of the coupling, the $g = 2.21$ signal being due to the interacting Ni(III) and $[Fe_4S_4]^{+1}$ centers bound, respectively, to hydride and proton.)

The midpoint redox potential for the development of Ni-signal C is below −330 mV, and this value is consistent with a catalytically active species (7). It is worth noticing that the midpoint redox potential (−220 mV) assigned here to the $[Fe_4S_4]$ cluster interacting with the nickel center is pH dependent and that of the 3Fe cluster (−70 mV) is pH independent.

Forms 5 and 6 represent further reduced forms of the enzyme. The nickel center is reduced into a Ni(II) state and becomes EPR silent. The proton is released from the $[Fe_4S_4]^{1+}$ cluster, and a "$g = 1.94$" type EPR signal typical of $[Fe_4S_4]^{1+}$ clusters is observed. During the catalytic cycle, all three forms of the enzyme (Forms 3, 4, and 5) can be present simultaneously resulting in a complex EPR spectrum (*e.g.* see Fig. 7*A*). When excess amounts of dithionite are added to the sample, a super-reduced state (Form 6) is attained. In this super-reduced state all metal centers are reduced. Both the Ni(II) and the $[Fe_3S_x]_{red}$ centers are EPR silent while the two $[Fe_4S_4]^{1+}$ are EPR active. The fact that two sets of EPR signals are observed may indicate different conformations for these two $[Fe_4S_4]$ clusters. The complexity of the EPR spectrum may also indicate weak interaction between the two

$[Fe_4S_4]^{1+}$ paramagnetic centers. It is proposed that Form 6 represents an inactive form of the enzyme as H_2 is not evolved in the presence of excess dithionite.

The role of the iron-sulfur clusters has not yet been clarified. Both the 3Fe and the second 4Fe cluster could be limited to electron transfer, since both high and low redox potential electrons are needed to either evolve or oxidize H_2 for the reduction of sulfate. The physiological characteristics of the organism (*D. gigas*) are compatible with such a hypothesis.

This proposed mechanism offers a framework for interpreting the present available data; however, it must be viewed as tentative and as a guide for future experimental work.

Acknowledgments—We thank Dr. T. Lissolo for very interesting discussions. We are indebted to I. Carvalho for her skillful technical help and M. Martinez for careful typing of the manuscript.

REFERENCES

1. LeGall, J., Moura, J. J. G., Peck, H. D., Jr., and Xavier, A. V. (1982) in *Iron-Sulfur Proteins* (Spiro, T., ed) pp. 177–246, John Wiley & Sons, New York
2. Odom, J. M., and Peck, H. D., Jr. (1984) *Annu. Rev. Microbiol.* **38**, 551–592
3. LeGall, J., Ljungdahl, P. O., Moura, I., Peck, H. D., Jr., Xavier, A. V., Moura, J. J. G., Teixeira, M., Huynh, B. H., and DerVartanian, D. V. (1982) *Biochem. Biophys. Res. Commun.* **106**, 610–616
4. Teixeira, M., Moura, I., Xavier, A. V., DerVartanian, D. V., LeGall, J., Peck, H. D., Jr., Huynh, B. H., and Moura, J. J. G. (1983) *Eur. J. Biochem.* **130**, 481–484
5. Cammack, R., Patil, D., Aguirre, R., and Hatchikian, E. C. (1982) *FEBS Lett.* **142**, 289–292
6. Moura, J. J. G., Moura, I., Huyhn, B. H., Krüger, H. J., Teixeira, M., DuVarney, R. C., DerVartanian, D. V., Xavier, A. V., Peck, H. D., Jr., and LeGall, J. (1982) *Biochem. Biophys. Res. Commun.* **108**, 1388–1393
7. Lissolo, T., Pulvin, S., and Thomas, D. (1984) *J. Biol. Chem.* **259**, 11725–11729
8. Huyhn, B. H., Czechowski, M. H., Krüger, H. J., DerVartanian, D. V., Peck, H. D., Jr., and LeGall, J. (1984) *Proc. Natl. Acad. Sci. U. S. A.* **81**, 3728–3732
9. van der Westen, H. M., Mayhew, S. G., and Veeger, C. (1978) *FEBS Lett.* **86**, 122–126
10. Bossu, F., Murray, C., and Margerum, D. (1978) *Inorg. Chem.* **17**, 1630–1634
11. Moura, J. J. G., Teixeira, M., Moura, I., Xavier, A. V., and LeGall, J. (1984) *J. Mol. Catal.* **23**, 303–314
12. Berlier, Y. M., Fauque, G., Lespinat, P. A., and LeGall, J. (1982) *FEBS Lett.* **140**, 185–188
13. LeGall, J., Mazza, G., and Dragoni, N. (1965) *Biochim. Biophys. Acta* **99**, 385–387
14. LeGall, J., and Forget, N. (1978) *Methods Enzymol.* **53**, 613–634
15. Fisher, D. S., and Price, D. C. (1964) *Clin. Chem.* **10**, 21–25
16. Bradford, M. M. (1976) *Anal. Biochem.* **72**, 248–254
17. Hatchikian, E. C., Bruschi, M., and Le Gall, J. (1978) *Biochem. Biophys. Res. Commun.* **82**, 451–461
18. Davis, B. J. (1964) *Ann. N. Y. Acad. Sci.* **121**, 404–427
19. Bruschi, M., Hatchikian, E. C., LeGall, J., Moura, J. J. G., and Xavier, A. V. (1976) *Biochim. Biophys. Acta* **449**, 275–284
20. Cammack, R., Rao, K. K., Hall, D. O., Moura, J. J. G., Xavier, A. V., Bruschi, M., LeGall, J., Deville, A., and Gayda, J. P. (1977) *Biochim. Biophys. Acta* **490**, 311–321
21. Krüger, H. J. (1983) Master thesis, University of Georgia
22. Fauque, G., Teixeira, M., Moura, I., Lespinat, P. A., Xavier, A. V., DerVartanian, D. V., Peck, H. D., Jr., LeGall, J., and Moura, J. G. (1984) *Eur. J. Biochem.* **142**, 21–28
23. Jolly, P. W. (1982) in *Comprehensive Organometallic Chemistry* (Wilkinson, G., ed) Vol. 1, Chapter 37.4, pp. 37–100, Pergamon Press, Oxford
24. Xavier, A. V., Moura, J. J. G., LeGall, J., and DerVartanian, D. V. (1979) *Biochimie (Paris)* **61**, 689–695
25. Nicholls, D. (1973) in *Comprehensive Inorganic Chemistry* (Bailar, J., Emeléus, H., Nyholm, R., and Dickerson, A., eds) Vol. III, Chapter 42, Pergamon Press, Oxford
26. Cotton, F. A., and Wilkinson, G. (1972) *Advanced Inorganic Chemistry*, John Wiley & Sons, New York
27. Nag, K., and Chakravorty, A. (1980) *Coord. Chem. Rev.* **33**, 87–147
28. Tomlinson, A. A. G. (1981) *Coord. Chem. Rev.* **37**, 221–236
29. Sabatini, L., and Fabbrizzi, L. (1979) *Inorg. Chem.* **18**, 438–494
30. Lovecchio, F., Gore, E., and Busch, D. (1979) *J. Am. Chem. Soc.* **96**, 3109–3117
31. Dixon, N. E., Gazzola, C., Blakeley, R. L., and Zeiner, B. (1975) *J. Am. Chem. Soc.* **97**, 4131–4133
32. Ragsdale, S. W., Ljungdahl, L. G., and DerVartanian, D. V. (1983) *Biochem. Biophys. Res. Commun.* **115**, 658–665
33. Diekert G., Klee, B., and Thauer, R. K. (1980) *Arch. Microbiol.* **124**, 103–106
34. Xavier, A. V., Moura, J. J. G., and Moura, I. (1981) *Struct. Bonding* **43**, 187–213
35. Scott, R. A., Wallis, S., Czechowski, M., DerVartanian, D. V., LeGall, J., Peck, H. D., Jr., and Moura, I. (1984) *J. Am. Chem. Soc.* **106**, 6864–6865
36. Sugiura, Y., Kuwahara, J., and Suzuki, T. (1983) *Biochem. Biophys. Res. Commun.* **115**, 878–881
37. Huynh, B. H., Moura, J. J. G., Moura, I., Kent, T. A., LeGall, J., Xavier, A. V., and Münck, E. (1980) *J. Biol. Chem.* **255**, 3242–3244
38. Janick, P. A., and Siegel, L. M. (1983) *Biochemistry* **22**, 504–515
39. Christner, J. A., Münck, E., Kent, T. A., Janick, P. A., Salerno, J. C., and Siegel, L. K. (1984) *J. Am. Chem. Soc.* **106**, 6786–6794
40. Albracht, S. P. J., van der Zwaan, J. W., and Fontijn, R. D. (1984) *Biochim. Biophys. Acta* **766**, 245–258
41. Ghosh, D., Furey, W., Jr., O'Donnell, S., and Stout, C. D. (1981) *J. Biol. Chem.* **256**, 4185–4192
42. António, M. R., Averill, B. A., Moura, I., Moura, J. J. G., Orme-Johnson, W. H., Teo, B-K., and Xavier, A. V. (1982) *J. Biol. Chem.* **257**, 6646–6649
43. Beinert, H., Emptage, M. H., Dreyer, J. L., Scott, R. A., Hahn, J. E., Hodgson, K. O., and Thomson, A. J. (1983) *Proc. Natl. Acad. Sci. U. S. A.* **80**, 393–396
44. Moura, J. J. G., Moura, I., Kent, T. A., Lipscomb, J. D., Huynh, B. H., LeGall, J., Xavier, A. V., and Münck, E. (1982) *J. Biol. Chem.* **257**, 6259–6267
45. Krüger, H-J., Huyhn, B. H., Ljungdahl, P. O., Xavier, A. V., DerVartanian, D. V., Moura, I., Peck, H. D., Jr., Teixeira, M., Moura, J. J. G., and LeGall, J. (1982) *J. Biol. Chem.* **257**, 14620–14622
46. Deleted in proof
47. Fabbrizzi, L. (1979) *Inorg. Chim. Acta* **36**, L391–L393
48. Sakurai, T., Hongo, T., Nakahara, A., and Nakao, J. (1980) *Inorg. Chim. Acta* **46**, 205–210
49. Bowmaker, G., Boyd, P. D. H., and Campbell, G. K. (1983) *Inorg. Chem.* **22**, 1208–1213
50. Sugiura, Y., and Mino, Y. (1979) *Inorg. Chem.* **18**, 1336–1339
51. Jubram, N., Ginzburg, G., Cohen, H., and Meyerstein, D. (1982) *J. Chem. Soc. Chem. Commun.* 517–519
52. Mines, T., and Geiger, W. (1973) *Inorg. Chem.* **12**, 1189–1191
53. Bowmaker, G., Boyd, P. D. H., Campbell, G. K., and Martin, R. L. (1982) *Inorg. Chem.* **21**, 1152–1159
54. Kojima, N., Fox, J., Hausinger, R., Daniels, L., Orme-Johnson, W. H., and Walsh, C. (1983) *Proc. Natl. Acad. Sci. U. S. A.* **80**, 378–382

[5] M. PIERROT, R. HASER, M. FREY, F. PAYAN, J.P. ASTIER, *J. Biol. Chem.*, **257**, 14341-14348 (1982).
[6] A.V. XAVIER, J.J.G. MOURA, J. LEGALL, D.V. DERVARTANIAN, *Biochimie*, **61**, 689-695 (1979).
[7] D.V. DERVARTANIAN, A.V. XAVIER, J. LEGALL, *Biochimie*, **60**, 321-326 (1978).
[8] R. CAMMACK, G. FAUQUE, J.J.G. MOURA, J. LEGALL, *Biochim. Biophys. Acta*, **784**, 68-74 (1984).
[9] G. PALMER, «Annual Summer Meeting of the Biochemical Society on Electron Spin/Paramagnetic Resonance in Biochemistry», Leeds, July 1984.
[10] A. WALKER, unpublished results cited in ref. [9].
[11] K. NIKI, personal communication.

PS1.46 – TH

A.R. LINO
J.J.G. MOURA
A.V. XAVIER
I. MOURA
Centro de Química Estrutural, UNL
Complexo I, IST
Av. Rovisco Pais, 1000 Lisboa
Portugal
G. FAUQUE
J. LEGALL
Centre d'Etudes Nucleaires de Cadarache
Departement of Biologie, SRA, Bl no. 1,
13115 Saint-Paul-lez-Durance
France

CHARACTERIZATION OF TWO LOW-SPIN BACTERIAL SIROHEME PROTEINS

Sulfite reductase catalyses the rather unusual six-electron reduction of $SO_3^{=}$ to $S^{=}$.
Two low molecular weight proteins with sulfite reductase activity have been isolated from *M. barkeri* (DSM 800) [1,2], 23 KD and *Drm. acetoxidans* (strain 5071) [2], 23.5 KD. The enzymes contain one siroheme (iron-tetrahydroporphyrin prosthetic group) and one $[Fe_4S_4]$ cluster per minimal molecular weight.
The visible spectrum characteristics of both enzymes are very similar to those of siroheme containing enzymes; however, no band at 715 nm, characteristic of high-spin Fe^{3+} complexes of isobacteriochlorins is observed [3]. Low temperature EPR studies show that as isolated the proteins siroheme is in a low-spin ferric state ($S = 1/2$) with g-values at 2.40, 2.30 and 1.88 for the *M. barkeri* enzyme and g-values at 2.44, 2.33 and 1.81 for the *Drm. acetoxidans* enzyme.
EPR studies on model complexes have shown that ferric isobacteriochlorins with a single axial ligand are always high-spin while ferric isobacteriochlorins with two axial ligands are low-spin. The fact that in these sulfite reductases the siroheme is low-spin ferric suggests that it is six-coordinated. The siroheme of all the other sulfite reductases characterized so far has been shown to be in a high-spin ferric state with EPR features at 6.63, 5.24 and 1.98[4].
The sulfite reductase from *M. barkeri* and *Drm. acetoxidans* together with the assimilatory sulfite reductase from *D. vulgaris* (strain Hildenborough) [5] which also shows a siroheme in the low-spin state belong to a new class of sulfite reductases. They are small molecular weight proteins with one siroheme and a $[Fe_4S_4]$ center per polypeptide chain. In the native state their siroheme is low-spin ferric. The physiological significance of this observation is not known and deserves further investigation.

ACKNOWLEDGEMENTS

This work was supported by Junta Nacional de Investigação Científica e Tecnológica, Instituto Nacional de Investigação Científica (Portugal) and U.S.A.I.D. Grant No. 936-5542-G-SS-4003-00.

REFERENCES

[1] J.J.G. MOURA, I. MOURA, H. SANTOS, A.V. XAVIER, M. SCANDELLARI, J. LEGALL, *Biochem. Biophys. Res. Commun.*, 108, 1002-1009 (1982).
[2] I. MOURA, A.R. LINO, J.J.G. MOURA, G. FAUQUE, A.V. XAVIER, J. LEGALL, *J. Biol. Chem.* (1985), in press.
[3] A.M. STOLZENBACH, S.H. STRAUSS, R.H. HOLM, *J. Am. Chem. Soc.*, **103**, 4763-4778 (1981).
[4] L.M. SIEGEL, D.C. RUEGER, M.J. BARBER, R.J. KRUEGER, N.R. ORME-JOHNSON, W.H. ORME-JOHNSON, *J. Biol. Chem.*, **257**, 6343-6350 (1982).
[5] B.H. HUYNH, L. KANG, D.V. DERVARTANIAN, H.D. PECK JR., J. LEGALL, *J. Biol. Chem.*, **259**, 15373-15376 (1984).

190

includes a protein carboxylate (Fig. 2), Glu-21, and it is possible that this plays an important role either by binding to the central metal ion of the reagent or by hydrogen bonding to its ligated H_2O. Whatever the exact cause of the selectivity these studies demonstrate that proteins do have the capacity for selecting between similar complexes. They also emphasize the need for care in interpreting reactivity parameters for redox reactions between proteins and small molecules especially in cases where there appears to be more than one possible reaction pathway, as with cytochrome *c*. Using chemically modified lysine derivatives of cytochrome *c* we hope to unravel the observed binding selectivities.

ACKNOWLEDGEMENTS

This work was supported by the Science and Engineering Research Council (SERC) and the Medical Research Council (MRC). GW thanks the MRC for a Training Fellowship and GRM thanks the SERC for an Advanced Fellowship.

REFERENCES

[1] C.G.S. Eley, G.R. Moore, G. Williams, R.J.P. Williams, *Eur. J. Biochem.*, 124, 295-303 (1982).

[2] G. Williams, C.G.S. Eley, G.R. Moore, M.N. Robinson, R.J.P. Williams, *FEBS Lett.*, 150, 293-299 (1982).

[3] G.R. Moore, C.G.S. Eley, G. Williams, *Adv. Inorg. Bioinorg. Mech.*, 3, 1-96 (1984).

[4] T. Takano, R.E. Dickerson, *J. Mol. Biol.*, 153, 79-115 (1981).

B-3

PS1.44 — TH

I. MOURA
A.V. XAVIER
J.J.G. MOURA
Centro de Química Estrutural, UNL
Complexo I
IST, Av. Rovisco Pais, 1000 Lisboa
Portugal
M.Y. LIU
G. PAI
H.D. PECK JR.
J. LEGALL
Department of Biochemistry
University of Georgia
Athens, Georgia 30602
U.S.A.
W.J. PAYNE
Department of Microbiology
University of Georgia
Athens, Georgia 30602
U.S.A.

NMR STUDIES OF A MONOHEME CYTOCHROME FROM *WOLINELLA SUCCINOGENES*, A NITRATE RESPIRING ORGANISM

An ascorbate reducible monoheme *c*-type cytochrome (8.2 KDa, E'_o – +100 mV) was purified from the nitrate "respiring" organism *Wolinella succinogenes* (VPI 10659). The optical spectrum in the ferro and ferric forms are typical of a *c*-type heme coordination. The oxidized state shows the 695 nm band taken as indicative of methionyl axial coordination, but additional optical bands are also observed at 619 nm and 498 nm (shoulder) reminiscent of the absorption bands of cytochrome *c'* [1]. These peculiarities of the optical spectrum prompted us to study this situation of spin-equilibrium by nuclear magnetic resonance (NMR) spectroscopy.

The NMR spectrum of the reduced state is shown in Fig. 1. The heme mesoproton resonances (9.88, 9.59, 9.30 and 9.25 ppm) and the resonances originated from the bound axial methionine ($S\text{-}CH_3$ at −3.72 ppm and methylene protons at −3.85, −1.66 and −0.70 ppm) are readily discernible.

191

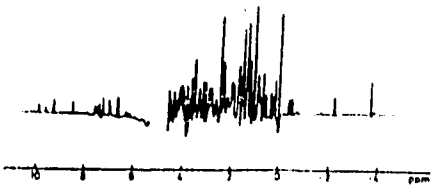

Fig. 1
Deconvoluted ^1H NMR spectrum of W. succinogenes ferricytochrome at 303 K, pH 7.2

The pH dependence of the NMR spectrum of ferricytochrome is shown in Fig. 2. As expected for a paramagnetic protein, several hyperfine shifted resonances are observable downfield of 10 ppm. The 3-proton intensity resonances designated M_i (i = 1,4) are assigned to heme methyl groups. The-

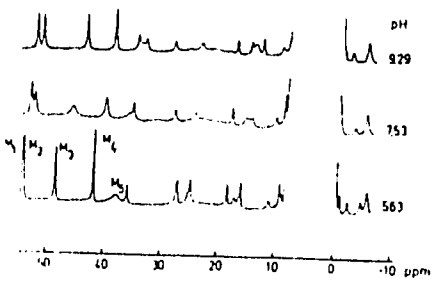

Fig. 2
^1H NMR spectra of W. succinogenes ferricytochrome at 303 K for three different pH values

se resonances have downfield shifts greater than 38 ppm which is unusual for a low-spin *c*-type situation. The temperature dependence of the ferricytochrome resonances shows that M_2 and M_4 are almost temperature invariant, M_1 shows a temperature dependence according to Curie's law and M_3 is anti-Curie dependent. Resonance 5 is extremely temperature dependent ($\delta_{50°C} - \delta_{0°C} = 7.15$ ppm at pH = 7.5) and also anti-Curie dependent.

The pH profile gives a pK_a value at ~7.3 and the linewidth variation is compatible with an intermediate rate for the exchange process between two forms.

Magnetic susceptibility measurements by a NMR method [2] were performed as a function of the pH. The results are indicated in Table I.

Table I
Magnetic susceptibility data for ferricytochrome at 308 K

pH	χ_M^P ($\times 10^3$)	μ_{eff}
4.90	7.59	4.31
7.50	4.64	3.38
9.98	2.52	2.48

The visible spectra, NMR and magnetic susceptibility measurements are indicative of a spin equilibrium which shifts towards the high-spin form when the pH is lowered. This is compatible with the increase in chemical shifts of the heme methyl resonances at low pH.

The assembly of these preliminary studies, indicates that there is a spin equilibrium in the ferric form. The high-spin/low-spin transition is relatively fast in the nuclear magnetic resonance time scale, since only four heme methyl resonances are observed in the lowfield region of the spectrum. The methyl resonance from the bound methionine axial ligand is not observed in the upfield spectral region. Thus, the high spin state could be produced by loss of the sixth axial ligand (methionyl sulfur) to the ferric ion.

The chemical exchange between the situation of bound and unbound axial ligand could induce a large chemical shift to the methionine methyl resonance [3]. Resonance M_3 is a plausible candidate for this S-CH_3 methionine, due to its chemical shift and strong temperature dependence.

ACKNOWLEDGEMENTS

This work was supported by grants from the Instituto Nacional de Investigação Científica, Junta Nacional de Investigação Científica e Tecnológica, Portugal and AID grant n. 936-5542-G-SS-4003-00.

REFERENCES

[1] R.G. Bartsch, M.D. Kamen, *J. Biol. Chem.*, 230, 41-63 (1958).

[2] W.D. Phillips, M. Poe, *Methods in Enzymol.*, 24, 304-317 (1972).

[3] R. Timkovich, M.S. Cork, *Biochemistry*, 23, 851-860 (1984).

B-4 49

PSI.45 — TH

I. MOURA
A.V. XAVIER
J.J.G. MOURA
Centro de Química Estrutural
Complexo I, U.N.L.
Av. Rovisco Pais, 1000 Lisboa
Portugal
G. FAUQUE
J. LeGALL
A.R.B.S., E.C.E., CEN Cadarache
13115 Saint Paul lez Durance
France
G.R. MOORE
Inorganic Chemistry Laboratory
University of Oxford
South Parks Road, Oxford OX1 3QR
U.K.
B.H. HUYNH
Department of Physics
Emory University
Atlanta, Georgia
U.S.A.

STRUCTURAL HOMOLOGY OF TETRAHEME CYTOCHROME c_3

Low potential tetraheme cytochromes c_3 (molecular mass 13 KDa) are found in sulfate reducing bacteria belonging to the genus *Desulfovibrio*. They seem to play an important role in electron transfer processes, but at the present moment their physiological role is still controversial. Cytochrome c_3 can act as an electron carrier for hydrogenase (although recently direct electron transfer was shown to occur between some of the electron carrier proteins, *e.g.*, *D. gigas* FdII and flavodoxin, and hydrogenase) and in some species involved in the reduction of elemental sulfur. Each heme, in this class of cytochromes, is bound to the protein by two thioether linkages involving cysteine residues, and the fifth and sixth ligands of each heme iron are histidinyl residues. Table I indicates all the tetraheme cytochromes c_3 that have been isolated until now as well as some of their physicochemical properties. The amino acid compositions are quite different from cytochrome to cytochrome originating very different isoelectric points. Tetraheme cytochromes are conserved in all the *Desulfovibrio* species analysed so far. It is interesting to note that even when the terminal acceptor is modified (*i.e.* nitrate by sulfate in *D. desulfuricans* (strain 27774) this multiheme cytochrome is still conserved. Cytochrome $c_{551.5}$ (c_7), a three heme containing cytochrome isolated from the sulfur reducing bacterium *Desulfuromonas acetoxidans*, is a close relative to cytochrome c_3. The four hemes in cytochrome c_3, are localized in nonequivalent protein environments (see below the comparison of the NMR and EPR spectral data) and each heme exhibits different redox midpoint potentials. The midpoint redox potentials of all the hemes are negative but the span in redox potential between the lowest and the highest one varies in this class of homologous proteins. As an example, in *D. vulgaris* cytochrome c_3 this difference is 80 mV, in *D. gigas* cytochrome c_3 100

Table I *

Desulfovibrio species	State of physico-chemical characterization	Isoelectric point	Number of residues	Molecular mass
D. gigas	P,A,S,NMR, EPR,MB	5.2	111	14400
D. vulgaris (Hildenborough)	P,A,S,NMR, EPR,MB	10.2	107	14100
D. vulgaris (Miyazaki)	P,A,S,X-ray, NMR,MB	10.6	107	14000
D. desulfuricans (Norway 4)	P,A,S,X-ray, NMR,EPR	7	118	15100
D. baculatus (strain 9974)	P,A,NMR, EPR	7	(118)	15100
D. desulfuricans (strain 27774)	P,A,NMR,EPR	n.d.	(103)	13500
D. desulfuricans (Berre eau)	P,NMR,EPR	8.6	n.d.	14000
D. desulfuricans (El Agheila Z)	P,A,S,NMR,EPR	10.0	102	13400
D. salexigens (British Guiana)	P,A,S,NMR	10.8	106	14000
D. desulfuricans (Cholinicus)	P,A	8.0	(108)	14300
D. africanus (Benghazi)	P,A	8.5	(109)	14900

P — Purified
A — Amino acid analysis
S — Sequence
NMR — Nuclear Magnetic Resonance
EPR — Electron Paramagnetic Resonance
MB — Mössbauer Spectroscopy
* Table composed from references [1-5] and references therein.

193

mV, and in *D. desulfuricans* (Norway strain) cytochrome c_3 this value is 200 mV (using the microscopic redox potentials determinated by EPR) [6-8].

A comparison of the NMR and EPR characteristics of this class of homologous proteins is presented in order to better understand the structure — function relationships.

Fig. 1 shows the low field region of the NMR spectra of several cytochromes c_3 isolated from different *Desulfovibriones*. An obvious common feature is the low downfield chemical shifts experienced by the heme methyl groups in this low spin paramagnetic state of the protein. The differences observed in the distribution of resonances are also striking. There is a wide variation in the distribution of heme methyl resonances between the different cytochromes c_3. These differences fall largely into three regions, the region downfield of 25 ppm, the region between 15 ppm and 25 ppm and the region upfield of 15 ppm. The presence of resonances downfield of 25 ppm is common to all cytochromes c_3. The fact that there are not many resonances in any of the spectra of Fig. 1 downfield of 25 ppm suggests that these proteins have similar structures. However, there is a striking difference: *D. gigas* cytochrome c_3 has three resonances in this region while the remaining five proteins have only two resonances. Similar differences can be seen in the regions between 15 ppm and 25 ppm. The heme methyl resonances in these regions of the spectra of some of the proteins, such as that from *D. desulfuricans* (Norway strain) are bunched together and cover a small range of chemical shift values whilst for other proteins, such as that from *D. salexigens*, they are better resolved and cover a wider range of chemical shift values. All of these differences may result from two causes: differences in the relative spatial orientations of the four heme groups, and differences in the electronic properties of the four heme groups.

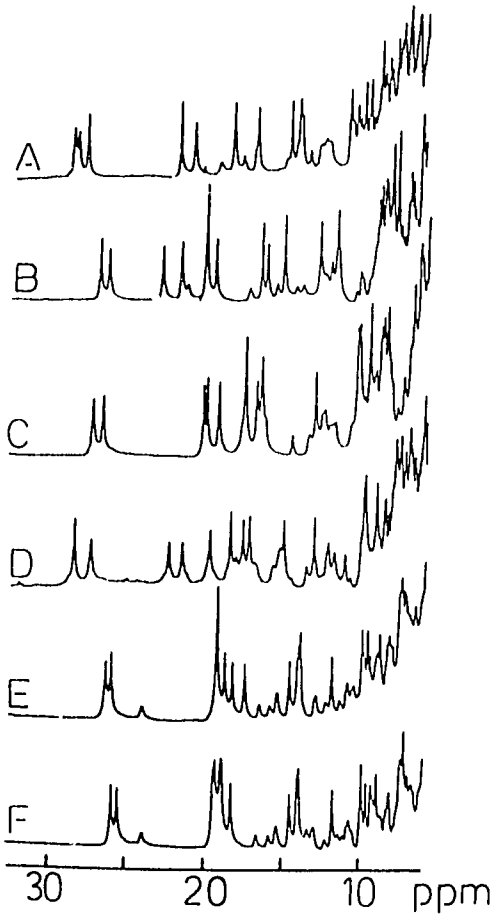

Fig. 1
Low-field NMR spectra of several ferricytochromes c_3 at 313 K. A — D. gigas; B — D. salexigens; C — D. vulgaris (strain Hildenborough); D — D. desulfuricans (El Agheila Z); E — D. desulfuricans (Norway 4); F — D. baculatus (strain 9974)

Despite of the emphasis upon the differences between the spectra of cytochromes c_3 it is relevant to notice that there is a high degree of similarity between them. For instance, in all cases there are 10 to 12 heme methyl resonances with chemical shift values >12 ppm.

Fig. 2 compares the EPR spectra of several cytochromes c_3 from different *Desulfovibrio* species. The cytochromes c_3 exhibit quite different EPR characteristics. Cytochrome c_3 from *D. desulfuricans* (Norway strain), *D. baculatus* (strain 9974) and *D. desulfuricans* (strain Berre eau) show quite similar characteristics. They all have broad features at $g \approx 3.3$, a resonance around $g = 3.0$ and a shoulder on this peak to lower g-values. For other cytochromes, like *D. gigas* and *D. desulfuricans* (El Agheila Z) cytochromes c_3, the broad peak around $g \approx 3.30$ is missing and only one prominent EPR signal is observed with a g_{max} around

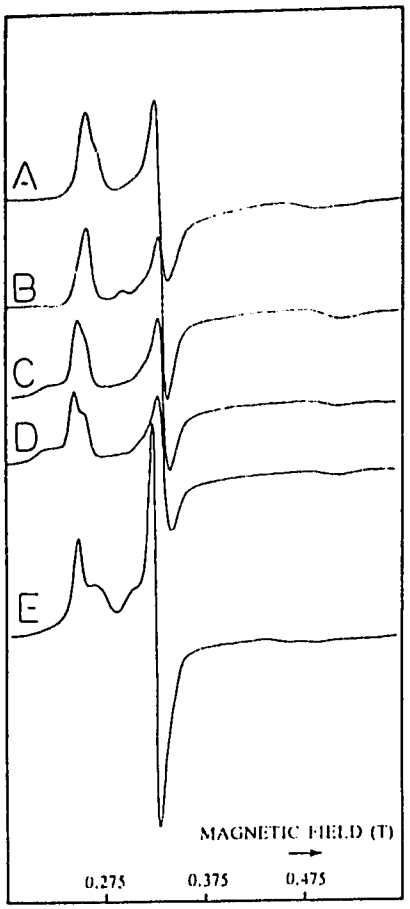

Fig. 2

EPR spectra of several cytochromes c_3 at 10 K, microwave power 0.63 mW and modulation amplitude 0.5 mT. A — D. gigas; B — D. desulfuricans (El Agheila); C — D. desulfuricans (Norway 4); D — D. baculatus (strain 9974); E — D. vulgaris (strain Hildenborough)

$g \simeq 3.0$-2.9, showing in some cases a shoulder. *D. vulgaris* cytochrome c_3 is still different since three g_{max} values are quite discernible at g-values 3.12, 2.97 and 2.87. The g_{med} is sharper when compared to the g_{med} signals from other cytochromes c_3. It was recently shown that in heme model compounds where the two imidazoles are perpendicular to each other, the EPR signals are extremely anisotropic with g_{max} values of the order of 3.4 [9,10]. The X-ray structure of cytochromes c_3 from *D. vulgaris* (strain Miyazaki) and *D. desulfuricans* (strain Norway) show that three of the heme groups have the two axial histidines in the same plane. Only one heme in both these cytochromes has the two axial histidines perpendicular to each other. This heme is also the one most exposed to the solvent [10].

In this context, re-examination of the EPR data indicates that the heme originating g-features above 3.0 in *D. vulgaris* (Hildenborough) and *D. desulfuricans* (Norway strain) should be assigned to the heme having two axial histidinyl residues perpendicular to each other. Also this heme has the lowest redox potential (−325 mV) in *D. desulfuricans* (strain Norway 4). However, in *D. gigas* and *D. desulfuricans* (El Agheila Z), the EPR characteristics are different and the signal with high g_{max} is not present. It is possible that in these proteins all the histidines are coplanar. The X-ray structures have not yet been determined.

Preliminar Mössbauer studies indicate that in the native state there is a weak magnetic interaction between the different hemes at 4.2 K in the absence of an external magnetic field. Also, measurable spectral differences that correlate with the EPR data are observed within this group of multiheme proteins. Comparison of Mössbauer spectra of *D. gigas* cytochrome c_3 (without high g_{max} features) and *D. vulgaris* (Hildenborough) cytochrome c_3 (having a g_{max} feature greater than 3.0) show that the magnetic component with the largest magnetic hyperfine constant is present in *D. vulgaris* cytochrome c_3 and absent in the *D. gigas* protein.

The screening of the EPR and NMR characteristics of this class of cytochromes would probably permit a division of this type of proteins into sub-groups with more similar properties, using structural criteria.

ACKNOWLEDGEMENTS

This work was supported by INIC, JNICT, NATO and USAID.

REFERENCES

[1] H. Santos, J.J.G. Moura, I. Moura, J. LeGall, A.V. Xavier, *Eur. J. Biochem.*, **141**, 283-296 (1984).

[2] J.J.G. Moura, H. Santos, I. Moura, J. LeGall, G.R. Moore, R.J.P. Williams, A.V. Xavier, *Eur. J. Biochem.*, **127**, 151-155 (1982).

[3] W. Shinkai, T. Hase, T. Yagi, H. Matsubara, *J. Biochem. (Tokyo)*, **87**, 1747-1756 (1980).

[4] Y. Higuchi, M. Kusunoki, Y. Matsuura, N. Yasuoka, M. Kakudo, *J. Mol. Biol.*, **172**, 109-139 (1984).

[5] M. Pierroy, R. Haser, M. Frey, F. Payan, J.P. Astier, *J. Biol. Chem.*, **257**, 14341-14348 (1982).
[6] A.V. Xavier, J.J.G. Moura, J. LeGall, D.V. DerVartanian, *Biochimie*, **61**, 689-695 (1979).
[7] D.V. DerVartanian, A.V. Xavier, J. LeGall, *Biochimie*, **60**, 321-326 (1978).
[8] R. Cammack, G. Fauque, J.J.G. Moura, J. LeGall, *Biochim. Biophys. Acta*, **784**, 68-74 (1984).
[9] G. Palmer, «Annual Summer Meeting of the Biochemical Society on Electron Spin/Paramagnetic Resonance in Biochemistry», Leeds, July 1984.
[10] A. Walker, unpublished results cited in ref. [9].
[11] K. Niki, personal communication.

PSI.46 -- TH

A.R. LINO
J.J.G. MOURA
A.V. XAVIER
I. MOURA
Centro de Química Estrutural, UNL
Complexo I, IST
Av. Rovisco Pais, 1000 Lisboa
Portugal
G. FAUQUE
J. LEGALL
Centre d'Etudes Nucléaires de Cadarache
Département of Biologie, SRA, Bl. no. 1,
13115 Saint-Paul-lez-Durance
France

CHARACTERIZATION OF TWO LOW-SPIN BACTERIAL SIROHEME PROTEINS

Sulfite reductase catalyses the rather unusual six-electron reduction of $SO_3^{=}$ to $S^{=}$.

Two low molecular weight proteins with sulfite reductase activity have been isolated from *M. barkeri* (DSM 800) [1,2], 23 KD and *Drm. acetoxidans* (strain 5071) [2], 23.5 KD. The enzymes contain one siroheme (iron-tetrahydroporphyrin prosthetic group) and one $[Fe_4S_4]$ cluster per minimal molecular weight.

The visible spectrum characteristics of both enzymes are very similar to those of siroheme containing enzymes; however, no band at 715 nm, characteristic of high-spin Fe^{3+} complexes of isobacteriochlorins is observed [3]. Low temperature EPR studies show that as isolated the proteins siroheme is in a low-spin ferric state (S = 1/2) with g-values at 2.40, 2.30 and 1.88 for the *M. barkeri* enzyme and g-values at 2.44, 2.33 and 1.81 for the *Drm. acetoxidans* enzyme.

EPR studies on model complexes have shown that ferric isobacteriochlorins with a single axial ligand are always high-spin while ferric isobacteriochlorins with two axial ligands are low-spin. The fact that in these sulfite reductases the siroheme is low-spin ferric suggests that it is six-coordinated. The siroheme of all the other sulfite reductases characterized so far has been shown to be in a high-spin ferric state with EPR features at 6.63, 5.24 and 1.98 [4].

The sulfite reductase from *M. barkeri* and *Drm. acetoxidans* together with the assimilatory sulfite reductase from *D. vulgaris* (strain Hildenborough) [5] which also shows a siroheme in the low-spin state belong to a new class of sulfite reductases. They are small molecular weight proteins with one siroheme and a $[Fe_4S_4]$ center per polypeptide chain. In the native state their siroheme is low-spin ferric. The physiological significance of this observation is not known and deserves further investigation.

ACKNOWLEDGEMENTS

This work was supported by Junta Nacional de Investigação Científica e Tecnológica, Instituto Nacional de Investigação Científica (Portugal) and U.S.A.I.D. Grant No. 936-5542-G-SS-4003-00.

REFERENCES

[1] J.J.G. Moura, I. Moura, H. Santos, A.V. Xavier, M. Scandellari, J. LeGall, *Biochem. Biophys. Res. Commun.*, **108**, 1002-1009 (1982).
[2] I. Moura, A.R. Lino, J.J.G. Moura, G. Fauque, A.V. Xavier, J. LeGall, *J. Biol. Chem.* (1985), in press.
[3] A.M. Stolzenbach, S.H. Strauss, R.H. Holm, *J. Am. Chem. Soc.*, **103**, 4763-4778 (1981).
[4] L.M. Siegel, D.C. Rueger, M.J. Barber, R.J. Krueger, N.R. Orme-Johnson, W.H. Orme-Johnson, *J. Biol. Chem.*, **257**, 6343-6350 (1982).
[5] B.H. Huynh, L. Kang, D.V. DerVartanian, H.D. Peck Jr., J. LeGall, *J. Biol. Chem.*, **259**, 15373-15376 (1984).

B-5

51

There is evidence that during turnover dioxygen is reduced to peroxy intermediates [7] via a 2--electron transfer process. How these intermediates are subsequently reduced to water is not clear. We have therefore studied the reaction of mixed--valence carboxy-cytochrome *c* oxidase, which contains 2 electrons, with hydrogen peroxide. This reaction can be studied by photolysis of the CO compound after mixing with H_2O_2 under anaerobic conditions. The results show that H_2O_2 reacts rapidly ($k = 2.5 \cdot 10^4\ M^{-1} \cdot s^{-1}$) with the partially reduced enzyme to form the fully oxidized enzyme. On the time scale of our experiments no other intermediates were observed. This demonstrates that under suitable conditions partially reduced cytochrome *c* oxidase can use hydrogen peroxide as a 2-electron acceptor instead of the 4-electron accepting dioxygen molecule. These results are in line of those of ORII [8], who showed that cytochrome *c* oxidase may act as a cytochrome *c* peroxidase.

REFERENCES

[1] M.K.F. WICKSTRÖM, *Nature*, 266, 271-273 (1979).
[2] L. POWERS, B. CHANCE, Y. CHING, P. ANGIOLILLO, *Biophys. J.*, 34, 465-498 (1981).
[3] R. BOELENS, H. RADEMAKER, R. WEVER, B.F. VAN GELDER, *Biochim. Biophys. Acta*, 756, 196-209 (1984).
[4] R. BOELENS, R. WEVER, B.F. VAN GELDER, H. RADEMAKER, *Biochim. Biophys. Acta*, 724, 176-183 (1983).
[5] R. BOELENS, R. WEVER, *FEBS Lett.*, 116, 223-226 (1980).
[6] R. BOELENS, R. WEVER, *Biochim. Biophys. Acta*, 517, 296-310 (1979).
[7] B. CHANCE, C. SARONIO, J.S. LEIGH JR., *J. Biol. Chem.*, 250, 9226-9237 (1975).
[8] Y. ORII, *J. Biol. Chem.*, 257, 9246-9248 (1982)..

RT4.5 — TH

A.V. XAVIER
H. SANTOS
J.J.G. MOURA
I. MOURA
Centro de Química Estrutural
U.N.L., Complexo I, I.S.T.
1000 Lisboa
Portugal
J. LEGALL
Department of Biochemistry
University of Georgia
Athens, GA 30602
U.S.A.

MECHANISM AND REGULATION FOR A COUPLED TWO-ELECTRON TRANSFER IN A TETRAHAEM CYTOCHROME

The need for a two-electron transfer process is a recurrent and elusive problem in biochemistry [1]. Analysis of the relative microscopic midpoint redox potentials for the four haems of *Desulfovibrio gigas* cytochrome c_3 [2] provides evidences that this molecule has the potential properties to optimize this function.

The oxidation of cytochrome c_3 can be considered to involve five steps which are obtained by successive loss of one electron [2]: Step 0 (all haems reduced) through Step IV (all haems oxidized). A full description of the redox equilibria involves 16 oxidation states and 32 microscopic midpoint redox potentials e_i^{jkl} (the presence of the upperscripts j, k, l, indicates those haems which are oxidized). The relative values, $\Delta e_{ij} = e_i - e_j$, as well as the haem-haem interacting potentials $I_{ij} = e_i - e_i^j = e_j - e_j^i$, were obtained for *D. gigas* cytochrome c_3 by a thorough NMR study (see Table 3 of reference [2]). The microscopic redox potentials are such that for a dynamic equilibrium (*e.g.*, in an electron transfer chain) a situation optimized for a two-electron transfer can be generated. In order to explain the mechanism by which this phenomenon is achieved, let us follow

the successive alterations of the microscopic midpoint redox potentials of each haem throughout the oxidation at pH = 7.2, starting with the fully reduced protein ($\Delta e_{12} = -35$ mV, $\Delta e_{13} = -36$ mV, and $\Delta e_{14} = -61$ mV). Oxidation of the haem with lowest midpoint redox potentials (haem 1, e_1) modifies the microscopic midpoint redox potentials of the other haems (e_i^1, i = 2, 3 or 4). It is important to notice that although I_{12} is positive (+19 mV), I_{13} is negative (−29 mV), altering the values of e_2 and e_3 in such way that $e_2^1 < e_2$, $e_3^1 > e_3$ and $e_3^1 \gg e_2^1$. Haem 2 is now easier to oxidize and haem 3 becomes more difficult to oxidize. Subsequent oxidation of haem 2 has a similar but even more drastic effect on haem 3 ($I_{23} = +42$ mV) and haem 4 ($I_{24} = -24$ mV). I_{23} is so large and positive that e_3^2 becomes equal to e_2^1, within experimental error. Thus, oxidation of haem 2 impels the concomitant oxidation of haem 3. Haem 4 is now more difficult to oxidize ($I_{34} = -18$ mV). Using the values given in the table cited above [2] it is easily seen that a similar situation is also observed both for the reduction at pH = 7.2 as well as for the oxidation/reduction at pH = 9.6 of *D. gigas* cytochrome c_3.

The above analysis depicts a situation of strong cooperativity (coupling) between the redox centers, of *Desulfovibrio gigas* cytochrome c_3, where oxidation (reduction) of haem 1 (haem 4) triggers a process by which two electrons are selected to be released (captured) in an essentially simultaneous way.

It is worth stressing that by purely electrostatic considerations, the values of the interacting potentials, I_{ij}, should be always negative and could never be of use for a similar mechanism. Redox-linked conformational modifications must be involved. These conformational changes result in the presence of regulatory redox centers as well as redox centers actually implicated in the electron transfer chain.

This regulatory role may be quite general. In particular, the present knowledge on *D. gigas* hydrogenase [3] for which cytochrome c_3 is a coupling protein, suggests the use of redox centers with a similar role.

Furthermore, the postulation of these centers makes it possible to reconcile the need for fast electron transfer with that of avoiding "short-circuits" [4]. The ready state for the redox centers involved in the electron transfer chain, *e.g.*, an entatic state [5], can only be generated after a signal has been emitted by the dispatcher redox center.

ACKNOWLEDGEMENTS

This work is supported by INIC, JNICT and USAID.

REFERENCES

[1] R.J.P. Williams, *Biochim. Biophys. Acta*, 505, 1-44 (1978).

[2] H. Santos, J.J.G. Moura, I. Moura, J. LeGall, A.V. Xavier, *Eur. J. Biochem.*, 141, 283-296 (1984).

[3] M. Teixeira, I. Moura, A.V. Xavier, B.H. Huynh, D.V. DerVartanian, H.D. Peck Jr., J. LeGall, J.J.G. Moura, *J. Biol. Chem.* (1985) in press.

[4] J. Kraut, *Biochem. Soc. Trans.*, 9, 197-202 (1981).

[5] B.L. Vallee, R.J.P. Williams, *Proc. Natl. Acad. Sci. USA*, 59, 498-505 (1968).

PS1.20 — MO

B. BARATA
I. MOURA
A.V. XAVIER
J.J.G. MOURA
Centro de Química Estrutural
FCL, UNL, Complexo I, IST
Av. Rovisco Pais, 1000 Lisboa
Portugal
J. LIANG
B.H. HUYNH
Department of Physics
Emory University
Atlanta, Georgia 30322
U.S.A.
J. LEGALL
Department of Biochemistry
University of Georgia
Athens, Georgia 30602
U.S.A.

EPR AND MÖSSBAUER STUDIES ON *DESULFOVIBRIO GIGAS* Mo(Fe-S) PROTEIN

The Mo(Fe-S) protein from *Desulfovibrio gigas*, a sulfate reducing organism, was shown to contain one Mo and approx. 12 Fe per molecule and a molecular weight of 120 KDa. No evidence was found for the presence of subunits. Its physiological role has not yet been determined. Optical, EPR and CD data strongly suggest the presence of [2Fe-2S] clusters. At ~70 K the EPR spectrum of the dithionite reduced sample exhibits a Mo signal centered around $g=1.97$ and signals at $g=2.02$, 1.94 and 1.93, corresponding to one type of [2Fe-2S] centers, named (Fe-S I). At lower temperature ($T<40$ K) an additional signal appears at $g=2.06$ and 1.90, indicating the presence of a second [2Fe-2S] center (Fe-S II). Redox titration studies revealed yet another Fe-S center with type I EPR signal. The two type I centers are termed (Fe-S I A) and (Fe-S I B).

When observed at temperatures lower than 40 K, the type I Fe-S EPR features at $g=2.02$ split into two peaks separated by approx. 15 G. Such splitting can be explained either by coupling of the paramagnetic site to a nearby $I=1/2$ nucleus, such as a proton, or a slight difference in the resonances of Fe-S I A and I B centers. The EPR signals of the Fe-S centers and molybdenum of the reduced protein are compared in H_2O and D_2O.

Recently, the protein was purified from ^{57}Fe grown cells. The quality of the Mössbauer data obtained in the native and partially reduced Mo(Fe-S) protein enabled us to pursue the characterization of the [Fe-S] centers in correlation with the previously reported EPR data.

In the native state, the Mössbauer parameters of the only quadrupole doublet observed at 4.2 K with an external field of 500 G applied parallel to the gama beam ($\Delta E_Q=(0.63\pm0.02)$ mm/s, and $\delta=(0.27\pm0.02)$ mm/s), are typical of high-spin ferric ions with tetrahedral sulfur coordination.

Partially reduced states of the protein show two types of doublets, at 150 K. The central quadrupole doublet is similar to that of the oxidized Mo(Fe-S) protein. The outer doublet represents the ferrous site in the reduced [2Fe-2S] clusters. The shape of the ferrous doublet indicates that it consists of at least two unresolved doublets. This observation is consistent with the EPR finding that the Mo(Fe-S) protein contains more than one type of [2Fe-2S] cluster. The Mössbauer parameters for the two ferrous sites are $\Delta E_Q=(3.27\pm0.02)$ mm/s, $\delta=(0.57\pm0.02)$ mm/s and $\Delta E_Q=(2.79\pm0.02)$ mm/s, $\delta=(0.59\pm0.02)$ mm/s.

Low temperature studies are being carried out in order to compare the above data with [2Fe-2S] clusters of reduced ferredoxin from spinach and Rieske centers.

ACKNOWLEDGEMENTS

This work was supported by INIC, JNICT and NATO.

REFERENCES

J.J.G. MOURA, A.V. XAVIER, R. CAMMACK, D.O. HALL, M. BRUSCHI, J. LEGALL, *Biochem. J.*, 173, 419-425 (1978).

199
6

PS1.32 — MO

J. LAMPREIA
I. MOURA
A. XAVIER
J.J.G. MOURA
Centro de Química Estrutural
Complexo I, UNL
Av. Rovisco Pais, 1000 Lisboa
Portugal
H.D. PECK JR.
J. LEGALL
Department of Biochemistry
University of Georgia
Athens, GA 30602
U.S.A.

EPR STUDIES ON ADENYLYL SULFATE (APS) REDUCTASE — A FLAVIN, IRON-SULFUR CONTAINING PROTEIN

Sulfate reducing bacteria (SRB) utilize sulfate as terminal electron acceptor (anaerobic "respiration") with concomitant accumulation of sulfite. This metabolic process, known as dissimilatory sulfate reduction is carried out by a complex enzymatic system as indicated schematically in Fig. 1 [1]. Adenylyl sulfate (APS) reductase is a key enzyme in the overall process, carrying out the reduction of APS the activated form of sulfate, to sulfite with the release of AMP [2].

ORGANISMS

APS reductases were purified to homogeneity from the following sulfate reducing bacteria: *Desulfovibrio gigas* (NCIB 9332), *D. desulfuricans* (ATCC 27774), *D. desulfuricans* (strain Berre eau), *D. baculatus* (strain 9974) and *D. vulgaris* (strain Hildenborough).

ACTIVE SITE COMPOSITION

The enzyme (molecular mass 440 KD, dimer) contains 12-16 gatm of iron (arranged in [Fe-S] clusters) and 1 FAD per monomeric unit. The chemical analysis (as well as the spectroscopic data, see below) are quite similar, despite the microbial origin of the enzyme.

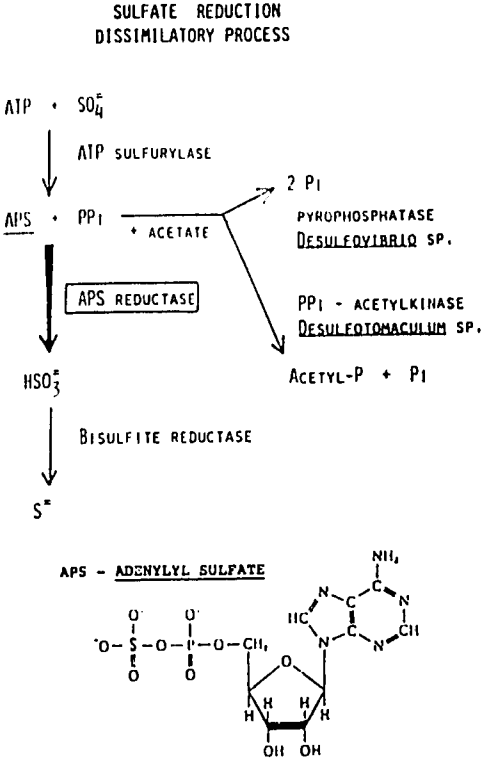

Fig. 1
Schematic representation of dissimilatory sulfate reduction pathway. Relevant enzymes

EPR SPECTROSCOPIC DATA — CHARACTERIZATION OF THE IRON-SULFUR CLUSTERS

Low temperature EPR studies were undertaken in order to characterize the redox centers present. In the native state all the samples examined so far show an almost isotropic EPR signal, centered around $g = 2.02$, only detectable below 25 K — Center I (Fig. 2-A). This signal shows measurable line broadening when the enzyme is isolated from ^{57}Fe grown cells (the experiments were conducted with ^{57}Fe *D. gigas* enzyme). The signal is compatible with the presence of a paramagnetic iron-sulfur cluster (see also below). The integration of this EPR signal varies slightly from preparation to preparation of the enzyme and also with its bacterial origin, but accounts always to less than one

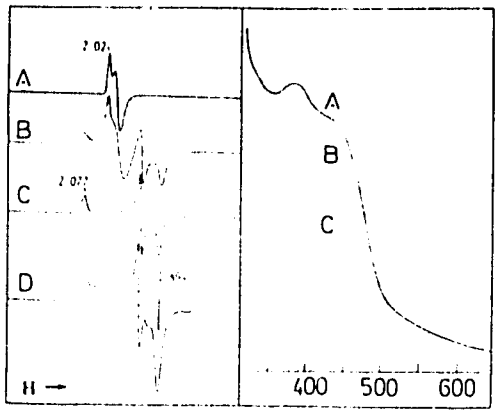

Fig. 2

Left part — EPR spectra of APS reductase from D. desulfuricans (strain 9974).

A — Native form; B — $SO_3^{=}$ + AMP; C — Dithionite reduced (20 sec.); D — Dithionite reduced (30 min.)

Spectrum B is represented with twice the gain of sepctra A and C. Spectrum D is represented with 1.25 of the gain of spectra A and C. Temperature 8 K; modulation amplitude 1 mT; power 2 mW.

Right part — Visible spectra of APS reductase from D. desulfuricains *(strain 9974).*

A — Native protein; B — Enzyme reacted with $SO_3^{=}$; C — Enzyme reacted with $SO_3^{=}$ + AMP

spin per monomeric unit (0.1-0.25 spin). The catalytic events occuring in the presence of natural interacting substrates (sulfite and AMP) as well as chemical reductants (ascorbate, dithionite and H_2 reduced methylviologen) can be followed by EPR in conjunction with visible spectroscopy. Different redox states of the enzyme can be attained using different reduction times.

Center II, EPR g-values 2.077, 1.935 and 1.894, integrates to approx. 0.7-0.9 spins per monomeric unit and is only observable below 25 K. These EPR features are trapped after a short dithionite reduction time (Fig. 2-C) or in the presence of H_2 reduced methylviologen. Sulfite plus AMP only reduce partially Center II and affect drastically the isotropic EPR signal (Fig. 2-B). Sulfite bleaches the flavin chromophore contribution (Fig. 3-A/B) but do not affect appreciably iron-sulfur centers. A complex EPR spectrum develops after a long reduction time, which accounts for at least three iron-sulfur clusters (Fig. 2-D). Center I and II seem to be catallytically envolved with the substrate ($AMP + SO_3^{=}$) as seen by EPR and visible spectroscopies. EPR redox titrations, in the presence of dye mediators, indicate that Center II has a relatively high midpoint redox potential (~ -50 mV). Preliminar Mössbauer spectroscopic studies on *D. gigas* ^{57}Fe APS reductase (in collaboration with B.H, Huynh, Emory University, Atlanta USA) indicate that the spectrum of the native enzyme is essentially dominated by diamagnetic quadrupole doublets typical of $[Fe_4S_4]$ clusters in the +2 oxidation state. The paramagnetic species detected by EPR (g = 2.02) may be in the limiting range for Mössbauer detection, due to its spin concentration. The presence of an extra metal center has been ruled out by a careful screening of the metal content of the enzyme. Further studies are in progress in order to fully characterize the APS reductase iron-sulfur centers.

ACKNOWLEDGEMENTS

Work supported by INIC, JNICT and USAID.

REFERENCES

[1] H.D. Peck Jr., J. LeGall, *Philos. Trans. R. Soc. London, Ser. B*, 298, 443-466 (1982).

[2] R.N. Bramlett, H.D. Peck Jr., *J. Biol. Chem.*, 250, 2979-2986 (1975).

201

B-8

PSI.34 — TU

M. TEIXEIRA
I. MOURA
A.V. XAVIER
J.J.G. MOURA
Centro de Química Estrutural
Complexo I, U.N.L.
Av. Rovisco Pais, 1000 Lisboa
Portugal
G. FAUQUE
B. PICKRIL
J. LEGALL
A.R.B.S., E.C.E.
CEN Cadarache
13115 Saint Paul lez Durance
France

NICKEL-IRON-SULFUR-SELENIUM CONTAINING HYDROGENASES ISOLATED FROM *DESULFOVIBRIO BACULATUS* STRAIN 9974

Hydrogenases from the periplasmic, cytoplasmic and membrane fractions of *Desulfovibrio baculatus* strain 9974 (DSM 1743) have been purified to apparent electrophoretic homogeneity.

PHYSICO-CHEMICAL DATA

Table I indicates the results of metal analysis as well as other physico-chemical data, namely the specific activity of the enzyme in respect to hydrogen evolution (μmoles H_2/min.mg.). Plasma emission metal analysis detects the presence of iron, and of nickel and selenium in equimolecular amounts. The U.V. and visible spectra show broad bands around 277 and 390-400 nm, typical of iron-sulfur containing proteins.

EPR DATA

The EPR spectra of the native ("as isolated") enzymes are shown in Fig. 1 A-C. All the enzymes show a weak isotropic EPR signal centered around g = 2.02 observable at low temperatures (below 20 K) that accounts for about 0.002 to 0.03 spins per molecule. The periplasmic and membrane bound enzymes also show additional

Table I

Physico-chemical data on D. baculatus *(9974) hydrogenases*

	Cytoplasmic	Periplasmic	Membrane bound
Specific Activity (μmoles H_2 evolved/min.mg.)	466	527	120
Molecular weight (kDa)	100[a] 81(54, 27)[b,c]	110[a] 75(49, 26)[b,c]	100[a] 89(62, 27)[b,c]
Metal content			
Fe	7.7 (14.1)[d]	9.25(13.5)	10.3(11.4)
Ni	0.54(1.0)	0.69(1.0)	0.90(1.0)
Se	0.56(1.03)	0.66(0.96)	0.86(0.95)
Ratio $A_{390/280}$	0.28	0.25	0.10

a) Molecular mass determined by high pressure liquid chromatography.
b) Molecular mass determined in the presence of SDS.
c) Molecular mass of subunits are indicated between brackets.
d) Values in ( ) were converted per 1 nickel per minimal molecular weight.

EPR signals with g-values greater than 2.0 assigned to nickel(III), which are detectable up to 77 K. The periplasmic hydrogenase shows EPR features at 2.20, 2.06 and ~2.00 (Fig. 1-B); the signals of the membrane bound enzyme can be

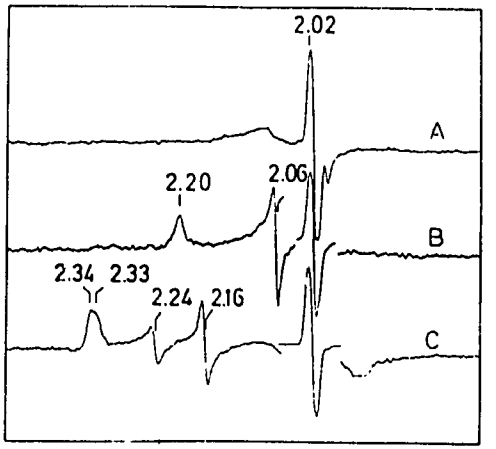

Fig. 1

EPR spectra of D. baculatus *(strain 9974) native hydrogenase: A — Cytoplasmic fraction; B — Periplasmic fraction; C — Membrane bound fraction.*

Experimental conditions: temperature 8 K; microwave power 2 mW; modulation amplitude 1 mT; microwave frequency 9.41 GHz

Rec'd with ... AUG 7 1987

decomposed into two sets of EPR signals with g-values at 2.34, 2.15 and ~2.00 (component I) and at 2.33, 2.24 and ~2.00 (component II) (Fig. 1-C).

In the hydrogen reduced state all the hydrogenase fractions show identical EPR spectra: signals typical of reduced iron-sulfur centers with g_{med} ~1.94, and additional EPR features with g-values greater than 2.0 that were assigned to nickel. The conjunction of EPR studies performed at different temperatures and microwave powers, as well as the observation of EPR signals in reduced samples (reduced either with H_2 gas or sodium dithionite, during different times), enables the identification of two sets of iron-sulfur centers: *center I* (2.03, 1.89 and 1.86) detected below 10 K and *center II* (2.06, 1.95 and 1.88) easily saturated at low temperature.

DISCUSSION

The hydrogenase fractions isolated from *D. baculatus* (strain 9974) show unusual spectroscopic properties which should be relevant for the understanding of the role of EPR detectable nickel in hydrogenases. The samples show a very weak EPR signal due to iron-sulfur centers in the oxidized state. Iron-sulfur EPR signals have been observed in the native state of other hydrogenases. *D. gigas* hydrogenase has an almost isotropic EPR signal centered around g = 2.02 assigned to a $[Fe_3S_x]$ center on the basis of complementary EPR and Mössbauer spectroscopic studies [1]. This signal integrates from 0.7 up to 1.0 spin/molecule depending on the preparation. However, the *D. vulgaris* (Hildenborough) enzyme also shows a very weak signal in the native state which only accounts for up to 0.05 spin/molecule [2] and the soluble *D. desulfuricans* (Norway strain) hydrogenase is EPR silent as isolated [3]. The cytoplasmic fraction of *D. baculatus* (strain 9974) hydrogenase is pratically EPR silent (the isotropic signal accounts for 0.002 spin/molecule). Additionally, EPR signals assigned to Ni(III) are observed in the periplasmic and the membrane bound form. The nickel EPR g-values observed in the membrane fraction are typical of Ni(III) as observed for other nickel containing hydrogenases as isolated. However the rhombic EPR signal observed for the periplasmic fraction as isolated is quite unusual. Similar g-values (2.20, 2.06 and 2.0) were also observed in the *D. desulfuricans* (Norway strain) enzyme isolated from the soluble fraction [3]. Other complex nickel EPR signals have been reported [4] and assigned as being the result of the interaction between the nickel and an iron-sulfur center.

Upon reduction under hydrogen atmosphere (or by addition of dithionite) the three hydrogenases gave the same type of EPR spectra despite its native state. These observations indicate that native hydrogenases isolated from different bacterial sources or from different fractions (soluble or membrane bound) yield different Ni(III) EPR signals [5]. They may contain the redox centers in different oxidation states depending on the enzyme conditions. In order to express full activity, certain enzymes (*e.g. D. gigas* yielding a 2.31, 2.23 and 2.0 native EPR nickel(III) signal) require an activation/reductive step. Others, as in the case of *D. baculatus* (strain 9974) do not show a lag time dependent activation step. The state of the nickel in the native preparation may be determinant for the behaviour of the enzyme towards the full expression of activity.

Remarkable is also the presence of selenium in equimolecular amounts to nickel. Selenium is also found in *Methanococcus vannielli* [6] and *D. desulfuricans* (Norway strain) hydrogenases [3].

ACKNOWLEDGEMENTS

This work was supported by INIC, JNICT, NATO and USAID.

REFERENCES

[1] M. Teixeira, I. Moura, A.V. Xavier, D.V. DerVartanian, J. LeGall, H.D. Peck Jr., B.H. Huynh, J.J.G. Moura, *Eur. J. Biochem.*, 130, 481-484 (1983).

[2] B.H. Huynh, M.H. Czechowski, H.J. Kruger, D.V. DerVartanian, H.D. Peck Jr., J. LeGall, *Proc. Natl. Acad. Sci. USA*, 81, 3728-3732 (1984).

[3] S.H. Bell, D.P.E. Dickson, R. Rieder, R. Cammack, D.S. Patil, D.O. Hall, K.K. Rao, *Eur. J. Biochem.*, 145, 645-651 (1984).

[4] S.D.J. Albracht, J.W. van der Zwaan, R.D. Fontijn, *Biochim. Biophys. Acta*, 766, 245-258 (1984).

[5] M. Teixeira, I. Moura, A.V. Xavier, B.H. Huynh, D.V. DerVartanian, H.D. Peck Jr., J. LeGall, J.J.G. Moura, 1985, submitted for publication.

[6] S. Yamazaki, *J. Biol. Chem.*, 257, 7926-7929 (1982).

CHAPTER 8

07
(A)

A LINK BETWEEN HYDROGEN AND SULFUR METABOLISMS IN *METHANOSARCINA BARKERI* (DSM 800)

G. Fauque, M. Teixeira**, I. Moura**, A.R. Lino**, P.A. Lespinat*, A.V. Xavier**, D.V. Dervartanian***, H.D. Peck, Jr.***, J. Leyall*, and J.J.G. Moura***

*A. R. B. S.
E. C. E.
CEN-Cadarache
Saint-Paul Lez Durance, France

**Centro de Quimica Estrutural
Lisbon, Portugal

***Department of Biochemistry
University of Georgia
Athens, Georgia

ABSTRACT

The hydrogenase of the acetoclastic methanogenic bacterium *Methanosarcina (M.) barkeri* strain DSM 800 grown on methanol has been purified to homogeneity. This soluble hydrogenase has a high molecular weight (800 kDa) and a final specific activity of 270 umoles of H_2 evolved per min. per mg of protein. It shows an absorption spectrum typical of a non-heme iron protein with a ratio A400/A275 = 0.29.

It contains 8-10 iron atoms, 0.6-0.8 nickel atoms and 1 FMN per subunit of molecular weight of 50 kDa. Under hydrogen the purified hydrogenase can reduce the F_{420} cofactor (either free or protein-bound) and the ferredoxin isolated from *M. barkeri* as well as cytochromes c_{553} and c_3 from *Desulfovibrio* and c_7 from *Desulfuromonas*. *M. barkeri* presents also sulfite, thiosulfate and trithionate

Biotechnological Advances in Processing Municipal Waste for Fuels and Chemicals

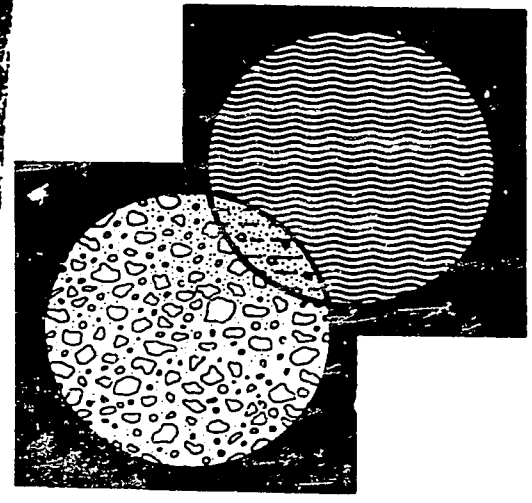

Proceedings of the First Symposium Minneapolis, Minnesota August 15-17, 1984

A. A. Antonopoulos, Editor
Energy and Environmental Systems Division
Argonne National Laboratory
9700 South Cass Avenue, Argonne, Illinois 60439
December 1985

Prepared for U. S. Department of Energy, Assistant Secretary for Conservation and Renewable Energy, Office of Renewable Technology

reductases activities. The *M. barkeri* sulfite reductase has been isolated (P_{590}); it contains 0.9 mol of sirohaem and 4.9 g atom of iron per subunit of molecular weight 23 KDa.

The EPR spectrum of P_{590} exhibits characteristics of low spin ferrihaem with g values at 2.40, 2.30 and 1.88.

INTRODUCTION

The methanogenic bacteria are a diverse group of strictly anaerobic microorganisms that produce methane from a limited number of substrates. *Methanosarcina barkeri* belongs to a group of methanogens that are characterized by their ability to grow not only chemoautotrophically on $H_2 + CO_2$ but also chemoorganotrophically with acetate, methanol or methylamines as energy sources (29).

The methanogenic bacteria have recently been reclassified as Archaebacteria in recognition of the fact that they are only distantly related in the evolutionary scale to eucaryotes (1) and the strictly anaerobic bacteria such as the sulfate reducing organisms and Clostridia (16). Several electron carriers and factors unique to methanogenic bacteria have been isolated from these organisms such as: coenzyme M (19), F_{420} (5), F_{342} (10) and F_{430} (29,6) which may be isolated in a protein-bound form (20). The metabolism of sulfur in methanogenic bacteria remains obscure although it is of special importance because of these organisms synthesize large amounts of coenzyme M, which contains both reduced and oxidized sulfur.

In this paper we report on the link between hydrogen and sulfur metabolisms in *M. barkeri* (DSM 800).

MATERIALS AND METHODS

Growth of the Microorganism and Preparation of the Crude Extract

M. barkeri (strain DSM 800) was grown at 37°C in a methanol-containing medium as previously described (3). The cells were suspended in 10 mM Tris-HCl buffer pH 7.6. DNase was added and the extract was ruptured once in a French press at 62 MPA under N_2 atmosphere. The extract was centrifuged at 12000 rpm for 30 min and the supernatant constituted the crude cell extract.

The sulfite reductase activity was measured by a manometric assay as described by Schedel et al. (24). It requires the generation of reduced methylviologen by an excess of hydrogenase under hydrogen atmosphere. The reduced dye then serves as electron donor to the sulfite reductase. The thiosulfate and trithionate reductases activities were also determined manometrically by the same technique.

The sulfite reductase (P_{590}) has been isolated from *M. barkeri* as previously described (21). The siroheme content of P_{590} was analyzed according to the method of Siegel et al. (25). The hydrogenase of *M. barkeri* has been purified as previously described (7). Three methods were used for the determination of hydrogenase activity: H_2 evolution with sodium dithionite (15 mM) as electron donor and methylviologen (1 mM) as mediator in 50 mM Tris-HCl buffer (23); H_2 uptake was followed by the reduction under H_2 of benzyl-viologen (10 mM) at pH 8.0; and D $-H^+$ exchange activity was followed directly in the liquid phase in a reaction vessel connected to a mass spectrometer via a teflon membrane allowing the diffusion of dissolved gases to the ion source (2).

The hydrogenase specific activities are expressed as moles of H_2 or HD produced and H_2 consumed per minute per mg of protein. Total iron was determined by the TPTZ method (8) and nickel by atomic absorption using a Perkin-Elmer model 403.

Protein was determined by the Lowry (18) and biuret (17) methods. The molecular mass of the native proteins was estimated by gel filtration on a column of Sephadex G-200 (30) and the subunit structure was determined on SDS polyacrylamide gel electrophoresis (28). The coupling effect of hydrogenase on the reduction of different electron carriers was assayed by a spectrophotometric method following the reduction of the chromophores at 553 nm (cytochromes), 420 nm (F_{420}) and 400 nm (ferredoxins) in the presence of hydrogenase under a hydrogen atmosphere (1 atm., 25°C).

troscopic Instrumentation

The ultraviolet and visible spectra were recorded on a eckman model 35 spectrophotometer. Electron paramagnetic sonance spectroscopy (EPR) was carried out on a Bruker 0-tt spectrometer, equipped with an ESR-9 flow cryostat nd a Nicolet 1180 computer with which mathematical manipu- ations were performed.

ESULTS

roperties of the Hydrogenase from M. barkeri

The hydrogenase of the acetoclastic methanogenic bac- rium *M. barkeri* (strain DSM 800) grown on methanol has en purified to homogeneity (7). This soluble hydrogenase is a high molecular weight (800 kDa) and a final specific tivity of 270 µmoles of H_2 evolved per min. per mg of otein in the dithionite reduced methylviologen assay. e protein is rather stable to high temperature and to posure to air at 4°C. It shows an absorption spectrum pical of a non-heme iron protein with maxima at 275, 380 d 403 nm and a ratio A400/A275 = 0.29 (Figure 1). It ntains 8-10 iron atoms, 0.6-0.8 nickel atoms and 1 FMN r subunit of molecular weight of 60 kDa.

The electron paramagnetic resonance (EPR) spectrum of e native enzyme shows a rhombic signal with g values at .24, 2.20 and ∿ 2.0 probably due to nickel which is opti- lly measured at 40 K. In the reduced state, using mole- lar hydrogen or dithionite as reductants, at least two pes of g = 1.94 EPR signals, due to iron-sulfur centers, uld be detected and differentiated on the basis of power temperature dependence.

Under hydrogen the purified hydrogenase can reduce the cofactor (either free or protein-bound) and the ferre- xin isolated from *M. barkeri* as well as cytochromes c_{553} d c_3 from *Desulfovibrio* and c_7 from *Desulfuromonas* (Table . In the same conditions, this protein can also reduce thyl and benzyl viologens.

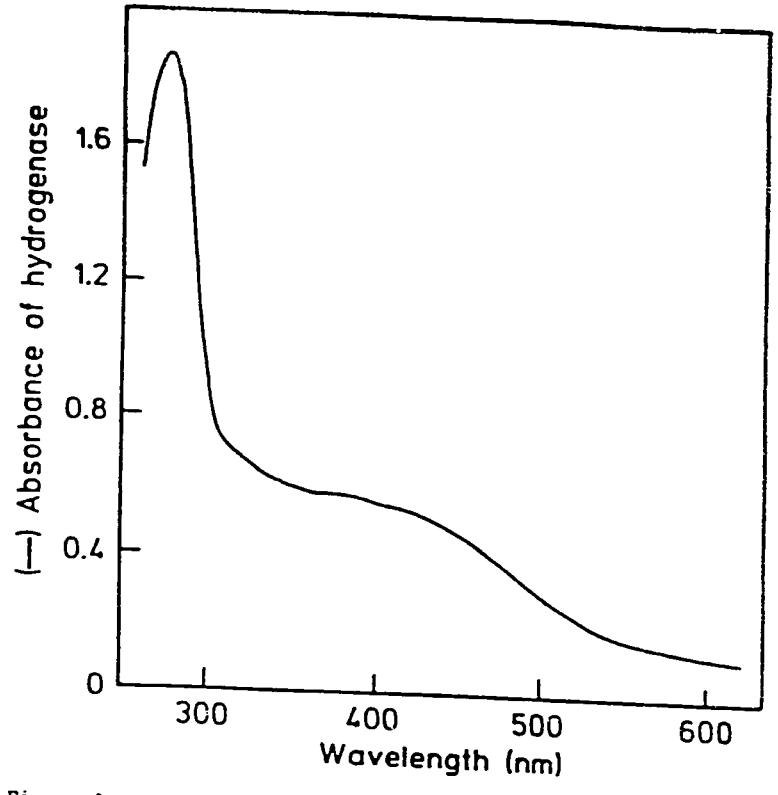

Figure 1. Electronic absorption spectrum of oxidized *M. barkeri* hydrogenase (0.62 mg/ml) at 25°C.

Table 1. Direct Coupling Between Electron Transfer Proteins and Hydrogenase from Methanosarcina barkeri (DSM 800)

Protein	Active Center	Reduction by Hydrogenase Under H_2
Cytochrome c_{553} D. Desulfuricans (Berre Eau)	1 Heme C (Met, His)	Yes
Cytochrome c_7 Desulfuromonas Acetoxidans	3 Heme C (His, His)	Yes
Cytochromes c_3* (M.W. 13000)	4 Heme C (His, His)	Yes
Ferredoxin M. Barkeri	(3 Fe - X S)	Yes
Ferredoxin II D. Desulfuricans (Berre Eau)	(4Fe-4S) + (3Fe-XS)	Partial
Factor F_{420} M. barkeri	5 - Deazaflavin Mononucleotide	Yes

* From D. gigas, D. desulfuricans Berre Eau, D. baculatus strain 9974.

A comparative study of two (Fe-Ni) hydrogenases (from *D. gigas* and *M. barkeri*) and one (Fe-) hydrogenase (from *D. vulgaris* Hildenborough) has been made (Table 2). The periplasmic hydrogenase from *D. vulgaris* Hildenborough is the most active in H_2 evolution, H_2 uptake and D_2-H^+ exchange

Sulfur Metabolism in M. barkeri

The *M. barkeri* crude extract exhibits sulfite, thiosulfate and trithionate reductases activities (Table 3). The sulfite reductase (P_{590}) has been purified from this strain as previously described (21). The optical spectrum of *M. barkeri* P_{590} shown in Figure 2 exhibits absorption bands at 590, 543, 395 and 275 nm. There is no band around 715 nm as is usually seen in other sulfite reductases; this band is characteristic of high spin Fe^{3+} complexes of isobacteriochlorins (26). The lack of this band in P_{590} is probably indicative that the siroheme is in a different spin state. The EPR spectrum of *M. barkeri* P_{590} shown in Figure 3 exhibits characteristics of low spin ferriheme with g values at 2.40, 2.30 and 1.88. Spin quantitation of this EPR signal yields a value close to 1 spin/siroheme. When P_{590} reacts with cyanide under reducing conditions (in the presence of methyl viologen) an EPR spectrum characteristic of reduced $[4Fe\text{-}4S]^{1+}$ center is observed (our unpublished results).

The chemical analysis of iron and siroheme together with EPR analysis show that P_{590} must contain one siroheme and probably one [4Fe-4S] center per mole of protein.

DISCUSSION

The specificity of the soluble hydrogenase from *M. barkeri* (DSM 800) for the reduction under H_2 of several electron carriers has been investigated. This protein is able to reduce some monoheme and multiheme cytochromes c isolated from sulfate and sulfur reducing bacteria. This hydrogenase reduces also completely the ferredoxin of *M. barkeri* and partially the *D. sulfuricans* (Berre Eau) ferredoxin. This protein can finally reduce the cofactor F_{420} from *M. barkeri* (free or protein-bound). We should note that the factor F_{420} is not reduced by the other (Fe-Ni) hydrogenase from *D. gigas* (G. Fauque and J. LeGall , unpublished).

Table 2. Comparison of Specific Activities of 2 Fe-Ni Hydrogenases (Desulfovibrio Gigas and Methanosarcina Barkeri) and 1 Fe-Hydrogenase (D. vulgaris Hildenborough)

Organism	H_2 Evolution (1 mM M.V. + 1/5 mM $Na_2S_2O_4$) pH 7.6	H_2 Uptake (10 mM MV) pH 8.0	HD Production (20% D_2 in Ar) pH 7.6
D. gigas	440	1 500	147
M. barkeri	270	960	35
D. vulgaris	3 800	37 000	607

The specific activities are expressed as µmoles of gases evolved or consumed per minute per milligram of protein.

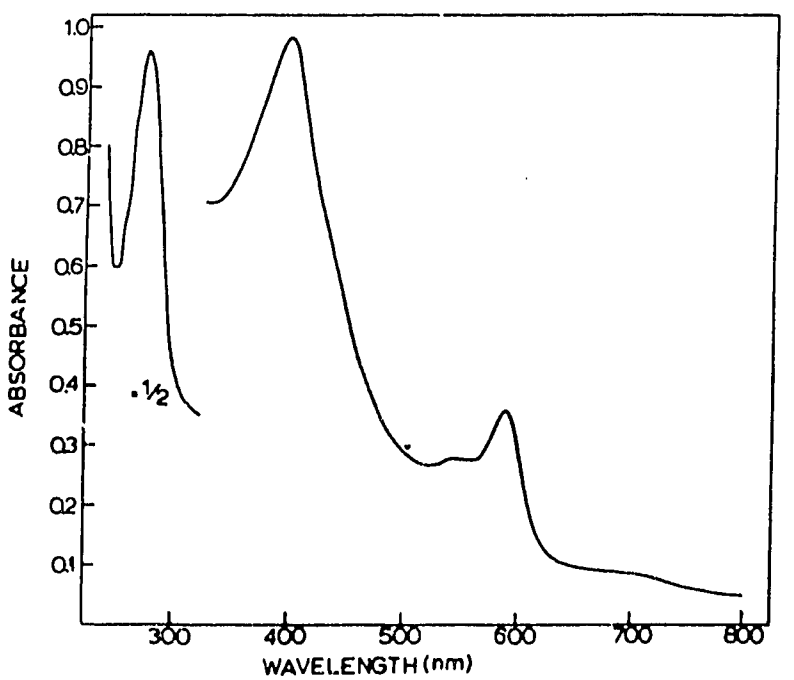

Figure 2. Ultraviolet and visible absorption spectra of the native M. barkeri P_{598} (sulfite reductase).

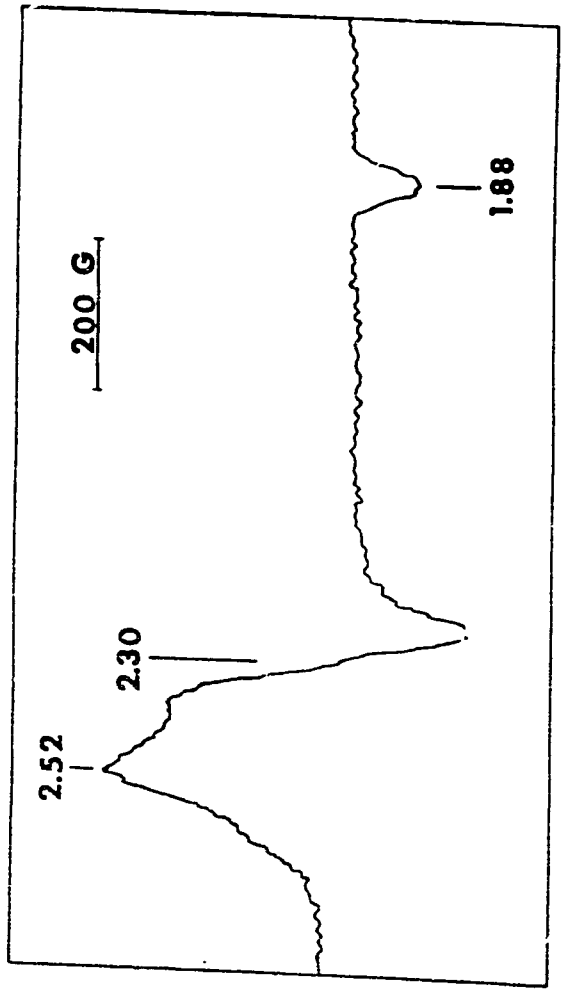

Figure 1. EPR spectrum of native *M. barkeri* P_{590}. Temperature 9.6 K, microwave power 2mW, gain 5 x 10^3.

Table 3. Reduction Under Hydrogen of Sulfite, Thiosulfate and Trithionate by a Crude Extract of M. barkeri

Additions	Activity
	µmoles H_2 min^{-1} mg^{-1}
None	0
Na_2SO_3	18
$Na_2S_2O_3$	5
$Na_2S_3O_6$	8
Na_2SO_4	0
plus ATP	

All reaction mixtures contained crude extract of M. barkeri (DSM 804) plus methyl viologen (5 mM), temp. 30°C; gas phase H_2. Na_2SO_3, 20 mM; phosphate buffer, pH 6.5, 0.2 M; $Na_2S_2O_3$, 20 mM; phosphate buffer, pH 7.6, 0.2 M; $Na_2S_3O_6$, 20 mM; Tris buffer, pH 7.5, 0.1 M; Na_2SO_4, 20 mM; $MgCl_2$, 20 mM, ATP, 20 mM, phosphate buffer, pH 7.0, 0.2 M.

Recently, EPR and Mössbauer studies of assimilative sulfite reductase isolated from *D. vulgaris* Heldenborough firmly establish that the siroheme is also in a low spin heme complex (12). Mössbauer spectroscopy demonstrated that the siroheme is exchange-coupled to the [4Fe-4S] center. The siroheme-[4Fe-4S] unit is a common prosthetic group found in *Escherichia coli* sulfite reductase and spinach nitrite reductase. However, *D. vulgaris* sulfite reductase and *M. barkeri* P_{590} are the only known examples where the native state of the enzyme contains a low-spin ferric siroheme.

CONCLUSIONS

The presence of sulfite, thiosulfate and trithionate reductase activities in *M. barkeri* shows that its sulfur metabolism is far more complex than was first suspected. Since sulfide ions are most probably predominant over oxidized sulfur compounds at the low redox potentials which are necessary for the growth of methanogenic organisms, it is not clear why these bacteria would need to reduce these

compounds. It has already been suggested (21) that *M. barkeri* sulfite reductase could actually function in a reverse direction, thus allowing the production of oxidized sulfur which is necessary for the biosynthesis of coenzyme M. Another attractive hypothesis is that a sulfur cycle might function when *M. barkeri* grows in association with sulfate reducing bacteria: a reoxidation of sulfide to sulfite would allow the latter organisms to obtain extra energy through oxidative phosphorylation coupled to methane formation and the constant cycling of sulfide and sulfite might prevent the accumulation of toxic levels of sulfide. A study of *Desulfovibrio vulgaris* growing through interspecies hydrogen and acetate transfer with *M. barkeri* has shown that the growth yield of the sulfate reducing bacterium is much higher than expected based on the loss of ATP originating from oxidative phosphorylation (27). The presence of a sulfite/sulfide cycle, eliminating the loss of ATP for the activation of sulfate and allowing the production of ATP through oxidative phosphorylation during sulfite reduction would explain the unexpected high growth yield of the sulfate reducing bacteria.

In contrast to the F_{420} hydrogenase isolated from *Methanobacterium formicicum* (22,13,14), *M. barkeri* hydrogenase appears to be extremely stable as far as its reactivity toward F_{420} is concerned. As seen in Table 1, its reactivity is extremely broad and is not limited to two electron acceptors since it can reduce the monoheme cytochrome c_{553} from sulfate reducing bacteria.

The sulfite reductase of *M. barkeri* appears similar to the so-called assimilatory sulfite reductase from *D. vulgaris* strain Hildenborough (15,12) in its molecular weight, heme and nonheme iron content and in the spin state of its siroheme. This is the second protein from a methanogenic "archaebacterium" that is shown to bear similarity with a protein from a sulfate reducing bacterium. With 26 direct homologies, the ferredoxin from *M. barkeri* (11) is more closely related to ferredoxin II from *D. desulfuricans* Norway 4 (9) than the later protein is to *D. gigas* ferredoxin (19 direct homologies) (4).

ACKNOWLEDGMENTS

This work was made possible thanks to a collaborative agreement between UGA, CNRS and CEA. Financial support from INIC, INICT and NATO are gratefully acknowledged, also Solar Energy Research Institute Contract XD-1-1155-1, and AID Grant No. 936-5542-G-SS-4003-00.

LITERATURE CITED

1. Balch, W.E., G.E. Fox, L.J. Magrum, C.R. Woese, and R.S. Wolfe, "Methanogens: Reevaluation of a Unique Biological Group," *Microbial. Rev., 43,* 260-296 (1979).
2. Berlier, Y.M., G. Fauque, P.A. Lespinat, and J. LeGall, "Activation, Reduction and Proton-deuterium Exchange Reaction of the Periplasmic Hydrogenase from *Desulfovibrio gigas* in Relation with the Role of Cytochrome c_3," *FEBS Lett., 140,* 185-188 (1982).
3. Blaylock, B.A. and T.C. Stadtman, "Methane Biosynthesis by *Methanosarcina barkeri* - Properties of the Soluble Enzyme System," *Arch. Biochem. Biophys., 116,* 138-152 (1966).
4. Bruschi, M., "Amino Acid Sequence of *Desulfovibrio* Ferredoxin: Revisions," *Biochem. Biophys. Res. Comm., 91,* 623-628 (1979).
5. Cheeseman, P., A. Tomswood, and R.S. Wolfe, "Isolation and Properties of a Fluorescent Compound, Factor$_{420}$ from *Methanobacterium* Strain M.O.H.," *J. Bacteriol, 112,* 527-531 (1972).
6. Diekert, G., H.P. Gilles, R. Jaenchen, and R.K. Thauer, "Incorporation of 8 Succinate Per Mol Nickel into F_{430} by *Methanobacterium thermoautotrophicum*," *Arch. Microbiol., 128,* 256-262 (1980).
7. Fauque, G., M. Teixeira, I. Moura, P.A. Lespinat, A.V. Xavier, D.V. DerVartanian, H.D. Peck, Jr., J. LeGall, and J.J.G. Moura, "Purification, Characterization and Redox Properties of Hydrogenase from *Methanosarcina barkeri* (DSM 800)," *Eur. J. Biochem., 142,* 21-28 (1984).
8. Fischer, D.S. and D.C. Price, "A Simple Serum Iron Method Using the New Sensitive Chromogen Tripyridyl-s-triazine," *Clin. Chem., 10,* 21-25 (1964).
9. Guerlesquin, F., M. Bruschi, G. Bovier-Lapierre, J. Bonicel, and P. Couchoud, "Primary Structure of the Two (4Fe-4S) Clusters Ferredoxin from *Desulfovibrio desulfuricans* (strain Norway 4)," *Biochimie, 65,* 43-47 (1983).

10. Gunsalus, R.P. and R.S. Wolfe, "Chromophoric Factors F_{342} and F_{430} of *Methanobacterium thermoautotrophicum*," *FEBS Lett.*, *3*, 191-193 (1978).
11. Hausinger, R.P., I. Moura, J.J.G. Moura, A.V. Xavier, H. Santos, J. LeGall, and J.B. Howard, "Amino Acid Sequence of a 3Fe-3S Ferredoxin from the Archebacterium *Methanosarcina barkeri*," *J. Biol. Chem.*, *257*, 14192-14194 (1982).
12. Huynh, B.H., L. Kang, D.V. DerVartanian, H.D. Peck, Jr., and J. LeGall, "Characterization of a Sulfite Reductase from *Desulfovibrio vulgaris*: Evidence for the Presence of a Low-Spin Siroheme and an Exchange-coupled Siroheme - 4Fe-4S Unit," *J. Biol. Chem.*, In press (1985).
13. Jin, S.L., D.K. Blanchard, and J.S. Chen, "Two Hydrogenases with Distinct Electron Carrier Specificity and Subunit Composition in *Methanobacterium formicium*," *Biochim. Biophys. Acta*, *748*, 8-20 (1983).
14. Kojima, N., J.A. Fox, R.P. Hausinger, L. Daniels, W.H. Orme-Johnson, and C. Walsch, "Paramagnetic Centers in the Nickel-containing, Deazaflavin Reducing Hydrogenase from *Methanobacterium thermoautotrophicum*," *Proc. Natl. Acad. Sci., USA*, *80*, 378-382 (1983).
15. Lee, J.P. and H.D. Peck, Jr., "Purification of the Enzyme Reducing Bisulfite to Trithionate from *Desulfovibrio gigas* and its Identification as Desulfoviridin," *Biochem. Biophys. Res. Comm.*, *45*, 583-589 (1971).
16. LeGall, J., J.J.G. Moura, H.D. Peck, Jr., and A.V. Xavier, "Hydrogenase and Other Iron Sulfur Proteins from the Sulfate-Reducing and Methane Forming Bacteria," *Iron-Sulfur Protein*, (T.G. Spiro, ed.), pp. 177-248, John Wiley and Sons, New York (1982).
17. Levin, R. and R.W. Brauer, "The Biuret Reaction for the Determination of Proteins. An Improved Reagent and its Application," *J. Lab. Clin. Med.*, *38*, 474-479 (1951).
18. Lowry, O.H., N.J. Rosebrough, A.L. Farr, and R.J. Randall, "Protein Measurement with the Folin Phenol Reagent," *J. Biol. Chem.*, *193*, 265-275 (1951).
19. MacBride B.C. and R.S. Wolfe, "A New Coenzyme of Methyl Transfer, Coenzyme M.," *Biochemistry*, *10*, 2317-2324 (1971).
20. Moura, I., J.J.G. Moura, H. Santos, A.V. Xavier, G. Burch, H.D. Peck, Jr., and J. LeGall, "Proteins Containing the Factor F_{430} from *Methanosarcina barkeri* and *Methanobacterium thermoautotrophicum*," *Biochim. Biophys. Acta*, *742*, 84-90 (1983).
21. Moura, J.J.G., I. Moura, H. Santos, A.V. Xavier, M. Scandellari, and J. LeGall, "Isolation of P_{598} from *Methanosarcina barkeri*: Evidence for the Presence of Sulfite Reductase Activity," *Biochem. Biophys. Res. Comm.*, *108*, 1002-1009 (1982).
22. Nelson, M.J.K., D.P. Brown, and J.G. Ferry, "FAD Requirement for the Reduction of Coenzyme F_{420} by Hydrogenase from *Methanobacterium formicium*," *Biochem. Biophys. Res. Comm.*, *120*, 775-781 (1984).
23. Peck, H.D., Jr., and H. Gest, "A New Procedure for the Assay of Bacterial Hydrogenases," *J. Bacteriol*, *71*, 70-80 (1956).
24. Schedel, M., J. LeGall, and J. Baldensberger, "Sulfur Metabolism in *Thiobacillus denitrificans*. Evidence for the Presence of a Dissimilatory Sulfite Reductase," *Arch. Microbiol.*, *105*, 339-341 (1975).
25. Siegel, L.M., M.Y. Murphy, and H. Kamin, "Siroheme: Methods of Isolation and Characterization," *Methods Enzymol.*, *52*, 436-447 (1978).
26. Stolzenbach, A.M., S.H. Strauss, and R.H. Holm, "Iron (II,III)-Chlorin and-Isobacteriochlorin Complexes. Models of the Heme Prosthetic Groups in Nitrite and Sulfite Reductases: Means of Formation and Spectroscopic and Redox Properties," *J. Am. Chem. Soc.*, *203*, 4763-4778 (1981).
27. Traore, S.A., C. Gaudin, C.E. Hatchikian, J. LeGall, and J.P. Belaich, "Energetics of Growth of a Defined Mixed Culture of *Desulfovibrio vulgaris* and *Methanosarcina barkeri*: Maintenance Energy Coefficient of the Sulfate Reducing Organism in the Absence of and Presence of its Partner," *J. Bacteriol.*, *155*, 1260-1264 (1983).
28. Weber, K. and M. Osborn, "The Reliability of Molecular Weight Determination of Dodecyl Sulfate Polyacrylamide Gel Electrophoresis," *J. Biol. Chem.*, *244*, 4406-4412 (1969).
29. Weimer, P.J. and J.G. Zeikus, "One Carbon Metabolism in Methanogenic Bacteria," *Arch. Microbiol.*, *119*, 49-57 (1978).
30. Whitaker, J.R., "Determination of Molecular Weights of Proteins by Gel Filtration of Sephadex," *Anal. Chem.*, *35*, 1950-1953 (1963).
31. Whitman, W.B. and R.S. Wolfe, "Presence of Nickel in Factor F_{430} from *Methanobacterium bryantii*," *Biochem. Biophys. Res. Comm.*, *92*, 1196-1201 (1980).

Evidence for the Formation of a $CoFe_3S_4$ Cluster in *Desulfovibrio gigas* Ferredoxin II

Isabel Moura and José J. G. Moura

Centro de Química Estrutural, UNL
1000 Lisboa, Portugal

Eckard Münck* and Vasilios Papaefthymiou

Gray Freshwater Biological Institute, University of Minnesota, Navarre, Minnesota 55392

Jean LeGall

Center for Biological Resource Recovery
Department of Biochemistry, University of Georgia
Athens, Georgia 30602

Received August 30, 1985

Using EPR and Mössbauer spectroscopy we have shown previously[1] that *Desulfovibrio gigas* ferredoxin II (Fd II) contains a 3Fe cluster. EXAFS studies[2] and chemical analyses[3] have suggested that this cluster has a cubane Fe_3S_4 core stoichiometry.

(1) Huynh, B. H.; Moura, J. J. G.; Moura, I.; Kent, T. A.; LeGall, J.; Xavier, A. V.; Münck, E. *J. Biol. Chem.* **1980**, *255*, 3242–3244.
(2) Antonio, M. R.; Averill, B. A.; Moura, I.; Moura, J. J. G.; Orme-Johnson, W. H.; Teo, B.-K.; and Xavier, A. V. *J. Biol. Chem.* **1982**, *257*, 6646–6649.
(3) Beinert, H.; Emptage, M. H.; Dreyer, J.-L.; Scott, R. A.; Hahn, J. E.; Hodgson, K. O.; Thomson, A. J. *Proc. Natl. Acad. Sci. U.S.A.* **1983**, *80*, 393–396.

0002-7863/86/1508-0349$01.50/0

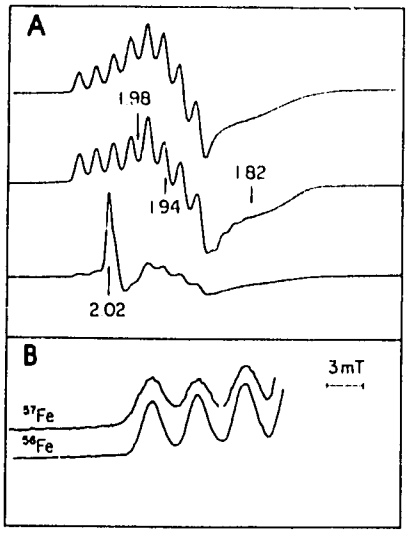

Figure 1. X-band EPR spectra of the oxidized CoFe cluster. (A) Middle trace: ^{56}Fe; $T = 40$ K; microwave power 1 mW; modulation amplitude, 0.5 mT. Lower trace: same as middle trace but $T = 9$ K. Upper trace: spectral simulation of 40 K spectrum using parameters quoted in the text. (B) Expanded view of low-field portion of 40 K spectra using samples containing ^{56}Fe ($I = 0$) and ^{57}Fe ($I = {}^1/_2$).

We have also shown[4] that the 3Fe cluster can be converted into a structure with a cubane Fe_4S_4 core. This conversion occurs with facility upon incubation of the protein with excess Fe^{2+} in the presence of dithiothreitol. Similar conversions have been reported for aconitase.[5] The facility of the $Fe_3S_4 \rightarrow Fe_4S_4$ conversions has suggested to us that one may be able to incorporate other metals into the vacant sites of a Fe_3S_4 cluster and thus generate a series of novel clusters. We report here evidence for the formation of a structure with a cubane $CoFe_3S_4$ core.

Fd II was purified and then incubated with excess metal similarly to the procedure described.[4] Typically 0.5 mL of dithionite-reduced Fd II, 0.5 mM in Fe_3S_4, was anaerobically incubated for 6–12 h with 15 mM $Co(NO_3)_2$ and 5 mM dithiothreitol and then repurified as described.[4] Addition of sulfide was not required. Metal analysis of four samples by plasma emission spectroscopy yielded, after correction for unconverted Fe_3S_4, (3 ± 0.3) Fe/Co. We call aerobically purified material the *oxidized* Co–Fe sample; this material is EPR-active. Upon addition of dithionite a *reduced*, EPR-silent, state was obtained.

Figure 1A (middle trace) shows an EPR spectrum of an oxidized sample. The spectrum exhibits eight well-resolved ^{59}Co ($I = {}^7/_2$) hyperfine lines centered around $g_z = 1.98$. The high-field portion of the g_z resonance is superimposed on a derivative-type feature at $g_y \approx 1.94$; the third principal resonance is centered at $g_x \approx 1.82$. Thus the spectrum of our *oxidized* sample is similar to the "$g = 1.94$" signals of *reduced* ($[Fe_4S_4]^+$) clusters. A spectral simulation (upper trace of Figure 1A) yielded $g_x \approx 1.82$, $g_y \approx 1.94$, $g_z = 1.98$ $A_x \approx A_y \approx 0$ mT, $A_z = 4.4$ mT, and line widths of 20, 15, and 2 mT along x, y, and z, respectively. A_x and A_y are quite uncertain because these parameters are strongly correlated with the widths along x and y.

In Figure 1B we show in an expanded view the first three low-field resonances for samples containing ^{56}Fe (lower trace) and ^{57}Fe (upper trace). The observation of line broadening of 0.6 mT by ^{57}Fe of the "^{59}Co hyperfine resonances" demonstrates that the EPR signal results from a cluster containing both Co and Fe, suggesting the Co has been incorporated into the vacant site of the Fe_3S_4 cluster. The observations of EPR signals around $g = 2$ suggests that the system has a spin $S = {}^1/_2$. Quantitation of the 40 K EPR signal against a copper perchlorate standard gave repeatedly ≈1 spin/Co. We have observed no other EPR-active species in either oxidized or reduced material, suggesting that the samples are free of adventitiously bound Co(II).

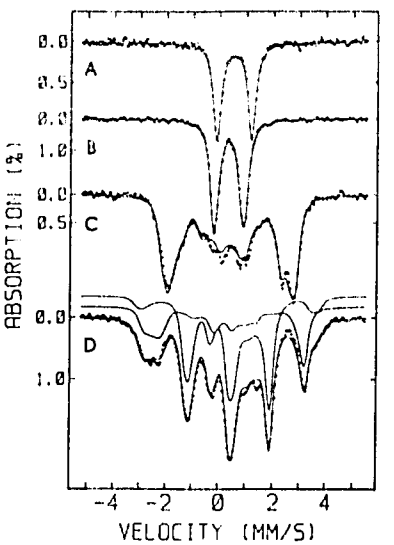

Figure 2. Mössbauer spectra of reduced (A) and oxidized (B–D) CoFe cluster. (A) Dithionite reduced sample at 4.2 K in zero applied field; (B) oxidized sample at T = 183 K, (C and D) oxidized sample at 4.2 K in 60 mT and 6.0 T parallel fields, respectively. Solid lines in (C) and (D) are computer simulations with parameters of Table I. Theoretical spectra of subsites I (two Fe atoms) and II are shown separately in (D).

Table I. Hyperfine Parameters of Oxidized Co–Fe Cluster at 4.2 K

	site I[a]	site II
A_x, MHz[b]	−35	+27
A_y, MHz	−38	+27
A_z, MHz	−31	+32
ΔE_Q, mm/s	+1.35	−1.1
η	0.4	0.4
δ, mm/s[c]	0.44	0.35

[a] Two equivalent Fe belong to site I. [b] Since $\tilde{g}$ is quite isotropic, the labels x, y, and z have no spatial relation to the g_x, g_y, and g_z. See ref 8. [c] Isomer shifts are quoted relative to Fe metal at 298 K.

The lower trace in Figure 1A shows a 9 K EPR spectrum recorded under conditions where the signal of the Co–Fe cluster is partially saturated. The resonance at $g = 2.01$ belongs to unconverted Fe_3S_4 clusters.[1] Thus, the EPR spectra (as well as the Mössbauer spectra) allow us to estimate the conversion yield. For five preparations we determined that 55%, 73%, 85%, 89%, and 94% of the total Fe belonged to $CoFe_3S_4$ clusters, with the remainder in unconverted Fe_3S_4. Typically 60–70% of the starting material was recovered.

The Mössbauer spectra of two samples[6] are shown in Figure 2. At 183 K the spectra of the oxidized Co–Fe cluster (Figure 2B) consist of one slightly asymmetric doublet (suggesting inequivalent irons) with quadrupole splitting $\Delta E_Q = 1.10$ mm/s and isomer shift $\delta = 0.36$ mm/s. At 4.2 K the spectra exhibit paramagnetic hyperfine interactions. The response of the spectral intensities to weak applied fields[7] shows that the spectra result

(4) Moura, J. J. G.; Moura, I.; Kent, T. A.; Lipscomb, J. D.; Huynh, B. H.; LeGall, J.; Xavier, A. V.; Münck, E. *J. Biol. Chem.* **1982**, *257*, 6259–6267.
(5) Kent, T. A.; Dreyer, J.-L.; Kennedy, M. C.; Huynh, B. H.; Emptage, M. H.; Beinert, H.; Münck, E. *Proc. Natl. Acad. Sci. U.S.A.* **1982**, *79*, 1096–1100.

(6) The raw data contained contributions from unconverted 3Fe clusters. The sample of Figure 2A contained 6% of Fe_3S_4 according to EPR and an undetectable amount of Fe_3S_4 according to the Mössbauer data (the Mössbauer sample was quite dilute). Both techniques suggest 25–30% unconverted Fe_3S_4 for the sample of Figure 2B–D. For clarity we have subtracted the spectral contributions of Fe_3S_4 from the raw data to obtain the spectra of Figure 2B–D.
(7) Münck, E. *Methods Enzymol.* **1978**, *54*, 346–379.

from three iron atoms residing in the cluster which yields the observed EPR signal. Analyses of the 4.2 K spectra reveals two distinct sites with occupancy ratio of 2:1. We have described the data by the spin Hamiltonian ($S = {}^1/_2$)

$$\hat{H} = \beta\vec{S}\cdot\vec{g}\cdot\vec{H} + \sum_{i=1}^{2}[\vec{S}\cdot\vec{A}(i)\cdot\vec{I}(i) - g_n\beta_n\vec{H}\cdot\vec{I}(i) + H_{quad}(i)]$$

where i designates the two distinct sites. For details of such analyses see ref 8. The solid lines in Figure 2C,D are simulations using the parameters of Table I. The hyperfine tensors of the two types of Fe sites have different signs, an indication of a spin-coupled system.

Figure 2A shows a 4.2 K spectrum ($\Delta E_Q = 1.28$ mm/s and $\delta = 0.53$ mm/s) of a dithionite-reduced sample. In strong applied fields the spectra (not shown) exhibit magnetic hyperfine structure; i.e., the complex is paramagnetic with integer spin S.

The values for δ, which is a useful oxidation state marker, can be compared with those[4] of the Fe_4S_4 cluster produced by reconstitution of apo-Fd II. The average shift $\delta_{av} = 0.41$ mm/s of the oxidized Co–Fe cluster compares well with $\delta_{av} = 0.44$ mm/s of the $[Fe_4S_4]^{2+}$ cluster. Likewise, $\delta_{av} = 0.53$ mm/s of the reduced Co–Fe cluster is very similar to $\delta_{av} = 0.57$ mm/s observed[4] for $[Fe_4S_4]^{+}$. These observations, as well as the EPR results, suggest that a $[CoFe_3S_4]^{2+}$ cluster is isoelectronic with a $[Fe_4S_4]^{+}$ cluster.

In summary, the Mössbauer and EPR studies as well as chemical analysis suggest the presence of a novel cluster with a $CoFe_3S_4$ core. The formation of a $CoFe_3S_4$ cluster in Fd II shows that Fe_3S_4 clusters, incorporated into a protein matrix, can serve as promising precursors for the formation of novel clusters. We have preliminary evidence for the formation of a cluster containing copper.

Acknowledgment. We thank Dr. J. D. Lipscomb for making his EPR facility available and P. Kelly, N. Hart, and the staff of the University of Georgia Fermentation Plant for growing *D.gigas* cells. This work was supported by the National Science Foundation, the National Institutes of Health, the Instituto de Investigação Cientifica Tecnologica, the Junta Nacional de Investigação Cientifica Tecnologica, and the Agency for International Development.

(8) Christner, J. A.; Janick, P. A.; Siegel, L. M.; Münck, E. *J. Biol. Chem.* **1983**, *258*, 11157–11164.

B-11

MINISYMPOSIA

1. *Ni-Biochemistry*
Convener: J.J.G. Moura
(Lisboa)

MS1.1 — MO

J.J.G. MOURA
M. TEIXEIRA
I. MOURA
A.V. XAVIER
Centro de Química Estrutural
U.N.L., Complexo I, I.S.T.
Av. Rovisco Pais, 1000 Lisboa
Portugal
J. LEGALL
Department of Biochemistry
University of Georgia
Athens, Georgia 30602
U.S.A.

DESULFOVIBRIO GIGAS HYDROGENASE; CATALYTIC CYCLE AND ACTIVATION PROCESS

Desulfovibrio gigas [NiFe] hydrogenase (E.C. 1.12.2.1) has a molecular weight of 89 kD (two subunits of 63 kD and 26 kD) and contains 1 gatm of nickel, 11 gatm of iron and 11-12 gatm of sulfide [1].

1 — NATIVE STATE

IRON-SULFUR-CENTERS

Mössbauer and EPR spectroscopic studies established that in the purified enzyme the iron-sulfur clusters are arranged in a $[Fe_3S_4]_{ox}$ cluster (EPR active) and two $[Fe_4S_4]^{2+}$ clusters (EPR silent) [2]. The $[Fe_3S_4]_{ox}$ cluster is the origin of an almost isotropic EPR signal centered around g = 2.02, observable below 30 K. The Mössbauer parameters of the $[Fe_4S_4]$ clusters (quadrupole splitting of 1.16 mm/s and isomeric shift of 0.46 mm/s, at 4.2 K) are typical of 4Fe centers in the +2 oxidation level [2].

NICKEL CENTER

In the native preparations, a rhombic EPR signal with g-values at 2.31, 2.23 and 2.02 (*Ni-signal A*) is observed up to 120 K (Fig. 1). This rhombic signal, assigned to nickel(III), accounts for 50-100% of the chemically detectable nickel depending on preparation. This assignment was confirmed by the observation of hyperfine coupling in ^{61}Ni-isotopic replaced hydrogenase [3]. A minor species can also be detected at g-values 2.33, 2.16 and ~2.0 (*Ni-Signal B*, Fig. 1). The relative intensities of *Ni-Signals A* and *B* varies with preparation and can be altered by anaerobic redox cycling of the enzyme. This indicates that there exists different Ni(III) environments in the oxidized enzyme.

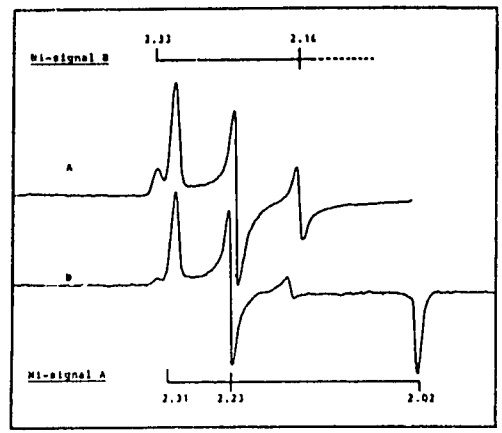

Fig. 1
EPR spectra of D. gigas *[NiFe] hydrogenase, recorded in a Bruker ER-200 II spectrometer, equipped with an Oxford Instruments continuous flow cryostat.*
A) and B) — Two different preparations of the enzyme. Temperature 100 K, modulation amplitude 1 mT, microwave power 2 mW, frequency 9.34 GHz

215

2 — INTERMEDIATE OXIDATION STATES

The first event occuring during the anaerobic reduction of *D. gigas* with hydrogen is the disappearance of *Ni-Signals A* and *B* and the isotropic g = 2.02 signal due to the $[Fe_3S_x]$ clusters [4]. An EPR silent state is then attained. Further reduction of the enzyme under H_2 atmosphere is accompanied by the development of a new rhombic EPR signal with g-values at 2.19, 2.16 and 2.02 (*Ni-Signal C*, Fig. 2-A). This signal was also attributed to a nickel species by the ^{61}Ni isotopic substitution [3].

During the course of the reduction experiment *Ni-Signal C* attains a maximum intensity (40-60% of the chemically detectable nickel). Longer incubation time under H_2 yields an EPR silent state, when measured at 77 K. At low temperature (below 15 K) EPR signals typical of $[Fe_4S_4]^{1+}$ clusters are observed [5].

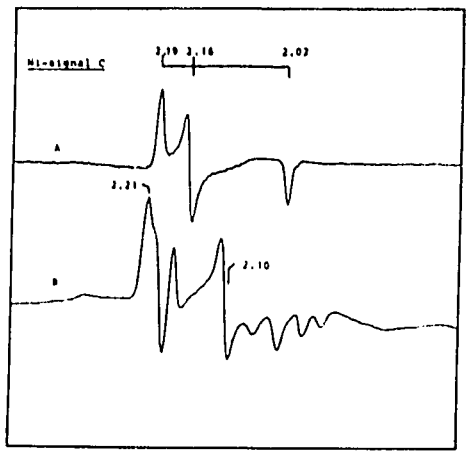

Fig. 2

EPR spectra of intermediate redox states of D. gigas *[NiFe] hydrogenase, in the presence of hydrogen. Experimental conditions as in Fig. 1.*

A) Temperature 77 K, microwave power 2 mW.

B) Same as A, at 4.2 K, microwave power 2 mW

At redox states of the enzyme such that *Ni-Signal C* develops, low temperature studies reveal the presence of another EPR active species: below 10 K, the shape of the EPR spectra changes drastically and a new set of signals at g = 2.21, 2.10 and broad components at higher field is clearly discernible at 4 K (Fig. 2-B). This set of g-values exhibits different power dependence from that of *Ni-Signal C* (readily saturated with low microwave power, typical of a slow relaxation species). The origin of the "2.21" signals is under discussion. Since these signals are only observable at low temperature with high microwave power levels (fast relaxing species), they may originate from an iron-sulfur center. Since the g-values appear to be too high, another explanation is that they originate from the Ni-center weakly interacting with another paramagnetic center in the vicinity (*e.g.* iron-sulfur center).

3 — MID-POINT REDOX POTENTIALS

Redox transitions were observed at -70 mV (measured by the disappearance of the 2.02 signal) and -220 mV (measured by the disappearance of the *Ni-Signal A* (Fig. 3 - insert A)). Only the second redox transition is pH dependent, with a slope of ~ −60 mV per pH unit [6]. *Ni-Signal C* develops at a mid-point redox potential below -300 mV, reaches a maximum around -350 mV and disappears below -400 mV (Fig. 3).

LISSOLO *et al.* [7] determined the activity of the enzyme as a function of the redox potential. Their study indicates that the hydrogenase activation is a one-electron process with a mid-point redox potential around -340 mV (Fig. 3 - insert B). This value correlates with the appearance of *Ni-Signal C*, suggesting that this signal may represent an activated state of the enzyme.

4 — ACTIVATION PROCESS AND CATALYTIC CYCLE

The definition of the role of the nickel during the redox cycle of [NiFe] hydrogenases requires the assignment of the oxidation states involved, the characterization of the ligation mode of the nickel center, as well as the elucidation of possible interactions between the redox centers.

The simplest interpretation of our redox data involves a redox scheme that requires the transition from Ni(III) to Ni(0). However, nickel chemistry shows that the very high and very low oxidation states are not stable chemical species; very negative and very positive redox potentials are associated with the transitions Ni(I) ⇌ Ni(0) and Ni(III) ⇌ Ni(II), respectively. Also, the Ni(III)/Ni(II)

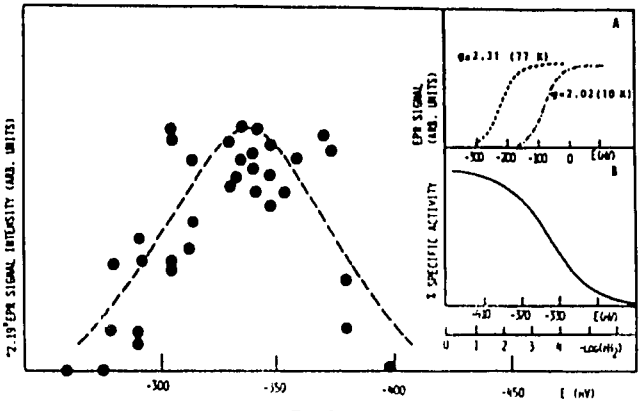

Fig. 3

EPR signal intensity (arbitrary units) of the Ni-signal C *in function of the redox potential. EPR signals were measured at 77 K. No attempt was made to fit the experimental points to a Nernst equation.*
Insert A — Redox titration followed at g = 2.02 (10 K) and g = 2.31 (77 K), data from reference [2].
Insert B — Activation profile of D. gigas *[NiFe] hydrogenase at different partial pressures of hydrogen, data from reference [7]*

chemistry offers a wide range of versatile properties namely: facile rearrangement of ligands, spin and conformational equilibria as well as alteration of the type and number of ligand in the nickel coordination sphere. The redox potential of the Ni(III)/Ni(II) couple can be brought, in principle, to physiological levels by preferential stabilization of the Ni(III) state. Thus, the utilization of fewer redox states seems more realistic in terms of the nickel chemistry.

Another important point to consider in the reactional mechanism of hydrogenase is that the so-called "oxygen stable" [NiFe] hydrogenases (*e.g. D. gigas* hydrogenase) are not fully active in the "as isolated" state. Studies of the hydrogenase activity [7] indicate that the enzyme must go through a lag phase as well as an activation one, in order to be fully active. This complex phenomenon seems to envolve the removal of oxygen (lag phase) followed by a reduction step (activation phase).

Taking into consideration the hydrogenase activity studies, the plausibility of the Ni(III) ⇄ Ni(II) redox cycling scheme, and the sequence of events observed by EPR spectroscopy upon exposure to H_2 atmosphere, a model is proposed for the mechanism of the [NiFe] hydrogenases in the context of both the catalytic and the activation processes:

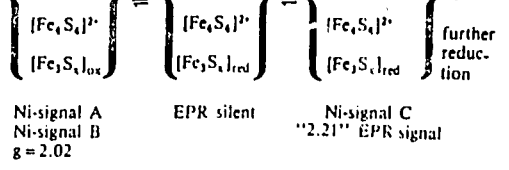

Ni-signal A
Ni-signal B
g = 2.02

EPR silent

Ni-signal C
"2.21" EPR signal

The "as isolated" state is fully characterized. EPR and Mössbauer studies in the enzyme "as isolated" [2] indicate that there is no magnetic interaction between these four redox centers.
The active state of the enzyme is EPR silent. During this activation process, both the isotropic g = 2.02 and the nickel signal disappear. The loss of the g = 2.02 signal is attributed to the reduction of the $[Fe_3S_4]$ cluster, $E_0 = -70$ mV (EPR silent $[Fe_3S_4]_{red}$).
In order to retain the Ni(III)/Ni(II) redox scheme, the disappearance of *Ni Signal A* and/or *Ni Signal B* requires a more complicated mechanism. We propose that one of the $[Fe_4S_4]$ clusters is reduced into a $[Fe_4S_4]^{1+}$ state (S = 1/2) and the reduced cluster is spin coupled with the Ni(III) center resulting in an EPR silent state. This proposal implies that the previously determined redox potential, -220 mV, for the disappearance of *Ni-Signal A* [2] is actually the mid-point redox potential for

one of the $[Fe_4S_4]$ clusters. Such a mechanism is supported by the optical studies which indicate that the activation process involves the reduction of iron-sulfur clusters. Preliminary Mössbauer data (our unpublished results in collaboration with B.H. Huynh) also show that approximately one $[Fe_4S_4]$ cluster is reduced in the EPR silent state and it is possible to recognize the normal "signature" of the reduced 3Fe cluster.

The events which follow the EPR silent state are the appearance of both the *Ni-Signal C* and the "g = 2.21" signal. In accordance with the heterolytic mechanism of hydrogen activation, we propose that in the presence of the natural substrate a hydride intermediate state is obtained. The nickel center is assigned as the hydride binding site and the $[Fe_4S_4]^{+1}$ cluster is the proton binding site. The spin coupling between the Ni(III) and the $[Fe_4S_4]^{1+}$ cluster is broken in this hydride intermediate, originating *Ni-Signal C*. Thus, this signal is assumed to represent the hydride-bound Ni(III) center and the g = 2.21 is attributed to the proton--bound $[Fe_4S_4]^{1+}$ cluster. Alternatively, the g = 2.19 EPR signal could be due to a transient Ni(III) state in a different coordination, resulting from the breaking of the coupling and the g = 2.21 signal could be due to the interacting Ni(III) and $[Fe_4S_4]^{1+}$ centers bound to hydride and proton, respectively. By further incubation with H_2 the *Ni-Signal C* disappears, suggesting reduction to Ni(II) with the concomitant development of reduced $[Fe_4S_4]$ center signals.

ACKNOWLEDGEMENTS

We thank Drs. T. Lissolo, B.H. Huynh, H.D. Peck Jr., and D.V. DerVartanian for very interesting discussions. This research was supported by grants from Instituto Nacional de Investigação Científica, Junta Nacional de Investigação Científica e Tecnológica, AID Grant 936-5542-G-SS-4003-00 and NATO Grant 0341/83.

REFERENCES

[1] J. LeGall, P.O. Ljungdahl, I. Moura, H.D. Peck Jr., A.V. Xavier, J.J.G. Moura, M. Teixeira, B.H. Huynh, D.V. DerVartanian, *Biochem. Biophys. Res. Commun.*, 106, 610-616 (1982).

[2] M. Teixeira, I. Moura, A.V. Xavier, D.V. DerVartanian, J. LeGall, H.D. Peck Jr., B.H. Huynh, J.J.G. Moura, *Eur. J. Biochem.*, 130, 481-484 (1983).

[3] J.J.G. Moura, I. Moura, B.H. Huynh, H.J. Krüger, M. Teixeira, R.C. DuVarney, D.V. DerVartanian, A.V. Xavier, H.D. Peck Jr., J. LeGall, *Biochem. Biophys. Res. Commun.*, 408, 1388-1393 (1982).

[4] J.J.G. Moura, M. Teixeira, I. Moura, A.V. Xavier, J. LeGall, *J. Mol. Cat.*, 23, 303-314 (1984).

[5] M. Teixeira, I. Moura, A.V. Xavier, B.H. Huynh, D.V. DerVartanian, H.D. Peck Jr., J. LeGall, J.J.G. Moura, *J. Biol. Chem.* (1985) in press.

[6] R. Cammack, D. Patil, R. Aguirre, E.C. Hatchikian, *FEBS Lett.*, 142, 289-292 (1982).

[7] T. Lissolo, S. Pulvin, D. Thomas, *J. Biol. Chem.*, 259, 11725-11729 (1984).

MS1.2 — MO

S.P.J. ALBRACHT
J.W. VAN DER ZWAAN
R.D. FONTIJN
E.C. SLATER
Laboratory of Biochemistry
University of Amsterdam
P.O. Box 20151, 1000 HD Amsterdam
The Netherlands

HYDROGENASE FROM *CHROMATIUM VINOSUM*: THE REDOX STATES OF NICKEL AND THE IRON-SULPHUR CLUSTER DURING CATALYSIS

The presence of nickel in a purified hydrogenase was first reported in 1981 by Graf and Thauer [1] for the enzyme from *Methanobacterium thermoautotrophicum*. EPR spectroscopy [2] showed that virtually all nickel was present as low-spin Ni(III) which could be reduced with H_2. No signals due to Fe-S clusters were observed. Hydrogenase from *Chromatium vinosum*, also a nickel--enzyme, clearly displays two signals in the $g = 2$ region which could be ascribed to Fe-S clusters [3]. An analysis of the 4 different EPR signals that can be detected in the enzyme as isolated led to the following hypothesis [3-5]. The preparation contains intact and defect enzyme molecules. Defect molecules, which are unreactive in the standard activity assays with viologens, contain one Ni(III) ion and one $[3Fe\text{-}xS]^{0+}$ cluster. Two forms of Ni(III), Ni-a and Ni-b, can be detected. Their ratio varies from preparation to preparation. In-

218

B-12

PSI.21 — TU

A.R. LINO
A.V. XAVIER
I. MOURA
Centro de Química Estrutural
and
UNL, Complexo I,
IST, Av. Rovisco Pais, 1000 Lisboa
Portugal
J. LEGALL
L.G. LJUNGDAHL
Department of Biochemistry
University of Georgia
Athens, Georgia 30602
U.S.A.

COBALT CONTAINING B_{12} COFACTORS FROM METHANOGENIC BACTERIA — SPECTROSCOPIC CHARACTERIZATION

Methanogens are primitive organims that use the reduction of CO_2 by H_2 to methane as a terminal metabolic electron transfer reaction [1]. They belong to a bacterial group designated as "archaebacteria", which are distantly related in the evolutive scale to eucharyotes and to the strict anaerobic bacteria such as clostridia and sulfate reducing bacteria.

Several electron carriers and factors, unique to methanogens, have been isolated from these bacteria (including F_{420}, coenzyme M, factors F_{430} and F_{342}).

Recently, a B_{12} containing protein was isolated from *Methanosarcina barkeri* (DSM 800) [2]. This protein contains bound aquocobalamine and when the cofactor is reduced and methylated with ^{14}C-methyl iodide, the resultant ^{14}C-methyl B_{12} protein is extremely active in the biosynthesis of ^{14}C-labeled methane [2].

Two B_{12} proteins have now been isolated from *M. barkeri* (DSM 800 and 804). The visible spectra of native B_{12} proteins from both strains are very similar and characteristic of bound aquocobalamine (Fig. 1). The enzyme cofactor can be reduced with mercaptoethanol or borohydride and methylated by methyl iodide, producing the methyl B_{12} form of the protein (Fig. 1). The methylated form of the enzyme can be converted by photolysis to a stable low-spin Co^{II} complex.

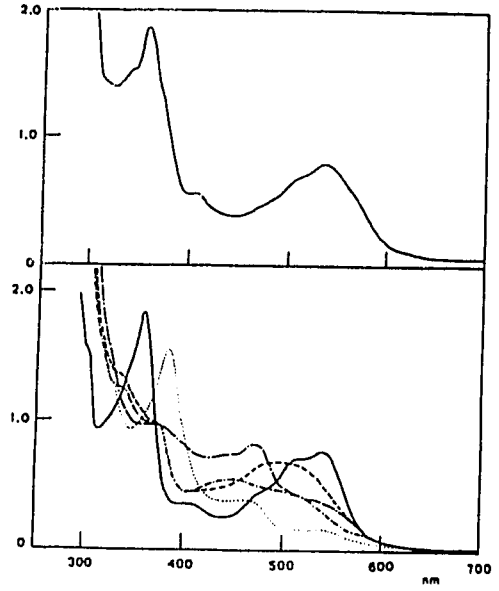

Fig. 1

(A) Absorption spectra of B_{12} containing protein from M. barkeri *(DSM 804) in the native form. (B) Absorption spectra of B_{12} containing protein from* M. barkeri *(DSM 800) in the native form (———), reduced with BH_4^- after 2 hours of reduction (·····), methylated with CH_3I (------) and after photolysis under reducing conditions*

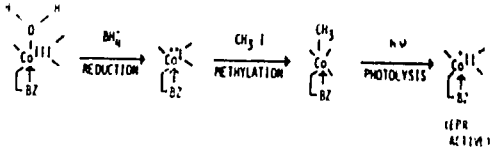

Amino-acid composition, cobalt and molecular weight of both proteins is shown in Table I. The proteins show similar amino-acid composition and the same Co content per monomer, in spite of their different oligomerization forms.

The corrinoids were extracted and purified from cell extracts and also from the purified proteins in their cyano form according to BERNHAUER *et al.* [3]. Different corrinoids are present in the cell ex-

29

Table I
Amino Acid Composition of M. barkeri *(DSM 800 and 804) B_{12} Protein*

Amino-acids	B_{12} protein from *M. barkeri* (DSM 800)		B_{12} Protein from *M. barkeri* (DSM 804)	
	from analysis	nearest integer	from analysis	nearest integer
Lysine	12.8	13	12.2	12
Hystidine	3.9	3	3.8	4
Arginine	4.2	4	4.6	5
Tryptophan	n.d.	n.d.	n.d.	n.d.
Aspartic Acid	17.2	17	18.4	18
Threonine	8.0	9	9.5	10
Serine	6.5	7	7.4	8
Glutamic Acid	20.9	21	18.7	19
Proline	7.1	7	7.1	7
Glycine	1.5	15	15.0	15
Alanine	18.3	18	15.3	15
Cysteine (Half)	n.d.	n.d.	3.2	4
Valine	11.9	12	12.5	13
Methionine	6.0	7	5.4	6
Isoleucine	10.0	10	9.9	10
Leucine	13.0	13	12.5	13
Tyrosine	4.4	5	4.5	5
Phenylalanine	5.6	6	4.5	5
Total Residues		168		169
Cobalt		1		1
Mol. Weight (subunit)		72 000 (18 100) α_4		50 000 (17 800) α_3

tract. The major one (~ – 90% of total) was completely purified and analysed. The visible spectra of dicyano and monocyano complexes of this corrinoid are shown in Fig. 2. The nuclear magnetic resonance spectra of this corrinoid as well as that of the corrinoid from the holoenzyme, are shown in Fig. 3. The NMR spectra of the corrinoids present six resonances in the aromatic region. Two of these resonances come from a *meso* (C-H) and a ribose (C_1-H) proton. The other four are assigned to base protons showing that the 5,6--dimethylbenzimidazole is replaced by 5--hydroxibenzimidazole. No resonance is observed in the region between 2 and 4 ppm, which could account for a metoxy group, showing that in *M. barkeri* factor III (and not factor III_m) is the corrinoid present in larger quantities. The corrinoid extracted from the purified B_{12} containing protein

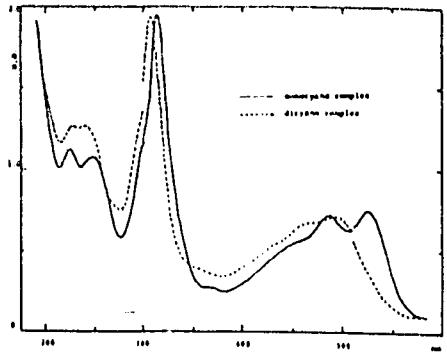

Fig. 2
Absorption spectra of 5-hydroxybenzimidazolcobalamine extracted from cells of M. barkeri *(DSM 800) in the monocyano and dicyano complex forms*

is spectroscopically identical to that isolated from the cells. The NMR spectra shown in Fig. 3 closely resembles the one published for factor III by Hensens *et al.* [4].

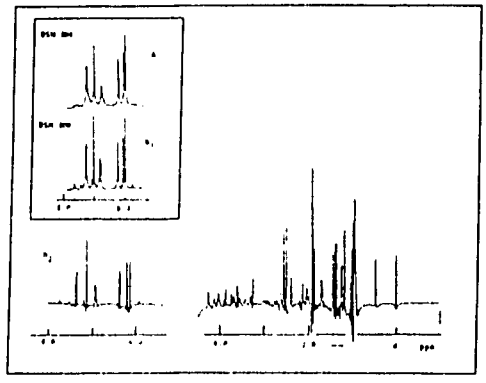

Fig. 3
300 MHz ^1H NMR spectra of factor III (5--hydroxybenzimidazolcobalamine) from M. barkeri. *(A) Corrinoid extracted from the purified B_{12} protein from* M. barkeri *(DSM 804); (B1) Corrinoid extracted from the purified B_{12} protein from* M. barkeri *(DSM 800); (B2) Corrinoid extracted from cells of* M. barkeri *(DSM 800)*

When the methyl B_{12} protein (from both strains) or the methyl extracted corrinoids are photolysed under reducing conditions, an EPR spectra at 77 K depicts typical signals of a stable Co^{II} complex (Fig. 4). Triplets are observed from the N-hyperfine interaction of the coordinated benzimidazole base showing that the nucleotide base is coordina-

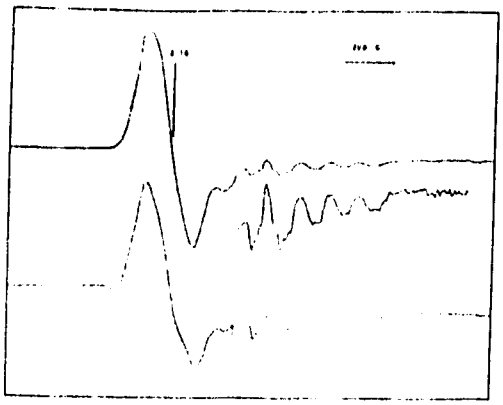

Fig. 4

(A) EPR spectra of B_{12} containing protein from M. barkeri *(DSM 800); (B) EPR spectra of the extracted corrinoid from cells of* M. barkeri *(DSM 800).*

Both methyl B_{12} protein and methyl extracted corrinoids were photolyzed under reducing conditions.

EPR Conditions: Microwave frequency 9.28 GHz; Temperature 77 K; Microwave power 20 mW; Field modulation 2 mT; Gain 8×10^4

ted to the cobalt both in its bound form to the protein and in the free form.

M. barkeri is until now the only methanogen where the presence of a B_{12} protein was reported [2,5]. In these bacteria it was shown that factor III is the most abundant corrinoid in the cells and that it is also the corrinoid associated with the B_{12} protein.

Although the physiological role of these proteins is not yet clearly established, they seem to be involved in the biosynthesis of CH_3S-CoM or CH_4 from CH_3OH [2].

ACKNOWLEDGEMENTS

Work supported by INIC, JNICT, U.S.A.I.D. and Quatrum.

REFERENCES

[1] J.G. Zeikus, *Bact. Rev.*, 41, 515-541 (1977).

[2] J.M. Wood, I. Moura, J.J.G. Moura, H. Santos, A.V. Xavier, J. LeGall, M. Scandellari, *Science*, 216, 303-305 (1982).

[3] K.Bernhauer, G. Wilharm, *Arch. Biochem. Biophys.*, 83, 248 (1939).

[4] O.D. Hensens, H.A.O. Hill, C.E. McClelland, R.J.P. Williams, in D. Dolphins (ed.), «B_{12}», vol. 1, Wiley, New York, 1092, pp. 463-500.

[5] P. Van der Meijden, H.J. Heythuysen, A. Powels, F.P. Howen, C. Van der Drift, G.D. Vogly, *Arch. Microbiol.*, 134, 238-242 (1983).

PS1.22 — TH

TINY VAN HOUWELINGEN
G.W. CANTERS
J.A. DUINE
J. FRANK, JZN.
G. STOBBELAAR
Department of Chemistry
Gorlaeus Laboratories
State University Leiden
P.O. Box 9502, 2300 RA Leiden
The Netherlands
and
Biochemical Laboratory
Technical University Delft
Julianalaan 67-67a, 2628 BC, Delft
The Netherlands

A BLUE COPPER PROTEIN FROM *THIOBACILLUS VERSUTUS*

The multifarious coordinating capabilities of copper are reflected by the variety of metalloproteins in which Cu occupies the catalytically active site. The usual classification of copper proteins distinguishes between three or four types [1].

As more and more copper proteins are discovered and characterised, it is becoming clear that within each class diversity reigns. For instance, for the type I blue copper proteins, the most extensively studied class up till now, it has been found that redox potentials may vary from 180 to 760 mV, molecular weights from 10 to 20 kD and pI points from 4 to 11. Most intriguing is the coordination of the Cu. It has been demonstrated by crystallographic techniques in a number of cases that the metal is surrounded in a distorted tetrahedral fashion by an N_2SS^* coordination [2-4]. The nitrogens are provided by two histidines and the sulfurs derive from a methionine and a cysteine. However, stellacyanin lacks methionine and Russian researchers have reported a blue copper protein which does not seem to contain cysteine [5,6]. It is not understood how the details of the Cu coordination relate to the spectroscopic properties and the redox potential of the protein and further structural studies and a search for new type I copper proteins are needed.

B-13

Biochimie, 68 (1986) 75–84
© Société de Chimie biologique / Elsevier, Paris

Redox properties and activity studies on a nickel-containing hydrogenase isolated from a halophilic sulfate reducer *Desulfovibrio salexigens*

M. TEIXEIRA*, I. MOURA*, G. FAUQUE**, M. CZECHOWSKI**, Y. BERLIER**, P.A. LESPINAT**, J. LE GALL**, A.V. XAVIER* and J.J.G. MOURA*

* *Centro de Quimica Estrutural and UNL, Complexo I, IST, Av. Rovisco Pais, 1000 Lisbon, Portugal*
** *ARBS, Equipe Commune d'Enzymologie CNRS-CEA, CEN Cadarache, 13108 Saint-Paul-lez-Durance, France*

(*Received 12-7-1985, accepted 12-9-1985*)

Summary — A soluble hydrogenase from the halophilic sulfate reducing bacterium *Desulfovibrio salexigens*, strain British Guiana (NCIB 8403) has been purified to apparent homogeneity with a final specific activity of 760 μmoles H_2 evolved/min/mg (an overall 180-fold purification with 20 % recovery yield). The enzyme is composed of two non-identical subunits of molecular masses 62 and 36 kDa, respectively, and contains approximately 1 Ni, 12-15 Fe and 1 Se atoms/mole. The hydrogenase shows a visible absorption spectrum typical of an iron-sulfur containing protein (A_{400} A_{280} = 0.275) and a molar absorbance of 54 $mM^{-1}cm^{-1}$ at 400 nm.

In the native state (as isolated, under aerobic conditions), the enzyme is almost EPR silent at 100 K and below. However, upon reduction under H_2 atmosphere a rhombic EPR signal develops at g-values 2.22, 2.16 and around 2.0, which is optimally detected at 40 K. This EPR signal is reminiscent of the *nickel signal C* (g-values 2.19, 2.16 and 2.02) observed in intermediate redox states of the well characterized *D. gigas* nickel containing hydrogenase and assigned to nickel by ^{61}Ni isotopic substitution (J.J.G. Moura, M. Teixeira, I. Moura, A.V. Xavier and J. LeGall (1984), *J. Mol. Cat.*, 23, 305-314). Upon longer incubation with H_2 the "2.22" EPR signal decreases. During the course of a redox titration under H_2, this EPR signal attains a maximal intensity around −380 mV. At redox states where this "2.22" signal develops (or at lower redox potentials), low temperature studies (below 10 K) reveals the presence of other EPR species with g-values at 2.23, 2.21, 2.14 with broad components at higher fields. This new signal (fast relaxing) exhibits a different microwave power dependence from that of the "2.22" signal, which readily saturates with microwave power (slow relaxing). Also at low temperature (8 K) typical reduced iron-sulfur EPR signals are concomitantly observed with $g_{med} \sim 1.94$. The catalytic properties of the enzyme were also followed by substrate isotopic exchange D_2/H^+ and H_2 production measurements.

* *To whom correspondence should be addressed*

Abbreviations
EPR = *electron paramagnetic resonance*

The general properties of the *D. salexigens* hydrogenase are compared with those of [NiFe] hydrogenases isolated from other sulfate reducers from the genus *Desulfovibrio*.

nickel / iron-sulfur clusters / hydrogenase / *Desulfovibrio* sp. / oxidation-reduction / EPR

Résumé — *Une hydrogénase soluble a été purifiée jusqu'à homogénéité apparente à partir de la bactérie sulfato-réductrice* Desulfovibrio salexigens *souche British Guiana (NCIB 8403). L'activité spécifique finale était de 760 µmoles H_2 produit / min / mg, soit une purification totale de 180 fois et un rendement de 20 %. L'enzyme est composée de deux sous-unités de masses moléculaires respectives 62 et 36 kDa et elle contient approximativement 1 atome de Ni, 12 à 15 atomes de Fe et 1 atome de Se par mole. L'hydrogénase présente un spectre d'absorption dans le visible typique d'une protéine à centres fer-soufre (A_{1} / A_{2} = 0,275) avec un coefficient d'extinction molaire de 54 mM^{-1} cm^{-1} à 400 nm.*

A l'état natif (sous conditions aérobies), l'enzyme ne présente pratiquement pas de signaux RPE à température égale ou inférieure à 100 K.

Cependant, après réduction sous atmosphère d'hydrogène, un signal RPE rhombique avec des valeurs g de 2,22, 2,16 et environ 2,0 peut être détecté préférentiellement à 40 K. Ce signal rappelle celui du nickel C (valeurs g de 2,19, 2,16 et 2,02) observé avec l'hydrogénase à nickel de D. gigas *dans des états intermédiaires d'oxydo-réduction. Il a été attribué à ce métal par substitution isotopique avec ^{61}Ni (J.J.G. Moura, M. Teixeira, I. Moura, A.V. Xavier and J. Le Gall, 1984), J. Mol. Cat., **23**, 305-314).*

Après une plus longue incubation sous H_2, le signal "2,22" diminue. Par titration redox en présence de H_2, l'intensité maximale est atteinte à environ − 380 mV. Pour un potentiel égal ou inférieur à cette dernière valeur mais à température inférieure à 10 K, apparaissent d'autres signaux RPE (g 2,23, 2,21, 2,14) et des composantes larges aux champs magnétiques plus élevés. Ce nouveau signal (à relaxation rapide) présente une dépendance vis-à-vis de la puissance micro-onde différente de celle du signal "2,22" qui, lui, sature rapidement avec celle-ci (relaxation lente). A basse température également (8 K) des signaux RPE typiques des centres fer-soufre réduits sont observés avec g moyen de 1,94 environ. Les propriétés catalytiques de l'enzyme ont été quant à elles suivies par la réaction d'échange deutérium-proton et par la mesure de la production d'hydrogène.

Les propriétés générales de l'hydrogénase de D. salexigens *sont comparées avec celles d'autres hydrogénases à nickel isolées à partir de différentes souches de bactéries sulfato-réductrices du genre* Desulfovibrio.

nickel / centres fer-soufre / hydrogénase / espèce* Desulfovibrio / *oxydation-réduction / RPE

Introduction

Several bacterial systems use the enzyme hydrogenase in order to metabolize the simplest molecule, H_2. During the metabolic energy-yielding process, H_2 is either oxidized or evolved as the product of reduction of protons, the reaction being expressed as $H_2 \rightleftarrows 2e^- + 2H^+$. In the forward reaction, H_2 serves as an electron donor and the reaction initiates an energy yielding process. In the backward reaction, the proton serves as one of the terminal electron acceptors in anaerobic metabolism [1, 2].

Although the importance of its biological function has been recognized a long time ago, only recently have the structural features and physico-chemical properties of its prosthetic groups begun to be understood, mainly through the application of low temperature EPR studies complemented with Mössbauer spectroscopy using metal isotopic substitutions (^{61}Ni and ^{57}Fe) [3, 4, 5].

Hydrogenases are generally recognized as iron-sulfur containing proteins, with four to twelve iron atoms in different cluster arrangements : [2Fe-2S], [3Fe-xS] and [4Fe-4S].

In the last few years, through physiological, chemical and spectroscopic studies (mainly EPR), nickel was found to be a constituent of several hydrogenases.

The metabolism of molecular H_2 has figured centrally in the development of our present concepts regarding the biochemistry and physiology of *respiratory* sulfate reduction carried out by *Desulfovibrio* sp. and the hydrogenase system has been extensively studied [6].

Generally, the hydrogenases isolated from this bacterial group have been found to be confined to the periplasmic space, but membrane bound and cytoplasm located enzymes have also been reported.

The results so far obtained enabled, within the *Desulfovibrio* genus, two types of hydrogenases to be distinguished: one type containing only iron-sulfur clusters (termed [Fe] hydrogenases) and the other the nickel-iron-sulfur containing hydrogenases (termed [NiFe] hydrogenases).

Within this bacterial group, the enzyme shows a large diversity with respect to structural features (*e.g.*, the presence of subunit structure), catalytic properties (H_2 evolution versus H_2 uptake and D_2/H^+ exchange activities), activation step requirements in order to express full activity, as well as sensitivity to thermal denaturation, unfolding agents, and CO.

The [Fe] hydrogenase type has been most extensively studied in *D. vulgaris* (Hildenborough) [7, 8] and the *D. gigas* enzyme has been considered the prototype of the [NiFe] hydrogenases [9-14].

A tentative catalytic and activation scheme has already been proposed, showing the involvement of all the redox centers in the simple electron transfer process ($2H^+ + 2e^- \rightleftharpoons H_2$) carried out by this complex enzyme [13]. The improvement of this scheme and the full understanding of the behaviour of this class of enzymes prompted us to characterize [NiFe] and [Fe] hydrogenases from other *Desulfovibrio* strains.

In this paper, we describe the biochemical characterization, redox properties (monitored by electron paramagnetic spectroscopic measurements), and some relevant catalytic properties of a [NiFe] hydrogenase isolated from *Desulfovibrio salexigens* strain British Guiana (NCIB 8403). This desulfovibrione is the only well known halophilic strain within the genus. A few electron transfer proteins have been previously isolated from *D. salexigens*: a cytochrome c_3 (M, 13000) [15], a flavodoxin and a rubredoxin [16], as well as desulfoviridin and a blue protein containing molybdenum and iron-sulfur centers (our unpublished data).

Material and Methods

All chemicals and reagents were of the highest purity available.

Assays

Hydrogenase activity was assayed by the rate of H_2 evolution with sodium dithionite (15 mM) as electron donor and methylviologen (1 mM) as redox mediator [17], at 30 °C and pH 7.6. Hydrogen evolved was determined by gas chromatography using an Aerograph A-90 P3 chromatograph.

The D_2/H^+ exchange reaction was performed as previously described [18] using a mass spectrometer (VG8-80 equipped with an AI 2050 II data acquisition system).

Total iron was determined by the 2,4,6-tripyridyl-S-1,3,5-triazine (TPTZ) method [19]. Metals were also screened and quantified by plasma emission spectroscopy using a Jarrell-Ash model 750 Atomcomp.

Protein was determined by Lowry's method [20], using a bovine serum albumin standard solution purchased from Sigma.

The homogeneity of the preparations was checked on 7% polyacrylamide gel electrophoresis at pH 8.0 [21]. The subunit structure was determined on SDS polyacrylamide gel electrophoresis [22], using the following molecular mass markers (Da): phosphorylase b (94 000), bovine serum albumin (67 000), ovalbumin (43 000), carbonic anhydrase (30 000), chymotrypsinogen (25 000), soybean trypsin (20 000) and lactoalbumin (14 400).

Spectroscopic instrumentation

Electron paramagnetic resonance spectroscopy (EPR) was carried out on a Bruker 200-tt spectrometer, equipped with an ESR-9 flow cryostat (Oxford Instruments Co., Oxford, UK), and a Nicolett 1180 Computer, on which mathematical manipulations were performed. The visible/ultraviolet spectra were obtained on a Shimadzu model 260.

Oxidation-reduction potentiometric titrations

Oxidation-reduction titrations were carried out in an apparatus similar to that described by Dutton [23], equilibrating the enzyme under different partial pressures of hydrogen (using different proportions of argon + hydrogen) at 30°C and pH 8.0 (100 mM Tris-HCl buffer), in the presence of the following oxidation-reduction mediators at a final concentration of 50 μM: methylene blue (E_m = 11 mV); indigotetrasulphonate (E_m = − 46 mV); 2-hydroxy-1,4-naphthoquinone (E_m = − 145 mV); anthraquinone-2-sulphonate (E_m = − 225 mV); phenosafranine (E_m = − 255 mV); benzylviologen (E_m = − 345 mV); methylviologen (E_m = − 440 mV); *N,N*-dimethyl-3-methyl-4,4-bipyridyl (E_m = − 617 mV).

All redox potentials measured using a platinum/saturated calomel electrode system are quoted relative to the standard hydrogen electrode. The protein concentration in the titration vessel was 40 μM, as estimated by the molar absorbance coefficient. Typically,

the sample was first reduced under pure hydrogen atmosphere (1 atm) and left to equilibrate. Sample reoxidation was accomplished varying the partial pressure of H_2 gas, using the hydrogen and argon mixture. After equilibration at a fixed redox potential, a sample was transferred into an EPR tube under the titration vessel pressure and immediately frozen at 77 K for further quantification.

Growth of the microorganisms and preparation of cell crude extracts

D. salexigens strain British Guiana (NCIB 8403) was grown at 37°C on a standard lactate-sulfate medium [24] supplemented with 3 % sodium chloride. The cells were then lysed and frozen until used. They were slowly unfrozen and centrifuged at 20 000 rpm for 1.5 h. The supernatant from 250 g of cells (wet weight) was then centrifuged twice at 40 000 rpm for 2 h.

Purification of hydrogenase (Table I)

Scheme A

All purification procedures were carried out in air at 4°C and the pH of the buffers (Tris-HCl and phosphate) was 7.6 (measured at 5°C). A summary of the purification steps is presented in Table I.

The centrifuged extract was loaded onto a hydroxylapatite (Biorad) column (5 × 29 cm) and the column washed with 500 ml of 0.2 M Tris-HCl. A reverse gradient of 500 ml of 0.2 M Tris-HCl to 500 ml of 0.01 M Tris-HCl was applied. The column was then washed with 300 ml 0.01 M KPB and a phosphate linear gradient of 0.01 up to 0.4 M phosphate buffer (1000 ml of each) was set up. No hydrogenase was found in the eluent. The column was further washed with 500 ml 0.4 M phosphate buffer and the hydrogenase finally eluted from the column. About 80 % of the hydrogenase activity (in the H_2 evolution) was recovered. The hydrogenase enzyme was then concentrated to 8 ml in a Diaflow apparatus using a YM 30 membrane. It was then dialyzed against 4500 ml 0.01 M Tris-HCl. The dialysis resulted in the formation of a precipitate which redissolved in 1 M Tris-HCl. The hydrogenase activity was then redetermined in the supernatant and found to have decreased by 50 %. The resuspended pellet was checked for activity and very little was found. A spectrum of the resuspended pellet showed only cytochromes.

The dialyzed protein was diluted 1:4 with 0.01 M Tris-HCl and then applied to a DEAE-Biogel A column (5 × 34 cm). The column was washed with 200 ml of 0.01 M Tris-HCl and a linear gradient was then constructed (1000 ml of 0.01 M Tris-HCl to 1000 ml of 0.3 M Tris-HCl).

The hydrogenase was collected at a concentration of about 0.25 M Tris-HCl. About 85 % of the hydrogenase was recovered in this step of purification. The A_{400}/A_{280} ratio was 0.275 and the specific activity was 602 μmoles H_2 produced/min/mg protein. The yield of purification after this step was 30 %.

After concentration in a YM 30 membrane, this hydrogenase fraction was introduced on a LKB HPLC gel filtration column (TSK G 3000 SW) equilibrated with 0.5 M phosphate buffer at pH 7.4. By this procedure, a pure hydrogenase fraction was obtained (as judged by polyacrylamide gel electrophoresis), containing 14.5 mg of hydrogenase, with an absorbance ratio A_{400}/A_{280} of 0.275 and a specific activity of 758 units of H_2 evolved.

Scheme B

Another purification scheme was outlined in order to decrease the number of chromatographic steps. Both schemes A and B yield homogeneous preparations with the same level of specific activity.

After disruption of the cells in a French Press at 62 MPa, the crude extract was centrifuged at 8000 rpm for 2 h and the supernatant dialyzed against distilled water for 24 h. The dialyzed solution was then applied onto a DEAE-Biogel A column (6 × 34 cm) equilibrated with 0.01 M Tris-HCl. After elution with a linear gradient of 0.01-0.5 M Tris-HCl (1000 ml of each), the hydrogenase activity was found in a fraction eluted at about 0.3 M Tris-HCl. This fraction was then applied

TABLE I

Purification (Scheme A) of hydrogenase from D. salexigens *(British Guiana).*

Fractions	Protein (mg)	Total activity (μmoles H_2/min)	Specific activity (μmoles H_2/min/mg)	Exchange activity (μmoles HD + H_2/min/mg)
Crude extract	12 690	54 000	4.3	2
Hydroxylapatite column	nd	42 500	nd	nd
Dialysis and centrifugation	210	19 500	93	28
DEAE-Bio-Gel	27	16 300	602	175
HPLC	14.5	11 000	758	378

Hydrogenase activity measured by the hydrogenase evolution assay or the D_2/H^+ exchange reaction (see Materials and Methods). nd = not determined

to a hydroxylapatite column, equilibrated with 0.4 M Tris-HCl. A discontinuous gradient of 0.4-0.01 M Tris-HCl was performed and then a continuous gradient of 0.001-0.6 M phosphate (500 ml of each) was set up. The hydrogenase fractions eluted at 0.5 M phosphate were concentrated on a Diaflo Amicon with a YM 30 membrane.

Results

Purity, metal content and optical absorption spectra

The purification procedure is summarized in Table I. The hydrogenase was purified 180-fold, showing a final specific activity of 760 units in H_2 evolution. The overall recovery yield was 30 %. The enzyme is composed of two subunits of molecular masses 62 and 36 kDa.

The native state of the enzyme (aerobically isolated) shows a typical U.V./visible spectrum of a non-heme iron protein with broad bands at 400 and 280 nm, and an absorbance ratio A_{400}/A_{280} of 0.275 (Fig. 1). The molar absorbance at 400 mn is 54 $mM^{-1} cm^{-1}$.

Reduction of the enzyme under H_2 gas decreases the absorbance in the visible region by approximately 15 % (Fig. 1).

Analysis of *D. salexigens* hydrogenase by the chemical (TPTZ) method gave a value of 12 ± 1 *g*-atms of iron per minimal molecular mass of 98 kDa. Plasma emission analysis detected the following metals in relevant amounts : 1.03 *g*-atms of nickel, 15.15 *g*-atms of iron, 1.08 *g*-atms of selenium and 0.163 *g*-atms of zinc per minimal molecular mass. The metal content of the enzyme obtained by the purification schemes described is therefore 1 Ni, 12-15 Fe, 1 Se and trace amounts of Zn.

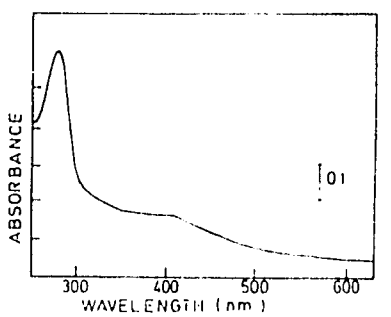

FIG. 1. — *Optical absorption spectra of* D. salexigens *hydrogenase*

Protein concentration 3.75 µM, at pH 7.6, 50 mM Tris-HCl buffer. —— native enzyme; - - - H_2 reduced (flushed under H_2 for 1 h)

Enzyme activity (H_2 evolution and D_2-H^+ exchange)

The aerobically isolated *D. salexigens* hydrogenase does not require a reductive activation step in order to catalyze the methylviologen mediated H^+ reduction. The H_2 evolution rate is practically constant from time zero and no lag phase period was observed. The enzyme preparation used has a specific activity of 760 units of H_2 evolved.

The hydrogenase activity was also followed at pH 7.6 by the D_2/H^+ exchange reaction using 20 % D_2 in N_2. The D_2/H^+ exchange kinetics mediated by the purified hydrogenase from *D. salexigens* is presented in Figure 2, with the three curves corresponding to D_2 uptake, HD transient evolution and then uptake, and H_2 production (mass-peaks 4, 3 and 2, respectively).

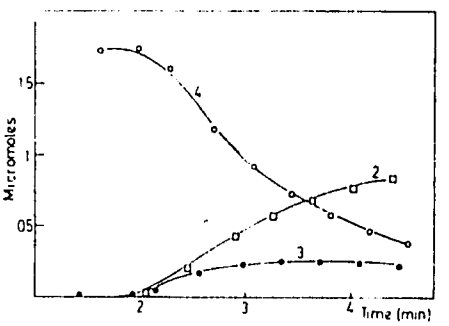

FIG. 2. — *(D_2/H^+) exchange activity of* D. salexigens *hydrogenase.*

The curves refer to : (○) D_2 uptake; (●) HD transient evolution then uptake; (□) H_2 production following mass-peaks 4, 3 and 2, respectively. Protein concentration 0.6 nM, gas-phase 20 % D_2 in N_2.

The ratio between the initial H_2 and HD evolution is higher than 1 and the sum of HD + H_2 evolved is lower than the H_2 production from dithionite reduced methylviologen (Table I).

EPR spectroscopy

The EPR spectrum of the native ("as isolated") enzyme is shown in Figure 3-A. It shows a very weak signal centered in the $g = 2.0$ region, observable only at low temperature. No EPR signals are observed when the sample is examined at 100 K.

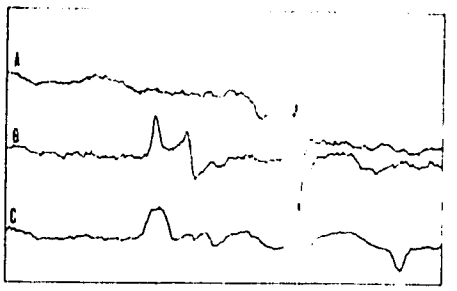

FIG. 3. — *EPR spectra of* D. salexigens *hydrogenase.*

A) Native state ("as isolated") at 11 K; gain 3.2×10^3. B) Intermediates H_2 reduced state at 25 K. The sample was poised at −380 mV under H_2 atmosphere (see redox titration conditions under Materials and Methods); gain 2×10^3. C) Same as B, at 4 K; gain 2×10^3. Other experimental conditions : microwave power 2 mW, modulation amplitude 1 mT, microwave frequency 9.45 GHz.

Upon exposure to different partial pressures of hydrogen gas, in the presence of redox mediators, a rhombic EPR signal develops with g-values at 2.22, 2.16 and around 2.0 (Fig. 3-B). During the course of the redox titration, using H_2 gas as electron donor, the "2.22" EPR signal reaches a maximal intensity (Fig. 4-A). This signal is optimally detected at 40 K and is readily saturated by microwave power at low temperature, being characteristic of a slow relaxing species.

Long incubation of the enzyme under H_2 atmosphere decreases the intensity of this signal. When the enzyme is poised at redox potentials where the "2.22" signal attains maximal intensity (~ −380 mV, Fig. 4-A), studies at low temperature reveal the presence of other EPR active species. Below 10 K the "$g = 2.22$" signal starts saturating and a new set of signals at 2.23, 2.21, 2.14, and broad features at higher field develop (Fig. 3-C). These latter signals exhibit a different power dependence from that of the previous EPR signal ("$g = 2.22$"), as shown in Figure 5. The complex set of signals only observable below 10 K shows fast electronic relaxation properties. At redox potentials below −300 mV, the low temperature (8 K) EPR spectra also reveal the presence of reduced iron-sulfur centers with g_{med} at 1.94. Temperature and microwave power dependence of this spectral region indicate that at least two types of iron-sulfur centers are present (Fe/S center I (g_{min} at 1.87) has faster relaxation properties than Fe/S center II (g_{min} at 1.90)). The low intensity of these signals prevents a detailed

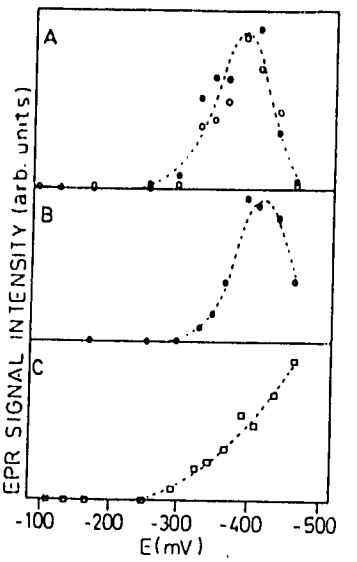

FIG. 4. — *EPR redox titration curves of the EPR active species detected in the hydrogen reduced states of* D. salexigens *hydrogenase.*

EPR signal intensities (arbitrary units) of the EPR signals detected upon poising the enzyme under different H_2 partial pressures at 25°C, pH 8.5, in the presence of redox mediators, as described in Materials and Methods, at the following g-values and temperatures : A) $g = 2.22$ (○) and 2.16 (●), at 20 K. B) $g = 2.23$ at 4 K (◑). C) $g = 1.87$ at 4 K (□).

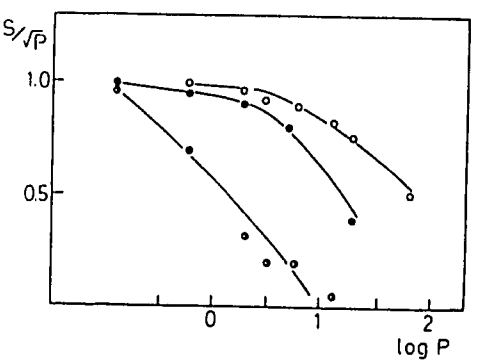

FIG. 5 — *Microwave power saturation curves of* D. salexigens *hydrogenase EPR detectable signals under H_2 atmosphere* (◑) $g = 2.22$, 4 K. (●) $g = 2.22$, 20 K. (○) $g = 2.23$, 4 K.

analysis of their spectral features. Figure 6 shows a temperature dependence of a *D. salexigens* hydrogenase sample poised at approximately −450 mV, a redox stage where the "2.22" EPR signal has decreased in intensity (Fig. 4-A). Low temperature reveals the presence of the "2.23" signal features (Fig. 6). The different relaxation properties for the two EPR signals detected in intermediate redox stages of the enzyme enable a complete description of the intensity profiles to be obtained by measuring the spectra at 20 and 4 K, respectively, as shown in Figure 4. This figure also indicates the development of the EPR features associated with the Fe S clusters.

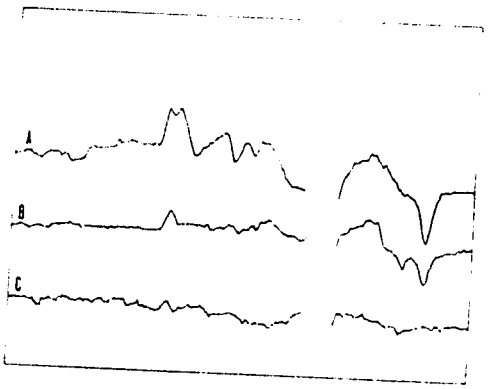

FIG. 6. — *EPR spectra of* D. salexigens *hydrogenase poised at −450 mV under H_2 atmosphere (see redox titration conditions under Materials and Methods)*

A) Temperature 4 K. B) Temperature 11 K. C) Temperature 22 K. Gain 10^4. Other experimental conditions as in caption of Figure 3. The top spectrum (insert) represents an identical spectrum of *D. gigas* hydrogenase, under the same experimental conditions as *D. salexigens* hydrogenase spectrum A.

Discussion

Sulfate reducing bacteria carry out the reduction of sulfur containing compounds, an important biological set of reactions with relevance to the biocycle of this element. Also *Desulfovibriones* is the only bacterial group which clearly participates in inter-species hydrogen transfer, working either as H_2-producing or as H_2-utilizing microorganisms [6].

The bidirectional hydrogenase functions as an "energy valve", supplementing or disposing of electrons. Thus, the system has considerable advantages for the study of the bioenergetics and the physiology of H_2 metabolism.

Hydrogenases isolated from *Desulfovibrio* sp. have recently been extensively studied. Table II summarizes the data on the localization, activity, metal center composition and relevant physicochemical data on hydrogenases isolated from this group of bacteria. A common feature emerges : all the enzymes contain nickel as a relevant constituent. So far, only *D. vulgaris* (Hildenborough) hydrogenase does not contain this transition metal [7].

D. salexigens hydrogenase is isolated from the only well characterized halophilic sulfate-reducer. Its properties have many common features with the group of the nickel containing hydrogenases isolated from sulfate-reducing bacteria of the genus *Desulfovibrio*. However, important differences are found within the group. *D. salexigens* hydrogenase is practically EPR silent, when isolated. The same is observed with the soluble *D. desulfuricans* (Norway 4) hydrogenase [25] and *D. baculatus* strain 9974 enzyme [26].

In contrast, *D. desulfuricans* (ATCC 27774) [4], membrane bound *D. desulfuricans* (Norway 4) [27], *D. multispirans* n.sp. [28] and *D. gigas* [10] hydrogenases exhibit a rhombic EPR signal with g-values around 2.3, 2.2 and 2.0. This signal has been termed *nickel signal A*. These rhombic EPR signals observed for the oxidized state of bacterial hydrogenases were assigned to Ni(III) based on Ni model compounds, relaxation properties (the signal is observable at 100 K), EPR g-values, and ^{61}Ni isotopic substitutions (performed for *D. gigas* [3] and *D. desulfuricans* (ATCC 27774) [4]). Besides the rhombic signal, this group of hydrogenases also exhibits a strong isotropic signal at $g = 2.02$, observable below 30 K. This signal is assigned to a [3Fe-xS] center, based on Mössbauer spectroscopic studies using unenriched naturally abundant and ^{57}Fe enriched *D. gigas* and *D. desulfuricans* (ATCC 27774) hydrogenases [4, 10].

The rhombic EPR nickel signal accounts for 50-100 % of the chemically detectable nickel, depending on the preparation and source. The "2.02" isotropic signal integrates from 0.2 spins (*D. multispirans* hydrogenase) [28] up to 0.9 spins (*D. gigas* hydrogenase) [10]. Redox titrations have only been performed for the *D. gigas* hydrogenase [10, 11]. The "2.02" signal titrates at −70 mV (at 10 K) and the *nickel signal A* disappearence is associated with a redox process which titrates at

TABLE II

Comparison of physico-chemical properties of Desulfovibrio *sp. hydrogenases.*

Property	*D. vulgaris* (Hildenborough)	*D. salexigens* (strain Brest Guinea) (NCIB 8403)	*D. gigas* (NCIB 9332)	*D. desulfuricans* (Norway 4)	*D. baculatus* (ATCC 9974)	*D. desulfuricans* (NRC 49001)	*D. desulfuricans* (ATCC 27774)	*D. multispirans* n sp.
Localization	periplasm	periplasm	periplasm	membrane*	periplasm*	periplasm	NR*	cytoplasm
Molecular weight	49 000	98 000	89 500	55 000	100 000	52 000	77 600	82 500
Subunits	1	2	2	1	1	1	2	2
Nickel	0	1	1	+ (EPR)	1	NR	1	1
Selenium	NR	1	0	1	1	NR	0	0
Non-heme iron	12	12-15	11	6		12	12	11
[Fe$_4$S$_4$]	0	NR	1	"$g = 2.02$"	NR	NR	1	1
[Fe$_2$S$_2$]	3	+ (probably 2)	2	NR	+ (probably 2)	NR	2	+ (probably 2)
Specific activity (μmoles H_2 min mg)								
Evolution	4 600	760	420	70	527	9 000	152	790
Consumption	50 000	NR	1 200	200	NR	NR	NR	590
References	[7, 8]	This work	[9, 10, 12]	[27]	[26]	[34]	[4]	[28]

* non reported

(a) A soluble form was also purified [25].

(b) A cytoplasmic and a membrane bound form were also purified [26].

-220 mV, and was shown to be pH-dependent (60 mV/pH unit) [11]. After the first sequence of reductive events, an EPR silent state is attained. Evidence was previously accumulated [13] suggesting that in this EPR silent state one $[Fe_4S_4]^{+1}$ cluster ($S = 1/2$) is present and coupled to the Ni(III) center. This proposal implies that the -220 mV redox transition represents the mid-point redox potential of the iron-sulfur center. In this context, *D. salexigens*, *D. baculatus* strain 9974 and soluble *D. desulfuricans* (Norway 4) hydrogenases would have been isolated in this spin coupled state. The low intensity of the Ni EPR signals in the native preparations or even its absence [26, 28], could be due to spin coupling between the Ni center and the Fe_4S_4 cluster.

The pattern observed for the reductive events following the EPR silent state are now common to all *Desulfovibrio* [NiFe] hydrogenases studied. The appearence of a transient rhombic signal (termed *nickel signal C*) detected in *D. gigas* hydrogenase with g-values 2.19, 2.16 and 2.0 [13] is also observed in *D. salexigens*, *D. baculatus* strain 9974 [26], *D. desulfuricans* (ATCC 27774) [4] and *D. multispirans* [28] enzymes. In all these cases, EPR studies reveal the presence of other EPR active species at redox stages where the transient is observed. Due to its relaxation properties (fast relaxing) this last signal is only observable at low temperature and with high levels of microwave power [13].

The redox titration data obtained for *D. salexigens* hydrogenase, under H_2 atmosphere, show a very similar behaviour to that of the *D. gigas* enzyme [13]. The transient nickel signal develops to maximal intensity at ~ -380 mV. Also, the study of the development of this signal followed at two temperatures (20 K and 4 K) clearly shows that the two species are not directly correlated.

Below -450 mV, the slow relaxing species disappears (not observable at 20 K) but the complex fast relaxing species is still detected. A similar study recently conducted in the *D. gigas* hydrogenase fully supports this data analysis (our unpublished results).

An important point to consider in the reactional mechanism, is that some of the so-called "oxygen stable" [NiFe] hydrogenases are not fully active when isolated. This state is EPR active (rhombic *nickel signal A* and isotropic $g = 2.02$" signal). A main conclusion is that these EPR active species are not relevant for the mechanism. The enzyme must go through an activation process that represents a complex phenomenon:

removal of oxygen (lag phase) followed by a reductive step [18, 19]. It is important to note that the enzymes which are EPR silent as isolated, do not show a lag phase for activation. The *D. salexigens* and *D. baculatus* hydrogenases have a constant rate of H_2 evolution, but for the *D. gigas* and *D. multispirans* enzymes an activation step (lag phase) is required in order to express full activity.

Upon reduction (either by long exposure to H_2 atmosphere or by chemical reduction with excess dithionite) $g_{med} \sim 1.94$ EPR signals have been observed for *D. gigas* [13], *D. desulfuricans* (ATCC 27774) [4], soluble *D. desulfuricans* (Norway 4) [25], and *D. baculatus* strain 9974 hydrogenases [26], as well as for the *D. salexigens* enzyme.

All these pieces of information have been discussed in general terms as a basis for a "working hypothesis" which represents a useful framework for discussing the mechanistic involvement of these redox species [13].

The analysis of the structural and physicochemical properties of the redox centers of these homologous hydrogenases will enable a wealth of information to be built up, useful to delineate a general approach to the mechanism of enzyme action.

Another important piece of information that has not been fully explored in the study of bacterial hydrogenases is the mechanism of activation of the hydrogen molecule by the enzyme active centers, which can be directly probed by D_2/H^+ exchange experiments. Activity measurements are generally only related with the measurement of the overall evolution or consumption of H_2. However, when these data are correlated with the exchange activities (D_2 H^+) of the reactional center it is possible to probe the operating mechanisms, *i.e.* homolytic or heterolytic cleavage [30, 31].

According to the ratio found for the initial HD and H_2 evolution in D_2/H^+ exchange reactions, the hydrogenases isolated from the *Desulfovibrio* genus can be divided into two classes. i) One class is represented by the hydrogenases from *D. salexigens* and *D. baculatus* strain 9974 (our unpublished results) which have a H_2/HD ratio higher than 1 (ratio $H_2/(HD + H_2)$ around 0.6). ii) Another class is represented by the hydrogenases from *D. gigas* and *D. multispirans* (our unpublished data) which have H_2/HD ratios lower than 1 (ratio $H_2/(HD + H_2)$ around 0.3). The soluble hydrogenase from *Methanosarcina barkeri* also has a H_2/HD ratio lower than 1 [32].

These H_2/HD ratios are generally used to differentiate between a heterolytic versus a homolytic cleavage of the hydrogen molecule. In similar experiments with metal salts, ratios of 0.95 with platinum oxide and of 0.30 with ruthenium chloride were obtained (Y. Berlier, G. Fauque, P.A. Lespinat and J. LeGall, unpublished results). These salts could serve as analogs for the homolytic and heterolytic activations of the hydrogen molecule.

Another possible explanation for these differences is the kinetics of the H_2 binding site of the enzymes with respect to the exchange with water. The general mechanism proposed for hydrogenase activity [30, 31] involves the heterolytic activation of hydrogen, with the formation of a hydride :

$$\text{Enzyme} + H_2 \rightleftharpoons E\text{-}H^- + B\text{-}H^+$$

where E represents the hydride binding site and B the proton accepting site. The mechanism, based on the primary formation of HD rather than D_2 in the H_2/D^+ exchange reaction, indicates that only one of the bound atoms of H_2 can freely exchange with the protons of the medium. However, this may represent only a limiting situation and it is possible that both sites exchange protons with water but with different velocities. Also, the lability of the H^+ site may be modulated by the pK_a value of the proton acceptor site. In this context an extreme situation within the framework of the heterolytic mechanism would correspond to very different exchange velocities of both sites, resulting in a H_2/HD ratio lower than 1.

The different exchange kinetics of hydrogen binding sites could reflect differences on the active center of the hydrogenases, either at the proton or at the hydride binding site. Assuming that nickel is the hydride binding center, as has been proposed for several nickel containing hydrogenases [13], the observed difference could reflect different ligation to this metal. In this respect, it is noteworthy that in the *D. salexigens* and the *D. baculatus* hydrogenases, the presence of selenium was detected in a 1:1 ratio with nickel. These are the hydrogenases where the H_2/HD ratio was found to be higher than 1. Selenium has also been found in *Methanococcus vannielii* [33], soluble *D. desulfuricans* (Norway 4) [25] (and *D. baculatus* strain 9974 hydrogenases). It is not yet known whether selenium is present at a new catalytic site. If this is so, it could be related with the observed differences.

This explanation is also in better agreement with the EPR studies of [NiFe] hydrogenases. In fact, not only do the hydrogen reduced states of the *D. gigas*, *D. baculatus* and *D. salexigens* hydrogenases show very similar EPR spectra, but the redox patterns of the EPR spectra upon incubation under hydrogen are also identical, suggesting a common mechanism for the activation and reduction/oxidation of the hydrogen molecule.

Acknowledgments

We thank M. Scandellari and R. Bourelli for growing the bacteria. We are indebted to N. Galliano, I. Carvalho, B. Dimon and P. Carrier for their skilltul technical help and to M. Martinez and I. Ribeiro for carefully typing this manuscript. This research was supported by grants from Instituto Nacional de Investigação Cientifica and Junta Nacional de Investigação Cientifica e Tecnologica (Portugal), NATO 0341/83 and AID 936-5542 G-SS-4003-00 (J.J.G. Moura), and National Science Foundation Grant DMB-8415632 (J. LeGall). Part of this work has been made possible thanks to a special collaborative agreement between the University of Georgia (USA), Centre National de la Recherche Scientifique and Commissariat à l'Energie Atomique (France).

References

1. Adams, M.W.W., Mortenson, L.E. & Chen, J.S. (1981) *Biochim. Biophys. Acta*, **594**, 105-176.
2. Schlegel, H.G., & Schneider, K. (1978) *in : Hydrogenases : their catalytic activity, structure and function*, (Schlegel, H.G. and Schneider, K., eds) pp. 15-44, E. Goltze, Gottingen.
3. Moura, J.J.G., Moura, I., Huyhn, B.H., Krüger, H.J., Teixeira, M., DuVarney, R.C., DerVartanian, D.V., Xavier, A.V., Peck, H.D., Jr., & LeGall, J. (1982) *Biochem Biophys Res. Commun.*, **108**, 1388-1393.
4. Krüger, H.J., Huyhn, B.H., Ljungdahl, P.O., Xavier, A.V., DerVartanian, D.V., Moura, I., Peck, H.D., Jr., Teixeira, M., Moura, J.J.G. & LeGall, J. (1982) *J. Biol. Chem.*, **257**, 14620-14622.
5. Albracht, S.P.J., Graft, E.G. & Thauer, R.K. (1982) *FEBS Lett.*, **140**, 311-313.
6. LeGall, J., Moura, J.J.G., Peck, H.D., Jr. & Xavier, A.V. (1982) *in : Iron-Sulfur Proteins* (Spiro, T.G., ed.) pp. 260-370, Academic Press, New York.
7. Huynh, B.H. Czechowski, M.H., Krüger, H.J., DerVartanian, D.V., Peck, H.D., Jr. & LeGall, J. (1984) *Proc. Natl. Acad. Sci. USA*, **81**, 3728-3732.
8. Van der Westen, H.M., Mayhew, S.G. & Veeger, C. (1978) FEBS *Lett.*, **86**, 122-126
9. LeGall, J., Ljungdahl, P.G., Moura, I., Peck, HD, Jr., Xavier, A.V., Moura, J.J.G., Teixeira, M., Huynh, B.H. & DerVartanian, D.V. (1982) *Biochem. Biophys. Res. Commun.*, **106**, 610-616.
10. Teixeira, M., Moura, I., Xavier, A.V., DerVartanian, D.V., LeGall, J., Peck, H.D., Jr., Huynh, B.H. & Moura, J.J.G. (1983) *Eur. J. Biochem.*, **130**, 481-484.
11. Cammack, R., Patil, D., Aguirre, R. & Hatchikian, E.C. (1982) *FEBS Lett.*, **142**, 481-484.
12. Moura, J.J.G., Teixeira, M., Moura, I., Xavier, A.V. & LeGall, J. (1984) *J. Mol. Catal.*, **23**, 303-314.
13. Teixeira, M., Moura, I., Xavier, A.V., Huynh, B.H., DerVartanian, D.V., Peck, H.D., Jr., LeGall, J. & Moura, J.J.G. (1985) *J. Biol. Chem.*, **260**, 8942-8950.
14. Moura, J.J.G., Teixeira, M., Moura, I., Xavier, A.V. & LeGall, J. (1985) *Rev. Port. Quim.*, **27**, 63-66.
15. Drucker, H., Transil, E.B. & Campbell, L.L. (1970) *Biochemistry*, **9**, 3395-3400.
16. Moura, I., Moura, J.J.G., Bruschi, M., & LeGall, J. (1980) *Biochim. Biophys. Acta*, **591**, 1-8.
17. Peck, H.D., Jr. & Gest, H. (1956) *J. Bacteriol.*, **71**, 70-80.
18. Berlier, Y., Fauque, G., Lespinat, P.A. & LeGall, J. (1982) *FEBS Lett.*, **140**, 185-188.
19. Fischer, D.S. & Price, D.C. (1964) *Clin. Chem.*, **10**, 21-25.
20. Lowry, O.H., Rosebrough, N.J., Tan, A.C. & Randall, R.J. (1951) *J. Biol. Chem.*, **193**, 265-275.
21. Davis, B.J. (1964) *Ann. N.Y. Acad. Sci.*, **121**, 404-427.
22. Weber, K. & Osborn, M. (1969) *J. Biol. Chem.*, **244**, 4406-4412.
23. Dutton, P.L. (1971) *Biochim. Biophys. Acta*, **226**, 63-80.
24. Starkey, R.L. (1938) *Arkh. Mikrobiol.*, **9**, 268-304.
25. Rieder, R., Cammack, R. & Hall, D.O. (1984) *Eur. J. Biochem.*, **145**, 637-643.
26. Teixeira, M., Moura, I., Xavier, A.V., Moura, J.J.G., Fauque, G., Pickril, B. & LeGall, J. (1985) *Rev. Port. Quim.*, **27**, 194-195.
27. Lalla-Maharajah, W.V., Hall, D.O., Cammack, R., Rao, K.K. & LeGall, J. (1983) *Biochem. J.*, **209**, 445-454.
28. Czechowski, M.H., He, S.H., Nacro, M., DerVartanian, D.V., Peck, H.D., Jr & LeGall, J. (1985) *Biochem. Biophys. Res. Commun.*, **108**, 1388-1393.
29. Lissolo, T., Pulvin, S. & Thomas, D. (1984) *J. Biol. Chem.*, **259**, 11725-11729.
30. Krasna, A.I. & Rittenberg, D. (1954) *J. Am. Chem. Soc.*, **76**, 3015-3020.
31. Spencer, R.W., Daniels, L., Fulton, G. & Ormejohnson W.H. (1980) *Biochemistry*, **19**, 3678-3683.
32. Fauque, G. (1985) PhD. Thesis, Compiègne, France, 222 pages.
33. Yamazaki, S. (1982) *J. Biol. Chem.*, **257**, 7926-7929.
34. Glick, B.R., Martin, W.G. & Martin, S.M. (1980) *Can. J. Microbiol.*, **26**, 1214-1223.

23

Journal of Industrial Microbiology, 1 (1986) 139–147
Elsevier
SIM 019

Purification and characterization of three proteins from a halophilic sulfate-reducing bacterium, *Desulfovibrio salexigens*

M. Czechowski[a], G. Fauque[a], N. Galliano[a], B. Dimon[a], I. Moura[b], J.J.G. Moura[b], A.V. Xavier[b], B.A.S. Barato[b], A.R. Lino[b] and J. LeGall[c]

[a]*A.R.B.S.-Section Enzymologie Biochimie Bactérienne, CEN-Cadarache, 13108 Saint Paul lez Durance Cedex, France,* [b]*Centro de Química Estrutural, Complexo Interdisciplinar, Instituto Superior Tecnico, Avenida Rovisco Pais, P-1000 Lisboa, Portugal,* and [c]*Department of Biochemistry, University of Georgia, Boyd Graduate Studies Research Center, Athens, GA 30602, U.S.A.*

Received 15 July 1985
Revised 20 January 1986
Accepted 4 April 1986

Key words. Halophilic sulfate-reducing bacteria; *D. salexigens;* Enzyme function; Metal corrosion

SUMMARY

Hydrogenase, desulfoviridin and molybdenum proteins have been isolated from a halophilic sulfate-reducing bacteria, *Desulfovibrio salexigens* strain British Guiana. At least 50% of the hydrogenase was found to be located in the periplasm. The hydrogenase has a typical absorption spectrum, a 400/280 nm ratio of 0.28, a molecular weight by sedimentation equilibrium of 81 000 and is composed of two subunits. It has one nickel, one selenium and 12 iron atoms per molecule. The sulfite reductase has a typical desulfoviridin absorption spectrum, a molecular weight of 191 000 and iron and zinc associated with it. The molybdenum-iron protein is gray-green in color and exhibits an absorbtion spectrum with peaks around 612, 410, 275 nm and a shoulder at 319 nm. It is composed of subunits of approximately 13 250 and has an approximate molecular weight of 110 000. Three molybdenum and 20 iron atoms are found associated with it.

An extensive study of these three proteins will allow a better understanding of the function of these enzymes and also of their possible role in microbially caused corrosion.

INTRODUCTION

Sulfate-reducing bacteria have been implicated in the phenomenon of microbially caused corrosion in neutral anaerobic environments [13]. Hydrogen consumption and sulfate reduction contribute to this corrosion process. Hydrogen is consumed by the hydrogenase enzyme from either the metal surface [58] or from the iron sulfide film on the metal [28]. Hydrogen sulfide is produced by the sulfate reduction system and acts as an anodic reactant [59], a cathodic reactant [12] or in the formation of a reactive phosphorous compound [26].

Desulfovibrio (D.) salexigens strain British Guiana is the only well known halophilic strain in the genus *Desulfovibrio* and only studies on its cytochrome C_3 [16] flavodoxin and rubredoxin [41] have been published.

Hydrogenases have been purified to apparent homogeneity from many bacterial species, including anaerobic microorganisms such as sulfate reducers [46] and methanogenic bacteria [5,18,27].

They are involved either in the hydrogen consumption in which hydrogen is used as a reductant for CO_2 fixation or for energy generation via electron transport or in hydrogen production which enables bacteria to dispose of excess electrons [1,50].

An important enzyme in sulfate reduction is dissimilatory sulfite reductase or bisulfite reductase [47]. This enzyme has been purified from the cytoplasm of many sulfate-reducing bacteria [46] and is believed to be involved in ATP production in these micro-organisms [44]. Reduction of sulfite either involves a cyclic scheme, utilizing intermediates trithionate and thiosulfate to sulfide [3] or a direct six electron reduction to sulfide [46].

A molybdenum protein has been found in some species of sulfate reducers from the genus *Desulfovibrio (D.) gigas* [40], *D. africanus* [21], *D. desulfuricans* strains Berre Eau [7] and Berre Sol (our unpublished results). It is characterized by not only containing molybdenum but also iron and labile sulfide. Its function is still unknown.

A purification scheme and partial characterization of hydrogenase, desulfoviridin (bisulfite reductase) and molybdenum protein from *D. salexigens* is reported. A study of these proteins may help elucidate the phenomenon of microbially caused corrosion.

MATERIALS AND METHODS

Growth of cells. Desulfovibrio salexigens strain British Guiana (NCIB 8403) was grown at 37°C on lactate/sulfate medium [54] with 3.0% NaCl. Cells for localization studies were harvested by centrifugation and immediately used. Cells (250 g) for enzyme purification were harvested, resuspended in 10 mM Tris-HCl (pH 7.6) lysed with a French press and then frozen at −80°C until used.

Assay and metal determinations. Hydrogenase activity was measured at 32°C either by the hydrogen evolution assay from dithionite-reduced methyl viologen [45] using an Aerograph A-90 P3 gas chromatograph or by hydrogen consumption with benzyl viologen as electron acceptor using Warburg respirometry [8]. One unit of hydrogenase activity is defined as the amount of enzyme which catalyses the evolution or the consumption of 1 μmol H_2/min. Dissimilatory sulfite reductase activity was measured by a manometric assay at 32°C [31] using pure hydrogenase from *D. gigas* to reduce methyl viologen under H_2. The initial rate of hydrogen utilization is proportional to the amount of sulfite reductase. Protein was determined by a modification of the Lowry method as proposed by Markwell et al. [38]. Iron and nickel were determined by plasma emission spectroscopy using the Jarrel-Ash Model 75 atomcomp.

Optical spectra. Ultraviolet and visible absorption spectra were recorded on a Beckman DU 7 spectrophotometer.

Electrophoresis and molecular weight determination. Purity of the enzymes was established by polyacrylamide disc electrophoresis [11] and by comparison of published absorption ratios for similar type pure proteins. Subunit structure was determined by SDS-polyacrylamide gel electrophoresis [17]. Molecular weight was determined by SDS electrophoresis, gel filtration using a TSK 3000 SW analytical column (high-pressure liquid chromatography) or sedimentation equilibrium [49].

RESULTS

Location of the hydrogenase

Lysing the cells with the French press and centrifuging a 120 000 × *g* for 70 min released about 80% of the hydrogenase as soluble protein. The cells were washed in a 1:1 w/v buffer solution (pH 8.0) of 50 mM Tris-HCl/10 mM EDTA/500 mM glucose/3% NaCl, incubated in the same buffer at a 1:50 w/v ratio with 8 mg of lysozyme/ml and then centrifuged. This results in 70–80% of the hydrogenase being found in the supernatant. A visible spectrum showed 30% of the desulfoviridin was also found in the supernatant. Further experiments using $MgCl_26H_2O$ instead of NaCl found almost 50% of the hydrogenase in the supernatant and less than 5% of desulfoviridin. This seems to indicate a periplasmic origin for at least 50% of the hydrogenase enzyme. It is important to add NaCl or

Table I

Purification of hydrogenase from *D. salexigens*

Fraction	Protein (mg)	Total activity* (μmol H_2/min)	Specific activity* (μmol H_2 min per mg)
Crude extract	10750	47290	4.4
DEAE Bio-Gel A column	562	24000	42.7
Hydroxylapatite column	28	15552	561
Gel exclusion by HPLC	3.9	7170	1830

* in H_2 evolution.

$MgCl_26H_2O$ to the washing or incubating buffers or the cells clump together. When Na_2SO_4 was substituted at the same concentration, the cells clumped together and there was some cell lysis.

Purification of hydrogenase, desulfoviridin and molybdenum-iron sulfur protein

All purification procedures were carried out in air at 4°C and the pH of the buffers, Tris-HCl and phosphate (KPB), were 7.6 (measured at 5°C).

The lysed cells were slowly defrosted and centrifuged for 1.5 h at 20 000 × *g*. The supernatant was centrifuged at 120 000 × *g* for 2 h, dialized against 10 vol. of 10 mM Tris-HCl for 24 h and then centrifuged at 120 000 × *g* for 1 h. The centrifuged extract was loaded onto a DEAE Bio-Gel A column (5 × 25 cm) equilibrated with 10 mM Tris-HCl and the column washed with 500 ml of the same buffer. A gradient of 1500 ml 10 mM Tris-HCl and 1500 ml 400 mM Tris-HCl was set up. A molybdenum-iron protein, gray in color, came off at 100–125 mM Tris-HCl. The hydrogenase and desulfoviridin eluted off together at about 200–250 mM Tris-HCl. The hydrogenase activity recovered in the H_2 evolution was 51%.

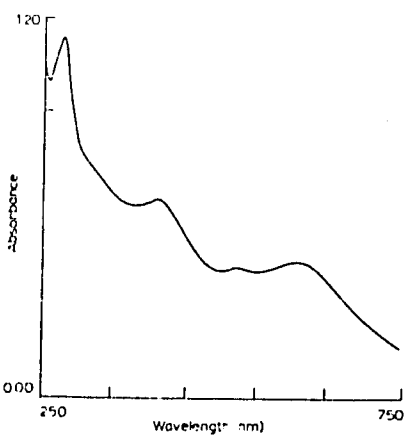

Fig. 1. Electronic absorption spectrum of oxidized molybdenum iron protein from *Desulfovibrio salexigens* recorded at 25°C.

This last fraction was loaded onto a Bio-Rad hydroxylapatite column (HTP) (4.3 × 26 cm) equilibrated with 250 mM Tris-HCl. The column was washed with 250 mM Tris-HCl and a reverse gradient of 400 ml 250 mM Tris-HCl and 400 ml 10 mM Tris-HCl was set up. The column was then washed with 200 ml of 10 mM KPB. A gradient of 1500 ml 10 mM KPB and 1500 ml 500 mM KPB was set up. The desulfoviridin eluted off at about 200 mM to 250 mM KPB and had a 409/630 nm ratio of 2.80 and a 279/630 nm ratio of 4.7. The hydrogenase band (brown) began to migrate at about 450 mM KPB and was collected at 500 mM KPB. The activity was 65% of that from the DEAE Bio-Gel column. The sample was concentrated in a diaflow apparatus using a YM 30 membrane. It was loaded onto a high-pressure liquid chromatography gel exclusion column which was equilibrated with 500 mM KPB (pH 7.5). Different fractions were analyzed spectroscopically and those with the highest 400/280 nm ratios were combined. Gel electrophoresis revealed one major band for the hydrogenase and the protein was estimated to be 95%

pure. The final yield of hydrogenase was 15.2%. A summary of the hydrogenase purification is found in Table 1.

The desulfoviridin appeared to be pure by the absorbancy ratios which were identical to that obtained for pure desulfoviridin from *D. gigas* [30] and *D. vulgaris* Hildenborough [31]. Before staining the electrophoresis gel there was one green band about 25% down the gel and a red band which migrated near the bromophenol blue. After staining, one major band was found in the location of the green band. The location of the red band stained but slowly dissipated after 24 h. This band is believed to be a siroheme which is part of the desulfoviridin [51]. The enzyme was judged to be about 95% pure.

The gray protein from the DEAE Bio-Gel column was loaded onto a HTP column (5 × 24 cm) equilibrated with 150 mM Tris-HCl. The column was developed with a KPB gradient up to 1 M and very little of the gray protein came off. The column was then washed with 2 M KPB and the majority of the protein eluted off the column. The 278/612 nm ratio is 2.92. The absorbance spectrum of this protein (Fig. 1) appears to be very similar to the molybdenum-iron-sulfur protein spectrum of *D. africanus* [21] and has the same 278.5:615 nm ratio.

Characterization of hydrogenase

The hydrogenase of *D. salexigens* is brown in color and its native form exhibits a typical hydrogenase UV/visible absorption spectrum with a broad shoulder around 400 nm (Fig. 2). SDS gel electrophoresis showed that it is composed of two different subunits of molecular weight 62 000 ± 5000 and 35 000 ± 3000. The total molecular weight by addition of the subunits is 97 000 but the molecular weight found by sedimentation equilibrium is 81 000. The ratio of 400/280 nm is 0.28 and the extinction coefficient at 400 nm using a molecular weight of 81 000 is 46 $mM^{-1} \cdot cm^{-1}$.

A metal content of 12.3 iron atoms, 0.8 nickel atoms and 0.86 selenium atoms per molecule of hydrogenase was determined. The hydrogenase does not exhibit an activation phase before maximum H_2 evolution activity. The specific activity in the H_2 evolution is 1830 μmol/min per mg protein and is 1300 μmol/min per mg protein in H_2 consumption.

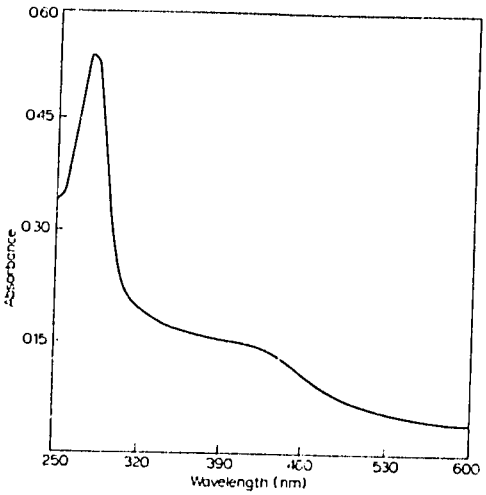

Fig. 2. Electronic absorption spectrum of oxidized *Desulfovibrio salexigens* hydrogenase at 25°C.

Characterization of desulfoviridin

The optical spectrum of desulfoviridin shows absorption bands at the following wavelengths (nm): 630 (0.595), 584 (0.374), 409 (1.668), 391.5 (1.544) and 279 (2.79); relative intensities are indicated in parenthesis. The molecular weight, determined by sedimentation equilibrium, is 191 000. The metal content is 31 iron atoms and 1.4 zinc atoms per molecule. The specific activity is 136 nmol H_2 consumed/min per mg protein. The activity was found to be greater at pH 6.0 than at pH 7.6 which indicates that bisulfite is the substrate [42]. An end product of the reaction was sulfide, appearing as a yellow precipitate of cadmium sulfide, which was formed in the center well of the reaction vial.

Characterization of molybdenum protein

The molybdenum-iron protein is gray-green in color and exhibits an absorbance spectrum with peaks around 612, 410, 275 nm and a shoulder at 319 nm (Fig. 1). Denaturing gel electrophoresis

Table 2

Properties of assimilatory (A) and dissimilatory (D) sulfite reductases from anaerobic bacteria

Sulfite reductase	Mr ($\times 10^{-3}$)	Activity[a]	Active center	Reference
Desulfuromonas acetoxidans (A)	23.5	906	Sir + Fe-S(α)	[35]
D. vulgaris (A) Hildenborough	27	900	Sir + Fe-S(α)	[25]
M. barkeri (DSM800) P 590 (A)	23	2790	Sir + Fe-S(α)	[42]
Desulfotomaculum nigrificans P 582 (D)	145	65[b]	Sir + Fe-S	[4]
D. gigas desulfoviridin (D)	200	632	Sir + Fe-S($\alpha_2\beta_2$)	[30]
D. vulgaris Hildenborough desulfoviridin (D)	226	260	Sir + Fe-S($\alpha_2\beta_2$)	[31]
D. desulfuricans Norway 4 desulforubidin (D)	225	410	Sir + Fe-S($\alpha_2\beta_2$)	[32]
D. baculatus 9974 desulforubidin (D)	n.d.	198	Sir + Fe-S($\alpha_2\beta_2$)	Fauque (unpublished)
Thermodesulfobacterium commune desulfofuscidin (D)	167	2000	Sir + Fe-S($\alpha_2\beta_2$)	[22]

[a] Activity expressed in nmol H_2 consumed/min per mg protein at pH 6 at 30°C except for *Thermodesulfobacterium commune* at 65°C.
[b] partially purified P 582.
Sir, sirohème; Fe-S: iron sulfur center.
n.d., not determined.

yielded bands of molecular weights of approximately 13 250, 26 000, 42 500 and 64 300. These results suggest a protein of several subunits of molecular weight of 13 250. The conditions were probably not sufficient to completely dissociate the protein. The molecular weight as determined by high-presure liquid chromatography analytical gel exclusion column is approxiately 110 000. The enzyme has three molybdenum atoms and 20 iron atoms for 110 000 molecular weight. The amount of molybdenum protein in the bacterium was large. The final amount is about 50 mg per 250 g of cells.

DISCUSSION

The location of a hydrogenase in the periplasmic space of *D. salexigens* is not unusual. Periplasmic origin of hydrogenase is common in sulfate-reducing bacteria of the genus *Desulfovibrio: D. Vulgaris* strains Hildenborough [57], Marburg [6], Miyazaki [2], *D. gigas* [9], *D. desulfuricans* (NRC 49001) [39], and *D. baculatus* strain 9974 [55].

The existence of more than one hydrogenase in the same species of the genus *Desulfovibrio* has been postulated [43].

The need for chloride at high concentration (> 2%) in order to prevent the clumping of cells from *D. salexigens* may be related to some function in the outer membrane or in response to the use of a high concentration of EDTA. It has been found that *D. salexigens* has an absolute requirement for chloride [37] and the cells in our buffer conditions exhibited an abnormal response to less than 2% of it.

It has been proposed that a periplasmic location

of hydrogenase in anaerobic bacteria is a specific adaptation important for utilization of low level of H_2 and for interspecies H_2 transfer [9]. The periplasmic location of hydrogenase would be important in hydrogen utilization from metal surfaces or iron sulfide films. However, attempts to show direct correlation between hydrogenase activity and bacterial corrosion have shown mixed results. [19]. Recently, a marine strain of a sulfate-reducing bacterium has been found to utilize cathodically produced hydrogen from a metal surface [20]. Conclusions concerning 'hydrogenase-less' sulfate-reducing bacteria will have to be revised because many of these strains are now known to have hydrogenase activity, e.g., *Desulfotomaculum orientis* [34] and *Desulfovibrio desulfuricans*, El Agheila Z (our own unpublished results).

Desulfovibrio salexigens hydrogenase is similar to the recently purified Fe-Ni-Se hydrogenases found in *D. desulfuricans* Norway 4 [48] and *D. baculatus* strain 9974 [55]. The only known selenium-containing hydrogenase without nickel is from *Methanococcus vanniellii* [60]. The function of selenium in this enzyme is not known. Other nickel-containing hydrogenases are present in sulfate-reducing bacteria of the genus *Desulfovibrio*, i.e., *D. gigas* [33], *D. desulfuricans* ATCC 27774 [29] and *D. multispirans* [15]. The *D. salexigens* hydrogenase does not exhibit an activation phase as found in two nickel-containing hydrogenases from *Desulfovibrio* [10,15,36]. There is no indication in the published results of an activation phase in the nickel-selenium-containing hydrogenases. The specific activity in hydrogen evolution of *D. salexigens* hydrogenase is the highest presently known value for nickel or nickel-selenium hydrogenases from *Desulfovibrio*. This specific activity is higher than previously reported with the hydrogenase isolated following a different purification procedure [14]. The native, partially reduced and fully reduced states, using hydrogen or dithionite as electron donors, of the *D. salexigens* hydrogenase have been analyzed by electron paramagnetic resonance spectroscopy [56].

The dissimilatory sulfite reductases of *Desulfovibrio* are complex structures ($\alpha_2\beta_2$ subunit structures) with molecular weights of about 200 000, Fe-S clusters and sirohemes (Table 2). The absorption spectrum and molecular weights of *D. salexigens* desulfoviridin are similar to that found in *D. gigas* [30] and *D. vulgaris* Hildenborough [31]. The specific activity of *D. salexigens* desulfoviridin is lower than other dissimilatory type sulfite reductases from *Desulfovibrio* and of assimilatory type sulfite reductases from sulfate or sulfur reducers and methanogenic bacteria (Table 2). Comparison of sulfite reductase activity from lysed cell extracts of different *Desulfovibrio* showed that *D. salexigens* had also the lowest activity (our unpublished results). Dissimilatory sulfite reductases may under different assay conditions form trithionate and thiosulfate in addition to sulfide. Desulfoviridin from this bacterium was able to qualitatively form sulfide in our assay conditions.

The optical absorbance spectrum and molybdenum iron content of the *D. salexigens* molybdenum iron protein are very similar to the one found in *D. africanus* [21]. Similarity between cytochrome c_3 of *D. africanus* Benghazi and *D. salexigens* British Guiana have also been found [52]. However, antiserum to *D. africanus* Benghazi cells reacts weakly to *D. salexigens* British Guiana cells [53].

The function of the molybdenum protein in *Desulfovibrio* is unknown. Molybdenum in bacteria is found associated with the nitrogenase, formate, dehydrogenase and nitrate reductase enzymes [24]. The amount of molybdenum protein in this bacterium is large as is found in *D. africanus* (30 mg/250 g wet weight cells) and implies an important function. In *D. salexigens* the amount of cytochromes is low and perhaps the molybdenum protein may function as an electron transport protein. The high molecular weight and the subunit structure may also imply a metal storage capacity for this protein. Further studies on the physiological function of this protein are in progress.

Metal corrosion in sea water is an important problem for the off-shore oil industry. *Desulfovibrio salexigens* is an obligative halophilic sulfate-reducing bacterium and may be used as an reference organism. Hydrogenase, sulfite reductase, and molybdenum protein (metal storage protein) which can be key enzymes in anaerobic bacterial corrosion

deserve to be well defined in this bacterium. A study of these important enzymes will allow a better understanding of how these enzymes function, their role in microbially caused corrosion, and a more rational development of biocides to control these bacteria.

ACKNOWLEDGMENTS

We are indebted to Dr. M. Scandellari and Mr. R. Bourelli for growing the bacteria which have been used for the present study, and to Dr. D. Patil and Mr. S.H. He for the metal analysis and the molecular weight determination by sedimentation equilibrium of the proteins. Financial aid support from the Agency of International Development, Grant No. 936-5542-G-SS-4003-00 is acknowledged.

REFERENCES

1 Adams, M.W.W., L.E. Mortenson and J.S. Chen. 1981. Hydrogenase. Biochim. Biophys. Acta 594: 105–176.

2 Aketagawa, J., K. Kobayashi and M. Ishimoto. 1983. Characterization of periplasmic hydrogenase from *Desulfovibrio vulgaris* Miyazaki. J. Biochem. 93: 755–762.

3 Akagi, J.M. 1981. Dissimilatory sulphate reduction, mechanistic aspects. In: Biology of Inorganic Nitrogen and Sulfur (Bothe, H. and A. Trebst, eds.), pp. 169–177, Springer-Verlag, Berlin).

4 Akagi, J.M. and V.L. Adams. 1973. Isolation of a bisulfite reductase activity from *Desulfotomaculum nigrificans* and its identification as the carbon monoxide-binding pigment, P_{582}. J. Bacteriol. 116: 392–398.

5 Albracht, S.P.J., E.G. Graf and R.K. Thauer. 1982. The EPR properties of nickel in hydrogenase from *Methanobacterium thermoautotrophicum*. FEBS. Lett. 140: 311–313.

6 Badziong, W. and R.K. Thauer. 1980. Vectorial electron transport in *Desulfovibrio vulgaris* (Marburg) growing on hydrogen plus sulfate as sole energy source. Arch. Microbiol. 125: 167–174.

7 Barata, B.A.S., I. Moura, A.V. Xavier, G. Fauque, J. LeGall and J.J.G. Moura. 1984. Molybdenum containing iron-sulfur protein from *Desulfovibrio desulfuricans* (Berre-Eau) – EPR spectroscopic characterization of the redox centers. PC3 in Setimo Encontro Anual da Sociedade Portuguesa de Quimica. 9 a 14 de Julho, 1984, Lisboa.

8 Bell, G.R., J.P. Lee, H.D. Peck, Jr. and J. LeGall. 1978. Reactivity of *Desulfovibrio gigas* hydrogenase towards artificial and natural electron donors. Biochimie 60: 315–320.

9 Bell, G.R., J. LeGall and H.D. Peck, Jr. 1974. Evidence for the periplasmic location of hydrogenase in *Desulfovibrio gigas*. J. Bacteriol. 120: 994–997.

10 Berlier, Y.M., G. Fauque, P.A. Lespinat and J. LeGall. 1982. Activation, reduction and proton-deuterium exchange reaction of the periplasmic hydrogenase from *Desulfovibrio gigas* in relation with the role of cytochrome c_3. FEBS. Lett. 140: 185–188.

11 Brewer, J.M. and R.B. Ashworth 1969. Disc electrophoresis. J. Chem. Educ. 46: 41–45.

12 Costello, J.A. 1974. Cathodic depolarization by sulfate reducing bacteria. S. Afr. J. Sci. 70: 202–204.

13 Crombie, D.J., G.J. Moody and J.D.R. Thomas. 1980. Corrosion of iron by sulfate-reducing bacteria. Chem. Indust. 21: 800–804.

14 Czechowski, M., G. Fauque, Y. Berlier, P.A. Lespinat and J. LeGall. 1985. Purification of an hydrogenase from an halophilic sulfate reducing bacterium: *Desulfovibrio salexigens* strain British Guiana. Rev. Port. Quim. 27: 196–197.

15 Czechowski, M.H., S.H. He, M. Nacro, D.V. DerVartanian, H.D. Peck, Jr. and J. LeGall. 1984. A cytoplasmic nickel-iron hydrogenase with high specific activity from *Desulfovibrio multispirans* sp. N., a new species of sulfate reducing bacterium. Biochem. Biophys. Res. Commun. 108: 1388–1393.

16 Drucker, H., E.B. Trousil and L.L. Campbell. 1970. Purification and properties of cytochrome c_3 from *Desulfovibrio salexigens*. Biochemistry 9: 3395–3400.

17 Fairbanks, G., T.L. Steck, and D.F.H. Wallach. 1971. Electrophoretic analysis of the major polypeptides of the human erythrocyte membrane. Biochemistry 10: 2600–2617.

18 Fauque, G., M. Teixeira, I. Moura, P.A. Lespinat, A.V. Xavier, D.V. DerVartanian, H.D. Peck, Jr., J. LeGall and J.J.G. Moura. 1984. Purification, characterization and redox properties of hydrogenase from *Methanosarcina barkeri* (DSM 800). Eur. J. Biochem. 142: 21–28.

19 Hamilton, W.A. 1985. Sulphate-reducing bacteria and anaerobic corrosion. Annu. Rev. Microbol. 39: 195–217.

20 Hardy, J.A. 1983. Utilization of cathodic hydrogen by sulfate-reducing bacteria. Br. Corros. J. 18: 190–193.

21 Hatchikian, E.C. and M. Bruschi. 1979. Isolation and characterization of a molybdenum iron-sulfur protein from *Desulfovibrio africanus*. Biochem. Biophys. Res. Commun. 86: 725–734.

22 Hatchikian, E.C. and J.G. Zeikus. 1983. Characterization of a new type of dissimilatory sulfite reductase present in *Thermodesulfobacterium commune*. J. Bacteriol. 153: 1211–1220.

23 Hatchikian, E.C., M. Bruschi and J. LeGall. 1978. Characterization of the periplasmic hydrogenase from *Desulfovibrio gigas*. Biochem. Biophys. Res. Commun. 82: 451–461.

24 Hinton, S.M. and L.E. Mortenson. 1985. Identification of molybdoproteins in *Clostridium pasteurianum*. J. Bacteriol. 162: 477–484.

25 Huynh, B.H., J. Kany, D.V. DerVartanian, H.D. Peck, Jr. and J. LeGall. 1984. Characterization of a sulfite reductase from *Desulfovibrio vulgaris*. Evidence for the presence of a low spin siroheme and an exchange coupled siroheme-(4Fe-4S) unit. J. Biol. Chem. 259: 15373–15376.

26 Iverson, W.P. 1974. Microbial corrosion of iron. In: Microbial Iron Metabolism (Neilands, J.B., ed.), pp. 475–513. Academic Press, New York.

27 Jacobson, F.S., L. Daniels, J.A. Fox, C.T. Walsh and W.H. Orme-Johnson. 1982. Purification and properties of an 8-hydroxy-5-deazaflavin-reducing hydrogenase from *Methanobacterium thermoautotrophicum*. J. Biol. Chem. 257: 3385–3388.

28 King, R.A. and J.D.A. Miller. 1971. Corrosion by the sulfate-reducing bacteria. Nature 233: 491–492.

29 Krueger, H.E., B.H. Huynh, P.O. Ljungdahl, A.V. Xavier, D.V. DerVartanian, I. Moura, H.D. Peck, Jr., M. Teixeira, J.J.G. Moura and J. LeGall. 1982. Evidence for nickel and three iron center in the hydrogenase of *Desulfovibrio desulfuricans*. J. Biol. Chem. 257: 14620–14623.

30 Lee, J.P. and H.D. Peck, Jr. 1971. Purification of the enzyme-reducing bisulfite to trithionate from *Desulfovibrio gigas* and its identification as desulfoviridin. Biochem. Biophys. Res. Commun. 45: 583–589.

31 Lee, J.P., J. LeGall and H.D. Peck, Jr. 1973. Isolation of assimilatory and dissimilatory-type sulfite reductase from *Desulfovibrio vulgaris*. J. Bacteriol. 115: 529–542.

32 Lee, J.P., C.S. Yi, J. LeGall and H.D. Peck, Jr. 1973. Isolation of a new pigment desulforubidin, from a *Desulfovibrio desulfuricans* (Norway strain) and its role in sulfite reduction. J. Bacteriol. 115: 453–455.

33 LeGall, J., P.O. Ljungdahl, I. Moura, H.D. Peck, Jr., A.V. Xavier, J.J.G. Moura, M. Teixeira, B.H. Huynh and D.V. DerVartanian. 1982. The presence of redox-sensitive in the periplasmic hydrogenase from *Desulfovibrio gigas*. Biochem. Biophys. Res. Commun. 106: 610–616.

34 Lespinat, P.A., G. Denariaz, G. Fauque, R. Toci, Y. Berlier and J. LeGall. 1985. Fixation de l'azote atmospherique et metabolisme de l'hydrogene chez une bacterie sulfato-reductrice sporulante. *Desulfotomaculum orientis*. C.R. Acad. Sci. Paris. T. 301, serie III, n 16: 707–710.

35 Lino, A.R., J.J.G. Moura, A.V. Xavier, I. Moura, G. Fauque and J. LeGall. 1985. Characterization of two low-spin bacterial siroheme proteins. Rev. Port. Quim. 27: 215.

36 Lissolo, T., S. Pulvin and D. Thomas. 1984. Reactivation of the hydrogenase from *Desulfovibrio gigas* by hydrogen. J. Biol. Chem. 9: 11725–11729.

37 Littlewood, D. and J.R. Postgate. 1957. Sodium chloride and the growth of *D. sulfovibrio desulfuricans*. J. Gen. Microbiol. 17: 378–389.

38 Markwell, M.K., S.M. Haas, L.L. Bieber and N.E. Tolbert. 1978. A modification of the Lowry procedure to simplify protein determination in membrane and lipoprotein samples. Anal. Biochem. 87: 206–210.

39 Martin, S.M., P.R. Glick and W.G. Martin. 1980. Factors affecting the production of hydrogenase by *Desulfovibrio desulfuricans*. Can. J. Microbiol. 26: 1209–1213.

40 Moura, J.J.G., A.V. Xavier, M. Bruschi, J. LeGall, D.O. Hall and R. Cammack. 1976. A molybdenum containing iron-sulfur protein from *D. gigas*. Biochem. Biophys. Res. Commun. 75: 1037–1044.

41 Moura, I., J.J.G. Moura, M. Bruschi and J. LeGall. 1980. Flavodoxin and rubredoxin from *Desulfovibrio salexigens*. Biochim. Biophys. Acta 591: 1–8.

42 Moura, J.J.G., I. Moura, H. Santos, A.V. Xavier, M. Scandellari and J. LeGall. 1982. Isolation of P-590 from *Methanosarcina barkeri*: evidence for the presence of sulfite reductase activity. Biochem. Biophys. Res. Commun. 108: 1002–1009.

43 Odom, J.M. and H.D. Peck, Jr. 1981. Hydrogen cycling as a general mechanism for energy coupling in the sulfate reducing bacteria *Desulfovibrio* sp. FEMS. Lett. 12: 47–50.

44 Peck, H.D., Jr. 1960. Evidence for oxidative phosphorylation during the reduction of sulfate with hydrogen by *Desulfovibrio desulfuricans*. J. Biol. Chem., 235: 2734–2738.

45 Peck, H.D., Jr. and H. Gest. 1956. A new procedure for assay of bacterial hydrogenase. J. Bacteriol. 71: 70–80.

46 Peck, H.D., Jr. and J. LeGall. 1982. Biochemistry of dissimilatory sulfate reduction. Phil. Trans. R. Soc. Lond. B 298: 443–466.

47 Postgate, J.R. 1956. Cytochrome c_3 and desulfoviridin, pigments of the anaerobic *Desulfovibrio desulphuricans*. J. Gen. Microbiol. 14: 545–572.

48 Rieder, R., R. Cammack and D.O. Hall. 1984. Purification and properties of the soluble hydrogenase from *Desulfovibrio desulfuricans* (strain Norway 4). Eur. J. Biochem. 145: 637–643.

49 Schachman, H.K. 1979. Ultracentrifugation in Biochemistry. Academic Press, New York.

50 Schlegel, H.G. and K. Schneider. 1978. Distribution and role of hydrogenases in microorganisms. In: Hydrogenases: their catalytic Activity, Structure and Function. (Schlegel, H.G. and K. Schneider, eds.), pp. 15–44, E. Goltz KG, Gottingen.

51 Siegel, L.M. 1978. Structure and function of siroheme and siroheme enzymes. In: Mechanisms of Oxidizing Enzymes (Singer, T.P. and R.H. Ondarza, eds.), pp. 201–214, Elsevier, New York.

52 Singleton, R., J. Denis and L.L. Campbell. 1984. Antigenic diversity of cytochromes c_3 from the anaerobic sulfate-reducing bacteria, *Desulfovibrio*. Arch. Microbiol. 139: 91–94.

53 Singleton, R., J. Denis and L.L. Campbell. 1985. Whole cell antigens of members of the sulfate reducing genus *Desulfovibrio*. Arch. Microbiol. 141: 195–197.

54 Starkey, R.L. 1938. A study of spore formation and other morphological characteristics of *Vibrio desulfuricans*. Arch. Mikrobiol. 8: 268–304.

55 Teixeira, M., I. Moura, A.V. Xavier, J.J.G. Moura, G. Fauque, B. Prickril and J. LeGall. 1985. Nickel-iron-sulfur-selenium containing hydrogenases isolated from *Desulfovibrio baculatus* strain 9974. Rev. Port. Quim. 27: 194–195.

56 Teixera, M., I. Moura, G. Fauque, M. Czechowski, Y. Berlier, P.A. Lespinat, J. LeGall, A.V. Xavier and J.J.G. Moura. 1986. Redox properties and activity studies on a nickel-containing hydrogenase isolated from a halophilic sulfate reducer *Desulfovibrio salexigens*. Biochimie 68: 75–84.

57 Van der Westen, H.M., S.G. Mayhew and C. Veeger. 1978. Separation of hydrogenase from intact cells of *Desulfovibrio vulgaris*, purification and properties. FEBS. Lett. 86: 122–126.

58 Von Wolzogen Kuhr, C.A.M. and L.S. Van der Vlugt. 1934. The graphitization of cast iron as an electrochemical process in anaerobic soils. Water (The Hague), 16: 147.

59 Wanklyn, J.N. and C.J.P. Spruit. 1952. Influence of sulphate-reducing bacteria on the corrosion potential of iron. Nature, 169: 928–929.

60 Yamazaki, S. 1982. A selenium-containing hydrogenase from *Methanococcus vannielii*. Identification of the selenium moiety as a selenocysteine residue. J. Biol. Chem. 257: 7926–7929.

Eur. J. Biochem. 162, 547–554 (1987)
© FEBS 1987

71

B-15

Characterization of the cytochrome system of a nitrogen-fixing strain of a sulfate-reducing bacterium: *Desulfovibrio desulfuricans* strain Berre-Eau

Isabel MOURA [1], Guy FAUQUE [2, 3], Jean LeGALL [3], Antonio V. XAVIER [1] and José J. G. MOURA [1]

[1] Centro de Quimica Estrutural, Universidade Nova de Lisboa
[2] A.R.B.S., Centre d'Etudes Nucléaires, Cadarache
[3] Department of Biochemistry, University of Georgia, Athens

(Received August 11/October 8, 1986) – EJB 86 0897

Two *c*-type cytochromes were purified and characterized by electron paramagnetic resonance (EPR) and nuclear magnetic resonance (NMR) spectroscopic techniques, from the sulfate-reducer nitrogen-fixing organism, *Desulfovibrio desulfuricans* strain Berre-Eau (NCIB 8387). The purification procedures included several chromatographic steps on alumina, carboxymethylcellulose and gel filtration. A tetrahaem and a monohaem cytochrome were identified. The multihaem cytochrome has visible, EPR and NMR spectra with general properties similar to other low-potential bis-histidinyl axially bound haem proteins, belonging to the class of tetrahaem cytochrome c_3 isolated from other *Desulfovibrio* species. The monohaem cytochrome c_{553} is ascorbate-reducible and its EPR and NMR data are characteristic of a cytochrome with methionine-histidine ligation. Their properties are compared with other homologous proteins isolated from sulfate-reducing bacteria.

Since the discovery by Postgate [1] and Ishimoto et al. [2] of tetrahaem cytochrome c_3 in the strict anaerobic sulfate-reducing bacteria, other *c*-type cytochromes have been reported in *Desulfovibrio* species. It is now known that several kinds of *c*-type cytochromes can be isolated from different *Desulfovibrio* species. A classification based on the number of haems per molecule, rather than their molecular masses, has recently been proposed [3] as follows.

Monohaem cytochromes
(methionine – haem-iron – histidine)

Cytochrome c_{553} is a low-molecular-mass protein and contains a single haem group with methionine and histidine as axial ligands. This cytochrome was only isolated from *Desulfovibrio* (*D.*) *vulgaris* strains Hildenborough and Miyazaki [4, 5]. It has a midpoint redox potential of approximately + 20 mV [6, 7] which is a low value compared with most other methionine-histidine-ligated monohaem cytochromes.

Cytochrome $c_{553\,(550)}$ is a haem protein found in *D. baculatus* strains Norway 4 [8] (formerly called *D. desulfuricans* strains Norway 4 [NCIB 8310] [3]) and 9974 (DSM 1743) [9]. This cytochrome has a N-terminal sequence showing little homology with *D. vulgaris* strain Hildenborough cytochrome c_{553}. EPR and NMR spectroscopies have been utilized to characterize the structure around the haem [10].

Tetrahaem cytochrome c_3
(histidine – haem-iron – histidine)

This is present in all *Desulfovibrio* species so far examined. The four haems, mesoporphyrins, are covalently bound to the polypeptide chain through thioether linkages provided by cysteinyl residues on either a -Cys-$(Xaa)_2$-Cys-His- sequence or a -Cys-$(Xaa)_4$-Cys-His- sequence. The axial ligands are two hystidinyl residues. The three-haem-containing cytochrome $c_{551.5}$ (c_7) isolated from the sulfur-reducing bacterium *Desulfuromonas* (*Drm.*) *acetoxidans* (strain 5071) is a close relative to this class of haem protein [11, 12].

Several tetrahaem cytochromes c_3 isolated from different strains of *Desulfovibrio* have been sequenced: *D. gigas*, *D. vulgaris* strains Hildenborough and Miyazaki, *D. baculatus* strain Norway 4, and *D. salexigens* strain British Guiana as well as cytochrome $c_{551.5}$ (c_7) from *Drm. acetoxidans* [11, 13–15]. Even when deletions are allowed to maximize homology, only about 30% of the amino-acid residues are conserved throughout the above series of proteins. They account mainly for the residues involved in the haem-attachment sites. There are only eight conserved residues not involved in binding the haem groups. This difference in amino-acid composition results in a wide variation of the physico-chemical properties.

Structural studies by X-ray crystallography have been reported for tetrahaem cytochromes c_3 from *D. vulgaris* strain Miyazaki [16] and *D. baculatus* strain Norway 4 [17, 18] at 0.26-nm resolution and a new sequence alignment has been proposed [19]. The relative positions and orientations of the haems are very similar for both proteins. Some of the features of interest coming from these structures are: the haem groups have different solvent exposition, the four haems are not parallel and they are attached in a compact cluster with iron-iron distances ranging over 1.09–1.73 nm.

Several physico-chemical techniques, mainly Mössbauer spectroscopy [20], circular dichroism (CD) [21], electron

Correspondence to J. J. G. Moura, Centro de Quimica Estrutural, Universidade Nova de Lisboa, Avenida Roviseo Pais, P-1096 Lisboa, Portugal

Abbreviations. EPR, electron paramagnetic resonance; SDS, sodium dodecyl sulphate.

5

241

Table 1. *Present knowledge of cytochromes characterization in sulfate-reducing bacteria of the genus* Desulfovibrio
This table was compiled from references indicated in text. Preliminar crystallographic data was recently reported on *D. vulgaris* Miyazaki cytochrome c_{553} [65]. S = sequenced; NMR, EPR, X-ray refer to spectroscopic characterization; P = purified; PNP = present but not purified; – = not reported

Desulfovibrio species	Tetrahaem cytochrome c_3	Octahaem cytochrome c_3	Monohaem cytochrome c_{553}
D. gigas	S, NMR, EPR	P	–
D. vulgaris Hildenborough	S, NMR, EPR	P	S, NMR, EPR
D. vulgaris Miyazaki	S, X-ray	–	P, X-ray
D. baculatus strain 9974	P, NMR, EPR	–	P[a]
D. baculatus Norway 4	S, NMR, EPR, X-ray	S	P, NMR, EPR[a]
D. desulfuricans ATCC 27774	P, NMR, EPR	–	–
D. desulfuricans Berre-Eau	P, NMR, EPR	–	P, NMR, EPR
D. desulfuricans El Algheila Z	S, NMR, EPR	P	–
D. salexigens British Guiana	S, NMR	PNP	PNP
D. desulfuricans Berre-Sol	P, NMR, EPR	–	P, NMR

[a] Refers to monohaem cytochrome $c_{553\ (550)}$.

paramagnetic resonance (EPR) [22–25], nuclear magnetic resonance (NMR) [26–32], cyclic voltametry, differential pulse polarography and pulse radiolysis [33–39] have also been applied to elucidate structural features and the mechanism of electron transfer in cytochromes from *Desulfovibrio* spp.

The midpoint redox potentials of the four haems have been measured by a wide range of techniques [24, 25, 33, 34, 40].

Octahaem cytochrome c_3 *(histidine–haem-iron–histidine)*

This cytochrome has been found in several *Desulfovibrio* species (see Table 1). Recently, Guerlesquin et al. [41] characterized the octahaem cytochrome c_3 from *D. baculatus* strain Norway 4. By removal of the haems they demonstrated that two identical subunits of molecular mass 13.5 kDa are obtained. Although the monomer form of octahaem cytochrome c_3 has a molecular mass somewhat similar to that of the tetrahaem cytochrome c_3 isolated from the same bacterium, the amino acid composition and the N-terminal sequence are different, confirming the presence of a different cytochrome [41].

Table 1 contains information about the purification and characterization of *c*-type cytochromes from these bacteria. The physiological role of cytochromes in sulfate-reducing organisms is far from being fully understood. Tetrahaem cytochrome c_3 plays an important role in relevant metabolic pathways of Desulfovibriones, namely in its direct interaction with the hydrogenase system and with the electron transfer chain to the terminal reductases involved in the reduction of sulfur compounds. Octahaem cytochrome c_3 seems to be an electron carrier for the electron transport chain of thiosulfate reduction in the *D. gigas* enzymatic systems [42] and cytochrome c_{553} was identified as a natural electron acceptor for the formate dehydrogenase systems in *D. vulgaris* strain Miyazaki [43].

Other *c*-type cytochromes were also detected in some *Desulfovibrio* spp. In *D. desulfuricans* (ATCC 27774) a sulfate-reducing bacterium that can grow on nitrate as terminal electron acceptor, the nitrite reductase is a hexahaem *c*-type cytochrome [44]. Another *c*-type cytochrome called 'split-soret' was also purified from this organism. It is a trimeric protein with subunit molecular masses of 26.4 kDa with two haems *c* per monomer [45].

In the present communication we report the purification and some properties of tetrahaem cytochrome c_3 and cytochrome c_{553} isolated from *D. desulfuricans* strain Berre-Eau. Another *c*-type cytochrome was also detected for which preliminary properties are presented. *D. desulfuricans* strain Berre-Eau is able to grow while fixing N_2 as has been reported for some strains of *Desulfovibrio* and *Desulfotomaculum* [46–48].

MATERIALS AND METHODS

Analytical procedures and instrumentation

Molecular masses were estimated by gel filtration on a Sephadex G-50 column, according to the method of Whitaker [49], using the following standards: chymotrypsin (M_r = 25000), *D. gigas* ferredoxin II (M_r = 24000), horse heart cytochrome *c* (M_r = 12500) and *D. gigas* rubredoxin (M_r = 6000) and also in the presence of sodium dodecyl sulfate (SDS) using the procedure of Weber and Osborn [50] with the following standards: soybean trypsin inhibitor (M_r = 21000), horse heart cytochrome *c* (M_r = 12500), and *D. vulgaris* strain Hildenborough cytochrome c_{553} (M_r = 9000).

The isoelectric point was determined by isoelectric focusing [51] on a LKB Multiphor apparatus.

Absorption spectra were obtained on a Beckman spectrophotometer, model 35.

For NMR measurements, the cytochromes were desalted and lyophilised three times from ^2H_2O and dissolved to the required concentration (1–2 mM). Reduction of the proteins was achieved by adding small amounts of solid sodium dithionite under an N_2 atmosphere. High-resolution proton NMR spectra were recorded on a Bruker CXP 300 spectrometer (300 MHz) equipped with an Aspect 2000 computer in which mathematical manipulations were carried out. The temperature was controlled to ± 0.5°C with a standard Bruker B-VT-1000 variable temperature control unit.

Selective Nuclear Overhauser effects were obtained by the TOE method [52]. Typically, one free induction decay was acquired with a gated irradiation pulse on the frequency chosen, and the next with the same gated irradiation pulse, but on an empty region of the spectrum. The spectra were subtracted in order to minimize external effects, the sequence was repeated 1000 times to obtain a good signal/noise ratio. All chemical shift values are quoted in parts per million (ppm)

from internal sodium 3-trimethylsilyl-(2,2,3,3,-$^2H_4$)propionate, positive values referring to low-field shifts.

EPR spectra were recorded in a Bruker ER-200 tt spectrometer equipped with an Oxford Instruments continuous helium flow cryostat interfaced to a Nicolett 1180 computer.

Growth of organisms and purification of D. desulfuricans *strain Berre-Eau cytochromes*

D. desulfuricans strain Berre-Eau (NCIB 8387) was grown in the medium of Starkey [53] on lactate/sulfate at 37 C and harvested as previously described [54].

All the purifications steps were performed at + 4 C using potassium phosphate and Tris/HCl buffers, pH 7.6, of appropriate molarity. The frozen cells (600 g, wet weight) were thawed and suspended in 1.4 l of 10 mM Tris/HCl buffer, containing a few deoxyribonuclease crystals. The cell suspension was treated in a French pressure cell; then the cell-free extract was centrifuged for 45 min at 12000 rev./min.

The crude extract was passed over a column (37 × 5.5 cm) of DEAE-cellulose (DE-52) equilibrated with 10 mM Tris HCl. The fraction not adsorbed on this column (1500 ml) contained most of the cytochromes and was passed over an alumina column (18 × 4.5 cm) equilibrated with 10 mM Tris HCl. A discontinuous gradient of potassium phosphate buffer (10 – 500 mM) was performed. Two main fractions containing cytochromes were eluted between 40 – 100 mM and at 400 mM. The first fraction contained an ascorbate-reducible cytochrome (cytochrome c_{553}), The second fraction contained mostly a cytochrome not reducible by ascorbate but dithionite-reducible (tetrahaem cytochrome c_3).

During the purification a purity coefficient will be defined as $[A_{553}$ (red)-A_{570} (red)]/A_{280} (oxid).

Cytochrome c_{553}

The fraction containing cytochrome c_{553} coming from alumina (V = 350 ml with a purity coefficient of 0.15) was dialysed overnight against 20 l distilled water. After dialysis this cytochrome was adsorbed on a column (19 × 4.5 cm) of carboxylmethycellulose (CMC-52) equilibrated with 10 mM Tris/HCl buffer and eluted with a discontinuous gradient of Tris/HCl buffer (10 – 250 mM). The cytochrome c_{553} with a coefficient of 0.82 in a total volume of 310 ml was dialysed again and a second step of purification was performed on another CMC-52 column with a similar elution gradient. At 25 – 50 mM Tris/HCl buffer the cytochrome c_{553} was eluted in a volume of 190 ml with a purity coefficient of 1.02. A last step of purification was done in column (5 × 3 cm) of hydroxyapatite (HTP) equilibrated with 50 mM Tris/HCl buffer. Cytochrome c_{553} was not retained but eluted in a volume of 150 ml having a purity coefficient of 1.2. This cytochrome was completely reduced by ascorbate.

Tetrahaem cytochrome c_3

The fraction containing mostly a cytochrome not reducible by ascorbate eluting from the first alumina column was dialyzed overnight against 20 l distilled water. This fraction, in a volume of 450 ml and with a purity coefficient of 0.19, was adsorbed on another alumina column (17 × 4 cm) equilibrated with 10 mM Tris/HCl buffer. During a discontinous gradient of phosphate buffer (10 – 700 mM), a 360-ml cytochrome fraction was collected at 400 mM. This cytochrome was not reducible by ascorbate and the purity coefficient was 1.88.

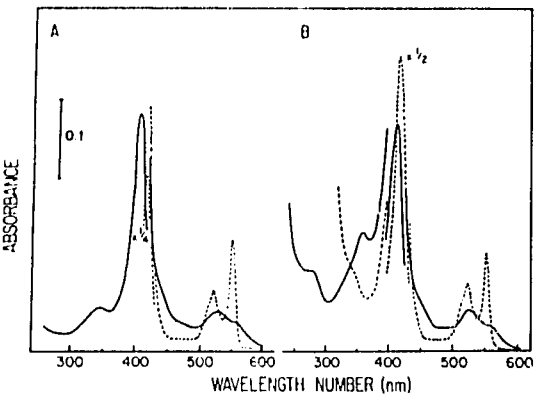

Fig. 1. *Ultraviolet and visible absorption spectra of* D. desulfuricans *strain Berre-Eau cytochromes.* (A) Tetrahaem cytochrome c_3 (1.25 μM): (——) oxidized form; (- - - -) dithionite-reduced form. (B) Monohaem cytochrome c_{553} (4.33 μM): (——) oxidized form; (- - - -) ascorbate-reduced form

After dialysis this cytochrome was adsorbed on an HTP column (11 × 4 cm) equilibrated with 10 mM Tris/HCl. A discontinous gradient in phosphate was performed (1 – 500 mM). Tetrahaem cytochrome c_3 was eluted between 200 – 400 mM in a volume of 175 ml with a purity coefficient of 1.95. After dialysis, the material was adsorbed onto a CMC-52 column (20 × 4.5 cm) and subjected to a discontinuous Tris/HCl gradient (10 – 170 mM). Tetrahaem cytochrome c_3 was eluted at 60 – 100 mM in a volume of 180 ml with a purity coefficient of 2.8 l. Another similar step on CMC-52 increased the purity coefficient to 2.85 and finally tetrahaem cytochrome c_3 was passed on a Sephadex G-50 column (90 × 4.5 cm) equilibrated with 10 mM Tris/HCl. Tetrahaem cytochrome c_3 was obtained in a volume of 70 ml with a purity coefficient of 3.22.

RESULTS

Homogeneity and molecular masses

Tetrahaem cytochrome c_3 and cytochrome c_{553} were judged to be pure by polyacrylamide gel electrophoresis at pH 8.9.

The molecular mass of cytochrome c_{553} was estimated to be 9 kDa by SDS gel electrophoresis. This value is similar to the molecular mass of three other monohaem cytochromes isolated from *Desulfovibrio* species [4, 5, 8, 9].

The molecular mass of tetrahaem cytochrome c_3 determined by gel filtration on Sephadex G-50 and on SDS gel was estimated to be 13.5 kDa. The isoelectric points were determined by isoelectric focusing to be 9.2 and 8.6 respectively for cytochromes c_{553} and c_3.

Ultraviolet and visible absorption spectral properties

The absorption spectra of oxidized and reduced forms of purified cytochrome c_{553} and tetrahaem cytochrome c_3 are shown in Fig. 1. Cytochrome c_{553} is completely reduced by ascorbate and cytochrome c_3 is only dithionite-reducible. In contrast with cytochrome c_3, cytochrome c_{553} shows in the oxidized form a peak in the 280-nm region and a weak shoul-

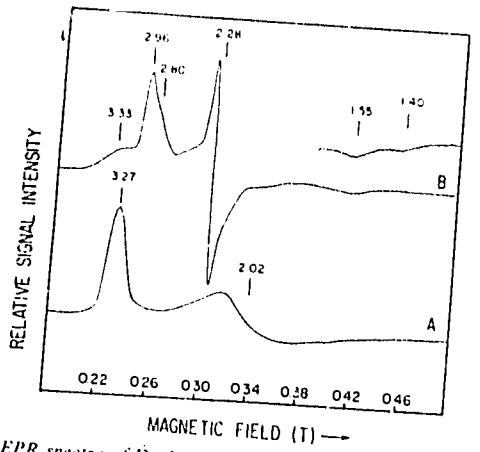

Fig. 2. *EPR spectra of* D. desulfuricans *strain Berre-Eau ferricytochrome* c_{553} *(A) and ferritetrahaem cytochrome* c_3 *(B).* (A) Measured at 5.2 K, microwave power 2 mW, field modulation 1 mT, gain 5×10^4; (B) measured at 4.8 K, other experimental conditions as in A

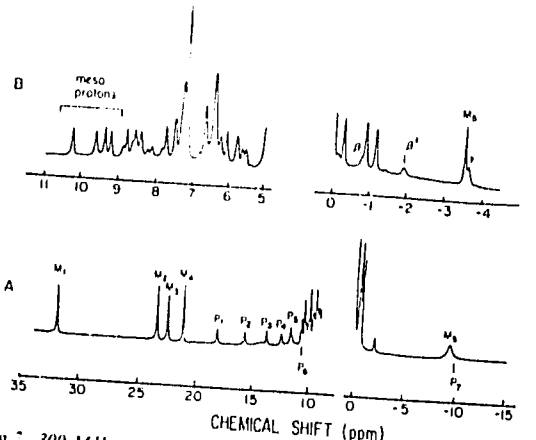

Fig. 3. *300-MHz spectra of* D. desulfuricans *Berre-Eau cytochrome* c_{553} *in (A) reduced form at 313 K and (B) oxidized form at 300 K.* Some relevant resonances are assigned

der at 690 nm (not shown), characteristic of the haem-methionine axial ligation.

The highest purity coefficient found for tetrahaem cytochrome c_3 is 3.22 and for cytochrome c_{553} is 1.20. The values are similar to the ones reported from other Desulfovibrione tetrahaem cytochromes c_3 and monohaem cytochromes c_{553}.

Electron paramagnetic resonance data

Ferricytochrome c_{553}. The EPR spectrum recorded at 6 K (Fig. 2A) contains two main components present at $g = 3.27$ and $g = 2.02$ which are assigned to a low-spin species. The third component of the corresponding rhombic g tensor is not observable, presumably being too broaden in the high field region.

Ferritetrahaemcytochrome c_3. Fig. 2B shows the EPR spectrum recorded at 10 K. The spectrum is quite complex, showing in the g_{max} region several superimposed signals. A very broad feature is detected around 3.33, a prominent feature at 2.96 and a shoulder at 2.80. A derivative peak is observed at 2.28 (probably g_{med}) and two broad signals at high field: 1.55 and 1.40 (g_{min}).

Nuclear magnetic resonance data

Ferricytochrome c_{553}. Fig. 3A shows the NMR spectrum of the low-field region of *D. desulfuricans* strain Berre-Eau ferricytochrome c_{553}. Four haem methyl resonances are observed (M_{1-4}) in a pattern very similar to that observed for *D. vulgaris* strain Hildenborough cytochrome c_{553} [10]. At high field the ε-methyl protons from the axial-ligated methionine can be observed at -9.34 ppm (300 K). A one-proton resonance, presumably from a methylene group of this residue, is underneath the ε-methyl methionine group (P_7) and can be separated when varying the temperature. The temperature dependence of selected resonances of the NMR spectra of ferricytochrome c_{553} (Fig. 4) indicates that the methyl resonances M_2, M_3 and M_4 do not follow a Curie law. Although the chemical shift of ε-methyl methionine resonance decreases

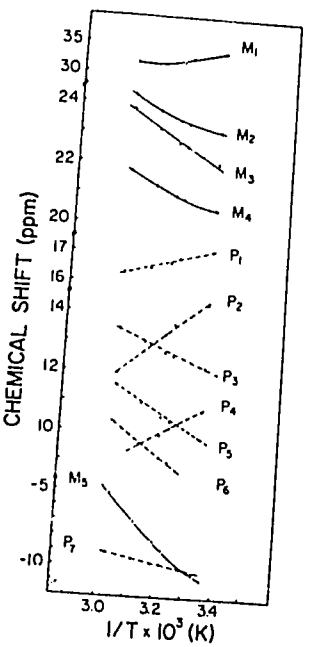

Fig. 4. *Temperature dependence of selected NMR resonances of* D. desulfuricans *strains Berre-Eau ferricytochrome* c_{553} *as indicated in Fig. 3*

when the temperature is increased, the temperature-dependence plot is complex and not linear. This is also observed for methyl resonances M_1, M_2 and M_4.

Ferrocytochrome c_{553}. Fig. 3B shows the 300-MHz NMR spectrum of *D. desulfuricans* strain Berre-Eau ferrocytochrome c_{553}. Four one-proton resonances assigned to haem mesoprotons are resolved at 10.24, 9.63, 9.39 and 9.27 ppm in the low-field region of the spectrum at 300 K. In the high-field region the typical pattern of the resonances from the methionine ligated to the haem iron can be observed. The

Table 2. *Chemical shift of axial methionine resonance in* D. desulfuricans *Berre-Eau ferrocytochrome* c_{553} *(313 K)*

Resonance	Chemical shift
	ppm
ε-Methyl	−3.51
γ'-Methylene	−3.60
γ-Methylene	−[a]
β'-Methylene	−1.89
β-Methylene	−0.76

[a] Not determined. Probably the methionyl γ-proton overlaps the ε-methyl group.

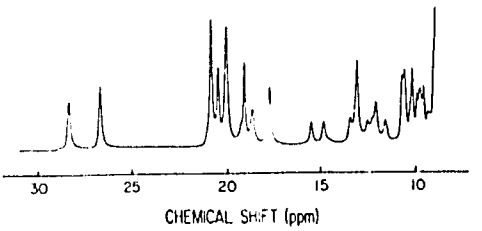

Fig. 5. *300-MHz NMR spectra of the low-field region of* D. desulfuricans *strain Berre-Eau tetrahaem cytochrome* c_3 *in the oxidized form at 313 K*

methyl protons at the ε position of the axial methionine are at −3.51 ppm, a value lower than those generally observed for methionine-histidine cytochromes (positive redox potential). The assignment of the methionyl β and γ protons was carried out as in [52]. The results are shown in Table 2.

Ferritetrahaemcytochrome c_3. In Fig. 5, the low-field region of the oxidized form of tetrahaem cytochrome c_3 is shown. Several resonances corresponding to three-proton intensity (haem methyl) can be detected in this region as is usual for tetrahaem cytochromes c_3 from other *Desulfovibrio* species. At least 14 haem methyl resonances of the 16 haem methyl groups are observed.

DISCUSSION

Sulfate-reducing bacteria are strict anaerobes that are considered as representative of organisms having an ancestral metabolic process. They are able to carry out the dissimilatory reduction of sulfate, the so-called 'sulfate respiration'. This process involves eight electrons to reduce sulfate up to hydrogen sulfide, coupled with an electron transfer chain.

Cytochromes seem to play an important role in these electron transfer processes, although at the present moment their precise physiological role is still controversial. More research on the cell localization must be undertaken in order to understand fully the involvement of the haem proteins. The localization of tetrahaem cytochrome c_3 is predominantly periplasmic [54] although Odom and Peck [55] have found relevant amounts of *c*-type cytochromes in *D. gigas* cytoplasm. Recently, comparing amino acid sequences of several periplasmic and cytoplasmic proteins from *Desulfovibrio* species, LeGall and Peck [56] proposed that periplasmic proteins have NH_2-terminal amino acid sequences indicative of recognition sites for signal peptidases. This is the case of tetrahaem cytochromes c_3 and supports their previous localization in the periplasmic space.

As indicated in Table 1, tetrahaem cytochromes c_3 are conserved in all the *Desulfovibrio* species analysed so far. It is interesting to note that even when the terminal acceptor is modified, i.e. nitrate by sulfate in *D. desulfuricans* (ATCC 27774) this multihaem cytochrome is conserved [45].

The presence of monohaem cytochromes has not been reported for most of Desulfovibriones (see Table 1).

The general EPR and NMR spectroscopic parameters of the monohaem cytochrome c_{553} isolated from *D. desulfuricans* strain Berre-Eau are very similar to those from *D. vulgaris* strain Hildenborough cytochrome c_{553}. According to the classification of Brautigan et al. [57], *D. desulfuricans* strain Berre-Eau cytochrome c_{553} belongs to the class of cytochromes like yeast iso-2, *Euglena, Rhodospirillum rubrum* and *Pseudomonas denitrificans* that have a major neutral pH form with g_{max} value near 3.2. The tuna, yeast iso-1 and horse cytochromes *c* belong to the other class having at neutral pH a major form with EPR absorption at $g = 3.06$. It was also suggested by Brautigan et al. [57] that in this last class of cytochromes the N-1 from the ligated imidazole is deprotonated or enhanced hydrogen bonding. The NMR pattern of the low-field-shifted methyl haem resonances in the ferric form as well as the chemical shift of the haem-meso proton resonances and the methyl group of the methionine in the ferrous state are identical (see Table 2 and Fig. 3). It was recently shown that in *D. vulgaris* strain Hildenborough cytochrome c_{553}, a different methionine chirality is observed when comparing the oxidized and reduced states of the protein [10]. In the reduced state the axial methionine has an *S* chirality and changes to *R* upon oxidation. The structure is most closely related to that found in cytochromes c_{551}, but it differs from these by a clockwise rotation of approximately 45° around the iron-sulfur bound.

Another monohaem cytochrome was isolated from *D. baculatus* strain Norway 4 [8]. With respect to the chirality of the bound axial methionine, it seems to have the same properties as *D. vulgaris* strain Hildenborough cytochrome c_{553}. However it presents different ring methyl hyperfine shifts in the oxidized form, that are explained as being due to a small rotation of the axial methionine about an axis through the haem iron and the methionine sulfur atom [10]. This cytochrome isolated from *D. baculatus* strain Norway 4 shows a splitting of the α band of the visible spectrum in the reduced state. A similar monohaem cytochrome also showing a split α band was purified from *D. baculatus* strain 9974 [9]. The EPR *g*-values of these two split α cytochromes differ from those observed for *D. vulgaris* strain Hildenborough and *D. desulfuricans* strain Berre-Eau cytochromes c_{553} (Table 3).

The similarities between the monohaem cytochromes from *D. vulgaris* strain Hildenborough and *D. desulfuricans* strain Berre-Eau as well as the similarities between the monohaem cytochromes from *D. baculatus* strains 9974 and Norway 4 are quite noticable [7–10, 58] confirming that two different types of monohaem cytochromes are present in *Desulfovibrio* species.

Table 3 compares some of the data available for monohaem cytochromes from *Desulfovibrio* species. As it was already pointed out the monohaem cytochromes from *Desulfovibrio* species have unusually low oxidation-reduction potentials [6, 7]. This might be correlated with the unusual low position obtained for the ε-methyl group of the axial methionine in the reduced state [59]. A similar value of chemical shift was also reported for the methionyl methyl group of *D. vulgaris* strain Hildenborough ($\delta_{30°C} = 3.62$ ppm)

Table 3. *Physico-chemical data on monohaem cytochromes isolated from sulfate-reducing bacteria of the genus* Desulfovibrio
This table was compiled from references indicated in the text. The midpoint redox potential of *D. vulgaris* Miyazaki was reported by Langone et al. [66]

Monohaem cytochromes c_{553}	Redox potential	EPR values		Isoelectric point	Molecular mass
		g_{max}	g_{med}		
	mV				kDa
D. vulgaris Hildenborough	20 ± 5	3.15	2.065	8.6	8.6
D. vulgaris Miyazaki	-260	– [c]	– [c]	10.2	8.2
D. baculatus Norway 4[a]	≥ – 50[b]	3.07	2.24	6.6	9.4
D. desulfuricans Berre-Eau	≥ – 50[b]	3.27	2.02	9.2	9.0
D. baculatus strain 9974[a]	≥ – 50[b]	3.08	2.25	– [c]	9.0

[a] Refers to monohaem cytochrome $c_{553\,(550)}$.
[b] Ascorbate-reducible.
[c] Not reported.

Table 4. *EPR g-values of tetrahaem cytochromes* c_3 *isolated from sulfate-reducing bacteria of the genus* Desulfovibrio

Tetrahaem cytochromes c_3	g_{max}	g_{med}	g_{min}
D. gigas	2.96, 2.85	2.30	1.58, 1.51
D. vulgaris Hildenborough	3.12, 2.97, 2.82	2.29	1.67, 1.57, 1.43
D. baculatus Norway 4	3.36, 3.01, 2.94	2.28	1.51, 1.38
D. baculatus strain 9974	3.36, 3.06, 2.95	2.27	1.51, 1.32
D. desulfuricans Berre-Eau	3.33, 2.96, 2.80	2.28	1.55, 1.40
D. desulfuricans El Agheila Z	2.95	2.28	≈ 1.51

and *D. baculatus* strain Norway 4 ($\delta_{30°C}$ = 3.60 ppm) ferrocytochromes c_{553} [10].

In Table 4 some of the EPR *g*-values of tetrahaem cytochromes c_3 are compiled. The tetrahaem cytochromes c_3 exhibit quite different EPR characteristics. Tetrahaem cytochrome c_3 from *D. baculatus* strains 9974 and Norway 4 and *D. desulfuricans* strain Berre-Eau (this study) show quite similar EPR characteristics [60]. They all have a broad feature at g = 3.3, a resonance around g = 3.0 with a shoulder on this peak to lower g values. For other tetrahaem cytochromes, like *D. gigas* and *D. desulfuricans* strain El Agheila Z. tetrahaem cytochromes c_3 the broad peak around g = 3.30 is missing and only a g_{max} value is prominent around 3.0–2.9, showing in some cases a shoulder. *D. vulgaris* strain Hildenborough tetrahaem cytochrome c_3 seems different in the fact that three g_{max} values are quite discernable at 3.12, 2.97 and 2.82. The g_{med} is sharper when compared to those from other cytochromes c_3 [7, 60].

Recently Palmer and Walker et al. have shown that, in haem model compounds where the two axial imidazoles are perpendicular to each other, the EPR signals are extremely anisotropic with g values at around 3.4 [61, 62]. The X-ray structures of tetrahaem cytochromes c_3 from *D. vulgaris* strain Miyazaki and *D. baculatus* strain Norway 4 show that three of the haem groups have the two axial histidines in the same plane in relation to each other. Only one haem in both of these cytochromes has the two axial histidines perpendicular to each other [8, 18]. In this context we can re-examine the EPR spectra of these cytochromes c_3 with g values greater than 3. This signal should correspond to the haem with the two histidines perpendicular to each other. This haem has the lowest redox potential (– 325 mV) in *D. baculatus* strain Norway 4 [40]. However, in *D. gigas* and *D. desulfuricans* strain El Agheila Z tetrahaem cytochromes c_3, where the X-ray structures are not yet determined, the EPR characteristics are different and the signal with high g_{max} is not present. The tetrahaem cytochrome c_3 purified from *D. desulfuricans* strain Berre-Eau is similar in many aspects to tetrahaem cytochromes c_3 from other sulfate-reducing bacteria of the genus *Desulfovibrio*. It is a tetrahaem protein with a molecular mass of 13.5 kDa. The redox potentials of the four haems are low, since only dithionite, not ascorbate, can reduce the protein. The EPR and NMR characteristics of the tetrahaem cytochrome c_3 are more closely related to the similar proteins isolated from *D. baculatus* strains 9974 and Norway 4. The screening of the EPR and NMR characteristics of tetrahaem cytochromes c_3 would probably permit this class of proteins to be subdivided into sub-groups with more similar properties. This class of cytochromes has been extensively proposed to be involved in the hydrogen metabolism of sulfate-reducing bacteria [3]. It was also shown that in some species of sulfate reducers, for instance in *D. baculatus* strains 9974 and Norway 4 and *D. gigas*, tetrahaem cytochrome c_3 can act as a sulfur reductase (reduction of elemental sulfur to sulfide), whereas that of *D. vulgaris* strain Hildenborough is rapidly inhibited by sulfide [63, 64].

The four haems of tetrahaem cytochromes c_3 have histidine-histidine ligation and, as shown by EPR and NMR spectroscopies, they are localized in non-equivalent protein environments and each haem has a different redox potential [25, 30, 31, 40]. Although the absolute values vary with the experimental method of measurement, there is a general agreement that the four haem groups exhibit different and negative redox potential values.

By redox studies, followed by monitoring changes in the haem methyl resonance by NMR spectroscopy, we have recently shown that there is a haem-haem redox interaction [31, 32]. The midpoint redox potentials of some of the haems, as well as their interacting potentials, are pH-dependent. From these studies it seems that tetrahaem cytochrome c_3 has the potential of donating or receiving two coupled electrons and can interact with other electron transfer proteins in different

246

physiological conditions by modulating its mid-point redox potentials [32]. A full characterization of this new tetrahaem cytochrome c_3 in the light of this model of the interaction between the four haems is under study and will probably contribute to a better understanding of the electron transfer mechanism in this class of cytochromes and of their physiological significance.

The cytochrome system in *D. desulfuricans* strain Berre-Eau is mainly constituted by cytochrome c_{553} and tetrahaem cytochrome c_3, a very small amount of another *c*-type cytochrome was also detected. This cytochrome has not yet been fully purified. It does not belong to the octahaem cytochrome c_3 type and is partially reduced by ascorbate. Its molecular mass is between that of tetrahaem cytochrome c_3 and cytochrome c_{553}. NMR and EPR show that it is a multihaem cytochrome with significant differences from tetrahaem cytochrome c_3. A complete study of this cytochrome is underway to elucidate its properties fully.

We thank M. Scandellari and R. Bourelli for growing the bacteria used for the present study. We are indebted to I. Pacheco for her skilful technical help. This research was supported by grants from *Instituto Nacional de Investigação Cientifica, Junta Nacional de Investigação Cientifica e Tecnologica* and Agency for International Development (J. J. G. Moura) and National Science Foundation Grant DMB-8602789 (J. LeGall). Part of this work has been made possible thanks to a special collaborative arrangement between the University of Georgia, Athens (USA) and the *Centre National de la Recherche Scientifique* and the *Comissariat de l'Energie Atomique* (France).

REFERENCES

1. Postgate, J. R. (1954) *Biochem. J. 59*, Xi.
2. Ishimoto, M. K., Kayama, J. & Nagai, Y. (1954) *Bull. Chem. Soc. Japan 27*, 564–565.
3. LeGall, J. & Fauque, G. (1986) in *Biology of anaerobic microorganisms (Environmental microbiology of anaerobes)*, (Zehnder, A. J. B. ed.) in the press.
4. Bruschi, M., LeGall, J. & Dus, K. (1970) *Biochem. Biophys. Res. Commun. 38*, 607–616.
5. Yagi, T. (1979) *Biochim. Biophys. Acta 548*, 96–105.
6. Bianco, P., Haladjian, J., Bruschi, M. & Pillard, R. (1982) *J. Electroanal. Chem. 136*, 129–299.
7. Bertrand, P., Bruschi, M., Denis, M., Gayda, J. P. & Manca, F. (1982) *Biochem. Biophys. Res. Commun. 106*, 756–760.
8. Fauque, G., Bruschi, M. & LeGall, J. (1979) *Biochem. Biophys. Res. Commun. 86*, 1020–1029.
9. Fauque, G. (1979) *These de Doctorat de Specialite*, University of Aix-Marseille I.
10. Senn, H., Guerlesquin, F., Bruschi, M. & Wuthrich, K. (1983) *Biochim. Biophys. Acta 748*, 194–204.
11. Ambler, R. P. (1971) *FEBS Lett. 18*, 351–353.
12. Probst, I., Bruschi, M., Pfennig, N. & LeGall, J. (1977) *Biochim. Biophys. Acta 460*, 58–64.
13. Ambler, R. P. (1973) *Syst. Zool. 22*, 554–565.
14. Shinkai, W., Hase, T., Yagi, T. & Matsuabara, H. (1980) *J. Biochem. (Tokyo) 87*, 1747–1756.
15. Bruschi, M. (1981) *Biochim. Biophys. Acta 1*, 219–226.
16. Higuchi, Y., Bando, S., Kusunoki, M., Matsuma, Y., Yasuoka, N., Kakudo, M., Yamanaka, T., Yagi, T. & Inokuchi, H. (1981) *J. Biochem. (Tokyo) 89*, 1659–1662.
17. Haser, R., Pierrot, M., Frey, M., Payan, F., Astier, J. P., Bruschi, M. & LeGall, J. (1979) *Nature (Lond.) 282*, 806–810.
18. Pierrot, M., Haser, R., Frey, M., Payan, F. & Astier, J. P. (1982) *J. Biol. Chem. 257*, 14341–14348.
19. Higuchi, Y., Kusanaki, M., Yasuaka, N., Kakudo, M. & Yagi, T. (1981) *J. Biochem (Tokyo) 90*, 1571.
20. Ono, K., Keisaku, K. & Kimmer, K. (1975) *J. Chem. Phys. 63*, 1640–1642.
21. Drucker, H. L., Campbell, L. & Woody, R. W. (1970) *Biochimistry 9*, 1519–1527.
22. LeGall, J., Bruschi-Heriaud, M. & DerVartanian, D. V. (1971) *Biochim. Biophys. Acta 234*, 499–512.
23. DerVartanian, D. V. & LeGall, J. (1974) *Biochim. Biophys. Acta 346*, 79–99.
24. DerVartanian, D. V., Xavier, A. V. & LeGall, J. (1978) *Biochimie (Paris) 60*, 315–320.
25. Xavier, A. V., Moura, J. J. G., Moura, I., LeGall, J. & DerVartanian, D. V. (1979) *Biochimie (Paris) 61*, 689–695.
26. McDonald, C. C., Philips, W. D. & LeGall, J. (1974) *Biochemistry 13*, 1952–1959.
27. Dobson, C. M., Hoyle, N. J., Geraldes, C. F., Bruschi, M., LeGall, J., Wright, P. E. & Williams, R. J. P. (1974) *Nature (Lond.) 249*, 425–429.
28. Xavier, A. V. & Moura, J. J. G. (1978) *Biochimie (Paris) 60*, 327–338.
29. Moura, I., Moura, J. J. G., Santos, H. & Xavier, A. V. (1980) *Cienc. Biol. 5*, 189–191.
30. Moura, J. J. G., Santos, H., Moura, I., LeGall, J., Moore, G. R., Williams, R. J. P. & Xavier, A. V. (1982) *Eur. J. Biochem. 127*, 151–155.
31. Santos, H., Moura, J. J. G., Moura, I., LeGall, J. & Xavier, A. V. (1984) *Eur. J. Biochem. 141*, 283–296.
32. Xavier, A. V., Santos, H., Moura, J. J. G., Moura, I. & LeGall, J. (1985) *Rev. Port. Quim. 27*, 149–150.
33. Niki, K., Yagi, T., Inokuchi, H. & Kimura, K. (1977) *J. Electrochem. Soc. 124*, 1979–1991.
34. Niki, K., Yagi, T., Inokuchi, H. & Kimura, K. (1979) *J. Am. Chem. Soc. 10*, 3335–3340.
35. Sokol, W. F., Evans, D. H., Niki, K. & Yagi, T. (1980) *J. Electroanal. Chem. 108*, 107–115.
36. Bianco, P. & Haladjian, J. (1981) *Electrochim. Acta 26*, 1001–1004.
37. Bianco, P. & Haladjian, J. (1979) *Biochim. Biophys. Acta 545*, 86–93.
38. Eddowers, M. J., Elzanouska, H. & Hill, H. A. O. (1979) *Biochem. Soc. Trans. 7*, 735–737.
39. Van Leeuwen, J. W., Van Dijk, C., Grande, H. J. & Veeger, C. (1982) *Eur. J. Biochem. 141*, 283–296.
40. Cammack, R., Fauque, G., Moura, J. J. G. & LeGall, J. (1984) *Biochim. Biophys. Acta 784*, 68–74.
41. Guerlesquin, F., Bovier-Lapierre, G. & Bruschi, M. (1982) *Biochem. Biophys. Res. Commun. 105*, 530–538.
42. Hatchikian, E. C., LeGall, J., Bruschi, M. & Dubourdieu, M. (1972) *Biochim. Biophys. Acta 258*, 701–708.
43. Yagi, T. (1979) *Biochim. Biophys. Acta 548*, 96–105.
44. Liu, M. C. & Peck, H. D. Jr (1981) *J. Biol. Chem. 256*, 13159–13164.
45. Liu, M. C., (1982) Ph. D. Thesis, University of Georgia, Athens GA.
46. Nazina, T. N., Rozanova, E. P. & Kaulininskaya, T. A. (1979) *Mikrobiologiya 48*, 133–136.
47. Lespinat, P. A., Denariaz, G., Fauque, G., Toci, R., Berlier, Y. & LeGall, J. (1985) *C. R. Acad. Sci. (Paris) 301*, 707–710.
48. Postgate, J. R. & Kent, H. M. (1985) *J. Gen. Microbiol. 131*, 2119–2122.
49. Whitaker, J. R. (1963) *Anal. Chem. 35*, 1950–1953.
50 Weber, K. & Osborn, M. (1961) *J. Biol. Chem. 244*, 4406–4412.
51. Vesterberg, O. (1972) *Biochim. Biophys. Acta 247*, 11–19.
52. Senn, H., Keller, R. M. & Wuthrich, K. (1980) *Biochem. Biophys. Res. Commun. 92*, 1362–1369.
53. Starkey, R. L. (1938) *Arch. Mikrobiol. 9*, 268–304.
54. LeGall, J., Mazza, G. & Dragoni, N. (1961) *Biochim. Biophys. Acta 99*, 385–387.
55. Odom, J. M. & Peck, H. D. Jr (1984) *Annu. Rev. Microbiol. 38*, 551–592.
56. LeGall, J. & Peck, H. D. Jr (1986) *FEMS Lett.*, in the press.
57. Brautigan, D. L., Feinberg, B. A., Hoffman, B. A., Margoliash, E., Peisach, J. & Blumberg, W. E. (1977) *J. Biol. Chem. 252*, 574–582.

58. Coutinho, I., Moura, I., Moura, J. J. G., Xavier, A. V., Fauque, G. & LeGall, J. (1984) *7 Encontro Anual da Sociedade Portuguesa de Química*, PC 4.
59. Moore, G. R. & Williams, R. J. P. (1977) *FEBS Lett. 79*, 229–232.
60. Moura, I., Xavier, A. V., Moura, J. J. G., Fauque, G., LeGall, J., Moore, G. R. & Huynh, B. H. (1985) *Rev. Port. Quim. 27*, 212–215.
61. Palmer, G. (1984) *Biochem. Soc. Trans. 13*, 548–560.
62. Walker, F. A., Huynh, B. H., Scheidt, W. R. & Osvath, S. R. (1986) *J. Am. Chem. Soc.* (accepted for publication).
63. Fauque, G., Herve, D. & LeGall, J. (1979) *Arch. Microbiol. 121*, 261–264.
64. Fauque, G., Barton, L. L. & LeGall, J. (1980) *CIBA Found. Symp. 72*, 71–86.
65. Nakagawa, A., Nagashima, E., Higuchi, Y., Kusumoki, M., Matsuura, Y., Yasuoka, N., Katsube, Y., Chichara, H. & Yagi, T. (1986) *J. Biochem. (Tokyo) 99*, 605–606.
66. Langone, J. J., Boyle, M. D. P. & Borsos, T. (1978) *J. Immunol. 121*, 327–332.

B.16

Energy Transduction Coupling Mechanisms in Multiredox Center Proteins

António V. Xavier

Centro de Quimica Estrutural, New University of Lisbon

ABSTRACT

The data obtained for the physicochemical parameters of *Desulfovibrio gigas* cytochrome c_3, a small tetraheme electron transfer protein, are analyzed in terms of its possible use as an electron/proton/phosphoryl group transfer potential coupling device.

INTRODUCTION

The understanding of the mechanism for the multifarious couplings of energy transduction is a fundamental problem that has interested biochemists for the last quarter of a century and in particular Professor R. J. P. Williams [1].

The types of energy transduction that have been considered generally deal with electron/proton/phosphoryl group transfer potential: electron/electron coupling is an indispensable condition for the ubiquitous need for the transfer of two electrons in a single step; electron/proton coupling is a well-recognized process necessary for the function of proton-carrying redox proteins; and proton/phosphoryl group transfer potential coupling has to be considered in order to explain input of energized H^+ and output of ATP.

My purpose with this article is to utilize the recently obtained data on the characterization of the multiredox center cytochrome c_3 isolated from *Desulfovibrio gigas*, in order to demonstrate its potential use as a model for these three types of energy coupling.

D.gigas cytochrome c_3 is a small protein with four *c* type hemes in a single polypeptide chain of approximately 13 kDa [2]. The axial ligands for the four hemes are two histidinyl residues [3]. Cytochrome c_3 has a central role in the physiology of

Address reprint requests to Dr. A. V. Xavier, Centro de Quimica Estrutural, UNL, IST, Av. Rovisco Pais, P-1000 Lisboa, Portugal.

Journal of Inorganic Biochemistry 28, 239-243 (1986)
 0162-0134/86/$3.50

VM

Desulfovibrio spp. since it couples the pyruvate dehydrogenase activity, where two protons and two electrons are released, and the hydrogenase activity, resulting in the production of H_2. Conversely, it also couples the uptake of H_2 by hydrogenase, where again two electrons and two protons are produced and sent to the sulfate reduction metabolic pathway. Although cytochrome c_3 is a soluble protein, it is believed to work when membrane bound [4].

RESULTS AND DISCUSSION

A thorough NMR study of *D.gigas* cytochrome c_3 has allowed the calculation of the microscopic midpoint redox potential for the 32 redox pairs that have to be considered in order to explain the redox titration of this tetraheme protein [5]. Indeed, the midpoint reduction potential for each of the four hemes is dependent on the redox state of the other three hemes, resulting in the presence of interaction potentials, I_{ij}, between heme i and heme j. Table 1 shows the data obtained for the six I_{ij} as well as for the six differences between the midpoint redox potential of two hemes with consecutive midpoint reduction potentials, both for the fully oxidized, Δ_{ij}^*, and for the fully reduced one, Δ_{ij}. The data reported have been obtained at two fairly different pH values, 7.2 and 9.6.

Even a qualitative analysis of Table 1 shows that (1) the microscopic midpoint redox potentials are pH dependent; (2) the interaction potentials are not negligible and are also pH dependent.

Furthermore, a preliminary analysis of the NMR redox titrations carried out in the presence of inorganic phosphate indicates that this anion interacts specifically with cytochrome c_3. This specific interaction is reflected by a decrease in the electron self-exchange, intermolecular, rate, as well as in a slight modification of the haem microscopic reduction potentials and their pK_a's (Ref. 6 and unpublished results from J. LeGall, I. Moura, J. J. G. Moura, H. Santos, and A. V. Xavier).

The pH dependence of the heme midpoint potentials (redox-Bohr effect) gives cytochrome c_3 the potential to function as an electron/proton coupling device, similar

TABLE 1. Interacting Potentials and Midpoint Reduction Potential Differences for *D.gigas* Cytochrome c_3 in mV (pH* are the Values Measured in D_2O)

	pH* = 7.2	pH* = 9.6
Δ_{21}^*	−3	>49
Δ_{12}^*	40	16
Δ_{43}^*	59	80
Δ_{34}^*	35 ± 5	51 ± 1
Δ_{21}	1 ± 8	5 ± 1
Δ_{12}	25 ± 8	75 ± 1
Δ_{43}	19 ± 5	14 ± 3
I_{12}	−26 ± 5	−29 ± 4
I_{13}	6 ± 1	36 ± 4
I_{14}	42 ± 4	41 ± 3
I_{23}	−24 ± 5	−31 ± 3
I_{24}	−18 ± 3	0 ± 1
I_{34}		

to that postulated for several other systems [7–9]. This effect is an indispensable one to achieve the coupled transfer of electrons and protons.

A quantitative analysis of the influence of the interaction potentials was previously reported [5]. This was done calculating the molar fractions for the different oxidation steps (step 0, corresponding to the oxidation step with no hemes oxidized; step I, to the oxidation step with only one heme oxidized; and so on up to step IV, which corresponds to having the four hemes oxidized) obtained along the redox titration (see Fig. 9 of Ref. 5). However, this analysis reflects only the chemical equilibrium data and is not relevant in order to try and examine the dynamic equilibrium in which each protein molecule will be involved for its physiological activity. A different analysis is depicted in Figure 1. In this analysis the assumption made is that for each molecule involved in the electron transfer process, the electrons are given (received) specifically

FIGURE 1. Cytochrome c_3 microscopic midpoint reduction potentials. Those actually involved in the electron transfer chain are represented in boxes. The evolution of the values for each heme before oxidation (——) and before reduction (- - -) are also shown. The interacting potentials are represented by broken lines, positive slopes indicating positive cooperativity ($I_{ij} > 0$) and vice versa. The combination of negative and positive cooperativities, at different oxidation stages, reinforces the dispatching effect (e.g., as $I_{12} > 0$ and $I_{13} < 0$, oxidation of heme 1 (e_1) makes heme 2 (e_2^1) easier and heme 3 (e_3^1) more difficult to oxidize).

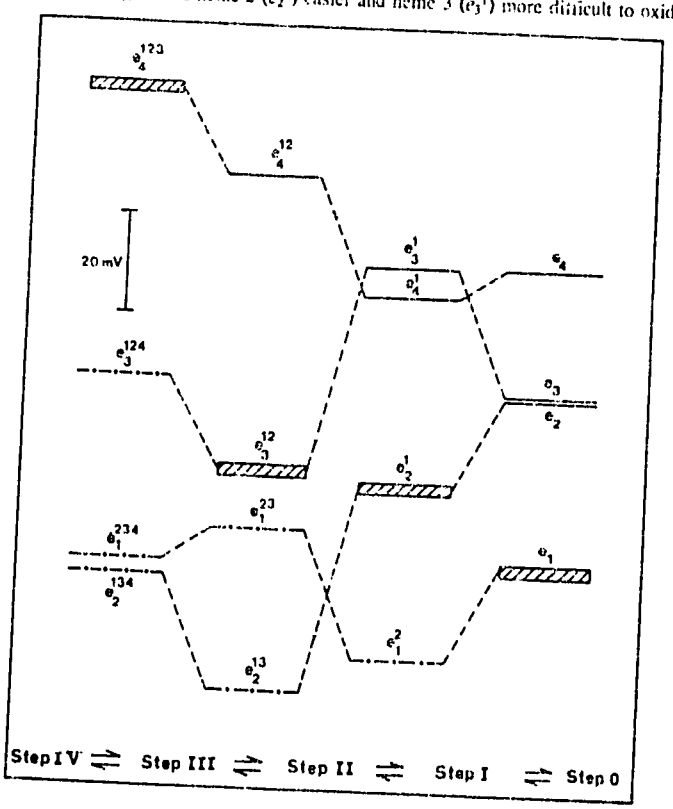

by one of the hemes and that the following electrons are given (received) so fast that there is no time for chemical equilibration to be attained. Thus, for each molecule when inserted in an electron transfer chain there is a specific order for the utilization of the hemes, which results in the utilization of only five redox states out of the 16 that can be obtained during a chemical redox titration of a tetraredox center protein.

The stepwise order is a direct result of the interaction potentials, which can be viewed as cooperativity effects, either positive (when $I_{ij} > 0$) or negative ones (when $I_{ij} < 0$), with the overall result of a vectorial use of the hemes. Thus, the physiologically useful microscopic reduction potentials are only those drawn as boxes in Figure 1: e_1, e_2^1, e_3^{12}, and e_4^{123}, respectively, for haem 1, the heme with the lowest midpoint reduction potential in the fully reduced state, and hemes 2, 3, and 4 the subsequent ones (the superscripts indicate the oxidized hemes).

Figure 1 also shows that in a dynamic equilibrium, due to the fairly strong positive cooperativity between hemes 2 and 3 ($I_{23} = +42$ mV), their midpoint reduction potential is the same, within experimental error ($e_2^1 = e_3^{12}$). Thus, owing to electron/electron coupling, the protein has the necessary properties to carry out a two-electron transfer [10, 11].

In this analysis the role of hemes 1 and 4 is interpreted as a regulatory one that sets the scene for a two-electron step to be operative: protein–protein recognition, with oxidation of heme 1 or reduction of heme 4, is a preparation step for a two-electron step to be activated, which is the one effectively used by the electron transfer chain. This mechanism of action also makes it possible to overcome the existing dilemma between the need for fast as well as for selective electron transfer [12]. Thus, the ready state for fast electron transfer by cytochrome c_3, e.g., an entatic state [13], would only be generated after the regulatory (dispatcher) centers have been activated, thus ensuring selectivity.

Although knowledge about the effects of the specific interaction of inorganic phosphate in the physicochemical properties of cytochrome c_3 is still scarce, it can be speculated that a further energy transduction coupling (to phosphoryl group transfer potential) may be achieved by this interesting molecule.

CONCLUSIONS

Molecular evolution has resulted in elaborated devices whose complexity has eluded the full understanding of the mechanisms involved in one of biology's best-kept secrets: that of energy transduction coupling.

Sulfate reducing bacteria are considered among the most ancient organisms in the evolutionary scale. Thus, they should be expected to rely on less sophisticated organization for the relevant structures.

It is quite remarkable that a small protein with a single polypeptide chain, hardly sufficient to cover its four covalently bond redox centers, concentrates the properties for such a broad range of potential energy transductions (electron/proton/phosphoryl group transfer potential). Although at this stage it is only possible to speculate on the physiological implications of these properties, which could lead as far as saying that cytochrome c_3 is a rudimentary (precursor) "respiratory" chain, the characterization so far obtained for this in many respects amazing protein warrants the importance of its complete study in order to use the acquired knowledge to further the understanding of the sophisticated systems used by more evolved cells.

I should like to thank J. LeGall, I. Moura, J. J. G. Moura, and H. Santos, with whom the

work reviewed in the present article has been carried out, for helpful discussions. This work was supported by INIC, JNICT, and USAID.

REFERENCES

1. R. J. P. Williams, *Biochim. Biophys. Acta* **505**, 1–14 (1978).
2. J. LeGall, *J. Bacteriol.* **86**, 1120 (1980).
3. M. Bruschi, C. E. Hatchikian, L. A. Golovleva, and J. LeGall, *J. Bacteriol.* **129**, 30–38 (1978).
4. J. LeGall, J. J. G. Moura, H. d. Peck Jr., and A. V. Xavier, in *Iron–Sulfur Proteins*, T. G. Spiro, Ed., Wiley, N. York, 1981, Vol. 4, pp. 177–247.
5. H. Santos, J. J. G. Moura, I. Moura, J. LeGall, and A. V. Xavier, *Eur. J. Biochem.* **141**, 283–296 (1984).
6. H. Santos, Ph.D. thesis, New University of Lisbon, Lisbon, Portugal, 1984.
7. G. R. Moore, G. W. Pettigrew, R. C. Pitt, and R. J. P. Williams, *Biochim. Biophys. Acta* **590**, 261–271 (1980).
8. S. Papa, *Biochim. Biophys. Acta* **456**, 39–84 (1976).
9. M. Losada, M. Hervas, M. A. de la Rosa, and F. F. de la Rosa, *Bioelectrochem. Bioenerg.* **6**, 205–225 (1983).
10. A. V. Xavier, H. Santos, J. J. G. Moura, I. Moura, and J. LeGall, *Rev. Port. Quim.* **27**, 149–150 (1985).
11. A. V. Xavier, in *Frontiers in Bioinorganic Chemistry*, A. V. Xavier, Ed., VCH Publishers, Weinheim, 1985, p. 722–725.
12. J. Kraut, *Biochem. Soc. Trans.* **9**, 197–202 (1981).
13. B. L. Vallee and R. J. P. Williams, *Proc. Natl. Acad. Sci. USA* **59**, 498–505 (1968).

Received May 1986